VOLUME 3 (1957) No. 2

NUCLEAR PHYSICS

MONTHLY JOURNAL DEVOTED TO THE EXPERIMENTAL AND THEORETICAL STUDY OF ATOMIC NUCLEI, NUCLEAR FIELDS AND THE FUNDAMENTAL ASPECTS OF COSMIC RADIATION

EDITOR: L. ROSENFELD - MANCHESTER

C. BLOCH, La fonction densité (strength function) dans la théorie statistique des réactions nucléaires 137

V. B. BERESTETSKY and YU. A. BYCHKOV, K-meson scattering with change of intrinsic parity 153

V. B. BERESTETSKY, On interference phenomena in the decay of strange particles. 157

C. J. HERRLANDER and T. R. GERHOLM, Excited levels in Hg^{200} studied from the decay of Tl^{200}. 161

R. ALPHONCE, A. JOHANSSON and G. TIBELL, The polarization of 155 MeV protons elastically and inelastically scattered from carbon 185

C. MARTY, Niveaux de rotation de noyaux sans axe de symétrie 193

DONALD STROMINGER and JOHN O. RASMUSSEN, Concerning lifetimes of low energy E1 gamma transitions in odd mass spheroidal nuclei 197

R. M. THALER and L. C. BIEDENHARN, A note on the calculation of coulomb penetration and coulomb wave functions 207

TH. A. J. MARIS, Polarization of high energy nucleons exciting a collective level 213

W. E. BURCHAM, W. M. GIBSON, D. J. PROWSE and J. ROTBLAT, Alpha-alpha scattering at 38.5 MeV 217

I. I. LEVINTOV, A. V. MILLER and V. N. SHAMSHEV, A new method of measurement of neutron polarization and n—He^4 phase analysis. 221

I. I. LEVINTOV, A. V. MILLER, E. Z. TARUMOV and V. N. SHAMSHEV, Dependence of (D+D) neutron polarization on deuteron energy. 237

F. VILLARS, A note on rotational energy levels in nuclei 240

(continued on p. 3 of cover)

NORTH-HOLLAND PUBLISHING COMPANY - AMSTERDAM

April 1957

EDITORIAL BOARD

AUSTRIA:	B. Karlik (Vienna), H. Thirring (Vienna)
BELGIUM:	M. de Hemptinne (Louvain), J. Verhaeghe (Ghent)
CANADA:	G. Volkoff (Vancouver)
DENMARK:	C. Møller (Copenhagen), S. Rozental (Copenhagen)
EGYPT & ARAB COUNTRIES:	F. El Bedewi (Alexandria), M. G. Nooh (Cairo)
FINLAND:	L. Simons (Helsinki)
FRANCE	A. Berthelot (Saclay), S. Gorodetzky (Strasbourg), F. Joliot (Paris)
GERMANY (FED. REP.):	W. Gentner (Freiburg i. B.), J. H. D. Jensen (Heidelberg)
GERMANY (DEM. REP.):	G. Hertz (Leipzig)
GREAT BRITAIN:	S. Devons (Manchester)
HUNGARY:	L. Janossy (Budapest)
INDIA:	H. Bhabha (Bombay), B. Peters (Bombay), R. Ramanna (Trombay)
IRISH REPUBLIC:	J. McConnell (Maynooth)
ISRAEL:	G. Racah (Jerusalem)
ITALY:	E. Amaldi (Rome)
JAPAN:	S. Kikuchi (Tokyo), S. Tomonaga (Tokyo)
NETHERLANDS:	H. Brinkman (Groningen), S. R. de Groot (Leiden)
NORWAY:	E. Hylleraas (Oslo), A. Lundby (Oslo), H. Wergeland (Trondheim)
POLAND:	L. Infeld (Warsaw)
PORTUGAL:	J. M. Araújo (Porto), J. R. de Almeida Santos (Coimbra)
SOUTH AMERICA:	G. Beck (Saõ Paulo), J. Leite Lopes (Rio de Janeiro)
SPAIN:	J. M. Otero (Madrid), C. Sanchez del Rio (Madrid)
SWEDEN:	O. Klein (Stockholm), K. Siegbahn (Uppsala), I. Waller (Uppsala)
SWITZERLAND:	P. Huber (Basel), P. Scherrer (Zürich)
U.S.S.R.:	M. A. Markov (Moscow), I. S. Shapiro (Moscow), D. V. Skobeltzyn (Moscow)
YUGOSLAVIA:	I. Supek (Zagreb)
U.S.A. & MEXICO:	V. Weisskopf (Cambridge, Mass.)
AUSTRALIA & NEW ZEALAND:	H. Messel (Sydney), M. L. Oliphant (Canberra)

CONTRIBUTIONS may be sent to the Editor, Professor L. Rosenfeld, Dept. of Theoretical Physics, The University, Manchester, either directly, or preferably through the intermediary of one of the members of the Editorial Board of the country or region in which the author is working. They may be written in English, French or German.

BOOKS FOR REVIEW should be sent to Professor Rosenfeld.

NUCLEAR PHYSICS is published in monthly issues. The subscription price is fl 57.00; 114s; $ 15.00. Postfree.

SUBSCRIPTIONS should be sent to the publishers, NORTH-HOLLAND PUBLISHING COMPANY, P.O.Box 103, Amsterdam or to any subscription-agent. Subscriptions for U.S.A. are to be sent exclusively to INTERSCIENCE PUBLISHERS, INC., 250 Fifth Avenue, New York 1, N.Y.

Printed in the Netherlands.

Nuclear Physics **3** (1957) 137—152; *North-Holland Publishing Co., Amsterdam*

LA FONCTION DENSITÉ (STRENGTH FUNCTION) DANS LA THÉORIE STATISTIQUE DES RÉACTIONS NUCLÉAIRES

CLAUDE BLOCH

Centre d'Études Nucléaires, Saclay (S. & O.) France

Reçu le 14 Novembre 1956

Abstract: It is shown by means of a simple model that the strength function corresponding to a single particle state of a nucleon interacting with a nucleus has a Lorentz shape in agreement with the analysis of the complex potential model in terms of giant resonances. The value of the imaginary part of the complex potential obtained from this calculation is not directly related to the second moment of the strength function which can be derived from a sum rule. It may, in fact, be appreciably smaller than the root square of the second moment.

1. Introduction

L'étude de la „fonction densité" [1]) (strength function) correspondant au modèle du potentiel complexe [2]) pour la diffusion nucléon-noyau a mis en évidence une relation statistique simple entre les fonctions d'onde du modèle des particules indépendantes et les fonctions d'onde véritables du noyau composé.

Dans le modèle des particules indépendantes on suppose que l'interaction du nucléon incident avec le noyau cible peut être décrite par un potentiel moyen. Nous désignerons par $|a\rangle$, $|b\rangle \ldots$; ε_a, $\varepsilon_b, \ldots$ les états et les niveaux d'énergie du système constitué par le noyau cible et le nucléon incident soumis au potentiel moyen représentant son interaction avec le noyau cible. Les fonctions d'ondes $|a\rangle$, $|b\rangle \ldots$ sont limitées à la région intérieure de l'espace de configuration et sont soumises à la surface nucléaire aux conditions aux limites habituelles de la théorie de Wigner [3]).

Nous désignerons par $|s\rangle$, $|t\rangle, \ldots$; ε_s, $\varepsilon_t, \ldots$ les états et les niveaux d'énergie du noyau composé réel formé par le nucléon incident et le noyau cible. Les fonctions $|s\rangle \ldots$ sont soumises aux mêmes conditions aux limites que les fonctions $|a\rangle \ldots$.

Le passage des fonctions $|a\rangle \ldots$ aux fonctions $|s\rangle \ldots$ est décrit par la matrice unitaire $\langle a|s\rangle$ dont la connaissance jointe à celle des états $|a\rangle \ldots$ permet le calcul de la fonction densité. L'analyse du phénomène des résonances géantes suggère que la matrice $\langle a|s\rangle$ (dont tous les éléments sont réels) peut être décrite statistiquement de la manière suivante:

a) les signes des éléments de matrice $\langle a|s\rangle$, $\langle a|t\rangle \ldots$ sont répartis au hasard;

b) la valeur moyenne (prise sur les niveaux ε_s, ε_t ... d'un petit intervalle d'énergie) de $|\langle a|s\rangle|^2$ est donnée par

$$\overline{|\langle a|s\rangle|^2} \equiv f(\varepsilon_a, \varepsilon_s) = \frac{1}{\pi} \frac{V\mathscr{D}}{(\varepsilon_s - \varepsilon_a - \Delta)^2 + V^2}, \tag{1}$$

où $\mathscr{D}$ est la distance moyenne des niveaux ε_s du noyau composé, V la partie imaginaire du potentiel complexe [4]). Le facteur $1/\pi$ est imposé par l'unitarité de la matrice. Le déplacement Δ du maximum de f est généralement négligé.

Nous désignerons par H l'Hamiltonien du noyau composé et par H_0, l'Hamiltonien du système simplifié ayant pour fonctions propres $|a\rangle$, $|b\rangle$ ... et pour valeurs propres ε_a, ε_b ...:

$$\begin{cases} H_0|a\rangle = \varepsilon_a|a\rangle, \\ H\ |s\rangle = \varepsilon_s|s\rangle. \end{cases} \tag{2}$$

La quantité

$$\vartheta = H - H_0 \tag{3}$$

est égale à la différence entre l'interaction vraie du nucléon incident avec le noyau cible et le potentiel moyen. C'est le potentiel qui produit le mélange de configurations décrit par la matrice unitaire $\langle a|s\rangle$.

Dans le but d'éclairer l'origine de la forme „de Lorentz" (1) de $f(\varepsilon_a, \varepsilon_s)$ nous allons calculer cette fonction pour un Hamiltonien fictif très simple défini par les conditions suivantes:

α) les valeurs propres ε_a ... de H_0 sont réparties au hasard indépendamment les unes des autres avec une distance moyenne D lentement variable avec l'énergie (la distance moyenne D des niveaux ε_a ... de H_0 n'est pas forcément égale à la distance moyenne $\mathscr{D}$ des niveaux ε_s de H);

β) les éléments de matrice ϑ_{ab} peuvent être considérés comme des variables aléatoires indépendantes, telles que les probabilités pour qu'un élément ait une valeur ou la valeur opposée soient égales.

Nous définissons ainsi un Hamiltonien aléatoire H pour lequel nous allons calculer la valeur moyenne ou valeur probable † de $|\langle a|s\rangle|^2$:

$$f(\varepsilon_a, \varepsilon_s) = \overline{|\langle a|s\rangle|^2}.$$

Les puissances impaires de tout élément de matrice ont des valeurs probables nulles:

$$\overline{\vartheta_{ab}^{2p+1}} = 0. \tag{4}$$

Nous supposerons que les valeurs probables des puissances paires de ϑ_{ab} sont des fonctions lentement variables de ε_a et ε_b, et nous écrirons

† E. Wigner [5]) a traité dans le même esprit le cas où les niveaux ε_a sont équidistants et où les éléments ϑ_{ab} peuvent prendre les valeurs $+\vartheta$ et $-\vartheta$ avec la même probabilité lorsque $|\varepsilon_a - \varepsilon_b| < \delta$ et sont nuls lorsque $|\varepsilon_a - \varepsilon_b| > \delta$.

$$\overline{\vartheta_{ab}^{2p}} = \vartheta^{(2p)}(\varepsilon_a, \varepsilon_b) = \vartheta^{(2p)}(\varepsilon_b, \varepsilon_a). \tag{5}$$

Aux fonctions $\vartheta^{(2p)}(\varepsilon_a, \varepsilon_b)$ nous associerons une notion de „portée" $\mathscr{E}$ définie par le fait que

$$\vartheta^{(2p)}(\varepsilon_a, \varepsilon_b) \approx 0 \text{ si } |\varepsilon_a - \varepsilon_b| > \mathscr{E}. \tag{6}$$

Nous allons montrer que dans le cas d'une „longue portée" c'est-à-dire lorsque

$$\mathscr{E} \gg V \gg D, \tag{7}$$

la fonction $f(\varepsilon_a, \varepsilon_s)$ prend effectivement la forme (1).

2. Formalisme Général

2.1. RELATION AVEC LA FONCTION DE GREEN

Nous allons d'abord établir entre la fonction $f(\varepsilon_a, \varepsilon_s)$ et la valeur probable de la fonction de Green

$$G(\varepsilon) = \frac{1}{\varepsilon - H} \tag{8}$$

de l'opérateur H, la relation

$$\frac{f(\varepsilon_a, \varepsilon_s)}{\mathscr{D}(\varepsilon_s)} = \frac{1}{2\pi i} \lim_{\delta \to +0} \langle a|\overline{G}(\varepsilon_s - i\delta) - \overline{G}(\varepsilon_s + i\delta)|a\rangle \tag{9}$$

$$= \frac{1}{\pi} \lim_{\delta \to +0} \operatorname{Im} \langle a|\overline{G}(\varepsilon_s - i\delta)|a\rangle.$$

Pour établir (9) il est commode de passer par l'intermédiaire de la transformée de Fourier de $f/\mathscr{D}$ considérée comme une fonction de ε_s:

$$F(t) = \int_{-\infty}^{+\infty} e^{i\varepsilon_s t} \frac{f(\varepsilon_a, \varepsilon_s)}{\mathscr{D}(\varepsilon_s)} d\varepsilon_s, \tag{10}$$

qui s'écrit aussi

$$F(t) = \sum_s e^{i\varepsilon_s t} \overline{|\langle a|s\rangle|^2} = \overline{\langle a|e^{iHt}|a\rangle}. \tag{11}$$

D'autre part, on a

$$e^{iHt} = \frac{1}{2\pi i} \int_C e^{i\varepsilon t} G(\varepsilon) d\varepsilon; \tag{12}$$

où C est un contour composé de parallèles à l'axe réel entourant celui-ci et parcouru dans le sens indiqué par la figure 1. On peut écrire en effet

$$G(\varepsilon) = \sum_s |s\rangle \frac{1}{\varepsilon - \varepsilon_s} \langle s|;$$

d'où, puisque le contour C entoure tout point ε_s,

$$\frac{1}{2\pi i} \int_C e^{i\varepsilon t} G(\varepsilon) d\varepsilon = \sum_s |s\rangle\langle s| \frac{1}{2\pi i} \int_C \frac{e^{i\varepsilon t} d\varepsilon}{\varepsilon - \varepsilon_s}$$

$$= \sum_s |s\rangle e^{i\varepsilon_s t} \langle s| = e^{iHt}.$$

Tout élément de matrice de la fonction de Green $G(\varepsilon)$ est une fonction analytique de ε ayant comme seules singularités des pôles aux points ε_s. De même, la valeur probable de tout élément de matrice de la fonction de Green sera analytique partout en dehors de l'axe réel. Par contre, tout

Fig. 1: Le contour d'intégration C dans le plan complexe ε.

point de l'axe réel ayant une certaine probabilité d'être valeur propre, la fonction $\overline{G}(\varepsilon)$ sera singulière sur toute la partie de l'axe réel où peuvent se trouver les valeurs propres ε_s de H. Nous montrerons plus loin que $\overline{G}(\varepsilon)$ tend vers une limite bien définie lorsque ε tend vers une valeur réelle en restant dans l'un des demi-plans délimités par l'axe réel. La valeur limite toutefois est différente suivant que ε est dans le demi-plan supérieur ou le demi-plan inférieur. En utilisant ces propriétés, on peut en faisant tendre le contour C vers l'axe réel écrire

$$\begin{aligned} F(t) &= \frac{1}{2\pi i}\int_C e^{\varepsilon t}\langle a|\overline{G}(\varepsilon)|a\rangle\, d\varepsilon \\ &= \lim_{\delta\to+0}\frac{1}{2\pi i}\int_{-\infty}^{+\infty} e^{\varepsilon_s t}\langle a|\overline{G}(\varepsilon_s-i\delta)-\overline{G}(\varepsilon_s+i\delta)|a\rangle\, d\varepsilon_s. \end{aligned} \tag{13}$$

Le terme $\overline{G}(\varepsilon_s-i\delta)$ correspond à la partie de C située en dessous de l'axe réel et $\overline{G}(\varepsilon_s+i\delta)$ à la partie située au-dessus de l'axe réel. En comparant (10) et (13) on obtient la relation à établir (9).

2.2. DEVELOPPEMENT DE LA FONCTION DE GREEN

Le problème est maintenant ramené au calcul de la valeur probable de G. Nous partirons du développement de G en série de puissances de ϑ:

$$G(\varepsilon) = \frac{1}{\varepsilon-H_0-\vartheta} = \frac{1}{\varepsilon-H_0} + \frac{1}{\varepsilon-H_0}\vartheta\frac{1}{\varepsilon-H_0} + \frac{1}{\varepsilon-H_0}\vartheta\frac{1}{\varepsilon-H_0}\vartheta\frac{1}{\varepsilon-H_0} + \ldots \tag{14}$$

Si on suppose que ϑ est une matrice bornée de norme † $||\vartheta||$ le développement (14) est majoré par la série

$$\sum_{n=0}^{\infty}\frac{||\vartheta||^n}{|\mathrm{Im}\,\varepsilon|^{n+1}}$$

qui converge si

$$|\mathrm{Im}\,\varepsilon| > ||\vartheta||.$$

† Rappelons que la norme $|\lambda|$ d'un vecteur $|\lambda>$ est définie par $|\lambda| = \sqrt{\langle\lambda|\lambda\rangle}$, et la norme d'une matrice A par $|A|\lambda>| \leqq ||A||\,|\lambda|$ quel que soit λ. La norme possède l'importante propriété que $||AB|| \leqq ||A||\,||B||$.

Sous la réserve que ϑ soit borné, le développement (14) permet donc de calculer $G(\varepsilon)$ loin de l'axe réel. La somme de la série peut ensuite, en principe, être prolongée analytiquement jusqu'au voisinage de l'axe réel afin de permettre l'application de la formule (9).

La norme de ϑ est donnée par

$$||\vartheta|| < \sum_{b} |\vartheta_{ab}| \sim \mathcal{N}\,\vartheta_M, \tag{15}$$

où ϑ_M désigne la valeur maximum d'un élément de matrice ϑ_{ab} et $\mathcal{N}$ le nombre de niveaux de H_0 se trouvant dans un intervalle d'énergie $2\mathscr{E}$. Cette estimation est valable si on suppose que ϑ_{ab} tombe rigoureusement à zéro lorsque $|\varepsilon_a - \varepsilon_b| > \mathscr{E}$. Le nombre $\mathcal{N}$ est en moyenne de l'ordre de $2\mathscr{E}/D$, mais avec les hypothèses faites sur la distribution des niveaux $\varepsilon_a, \varepsilon_b, \ldots$, il existe une probabilité petite mais non nulle que $\mathcal{N}$ dépasse tout nombre fixé à l'avance. Strictement parlant, ϑ n'est donc pas borné dans le modèle utilisé. Pour rendre ϑ borné, on pourrait modifier légèrement la distribution des niveaux de H_0 en spécifiant par exemple, que la distance de deux niveaux consécutifs ne peut être inférieure à une quantité fixée D_M. On aurait alors

$$||\vartheta|| < 2\mathscr{E}\vartheta_M/D_M.$$

2.3. REPRÉSENTATION GRAPHIQUE

Nous avons besoin de calculer un élément diagonal de $G(\varepsilon)$ que nous désignerons par la notation abrégée

$$G_a(\varepsilon) = \langle a|G(\varepsilon)|a\rangle.$$

D'après (14), $G_a(\varepsilon)$ est une somme de termes de la forme

$$G_a(\varepsilon) = \sum \frac{1}{\varepsilon-\varepsilon_a}\vartheta_{ab}\frac{1}{\varepsilon-\varepsilon_b}\vartheta_{bc}\frac{1}{\varepsilon-\varepsilon_c}\ldots\vartheta_{za}\frac{1}{\varepsilon-\varepsilon_a}. \tag{16}$$

Les valeurs propres de H_0, $\varepsilon_a, \varepsilon_b, \varepsilon_c, \ldots$ ne sont pas forcément toutes distinctes. Nous désignerons par $\varepsilon_a, \varepsilon_1, \varepsilon_2, \ldots \varepsilon_q$ celles qui sont effectivement distinctes. D'autre part, dans chaque terme, tout élément de matrice $\vartheta_{ab}, \vartheta_{bc}$ etc. . . . doit figurer un nombre pair de fois, sinon la valeur moyenne serait nulle.

Il sera commode de représenter chaque terme (16) par un diagramme Γ constitué de $q+1$ *points* correspondant aux valeurs propres $\varepsilon_a, \varepsilon_1, \ldots \varepsilon_q$ joints par k *traits* correspondant aux éléments de matrice $\vartheta_{ab}, \vartheta_{bc}, \ldots \vartheta_{za}$. A chaque terme est de plus associé un *mode de parcours* de l'ensemble du diagramme avec départ et arrivée au *point origine* a. Ce mode de parcours décrit *l'ordre* dans lequel se trouvent les facteurs constituant le terme.

Tout diagramme doit être connexe et constitué de traits doubles (ou plus généralement de multiplicité paire). La fig. 2 donne quelques exemples de diagrammes de degré $k = 10$ en ϑ. Le point origine a a été représenté par un petit cercle.

Il reste à faire la moyenne sur les valeurs des éléments de matrice ϑ_{ab} et sur les positions des niveaux $\varepsilon_1, \varepsilon_2, \ldots \varepsilon_q$. Le résultat s'écrit

$$G_a(\varepsilon) = \sum_\Gamma \mathscr{P}_\Gamma \int_{-\infty}^{+\infty} \frac{d\varepsilon_1\, d\varepsilon_2 \ldots d\varepsilon_q}{D_1 D_2 \ldots D_q} \frac{\Pi\vartheta^{(2p)}(\varepsilon_a, \varepsilon_b)}{(\varepsilon-\varepsilon_a)^{\nu_a+1}(\varepsilon-\varepsilon_1)^{\nu_1} \ldots (\varepsilon-\varepsilon_q)^{\nu_q}} \quad (17)$$

Ici nous avons désigné par $2\nu_a, 2\nu_1, \ldots 2\nu_q$ le nombre de traits aboutissant aux points a, 1, 2, ... q du diagramme. Le produit $\Pi\vartheta^{(2p)}$ désigne la valeur moyenne du produit des éléments de matrice $\vartheta_{ab} \ldots$. Nous avons écrit $D_1, D_2 \ldots$ pour $D(\varepsilon_1), D(\varepsilon_2) \ldots$.

La quantité $\mathscr{P}_\Gamma$ ou *poids* du diagramme Γ est le nombre d'éléments de matrice du produit (16) ayant le même diagramme. La sommation $\sum_\Gamma$

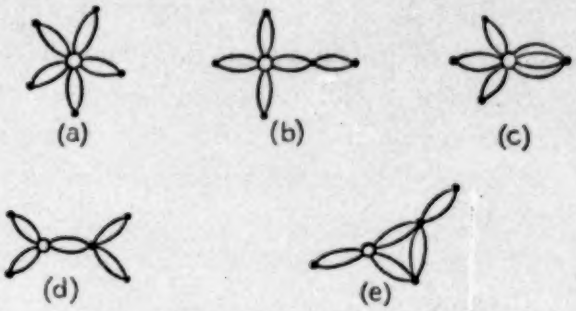

Fig. 2. Exemples de diagrammes de degré $k = 10$.

dans (17) porte alors seulement sur les diagrammes topologiquement différents. Les différents éléments du produit (16) ayant le même diagramme ne diffèrent que par l'ordre des facteurs. Le poids $\mathscr{P}_\Gamma$ est donc égal au nombre de façons dont il est possible de parcourir Γ en partant de l'origine et en y retournant. Deux façons de parcourir Γ qui ne diffèrent que par une permutation des points 1, 2, ... ne doivent pas être considérées comme distinctes. Ainsi les poids des diagrammes des types (a) (b) et (c) de la figure 2 sont

$$\mathscr{P}_a = 1, \qquad \mathscr{P}_b = q-1, \qquad \mathscr{P}_c = q(q+1)/2. \quad (18)$$

Notons enfin la relation

$$\nu_a+\nu_1+\nu_2+ \ldots +\nu_q = k \quad (19)$$

qui s'obtient en comptant les extrêmités de traits sur le diagramme soit sommet par sommet soit trait par trait.

3. Classification des Termes

La méthode de calcul de $\bar{G}_a(\varepsilon)$ que nous allons utiliser repose sur une classification des termes du développement (17) d'après leur dépendance en $\mathscr{E}$. Nous allons montrer que chaque terme est proportionnel à une puissance positive ou nulle de $1/\mathscr{E}$. En conservant uniquement les termes pour lesquels cette puissance est nulle, nous obtiendrons la valeur limite de $f(\varepsilon_a, \varepsilon_s)$ lorsque $\mathscr{E} \to \infty$, tous les autres paramètres du problème restant

constants. En prenant ensuite les termes en $1/\mathscr{E}$, $(1/\mathscr{E})^2$, etc. . . . il sera possible de déterminer des corrections à la première approximation de $f(\varepsilon_a, \varepsilon_a)$ et de fixer la valeur au-delà de laquelle $\mathscr{E}$ peut être considéré comme étant effectivement très grand.

Pour mettre en évidence la dépendence en $\mathscr{E}$ des termes de (16) nous allons simplifier les données du problème en posant

$$\begin{aligned} \vartheta^{(2)}(\varepsilon_a, \varepsilon_b) &= \vartheta^2 v^{(2)}\left(\frac{\varepsilon_a - \varepsilon_b}{\mathscr{E}}\right), \qquad v^{(2)}(0) = 1; \\ \vartheta^{(4)}(\varepsilon_a, \varepsilon_b) &= \vartheta^4 v^{(4)}\left(\frac{\varepsilon_a - \varepsilon_b}{\mathscr{E}}\right); \qquad \text{etc.} \ldots . \end{aligned} \tag{20}$$

Ici ϑ est une énergie qui fixe l'ordre de grandeur des éléments de matrice ϑ_{ab} pour $|\varepsilon_a - \varepsilon_b| \ll \mathscr{E}$. Nous supposerons que les fonctions $v^{(2p)}$ sont de l'ordre de l'unité lorsque l'argument est inférieur à 1 en valeur absolue, et pratiquement nulles lorsque l'argument est très supérieur à 1.

En introduisant les variables sans dimension

$$x = \frac{\varepsilon}{\mathscr{E}}, \qquad x_a = \frac{\varepsilon_a}{\mathscr{E}}, \qquad x_1 = \frac{\varepsilon_1}{\mathscr{E}}, \qquad \text{etc.} \ldots .$$

le développement (17) prend la forme

$$\bar{G}_a(\varepsilon) = \sum \frac{\vartheta^k}{D^q (\varepsilon - \varepsilon_a)^{\nu_a + 1} \mathscr{E}^{k-q-\nu_a}} I(x), \tag{21}$$

où $I(x)$ désigne l'intégrale sans dimension

$$I(x) = \int_{-\infty}^{+\infty} \mathrm{d}x_1 \ldots \mathrm{d}x_q \, \frac{\Pi v^{(2p)}}{(x - x_1)^{\nu_1} \ldots (x - x_q)^{\nu_q}}. \tag{22}$$

Dans le calcul de l'exposant de $\mathscr{E}$ on a tenu compte de la relation (19).

Sans chercher à faire ici une évaluation de I, nous noterons la présence du facteur

$$(1/\mathscr{E})^{k-q-\nu_a}.$$

Lorsque $\mathscr{E}$ est très grand (on précisera plus loin par rapport à quelles quantités) les termes dominants sont ceux pour lesquels l'exposant $k-q-\nu_a$ est aussi petit que possible. On a toujours quel que soit le diagramme

$$k - q - \nu_a \geqq 0$$

(en effet, dans la relation (19), les nombres $\nu_1, \nu_2, \ldots \nu_q$ sont supérieurs ou égaux à 1.) Les seuls diagrammes pour lesquels $k-q-\nu_a = 0$ sont les „étoiles simples" du type (a) (fig. 2). Les seuls diagrammes pour lesquels $k-q-\nu_a = 1$ sont les „étoiles à une branche aberrante" des types (b) et (c) etc. . . . . En prenant successivement les termes contenant des puissances de $(1/\mathscr{E})$ de plus en plus élevées, nous obtiendrons le développement

$$\bar{G}_a(\varepsilon) = \bar{G}_a^{(0)}(\varepsilon)+\bar{G}_a^{(1)}(\varepsilon)+\bar{G}_a^{(2)}(\varepsilon) + \ldots; \tag{23}$$

où le terme $G_a^{(k)}(\varepsilon)$ est proportionnel à $(1/\mathscr{E})^k$. A (23) correspond le développement

$$f = f^{(0)}+f^{(1)}+f^{(2)}+ \ldots \tag{24}$$

de $f(\varepsilon_a, \varepsilon_s)$ où

$$\frac{f^{(k)}(\varepsilon_a, \varepsilon_s)}{\mathscr{D}(\varepsilon_s)} = \frac{1}{2\pi i}[\bar{G}_a^{(k)}(\varepsilon_s - i\delta) - \bar{G}_a^{(k)}(\varepsilon_s + i\delta)]. \tag{25}$$

Nous allons dans les paragraphes suivants calculer explicitement $f^{(0)}$ et $f^{(1)}$.

4. Calcul de f pour une Portée Infinie

4.1. FORME DE LA FONCTION

Nous allons ici calculer la limite de $f(\varepsilon_a, \varepsilon_s)$ pour $\mathscr{E} \to \infty$. Seuls subsistent dans le développement (16) les termes pour lesquels $k-q-\nu_a = 0$, c'est-à-dire dont le diagramme est une „étoile" (fig. 2, a). D'après (16) on a

$$\bar{G}_a^{(0)}(\varepsilon) = \sum_{q=0}^{\infty} \int_{-\infty}^{+\infty} \frac{d\varepsilon_1 d\varepsilon_2 \ldots d\varepsilon_q}{D_1 D_2 \ldots D_q} \frac{\vartheta^{(2)}(\varepsilon_a, \varepsilon_1)\vartheta^{(2)}(\varepsilon_{a_1}, \varepsilon_2) \ldots \vartheta^{(2)}(\varepsilon_{a_1}, \varepsilon_q)}{(\varepsilon-\varepsilon_a)^{q+1}(\varepsilon-\varepsilon_1)(\varepsilon-\varepsilon_2) \ldots (\varepsilon-\varepsilon_q)} \tag{26}$$

car le poids de chaque diagramme est égal à 1 et $\nu_a = q = k/2$. En posant

$$\varphi(\varepsilon) = \int_{-\infty}^{+\infty} \frac{d\varepsilon_1}{D_1} \frac{\vartheta^{(2)}(\varepsilon_a, \varepsilon_1)}{\varepsilon-\varepsilon_1} \tag{27}$$

on peut écrire †

$$\begin{aligned} \bar{G}_a^{(0)}(\varepsilon) &= \sum_{q=0}^{\infty} \frac{1}{\varepsilon-\varepsilon_a} \left[\frac{\varphi(\varepsilon)}{\varepsilon-\varepsilon_a}\right]^q \\ &= \frac{1}{\varepsilon-\varepsilon_a-\varphi(\varepsilon)}. \end{aligned} \tag{28}$$

La fonction $\varphi(\varepsilon)$ et par conséquent aussi $G_a^{(0)}(\varepsilon)$ est analytique dans les deux demi-plans délimités par l'axe réel. On montre facilement à partir de l'expression (27) (en supposant que $\vartheta^{(2)}$ est une fonction continue de ε_1) que $\varphi(\varepsilon)$ tend vers deux limites distinctes suivant que ε approche l'axe réel dans le demi-plan inférieur ou le demi-plan supérieur. Pour δ infiniment petit positif et ε réel, on trouve que

$$\begin{aligned} \varphi(\varepsilon+i\delta) &= \Delta(\varepsilon) - \frac{i\pi}{D(\varepsilon)} \vartheta^{(2)}(\varepsilon_a, \varepsilon), \\ \varphi(\varepsilon-i\delta) &= \Delta(\varepsilon) + \frac{i\pi}{D(\varepsilon)} \vartheta^{(2)}(\varepsilon_a, \varepsilon), \end{aligned} \tag{29}$$

† La série n'est convergente que si $|\varepsilon-\varepsilon_a|$ est assez grand. L'expression finale est par contre analytique partout sauf sur l'axe réel. Elle constitue par conséquent le prolongement analytique de la série là où celle-ci n'est pas convergente.

où $\Delta(\varepsilon)$ est défini par la valeur principale de l'intégrale

$$\Delta(\varepsilon) = \text{V.P.} \int_{-\infty}^{+\infty} \frac{d\varepsilon_1}{D_1} \frac{\vartheta^{(2)}(\varepsilon_a, \varepsilon_1)}{\varepsilon - \varepsilon_1}. \tag{30}$$

Pour obtenir $f^{(0)}(\varepsilon_a, \varepsilon_s)$, il suffit d'appliquer à $\bar{G}_a^{(0)}$ la formule (25). En utilisant (28) et (29) il vient

$$\frac{f^{(0)}(\varepsilon_a, \varepsilon_s)}{\mathscr{D}(\varepsilon_s)} = \frac{\vartheta^{(2)}(\varepsilon_a, \varepsilon_s)/D(\varepsilon_s)}{[\varepsilon_s - \varepsilon_a - \Delta(\varepsilon_s)]^2 + [\pi\vartheta^{(2)}(\varepsilon_a, \varepsilon_s)/D(\varepsilon_s)]^2}. \tag{31}$$

Si lorsque ε_s varie dans un intervalle de l'ordre de

$$\boxed{V = \pi \frac{\vartheta^{(2)}(\varepsilon_a, \varepsilon_a)}{D(\varepsilon_a)}} \tag{32}$$

entourant ε_a, les fonctions $\vartheta^{(2)}(\varepsilon_a, \varepsilon_s)$, $\Delta(\varepsilon_s)$ et $D(\varepsilon_s)$ varient peu, on peut les remplacer par leurs valeurs prises pour $\varepsilon_s = \varepsilon_a$. On obtient alors la forme habituelle

$$\frac{f^{(0)}(\varepsilon_a, \varepsilon_s)}{\mathscr{D}(\varepsilon_s)} = \frac{1}{\pi} \frac{V}{(\varepsilon_s - \varepsilon_a - \Delta)^2 + V^2}. \tag{33}$$

4.2. VALEUR DE V

La relation † (32) est intéressante car elle donne la valeur de V c'est-à-dire de la partie imaginaire du potentiel complexe en fonction de l'interaction ϑ. On notera en particulier que V n'est pas lié directement au second moment de la fonction donné par les règles de somme [7])

$$\begin{aligned} M_2 &= \sum_s (\varepsilon_s - \varepsilon_a)^2 |\langle a|s\rangle|^2 \\ &= \langle a|\vartheta^2|a\rangle = \int \frac{d\varepsilon_b}{D_b} \vartheta^{(2)}(\varepsilon_a, \varepsilon_b). \end{aligned} \tag{34}$$

Pour simplifier la comparaison, admettons que D est approximativement constant ainsi que $\vartheta^{(2)}(\varepsilon_a, \varepsilon_b)$ lorsque $|\varepsilon_a - \varepsilon_b| < \mathscr{E}$, et que $\vartheta^{(2)}(\varepsilon_a, \varepsilon_b) \approx 0$ lorsque $|\varepsilon_a - \varepsilon_b| > \mathscr{E}$. On a alors

$$M_2 \approx 2\vartheta^{(2)}\mathscr{E}/D$$

et

$$\frac{V}{\sqrt{M_2}} \approx \sqrt{\frac{\pi}{2}\frac{V}{\mathscr{E}}}.$$

Dans l'approximation de la „longue portée", $\mathscr{E} \gg V$ et par conséquent

$$V \ll \sqrt{M_2}.$$

Il en résulte que dans ces conditions, le calcul de M_2 ne donne aucun ren-

† Une relation très analogue a été obtenue par K. A. Brueckner, R. Eden et N. Francis [6]).

seignement sur la valeur de V. D'une manière générale, les moments sont des paramètres „globaux" caractérisant l'ensemble de la fonction $f(\varepsilon_a, \varepsilon_s)$ alors que les paramètres „centraux" V et Δ dépendent seulement des valeurs des éléments de matrice ϑ_{ab} pour $\varepsilon_b \approx \varepsilon_a$.

On notera que l'expression approchée (33) donne un second moment M_2 infini alors que la valeur plus exacte (31) conduit à une valeur finie parce que $\vartheta^{(2)}(\varepsilon_a, \varepsilon_s)$ tend vers zéro lorsque $|\varepsilon_s - \varepsilon_a|$ devient supérieur à $\mathscr{E}$. On peut montrer (voir appendice) que le second moment de (31) est effectivement égal à la valeur (34) calculée rigoureusement.

5. Corrections en $1/\mathscr{E}$

Les corrections en $1/\mathscr{E}$ proviennent des diagrammes des types (b) et (c) de la figure 2. Leur contribution s'écrit

$$\bar{G}_0^{(1)}(\varepsilon) = \sum_{q=2}^{\infty} (q-1) \int_{-\infty}^{+\infty} \frac{d\varepsilon_1 \dots d\varepsilon_q}{D_1 \dots D_q} \frac{\vartheta^{(2)}(\varepsilon_a, \varepsilon_1) \dots \vartheta^{(2)}(\varepsilon_a, \varepsilon_{q-1}) \vartheta^{(2)}(\varepsilon_{q-1}, \varepsilon_q)}{(\varepsilon - \varepsilon_a)^q (\varepsilon - \varepsilon_1) \dots (\varepsilon - \varepsilon_{q-2}) (\varepsilon - \varepsilon_{q-1})^2 (\varepsilon - \varepsilon_q)}$$
$$+ \sum_{q=1}^{\infty} \frac{q(q+1)}{2} \int_{-\infty}^{+\infty} \frac{d\varepsilon_1 \dots d\varepsilon_q}{D_1 \dots D_q} \frac{\vartheta^{(2)}(\varepsilon_a, \varepsilon_1) \dots \vartheta^{(2)}(\varepsilon_a, \varepsilon_{q-1}) \vartheta^{(4)}(\varepsilon_a, \varepsilon_q)}{(\varepsilon - \varepsilon_a)^{q+2} (\varepsilon - \varepsilon_1) \dots (\varepsilon - \varepsilon_{q-1}) (\varepsilon - \varepsilon_q)^2},$$

où la première ligne correspond aux types (b) et la deuxième ligne aux types (c). Rappelons que le poids des diagrammes (b) est égal à $q-1$ et que $\nu_a = q-1$ alors que le poids des diagrammes (c) est égal à $q(q+1)/2$ et que $\nu_a = q+1$.

En posant

$$\psi(\varepsilon) = \int_{-\infty}^{+\infty} \frac{d\varepsilon_{q-1}\, d\varepsilon_q}{D_{q-1} D_q} \frac{\vartheta^{(2)}(\varepsilon_a, \varepsilon_{q-1}) \vartheta^{(2)}(\varepsilon_{q-1}, \varepsilon_q)}{(\varepsilon - \varepsilon_{q-1})^2 (\varepsilon - \varepsilon_q)},$$
$$\chi(\varepsilon) = \int_{-\infty}^{+\infty} \frac{d\varepsilon_q}{D_q} \frac{\vartheta^{(4)}(\varepsilon_a, \varepsilon_q)}{(\varepsilon - \varepsilon_q)^2}; \tag{35}$$

on peut écrire

$$\bar{G}_0^{(1)}(\varepsilon) = \frac{\psi(\varepsilon)}{(\varepsilon - \varepsilon_a)^2} \sum_{q=2}^{\infty} (q-1) \left[\frac{\varphi(\varepsilon)}{\varepsilon - \varepsilon_a}\right]^{q-2}$$
$$+ \frac{\chi(\varepsilon)}{(\varepsilon - \varepsilon_a)^3} \sum_{q=1}^{\infty} \frac{q(q+1)}{2} \left[\frac{\varphi(\varepsilon)}{\varepsilon - \varepsilon_a}\right]^{q-1}.$$

La sommation des séries est immédiate et on obtient

$$\bar{G}_a^{(1)}(\varepsilon) = \frac{\psi(\varepsilon)}{[\varepsilon - \varepsilon_a - \varphi(\varepsilon)]^2} + \frac{\chi(\varepsilon)}{[\varepsilon - \varepsilon_a - \varphi(\varepsilon)]^3}. \tag{36}$$

Pour obtenir explicitement $\psi(\varepsilon)$ et $\chi(\varepsilon)$ nous prendrons une forme particulière pour $\vartheta^{(2)}$ et $\vartheta^{(4)}$. La forme

$$\vartheta^{(2)}(\varepsilon_a, \varepsilon_s) = \frac{\vartheta^{(2)}(0)}{1+(\varepsilon_a-\varepsilon_s)^2/\mathscr{E}^2},$$
$$\vartheta^{(4)}(\varepsilon_a, \varepsilon_s) = \frac{\vartheta^{(4)}(0)}{1+(\varepsilon_a-\varepsilon_s)^2/\mathscr{E}^2}, \tag{37}$$

rend le calcul des intégrales particulièrement simple. On trouve, en supposant naturellement D constant,

$$\left.\begin{aligned} \varphi(\varepsilon) &= \frac{V}{x+i}, \\ \psi(\varepsilon) &= \frac{1}{\mathscr{E}}\frac{V^2}{(x+i)^2(x+2i)}, \\ \chi(\varepsilon) &= \frac{\pi\vartheta^{(4)}(0)}{\mathscr{E}D}\frac{1}{(x+i)^2}; \end{aligned}\right\} \text{ pour } \operatorname{Im}\varepsilon > 0 \tag{38}$$

où nous avons posé

$$x = \frac{\varepsilon-\varepsilon_a}{\mathscr{E}}, \qquad V = \pi\frac{\vartheta^{(2)}(0)}{D}.$$

Si la partie imaginaire de ε est négative il faut dans les formules (38) changer i en $-i$. Pour écrire simplement la correction $\bar{G}_a^{(1)}$ nous supposerons que

$$|x| \ll 1, \qquad \vartheta^{(4)}(0) \approx [\vartheta^{(2)}(0)]^2.$$

On peut alors mettre $\bar{G}_a^{(1)}$ sous la forme

$$\bar{G}_a^{(1)} = \bar{G}_a^{(0)}\left[\frac{V}{\mathscr{E}}\frac{iV}{\varepsilon-\varepsilon_a+iV} - \frac{1}{\pi}\frac{D}{\mathscr{E}}\frac{V^2}{(\varepsilon-\varepsilon_a+iV)^2}\right]; \tag{39}$$

d'où on tire sans peine la correction $f^{(1)}(\varepsilon_a, \varepsilon_s)$ à l'aide de la formule (25).

On notera sur l'expression (39) que la correction due aux termes du type (b) (fig. 2) est $V/\mathscr{E}$ et celle qui provient des termes du type (c) en $D/\mathscr{E}$. Il faut donc, pour que la méthode d'approximation ait un sens, que

$$V \ll \mathscr{E}, \qquad D \ll \mathscr{E}. \tag{40}$$

6. Les Termes d'Ordre Supérieur; Convergence du Développement

Les considérations du paragraphe précédent peuvent être étendues aux ordres supérieurs.

Les termes contenant une puissance donnée de $1/\mathscr{E}$ proviennent d'un nombre infini de diagrammes. Ceux-ci, toutefois, se déduisent, comme dans le cas des termes en $1/\mathscr{E}$, d'un nombre fini de diagrammes par l'addition de nombres quelconques de branches d'étoile simples. Soit Γ_0 un diagramme ne contenant aucune branche d'étoile simple, $\mathscr{P}_0$ son poids, $2\nu_a^0$ le nombre de traits de Γ_0 aboutissant en a et

$$\xi_0(\varepsilon) = \int \frac{d\varepsilon_1\, d\varepsilon_2 \dots}{D_1 D_2 \dots} \frac{\Pi \vartheta^{(2p)}}{\Pi(\varepsilon - \varepsilon_i)^{\nu_i}} \tag{41}$$

l'intégrale semblable à $\psi(\varepsilon)$ et $\chi(\varepsilon)$ relative à Γ_0. Le développement de $\bar{G}_a(\varepsilon)$ s'écrit alors

$$\begin{aligned} \bar{G}_a(\varepsilon) &= \sum_{\Gamma_0} \sum_{n=0}^{\infty} \mathscr{P}_0 \frac{(n+\nu_a^0)!}{n!\quad \nu_a^0!} \left[\frac{\varphi(\varepsilon)}{\varepsilon - \varepsilon_a}\right]^n \frac{\xi_0(\varepsilon)}{(\varepsilon-\varepsilon_a)^{\nu_a^0+1}} \\ &= \sum_{\Gamma_0} \frac{\mathscr{P}_0 \xi_0(\varepsilon)}{[\varepsilon - \varepsilon_a - \varphi(\varepsilon)]^{\nu_a^0+1}}, \end{aligned} \tag{42}$$

car on vérifie sans peine que le poids du diagramme résultant de l'addition de n branches d'étoile simples à Γ_0 est

$$\mathscr{P}_0 \frac{(n+\nu_a^0)!}{n!\quad \nu_a^0!}. \tag{43}$$

Dans (42) la sommation est étendue à tous les diagrammes Γ_0 ne contenant aucune branche d'étoile simple. Dans ce développement, le coefficient de chaque puissance de $1/\mathscr{E}$ est une somme d'un nombre fini de termes. Les intégrales $\xi_0(\varepsilon)$ sont toujours des fonctions analytiques dans les demi-plans inférieur et supérieur. Les différents termes du développement de $G_a(\varepsilon)$ possèdent donc aussi ces propriétés. Il en résulte que les termes du développement de $f(\varepsilon_a, \varepsilon_s)$ en puissances de $1/\mathscr{E}$ sont tous bien définis.

Nous allons montrer maintenant qu'on peut extraire de ce développement un développement partiel *divergent*. Considérons en effet la série partielle extraite de (42) dont les termes ont pour diagrammes

$$\Gamma_0, \qquad 2\Gamma_0, \qquad \dots p\Gamma_0, \qquad \dots$$

où Γ_0 est un diagramme quelconque. Le poids du diagramme $p\Gamma_0$ est égal à †

$$\mathscr{P}_0{}^p \frac{(p\nu_a^0)!}{p![\nu_a^0!]^p} \tag{44}$$

et la série s'écrit

$$\frac{1}{\varepsilon - \varepsilon_a - \varphi(\varepsilon)} \sum_{p=1}^{\infty} \frac{(p\nu_a^0)!}{p!} \left\{\frac{\mathscr{P}_0 \xi_0(\varepsilon)}{\nu_a^0![\varepsilon - \varepsilon_a - \varphi(\varepsilon)]^{\nu_a^0}}\right\}^p. \tag{45}$$

La présence du facteur $(p\nu_a^0)!$ rend cette série divergente si $\nu_a^0 \geqq 2$.

Pour analyser le sens de cette divergence nous allons estimer l'ordre de grandeur des termes de la série comme au paragraphe III. En désignant par q le nombre des points autres que a et par k le nombre des traits du diagramme Γ_0, on a

$$\frac{\xi_0(\varepsilon)}{[\varepsilon - \varepsilon_a - \varphi(\varepsilon)]^{\nu_a^0}} \approx \frac{\vartheta^k}{V^{\nu_a^0} D^q \mathscr{E}^{k-q-\nu_a^0}}$$

† Cette expression n'est exacte que si le diagramme Γ_0 est „indécomposable" c'est-à-dire s'il ne peut être considéré comme la somme de deux diagrammes indépendants sans liaison l'un avec l'autre en dehors des liens avec le point origine a.

en remplaçant $|\varepsilon-\varepsilon_a-\varphi|$ par V. En utilisant ensuite la relation $\vartheta^2 \approx VD$ il vient

$$\frac{\xi_0(\varepsilon)}{[\varepsilon-\varepsilon_0-\varphi(\varepsilon)]^{\nu_a^0}} \approx \left(\frac{D}{\mathscr{E}}\right)^{\frac{1}{2}k-q} \left(\frac{V}{\mathscr{E}}\right)^{\frac{1}{2}k-\nu_a^0}. \tag{46}$$

Si on suppose le diagramme Γ_0 indécomposable (au sens de la note de la p. 148), on a

$$\tfrac{1}{2}k-q \geqq \nu_a^0-1. \tag{47}$$

En effet si on supprime de Γ_0 les $2\nu_a^0$ traits qui le lient à a, les $k-2\nu_a^0$ traits restant doivent suffire à construire un diagramme connexe de q points. Les traits étant au moins doubles, il en faut pour cela au moins $2(q-1)$; ce qui entraîne l'inégalité (47). Nous pouvons donc écrire

$$\frac{\xi_0(\varepsilon)}{[\varepsilon-\varepsilon_a-\varphi(\varepsilon)]^{\nu_a^0}} \approx \left(\frac{D}{\mathscr{E}}\right)^{\nu_a^0-1} \eta; \tag{48}$$

où η est un nombre inférieur à l'unité. Le rapport du $p^{\text{ème}}$ terme de la série (45) au $(p-1)^{\text{ème}}$ est (en supposant $p \gg \nu_a^0$) de l'ordre de

$$\left(\frac{pD}{\mathscr{E}}\right)^{\nu_a^0-1} \eta.$$

On voit ainsi que les termes de la série vont en diminuant jusqu'à une valeur de p de l'ordre de $\mathscr{E}/D$ et croissent ensuite indéfiniment lorsqu'on dépasse cette valeur. Ceci rend la série divergente. Le nombre $\mathscr{E}/D$ est le nombre moyen de niveaux de H_0 existant dans un intervalle $\mathscr{E}$. D'autre part, pour que les intégrales $\xi(\varepsilon)$ ne soient pas nulles il faut que les $p\nu_a^0$ points du diagramme $p\Gamma_0$ liés directement à l'origine a soient à une distance de a au plus de l'ordre de $\mathscr{E}$. On voit donc que la croissance des termes se produit pour des valeurs de p correspondant à des diagrammes ayant des nombres de points si grands qu'il est nécessaire que la densité des niveaux de H_0 dans un intervalle de l'ordre de $\mathscr{E}$ de part et d'autre de $\mathscr{E}_a$ soit supérieure à la densité moyenne $1/D$. La divergence de la série envisagée est ainsi rattachée aux fluctuations de densité des niveaux de H_0 rendues possibles par l'hypothèse que ces niveaux sont distribués au hasard indépendamment les uns des autres. Nous avons déjà signalé à la fin du paragraphe 2 que cette hypothèse entraînait que ϑ n'était pas un opérateur borné. La divergence du développement en $1/\mathscr{E}$ est une conséquence de ce fait.

Pour éviter ces difficultés on peut imposer une séparation minimum D_m aux niveaux de H_0. Dans ce cas la série (44) a un nombre de termes fini inférieur à $2\mathscr{E}/D_m$ et la divergence disparaît. Malheureusement cette hypothèse qui rend le développement convergent à coup sûr empêche la factorisation des intégrales même dans le cas des „étoiles simples" et rend le calcul des différents termes du développement en puissances de $1/\mathscr{E}$

beaucoup plus difficile. Pour les *premiers termes* de ce développement, les diagrammes font intervenir des nombres petits de niveaux de H_0. La probabilité que ces niveaux soient très proches est donc faible et l'introduction d'une distance minimum entre les niveaux modifiera peu la valeur des intégrales. Les termes lointains qui rendent la série divergente sont au contraire supprimés par l'introduction d'une distance minimum. Ces remarques, sans constituer une démonstration rigoureuse suggèrent que le développement en puissances de $1/\mathscr{E}$ doit en fait être considéré comme un *développement asymptotique.*

Appendice

RELATION AVEC LE CALCUL DES MOMENTS

Les moments de la fonction $f(\varepsilon_a, \varepsilon_s)$,

$$M_n = \sum_s (\varepsilon_s - \varepsilon_a)^n |\langle a|s\rangle|^2 = \int_{-\infty}^{+\infty} \frac{d\varepsilon_s}{\mathscr{D}_s} (\varepsilon_s - \varepsilon_a)^n f(\varepsilon_a, \varepsilon_s) \qquad (A,1)$$

peuvent être calculés directement à partir de H. On a en effet

$$M_n = \langle a|(\sum_s |s\rangle(\varepsilon_s - \varepsilon_a)^n \langle s|)|a\rangle = \langle a|(H-\varepsilon_a)^n|a\rangle. \qquad (A,2)$$

Les hypothèses statistiques faites sur H_0 et ϑ permettent de calculer les valeurs probables des moments successifs. On trouve ainsi:

$$\begin{aligned}
M_1 &= \overline{\langle a|\vartheta|a\rangle} = \vartheta^{(1)}(\varepsilon_a, \varepsilon_a) = 0;\\
M_2 &= \overline{\langle a|\vartheta^2|a\rangle} = \int_{-\infty}^{+\infty} \frac{d\varepsilon_b}{D_b} \vartheta^{(2)}(\varepsilon_a, \varepsilon_b);\\
M_3 &= \overline{\langle a|\vartheta(H_0-\varepsilon_a)\vartheta|a\rangle} + \overline{\langle a|\vartheta^3|a\rangle}\\
&= \int_{-\infty}^{+\infty} \frac{d\varepsilon_b}{D_b} (\varepsilon_b - \varepsilon_a)\vartheta^{(2)}(\varepsilon_a, \varepsilon_b); \qquad (A,3)\\
M^4 &= \overline{\langle a|\vartheta(H_0-\varepsilon_a)^2\vartheta|a\rangle} + \overline{\langle a|\vartheta^4|a\rangle}\\
&= \int_{-\infty}^{+\infty} \frac{d\varepsilon_b}{D_b} (\varepsilon_b - \varepsilon_a)^2\vartheta^{(2)}(\varepsilon_a, \varepsilon_b) + \left[\int_{-\infty}^{+\infty} \frac{d\varepsilon_b}{D_b} \vartheta^{(2)}(\varepsilon_a, \varepsilon_b)\right]^2\\
&\quad + \int_{-\infty}^{+\infty} \frac{d\varepsilon_b\, d\varepsilon_c}{D_b D_c} \vartheta^{(2)}(\varepsilon_a, \varepsilon_b)\vartheta^{(2)}(\varepsilon_b, \varepsilon_c) + \int_{-\infty}^{+\infty} \frac{d\varepsilon_b}{D_b} \vartheta^{(4)}(\varepsilon_a, \varepsilon_b); \quad \text{etc.} \ldots ..
\end{aligned}$$

Il est intéressant de comparer ces valeurs des moments qui sont exactes pour le modèle choisi avec les moments des fonctions approchées $f(\varepsilon_a, \varepsilon_s)$ que nous avons obtenues.

Pour cela, nous allons calculer les premiers moments de la fonction (31). Les équations (11) et (13) permettent d'écrire

$$M_n^{(0)} = \left[\left(\frac{1}{i}\frac{\mathrm{d}}{\mathrm{d}t}\right)^n F^{(0)}(t)\right]_{t=0} = \frac{1}{2\pi i}\int_C (\varepsilon-\varepsilon_a)^n G_a^{(0)}(\varepsilon)\mathrm{d}\varepsilon$$
$$= \frac{1}{2\pi i}\int_C \frac{(\varepsilon-\varepsilon_a)^n \mathrm{d}\varepsilon}{\varepsilon-\varepsilon_a-\varphi(\varepsilon)}. \qquad \text{(A,4)}$$

Si on admet que $\vartheta^{(2)}(\varepsilon_a, \varepsilon_b)$ tombe rigoureusement à zéro si $|\varepsilon_a-\varepsilon_b| > \mathscr{E}'$ (où $\mathscr{E}'$ peut éventuellement être très supérieur à $\mathscr{E}$) on voit d'après la définition (27) de $\varphi(\varepsilon)$ que cette fonction est partout analytique en dehors du segment $(\varepsilon_a-\mathscr{E}', \varepsilon_a+\mathscr{E}')$. Il en est de même de la fonction

$$G_a^{(0)}(\varepsilon) = \frac{1}{\varepsilon-\varepsilon_a-\varphi(\varepsilon)}. \qquad \text{(A,5)}$$

On peut en effet vérifier sur la relation (27) que pour ε complexe, la partie imaginaire de $\varphi(\varepsilon)$ a toujours un signe opposé à celui de la partie imaginaire de ε†. Le dénominateur de (A,5) a donc toujours au moins une partie imaginaire non nulle lorsque ε n'est pas réel. On peut en plus affirmer qu'il existe un nombre $\mathscr{E}''$ tel que (A,5) n'ait pas de pole sur l'axe réel en dehors du segment $(\varepsilon_a-\mathscr{E}'', \varepsilon_a+\mathscr{E}'')$. En effet, puisque $|\varphi(\varepsilon)| \to 0$ lorsque $|\varepsilon-\varepsilon_a| \to \infty$, on peut trouver un nombre $\mathscr{E}'''$ tel que $|\varphi(\varepsilon)|$ reste inférieur à tout nombre fixé à l'avance, $\mathscr{E}$ par exemple, lorsque $|\varepsilon-\varepsilon_a|$ reste supérieur à $\mathscr{E}'''$. Il suffit alors de prendre pour $\mathscr{E}''$ le plus grand des deux nombres $\mathscr{E}'$ et $\mathscr{E}'''$.

En conclusion, la fonction à intégrer dans (A,4) est analytique partout à distance finie dans le plan complexe en dehors d'un certain segment $(\varepsilon_a-\mathscr{E}'', \varepsilon_a+\mathscr{E}'')$ de l'axe réel. Ceci permet sans changer la valeur de l'intégrale de transformer le contour d'intégration C en un cercle centré en ε_a de rayon arbitrairement grand (pourvu qu'il soit supérieur à $\mathscr{E}''$). Or pour $|\varepsilon-\varepsilon_a| \to \infty$ on peut développer $\varphi(\varepsilon)$:

$$\varphi(\varepsilon) = \frac{A_0}{\varepsilon-\varepsilon_a} + \frac{A_1}{(\varepsilon-\varepsilon_a)^2} + \ldots \frac{A_{k-1}}{(\varepsilon-\varepsilon_a)^k} + \ldots; \qquad \text{(A,6)}$$

où d'après (27) les A_k sont les moments de la fonction $\vartheta^{(2)}(\varepsilon_a, \varepsilon_b)/D_b$:

$$A_k = \int_{-\infty}^{+\infty} \frac{\mathrm{d}\varepsilon_b}{D_b} (\varepsilon_b-\varepsilon_a)^k \vartheta^{(2)}(\varepsilon_a, \varepsilon_b). \qquad \text{(A,7)}$$

De (A,6) on tire le développement de (A,5) pour les grandes valeurs de $\varepsilon-\varepsilon_a$:

$$G_a^{(0)}(\varepsilon) = \frac{1}{\varepsilon-\varepsilon_a-\varphi(\varepsilon)} = \frac{1}{\varepsilon-\varepsilon_a} + \frac{A_0}{(\varepsilon-\varepsilon_a)^3} + \frac{A_1}{(\varepsilon-\varepsilon_a)^4} + \frac{A_2+A_0^2}{(\varepsilon-\varepsilon_a)^5} + \ldots$$

Ce développement reporté dans l'intégrale (A,4) où C est un cercle de grand rayon donne immédiatement les valeurs des premiers moments:

† E. P. Wigner [1]) appelle „following functions" les fonctions analytiques ayant cette propriété (les fonctions $R(E)$ par exemple).

$$M_0^{(0)} = 1, \quad M_1^{(0)} = 0, \quad M_2^{(0)} = A_0,$$
$$M_3^{(0)} = A_1, \quad M_4^{(0)} = A_2 + A_0^2, \quad \text{etc.} \ldots . \tag{A,8}$$

Le résultat $M_0 = 1$ montre que la fonction (31) est bien normalisée à l'unité comme l'unitarité de la matrice $\langle a|s\rangle$ l'impose. Il en est de même d'ailleurs de la fonction simplifiée (33). Par contre les moments d'ordre 1, 2 et 3 de la fonction (31) ont exactement les valeurs prévues directement (A,3), alors que la fonction simplifiée (33) a un moment M_1 non nul (sauf si $\Delta = 0$) et des moments d'ordre supérieur divergents.

Le moment d'ordre 4 de (33) est inexact. Calculons alors les moments de la correction $f^{(1)}(\varepsilon_a, \varepsilon_s)$ donnée par (36). La méthode suivie pour les moments de $f^{(0)}(\varepsilon_a, \varepsilon_s)$ s'applique sans changement. Pour les grandes valeurs de $|\varepsilon - \varepsilon_a|$ on a d'après (35) en se limitant au premier terme,

$$\psi(\varepsilon) = \frac{1}{(\varepsilon - \varepsilon_a)^3} \int_{-\infty}^{+\infty} \frac{d\varepsilon_b\, d\varepsilon_c}{D_b D_c}\, \vartheta^{(2)}(\varepsilon_a, \varepsilon_b)\vartheta^{(2)}(\varepsilon_b, \varepsilon_c) + \ldots$$

$$\chi(\varepsilon) = \frac{1}{(\varepsilon - \varepsilon_a)^2} \int_{-\infty}^{+\infty} \frac{d\varepsilon_b}{D_b}\, \vartheta^{(4)}(\varepsilon_a, \varepsilon_b) + \ldots .$$

D'où le développement de $G_a^{(1)}(\varepsilon)$ pour les grandeurs valeurs de $|\varepsilon - \varepsilon_a|$:

$$G_a^{(1)}(\varepsilon) = \frac{1}{(\varepsilon - \varepsilon_a)^5} \left[\int_{-\infty}^{+\infty} \frac{d\varepsilon_b\, d\varepsilon_c}{D_b D_c}\, \vartheta^{(2)}(\varepsilon_a, \varepsilon_b)\vartheta^{(2)}(\varepsilon_b, \varepsilon_c) + \int_{-\infty}^{+\infty} \frac{d\varepsilon_b}{D_b}\, \vartheta^{(4)}(\varepsilon_a, \varepsilon_b) \right] + \ldots$$

En reportant cette expression dans (A,4) on voit que les moments d'ordre 0, 1, 2, 3 de $f^{(1)}(\varepsilon_a, \varepsilon_s)$ sont nuls. Par contre la contribution à M_4 est

$$M_4^{(1)} = \int_{-\infty}^{+\infty} \frac{d\varepsilon_b\, d\varepsilon_c}{D_b D_c}\, \vartheta^{(2)}(\varepsilon_a, \varepsilon_b)\vartheta^{(2)}(\varepsilon_b, \varepsilon_c) + \int_{-\infty}^{+\infty} \frac{d\varepsilon_b}{D_b}\, \vartheta^{(4)}(\varepsilon_a, \varepsilon_b).$$

L'addition de cette correction à la valeur (A,8) donne bien l'expression exacte (A,3) du moment.

Sans poursuivre plus loin ces considérations on voit que la méthode d'approximation décrite ici revient à sélectionner parmi les moments de chaque ordre les termes qui deviennent dominants lorsque $\mathscr{E}$ devient très grand.

Références

1) E. P. Wigner, Ann. Math. **53** (1951) 36; **55** (1952) 7
2) R. G. Thomas, Phys. Rev. **97** (1955) 224; A. M. Lane, R. G. Thomas and E. P. Wigner, Phys. Rev. **98** (1955) 693; C. Bloch, Journ. Phys. Rad. **17** (1956) 510
3) E. P. Wigner and L. Eisenbud, Phys. Rev. **72** (1947) 29; T. Teichmann and E. P. Wigner, Phys. Rev. **87** (1952) 123
4) H. Feshbach, C. Porter and V. Weisskopf, Phys. Rev. **96** (1954) 448
5) E. P. Wigner, Ann. of Math. **62** (1955) 548
6) K. A. Brueckner, R. Eden and N. Francis, Phys Rev. **100** (1955) 891
7) A. M. Lane, R. G. Thomas and E. P. Wigner, Phys. Rev. **98** (1955) 693

Nuclear Physics **3** (1957) 153—156; *North-Holland Publishing Co., Amsterdam*

K-MESON SCATTERING WITH CHANGE OF INTRINSIC PARITY

V. B. BERESTETSKY AND Yu. A. BYCHKOV
USSR Academy of Sciences, Moscow

Received 5 December 1956

Analysis of the experimental data on K-meson decay [1]) leads, with a high degree of probability, to the conclusion that 1) the K-meson spin is zero and 2) K-mesons can exist in states with different intrinsic parities, i.e., positive (θ-mesons) or negative (τ-mesons).

In collisions between K-mesons and nucleons the intrinsic parity of the former may change (transformation of θ-mesons into τ-mesons and vice versa). In order to consider some general properties of this type of process we shall represent the K meson-nucleon wave function ψ as a combination of two spinors ψ_θ and ψ_τ which transform differently on space inversion:

$$\psi = \begin{pmatrix} \psi_\theta \\ \psi_\tau \end{pmatrix}$$

where

$$I\psi_\theta = \psi_\theta; \qquad I\psi_\tau = -\psi_\tau,$$

I being the inversion operator.

In a scattering problem ψ, as usual, has the form

$$\psi = ue^{ikn_0 \cdot r} + F(\mathbf{n})e^{ikr}/r$$

where $\mathbf{n}_0$ and $\mathbf{n}$ are unit direction vectors of the incoming and scattered waves respectively and u and F are the corresponding amplitudes which, similarly to ψ, are bispinor quantities. Amplitude F can be represented in the form

$$F = Ru$$

where R is a two-dimensional matrix (each element of which is a two-dimensional matrix with respect to the spin variables).

If the interactions between θ and τ mesons on the one hand and nucleons on the other are the same, the latter relation will hold for "parity conjugated" amplitudes:

$$u' = C_p u; \qquad F' = C_p F$$

where C_p is the "parity conjugation" operator introduced by Lee and Yang [2]):

$$C_p = \begin{pmatrix} 0 & 1 \\ 1 & 0 \end{pmatrix}.$$

Thus matrix R must satisfy the condition

$$RC_p = C_p R$$

and can be represented in the form

$$R = a + bC_p$$

where a is a scalar and b a pseudoscalar (or, more precisely, the corresponding matrices in spin variables). Amplitude au describes the usual type of scattering (without a change in intrinsic parity) and has the form which is so familiar from spinor wave scattering theory. Our aim is to find the general form of amplitude bu which describes scattering involving a change of intrinsic parity.

For this purpose consider the relation between the incoming and outgoing waves with definite angular momentum and parity values. It can be written in the form

$$\psi^{\text{out}}_{jMg} = S(j, g)\psi^{\text{in}}_{jMg}$$

where j, M and g are respectively the angular momentum quantum numbers, its projection and parity and S is a two-dimensional matrix in the same sense as R. It can be written in the form

$$S(j, g) = \begin{pmatrix} S_{ll} & S_{ll'} \\ S_{l'l} & S_{l'l'} \end{pmatrix}$$

where $g = (-1)^l = (-1)^{l'+1}$; $l = j \pm \frac{1}{2}$ is the θ meson orbital moment and $l' = j \mp \frac{1}{2}$ is the τ meson orbital moment. On the basis of general symmetry properties of the S matrix

$$S_{ll'} = S_{l'l}.$$

Furthermore, since

$$\psi_{jM-g} = C_p \psi_{jMg}$$

invariance of interactions with respect to parity conjugation transformation yields the relationship

$$S(j, -g) = C_p S(j, g) C_p^{-1},$$

that is

$$S(j, -g) = \begin{pmatrix} S_{l'l'} & S_{ll'} \\ S_{l'l} & S_{ll} \end{pmatrix}.$$

It can be seen that the nondiagonal elements $S_{ll'}$ do not depend on the parity of state g.

We can now construct an expression for the scattering amplitude bu. To do this consider the amplitude of the incident wave in the form

$$u = \begin{pmatrix} v \\ 0 \end{pmatrix} \quad (\theta \text{ meson}).$$

Incoming waves of the following form correspond to it:

$$\psi^{\text{in}}_{jM_g} = \begin{pmatrix} c\Omega_{jlM}(\mathbf{n}) \\ 0 \end{pmatrix} e^{-ikr}/r$$

where $g = (-1)^l$; Ω_{jlM} is a spherical spinor, and

$$c = \frac{2\pi i^l}{k} (\Omega^*_{jlM}(\mathbf{n}_0)v).$$

The outgoing waves will have the form

$$\psi^{\text{out}}_{jM_g} = \begin{pmatrix} S_{ll}\ c\Omega_{jlM}(\mathbf{n}) \\ S_{ll'}\ c\Omega_{jl'M}(\mathbf{n}) \end{pmatrix} (-1)^{l+1} e^{ikr}/r$$

and therefore

$$bv = \frac{2\pi}{ik} \sum_{jlM} (\Omega^*_{jlM}(\mathbf{n}_0)v)\Omega_{jl'M}(\mathbf{n})S_{ll'}.$$

By making use of the following transformations [3]):

$$\Omega_{jl'M}(\mathbf{n}) = \boldsymbol{\sigma} \cdot \mathbf{n}\Omega_{jlM}(\mathbf{n})$$

$$\sum_M (\Omega^*_j(\mathbf{n}_0)u)\Omega_{jlM}(\mathbf{n}) = \frac{1}{4\pi}\left(\alpha_{jl} + \frac{\beta_{jl}}{i \sin\vartheta}\right)(\mathbf{n}_0 \wedge \mathbf{n}) \cdot \boldsymbol{\sigma}$$

where

$$\alpha_{jl} = (j+\tfrac{1}{2})P_l(\cos\vartheta)$$

$$\beta_{jl} = \mp P_l^1 \quad \text{for} \quad l = j \mp \tfrac{1}{2}$$

$$\cos\vartheta = \mathbf{n}_0 \cdot \mathbf{n}$$

(P_l, P_l^1 are the respective Legendre polynomials), we obtain

$$\sum_M (\Omega^*_{jlM}(\mathbf{n}_0)v)\Omega_{jlM}(\mathbf{n}) = \boldsymbol{\sigma} \cdot (\mathbf{n}r_{jl} + \mathbf{n}_0 q_{jl})$$

where

$$r_{jl} = \beta_{jl}/\sin\vartheta; \qquad q_{jl} = \alpha_{jl} - \beta_{jl} \operatorname{tg}\vartheta.$$

Application of well-known relations between Legendre polynomials leads to the equality

$$r_{j,j+\frac{1}{2}} + r_{j,j-\frac{1}{2}} = q_{j,j+\frac{1}{2}} + q_{j,j-\frac{1}{2}} = \frac{\mathrm{d}}{\mathrm{d}\cos\vartheta}(P_{j+\frac{1}{2}} - P_{j-\frac{1}{2}}).$$

Inserting all this into the expression for b we finally obtain

$$b = B(\vartheta)\boldsymbol{\sigma} \cdot (\mathbf{n}_0 + \mathbf{n})$$

where

$$B(\vartheta) = \frac{1}{2ik} \sum_j S_{j+\frac{1}{2},\,j-\frac{1}{2}} \frac{\mathrm{d}}{\mathrm{d}\cos\vartheta}(P_{j+\frac{1}{2}} - P_{j-\frac{1}{2}}).$$

For small momenta only the term with $j = \frac{1}{2}$ which corresponds to transitions $s_{\frac{1}{2}} \rightleftarrows p_{\frac{1}{2}}$ can be retained. B is then independent of the angles and the differential cross section for scattering with change in intrinsic parity takes the form

$$|b|^2 = \sigma_0(1+\cos\vartheta)$$

where σ_0 is a constant and, in accord with the general properties of the scattering matrix elements, $\sigma_0 \approx k^2$. Unfortunately, this dependence of the cross section on angle and momenta is in itself insufficient for experimental separation of the process under consideration as the differential cross section for scattering of the usual type involves a similar dependence at small momenta values

$$|a|^2 = c_1+c_2 k^2 \cos\vartheta$$

where c_1 and c_2 are constants (the first term corresponding to a s wave and the second to interference of s and p waves).

It follows from the expression for b that during this type of scattering nucleon polarization does not take place. If, however, the nucleon was polarized prior to scattering, the spin components perpendicular to the vector $\mathbf{n}_0+\mathbf{n}$ would change sign.

The foregoing discussion also pertains to scattering of Σ and Λ particles on nuclei with spin 0, providing the spin of these particles is $\frac{1}{2}$. The same expressions are also valid for the processes

$$K+N \to \Sigma+\pi; \qquad K+N \to \Lambda+\pi,$$

amplitude b in this case referring to the creation of a $\Lambda(\Sigma)$ particle of the same intrinsic parity as that of the incident K-particle (since an odd π meson appears in this case).

The authors express their sincere thanks to I. Pomeranchuk for numerous helpful discussions.

References

1) R. H. Dalitz, Phil. Mag. **44** (1953) 1068; Phys. Rev. **94** (1954) 1046;
E. Fabri, Nuovo Cimento **11** (1954) 479;
R. P. Haddock, Nuovo Cimento **4** (1956) 240;
C. N. Yang, Report at Rochester Conference (1956)
2) T. D. Lee and C. N. Yang, Phys. Rev. **102** (1956) 290
3) See, for example, A. Akhiezer and V. Berestetsky, Quantum Electrodynamics

Nuclear Physics **3** (1957) 157—160; *North-Holland Publishing Co., Amsterdam*

ON INTERFERENCE PHENOMENA IN THE DECAY OF STRANGE PARTICLES

V. B. BERESTETSKY

USSR Academy of Sciences, Moscow

Received 5 December 1956

Lee and Yang [1]) have shown that the hypothesis that K, Λ and Σ particles are parity degenerate doublets [2]) leads to interference phenomena which should be manifest in asymmetry of the angular distribution of the decay products with respect to a plane perpendicular to the direction of motion of the decaying particle. These authors studied the decay of Λ and Σ particles into nucleons and π mesons. We present here some examples of other similar processes.

The cascade decay

$$\Xi^- \to \Lambda^0 + \pi_1^- \to \mathrm{p} + \pi_1^- + \pi_2^-$$

is completely analogous to the decay of a Σ particle created during capture of a K-meson by a nucleon, a process which has been considered by Lee and Yang.

The first step of this cascade corresponds to the expansion of the Ξ particle (or $\Lambda+\pi_1$ system) wave function, Ψ, into wave functions of the Λ particle. We shall assume that the hyperon spin is $\frac{1}{2}$ and for the sake of definiteness, the parity of the Ξ particle will be considered to be positive, that is, to coincide with the nucleon parity. The Λ particle may exist in states of various intrinsic parity which are described by spinors ψ_1 and ψ_2 which transform differently upon space inversion. Let

$$I\,\psi_1 = -\psi_1; \qquad I\,\psi_2 = \psi_2$$

where I is the inversion operator. Then

$$\Psi = f_1\psi_1 + f_2\psi_2 \tag{1}$$

where f_1 is a scalar and f_2 a pseudoscalar. (Negative parity of the π meson has been taken into account here). It is evident that these coefficients have the following form

$$f_1 = a; \qquad f_2 = b\boldsymbol{\sigma}\cdot\mathbf{n} \tag{2}$$

where a and b are constants, $\mathbf{n}$ is the direction vector of the π_1 meson motion and $\boldsymbol{\sigma}$ is the Pauli matrix. f_1 and f_2 contain the wave functions of relative motion of the $\Lambda+\pi_1$ system: f_1 corresponds to the s state and f_2 to the p state.

After decay of the Λ particle ψ_1 and ψ_2 should be considered as wave functions of the $p+\pi_2$ system. Their expansion in terms of the nucleon spin functions should have the form

$$\psi_1 = Au; \qquad \psi_2 = B\boldsymbol{\sigma}\cdot\mathbf{n}'u \tag{3}$$

where A and B are constants, $\mathbf{n}'$ is the direction vector of π_2 in the system of rest of the Λ particle.

Thus the wave function of the $p+\pi_1+\pi_2$ system has the form

$$\Psi = \{aA+bB(\boldsymbol{\sigma}\cdot\mathbf{n})(\boldsymbol{\sigma}\cdot\mathbf{n}')\}u. \tag{4}$$

The angular distribution of the decay products is determined by the function

$$W = \langle|\Psi|^2\rangle = \tfrac{1}{2}\,\mathrm{tr}\,|\Psi|^2$$

where the parentheses designate averaging over spin states. The final result is

$$W = c_1+c_2\mathbf{n}\cdot\mathbf{n}' \tag{5}$$

where

$$c_1 = |aA|^2+|bB|^2,$$
$$c_2 = aA\,(bB)^*+(aA)^*bB.$$

This formula coincides with the analogous formula of Lee and Yang. Exploiting conservation of momentum, we can also express W in the form

$$W = c_1'+c_2'\cos\vartheta$$

where ϑ is the angle between the directions of motion of the π_2 and π_1, or π_1 and p.

Consider, further, the cascade decay

$$\Sigma^0 \to \Lambda^0+\gamma \to p+\pi^-+\gamma.$$

At first we shall assume that the Σ^0 particle has a definite parity, say, a positive one. The expansion of the wave function of the system Ψ can be expressed in the form

$$\Psi = g_1\psi_1+g_2\psi_2.$$

Here ψ_1 and ψ_2 have their previous meaning, g_1 is a pseudoscalar and g_2 a scalar, both of these coefficients depending linearly on the spin wave function of the photon, i.e., on the polarization vector $\mathbf{e}$. It follows from here that

$$g_1 = \alpha(\mathbf{e}\cdot\boldsymbol{\sigma}); \qquad g_2 = \beta(\mathbf{n}\wedge\mathbf{e})\cdot\boldsymbol{\sigma} \tag{6}$$

where $\mathbf{n}$ is the direction vector of the photon motion. g_1 corresponds to electric dipole photon emission and g_2 to magnetic dipole photon emission.

Formula (3) is valid for the second cascade step and hence the wave function of the $p+\pi+\gamma$ system has the form

$$\psi = \{\alpha A\boldsymbol{\sigma}+\beta B(\boldsymbol{\sigma}\wedge\mathbf{n}')(\boldsymbol{\sigma}) \quad (7\cdot\mathbf{n})\}\cdot\mathbf{e}u.$$

The angular distribution is defined by the formula

$$W = \langle|\Psi|^2\rangle,$$

the parentheses designating averaging over the nucleon as well as photon polarization. Inserting (7) we get

$$W = c_1+c_2(\mathbf{n}\cdot\mathbf{n}') \tag{8}$$

where

$$c_1 = |\alpha A|^2+|\beta B|^2,$$
$$c_2 = i[(\alpha A)^*\beta B-\alpha A(\beta B)^*].$$

In the general case the Σ-particle does not possess a definite parity. It can be described by a density matrix with respect to the two parity signs [1]). Employing parity conjugation invariance of the interaction [2]) the density matrix ϱ can be written in the form

$$\varrho = \varrho_1+\varrho_2 C_\mathrm{p} \tag{9}$$

where C_p is the parity conjugation operator:

$$C_\mathrm{p} = \begin{pmatrix}0 & 1\\ 1 & 0\end{pmatrix}.$$

ϱ_1 is a scalar and ϱ_2 a pseudoscalar, these having the following form:

$$\varrho_1 = \lambda+\mu(\mathbf{n}_1\wedge\mathbf{n}_0)\cdot\boldsymbol{\sigma}$$
$$\varrho_2 = (\nu_1\mathbf{n}_1+\nu_2\mathbf{n}_0)\cdot\boldsymbol{\sigma}$$

where λ, μ, ν_1 and ν_2 are constants, $\mathbf{n}_0$ is the direction of the Σ particle momentum and $\mathbf{n}_1$ the direction of relative momentum of the particles which composed the Σ particle.

The $\Sigma^0\to\Lambda^0+\gamma$ decay can be characterized by the matrix

$$S = S_1+S_2C_\mathrm{p} \tag{10}$$

where, in accord with (6)

$$S_1 = \beta(\mathbf{n}\wedge\mathbf{e})\cdot\boldsymbol{\sigma}; \qquad S_2 = \alpha(\mathbf{e}\cdot\boldsymbol{\sigma}).$$

The ϱ'-particle density matrix Λ can be constructed with the help of matrix S.

$$\varrho' = \langle S^+\varrho S\rangle_\mathrm{e}, \tag{11}$$

the parentheses signifying averaging over the photon polarization. ϱ' can also be written in the form

$$\varrho' = \varrho_1'+\varrho_2'C_\mathrm{p}$$

where

$$\varrho_1' = \langle S_1^+\varrho_1 S_1+S_2^+\varrho_1 S_2+S_1^+\varrho_2 S_2+S_2^+\varrho_2 S_1\rangle_\mathrm{e},$$
$$\varrho_2' = \langle S_1^+\varrho_2 S_1+S_2^+\varrho_2 S_2+S_1^+\varrho_1 S_2+S_2^+\varrho_1 S_1\rangle_\mathrm{e}.$$

In accord with (2), $\Lambda\to\mathrm{p}+\pi$ decay can be characterized by the matrix (column)

$$S' = \begin{pmatrix} B\boldsymbol{\sigma}\cdot\mathbf{n}' \\ A \end{pmatrix}. \tag{12}$$

The angular distribution of the decay products is given by the following formula

$$W = \tfrac{1}{2}\,\mathrm{tr}\, S'^{+}\varrho' S' = \tfrac{1}{2}\,\mathrm{tr}\,\langle S'^{+} S^{+}\varrho S S'\rangle_e \tag{13}$$

or

$$W = (|A|^2+|B|^2)\,\mathrm{tr}\,\varrho_1'+(A^*B+AB^*)\,\mathrm{tr}\,\varrho_2'\boldsymbol{\sigma}\cdot\mathbf{n}'.$$

Inserting the expressions for ϱ, S and S' we get

$$W = c_1+c_2(\mathbf{n}\cdot\mathbf{n}')+c_3\mathbf{n}\cdot(p_1\mathbf{n}_1+p_2\mathbf{n}_0)+c_4(\mathbf{n}\cdot\mathbf{n}')\mathbf{n}\cdot(p_1\mathbf{n}_1+p_2\mathbf{n}_0) \tag{14}$$

where

$$\begin{aligned} c_1 &= \lambda(|A|^2+|B|^2)(|\alpha|^2+|\beta|^2)\\ c_2 &= i\lambda(AB^*+A^*B)(\alpha\beta^*-\alpha^*\beta)\\ c_3 &= i(|A|^2+|B|^2)(\alpha\beta^*-\alpha^*\beta)\\ c_4 &= -(|\alpha|^2+|\beta|^2)(AB^*+A^*B). \end{aligned}$$

Formulae (10) and (11) can also be used to determine the influence of scattering on the structure of the Σ or Λ particle density matrix. Scattering on a nucleus with spin 0 is described by a matrix which is similar to (10):

$$S = S_1+S_2C_p$$

where

$$\begin{aligned} S_1 &= \alpha+\beta(\mathbf{n}_0\,\mathbf{n}_1)\cdot\boldsymbol{\sigma} \\ S_2 &= \gamma(\mathbf{n}_0+\mathbf{n}_1)\cdot\boldsymbol{\sigma} \end{aligned} \tag{15}$$

and $\mathbf{n}_1$ is the direction of the scattered particle. The form of the density matrix after scattering is similar to that of (11). If the angular distribution of the decay products before scattering was given by the expression

$$W = \langle S'^{+}\varrho S'\rangle$$

then after scattering it will be

$$W' = \langle S'^{+}\varrho' S'\rangle$$

where S' is given by formula (13).

The author expresses his appreciation to I. Ya. Pomeranchuk for numerous helpful discussions.

References

1) T. D. Lee and C. N. Yang, Phys. Rev. (in print)
2) T. D. Lee and C. N. Yang, Phys. Rev. **102** (1956) 290

Nuclear Physics **3** (1957) 161—184; *North-Holland Publishing Co., Amsterdam*

EXCITED LEVELS IN Hg^{200} STUDIED FROM THE DECAY OF Tl^{200}

C. J. HERRLANDER
Nobel Institute of Physics, Stockholm
and
T. R. GERHOLM
Institute of Physics, University of Uppsala

Received 5 Decemer 1956

Abstract: The half-life of Tl^{200} has been found to be (26.1 ± 0.4) h. Conversion lines corresponding to 14 transitions in Hg^{200} were found. In addition, a few unidentified conversion lines were also observed. With the aid of coincidence spectrometer measurements, a level scheme was established, including the following excited levels: 368.0, 947.4, 1574.8, 1594.9, 1659.6, 1732.3, 1776.0, 1884.7 and 2136.7 keV. Conversion coefficients and K/L-ratios were measured. The 368 and 579 keV transitions were found to be pure E2 transitions, suggesting the assignments 2+ and 4+ for the two first excited levels. For most of the other transitions in the decay-scheme, multipolarity assignments are discussed.

A weak positon spectrum was also found in the decay of Tl^{200}, probably consisting of three components going to the ground-state and the two first excited levels. The log *ft*-values of the two most energetic transitions are found to be 9.1 and 7.8, consistent with first forbidden transitions. The ground-state of Tl^{200} is 2−, and the mass excess, as calculated from our data, is (34550 ± 3020) μMU. Finally, the level-scheme is compared with the results obtained by Adyasevich *et al.* in neutron-capture experiments on mercury.

1. Introduction

The investigation presented here was started in 1954. It forms a part of an extensive study devoted to the decays of the isotopes with mass-numbers close below 208. The purpose of these investigations is to make possible a systematic comparison between the excited energy levels in these nuclei. A preliminary report on this work was published in 1955 (Bergkvist *et al.* [1])).

In 1949 Orth *et al.* [2]) reported three half-lives in thallium produced by bombarding gold with 38 MeV alpha-particles. They assigned these activities to Tl^{198} (1.8 h), Tl^{199} (7 h) and Tl^{200} (27 h), all decaying by electron capture. In absorption measurements they found conversion electrons with an energy of about 400 keV, which probably corresponds to transitions from the first excited levels in Hg^{198} and Hg^{200}. A decay-scheme of Tl^{200} was first proposed by Israel and Wilkinson [3]). A search for positons in the decay of Tl^{200} was carried out by the same authors but the result was negative, although the available energy (> 1360 keV) would be sufficient for positon decay.

Bergström *et al.* [4]) found a large number of conversion lines corresponding to gamma rays with a half-life of 27 h, Many of these gamma rays had been observed by Wilkinson in unpublished measurements (Bergström *et al.* [4]), ref. [3])). Wilkinson also showed that all strong gamma rays were in coincidence with a 368 keV transition, which very probably should go from the first excited level to the ground-state in Hg^{200}. Bergström *et al.* [4]) found the energy of this transition to be 367.8 keV, with an accuracy of better than 1 : 1000.

In the measurements reported by Bergkvist *et al.* [1]) Pb-sources were used and Tl^{200} was present only as a growing-in product. All the transitions reported by Bergström *et al.* [4]) were observed, as well as several weak conversion lines not classified by the authors. Some of these conversion lines were found to belong to the decay of Tl^{200}.

Davis *et al.* [5]) and Barloutaud *et al.* [6]) have shown by Coulomb excitation that the 368 keV level mentioned above is the first excited level in Hg^{200}. The latter authors also give an estimate of the gamma mean-life of this level (6.8×10^{-11} sec).

Butement and Shillito [7]) observed two gamma rays of energies 0.39 and 1.13 MeV from the 48 min activity of Au^{200}, decaying to Hg^{200} with beta rays with a maximum energy of 2.2 MeV. The 0.39 MeV gamma ray very probably corresponds to the transition from the first excited level mentioned above.

The reaction Hg^{199} (n, γ) Hg^{200} has been the subject of several investigations. Kinsey and Bartholomew [8]) found several gamma rays in the energy region 4.5 to 6.5 MeV. Adyasevich *et al.* [9]) measured the transition energies by means of the Compton secondaries expelled from a converter by a collimated beam of gamma rays. They report over 40 transitions in Hg^{200}, and have constructed a level-scheme with the highest level at 8.03 MeV. Their lowest levels will be compared with our level-scheme in section 5.

2. Experimental Procedures

2.1. SOURCE PREPARATION

For reasons mentioned below the Tl-activity was produced in two ways: a) By bombarding gold with 35 MeV alpha-particles in the 225 cm cyclotron of the Nobel Institute and b) by milking thallium from active lead produced by bombarding thallium with 65 MeV protons in the synchrocyclotron of the Gustaf Werner Institute at Uppsala.

A thin layer of gold containing the active thallium was scraped off and dissolved in aqua regia. To remove acids, the solution was dried and dissolved in water, whereafter most of the $AuCl_3$ was reduced to metallic gold with hydroxylaminehydrochloride (NH_2OH-HCl) and centrifuged off. Concentrated HCl was added to make the solution 6 *N*, and the thallium

was oxidized from Tl^{+} to Tl^{3+} with $KMnO_4$. The thallium and the remaining gold were extracted with ether saturated with 6*N* HCl. The ether was then evaporated over about 0.5 cm^3 6*N* HCl and the active solution deposited on an ion exchange column (Dowex 1, mesh 200, column size ø 2×100 mm^3). The column was washed with decreasing concentrations of HCl, and finally the thallium was washed off with water saturated with SO_2. Au is reduced to metallic gold at the top of the column.

The technique for separating lead from irradiated thallium is described in detail elsewhere [10]). The grown-in Tl activity was extracted with ether in 6*N* HCl solution after about 35 h.

Apart from Tl^{200}, the sources prepared by the first method also contain thallium isotopes with mass numbers lower than 200, while sources obtained according to the second method were mixed with thallium isotopes of mass numbers above 200.

The activity was then evaporated [11]) onto an aluminium foil used as backing for spectrometer sources. The size of the sources for the double-focusing spectrometer was 2×12 mm^2, while for the lens spectrometer and coincidence spectrometer circular sources with a diameter of about 2 mm were used.

2.2. INSTRUMENTS

The conversion lines from the decay of Tl^{200} have been studied in a double-focusing spectrometer [12]) adjusted to a relative half-width of about 0.3 per cent and a transmission of 0.15 per cent of 4π. For the scintillation spectra a single pulse height analyzer was used. The scintillation spectrometer was fitted with a counting rate feedback stabilizer due to de Waard [13]). The positon spectrum was measured in an intermediate image spectrometer [14]). This instrument was provided with a helical baffle used to prevent the conversion electrons from reaching the detector. The coincidence measurements were carried out in a double lens spectrometer [15]). The resolving time of the coincidence circuit used in these measurements was 0.15 μs $(=2\tau)$.

3. Results

3.1. HALF-LIFE MEASUREMENTS

The half-life of Tl^{200} was measured by following the decay of the K-conversion line of the 368 keV transition for about four half-lives. To avoid influence from a weak 367 keV transition in Tl^{199}, these measurements had to be carried out with a sample milked from Pb-activities. The resulting decay-curve, corrected for the background, is shown in fig. 1.

The half-life was found to be

$$T_{\frac{1}{2}}(Tl^{200})=(26.1\pm0.4)\ \text{h},$$

which is within the limits of the value given by Michel and Templeton [16] (27±1 h).

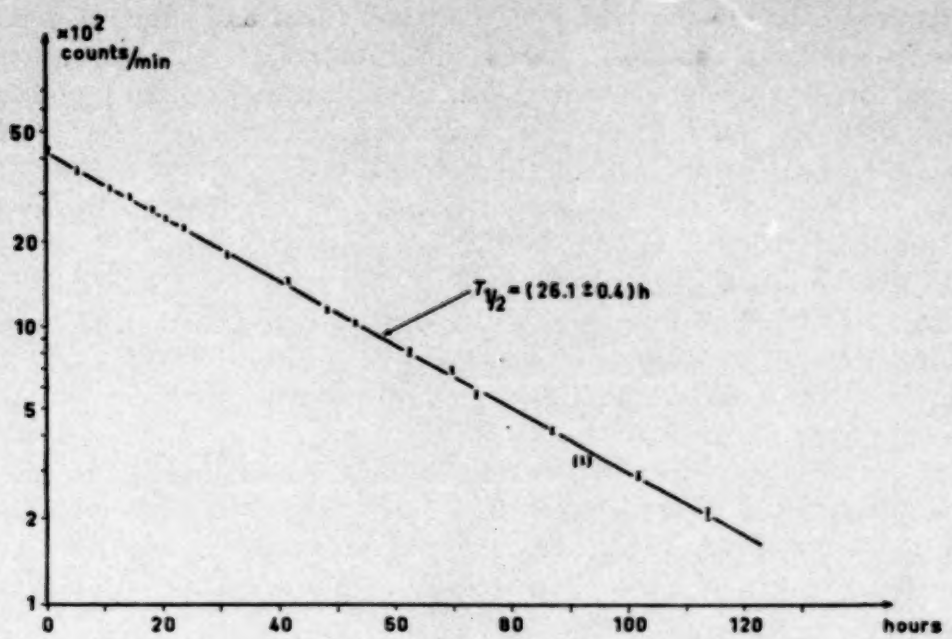

Fig. 1. Half-life of Tl^{200} obtained from the decay of the K-conversion line of the 368 keV transition. Corrected for the background of the line.

3.2. ENERGY AND INTENSITY MEASUREMENTS OF CONVERSION LINES

The energies and intensities of the conversion lines have been measured in a double-focusing spectrometer. A preliminary search for electron lines was carried out on a lead source containing, apart from Tl^{200}, admixtures of Pb^{204m} (67.5 min), Pb^{203} (52 h), Pb^{202m}(3.6 h), Pb^{201} (9.4 h), and Pb^{200} (21.5 h), as well as the growing-in Tl activities. A list of possible Tl^{200} transitions was thus obtained. The energies and the intensities of the conversion lines for most of the observed transitions assigned to Tl^{200} were then measured using pure Tl sources. The calibration of the spectrometer was checked against the standard conversion lines of ThB (F and I lines), Cs^{137} and Bi^{207}. The energies and relative intensities found are given in table I. In the last column the energies of the corresponding gamma transitions are given. The isotopic assignments of the transitions given in table I are based on half-life meosurements of the K-lines.

All the energies fit into the level-scheme given in fig. 10 (page 179), although the energy values 628.9 and 787.3 are just outside the errors. More convincing proofs of the energy levels are given below (cf. subsection 3.4).

Three very weak electron lines exist, having energies of 81.4, 301.5 and 305.0 keV, which are not with certainty assigned to Tl^{200}. Three other

lines are also found probably corresponding to the transition energies 591.6 and 661.6 keV ($L_{591.6}$ and $K_{661.6}$ are less than 2 keV apart and cannot be resolved). However, these lines have not been assigned to Tl^{200} with certainty.

TABLE I

E_e- (keV)	Assignments	corresponding γ-energy (keV)	rel. conv. int. ($K_{368} = 100$)	E_γ (keV)
33.4	K	116.5	>3	116.5±0.1
101.7	L_I	116.5	2.3±0.3	
168.9	K	252.0	4.8±0.5	252.0±0.2
237.3	L_I	252.1	1.0±0.2	
206.2	K	289.3	5.5±0.5	289.3±0.2
274.7	L_I	289.5	1.6±0.2	
226.2	K	309.3	1.8±0.3	309.3±0.2
294.6	L_I	309.4	0.3±0.1	
284.9	K	368.0	100	368.0±0.2
353.4	L_I	368.2	40 ±3	
	L_{II}	367.6		
496.3	K	579.4	5.9±0.5	579.4±0.3
565.1	L_I	579.9	1.8±0.3	
	L_{II}	579.3		
545.8	K	628.9	1.3±0.2	628.9±0.5
614.4	L_I	629.4	0.2±0.1	
629.1	K	712.2	0.3±0.1	712.2±0.4
704.2	K	787.3	0.8±0.2	787.3±0.5
745.5	K	828.6	6.4±0.7	
814.4	L_I	829.2	1.3±0.2	828.6±0.4
	L_{II}	828.6		
1123.7	K	1206.8	6.9±0.7	1206.8±0.5
1192.1	L_I	1206.9	1.8±0.2	
1143.8	K	1226.9	0.9±0.2	1226.9±0.7
—	L	—	< 0.15	
1281.2	K	1364.3	1.0±0.2	1364.3±1.0
1433.6	K	1516.7	0.5±0.1	1516.7±0.8
—	L	—	0.2±0.1	

Search for the K-lines of two possible transitions of (368+579) and (368+1517) keV has been carried out. The following limits of the K-line intensities are found:

$$K_{(368+579)} < 0.05$$

$$K_{(368+1517)} < 0.03. \qquad (K_{368} = 100)$$

3.3 SCINTILLATION SPECTRUM

Scintillation spectra have been measured in order to get information on relative gamma intensities. From these measurements, and from the relative intensities of the conversion lines the conversion coefficients are obtained by comparison with the theoretically known conversion coefficient

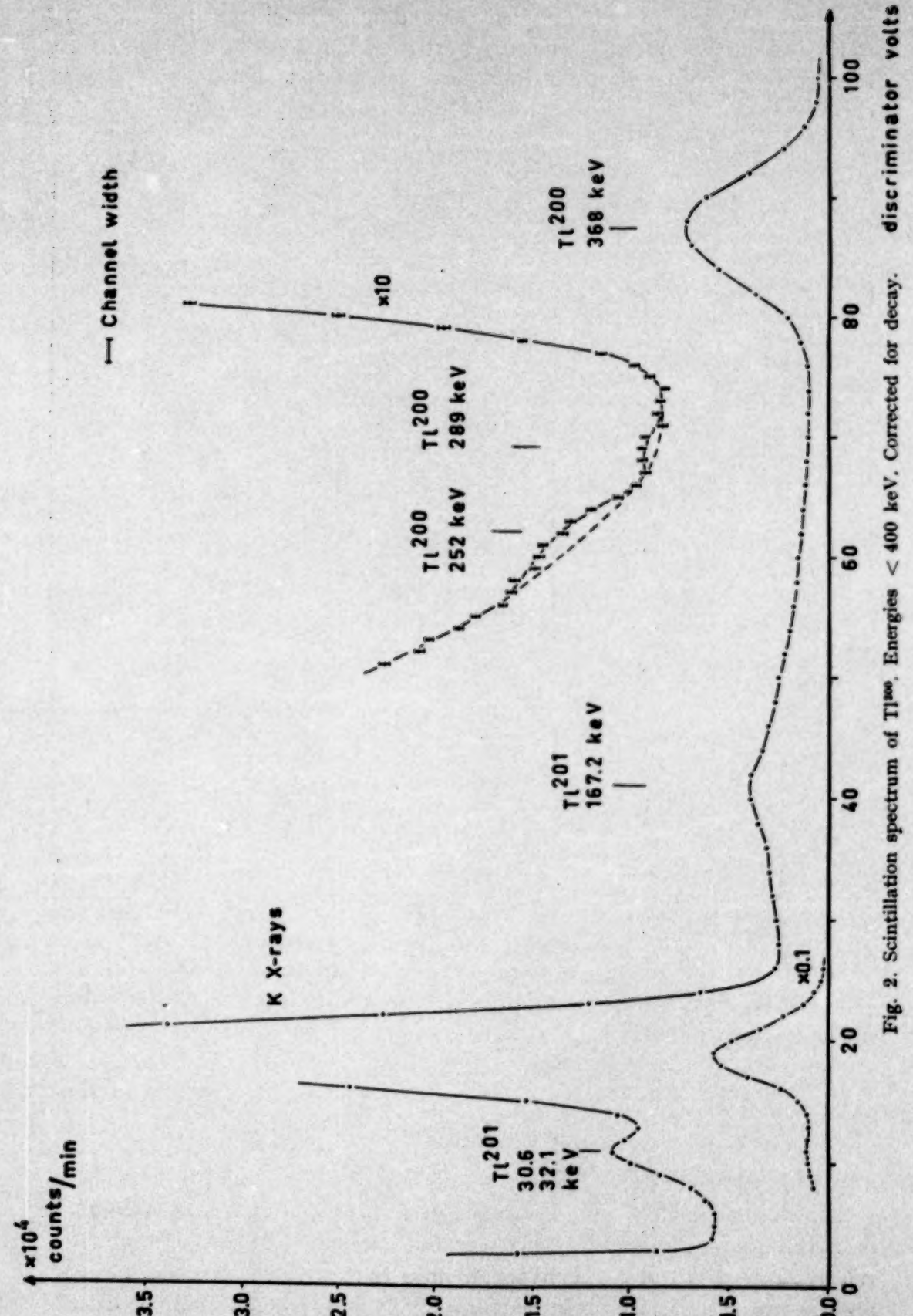

Fig. 2. Scintillation spectrum of Tl^{200}. Energies < 400 keV. Corrected for decay.

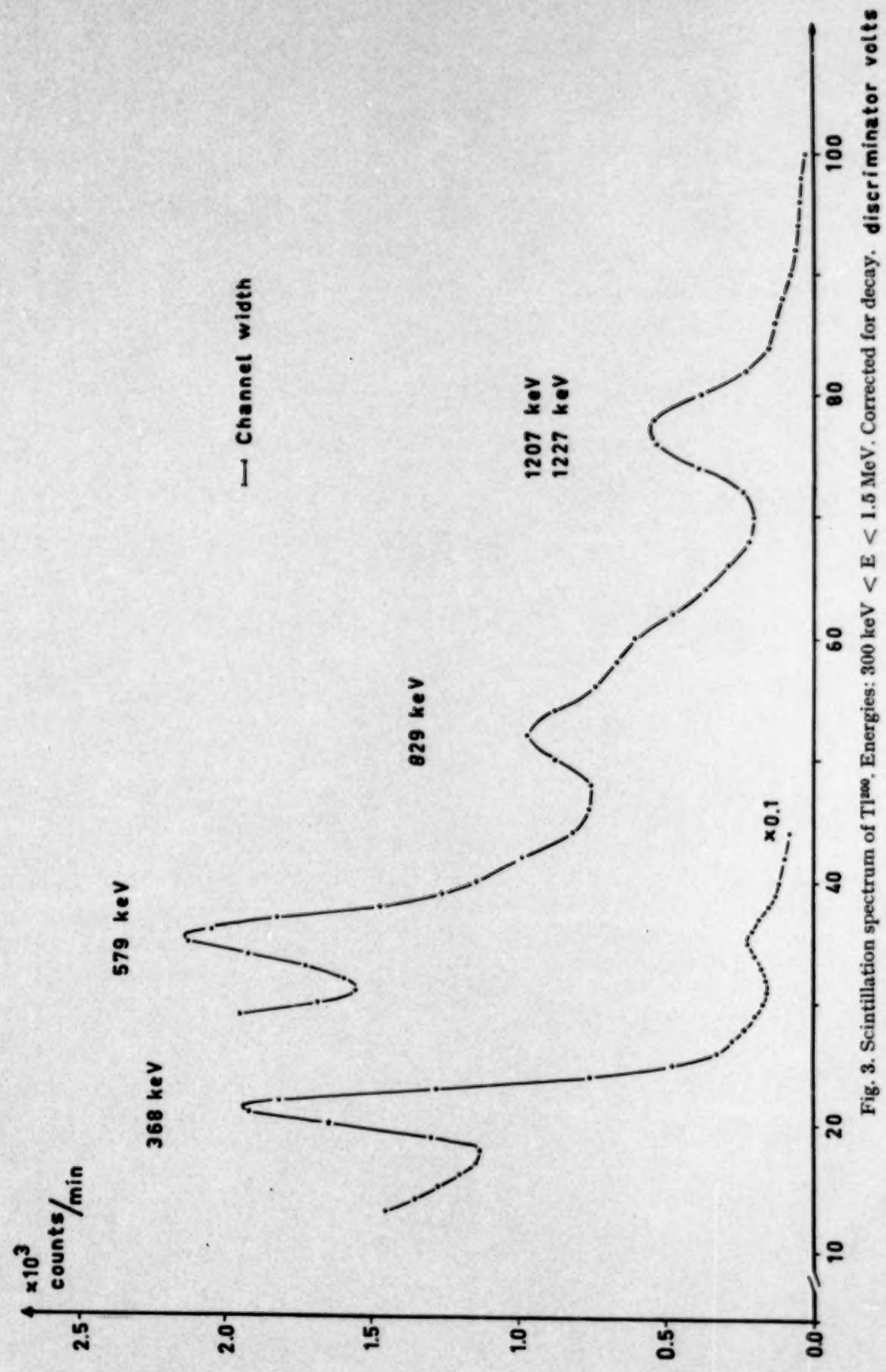

Fig. 3. Scintillation spectrum of Tl^{200}. Energies: 300 keV < E < 1.5 MeV. Corrected for decay.

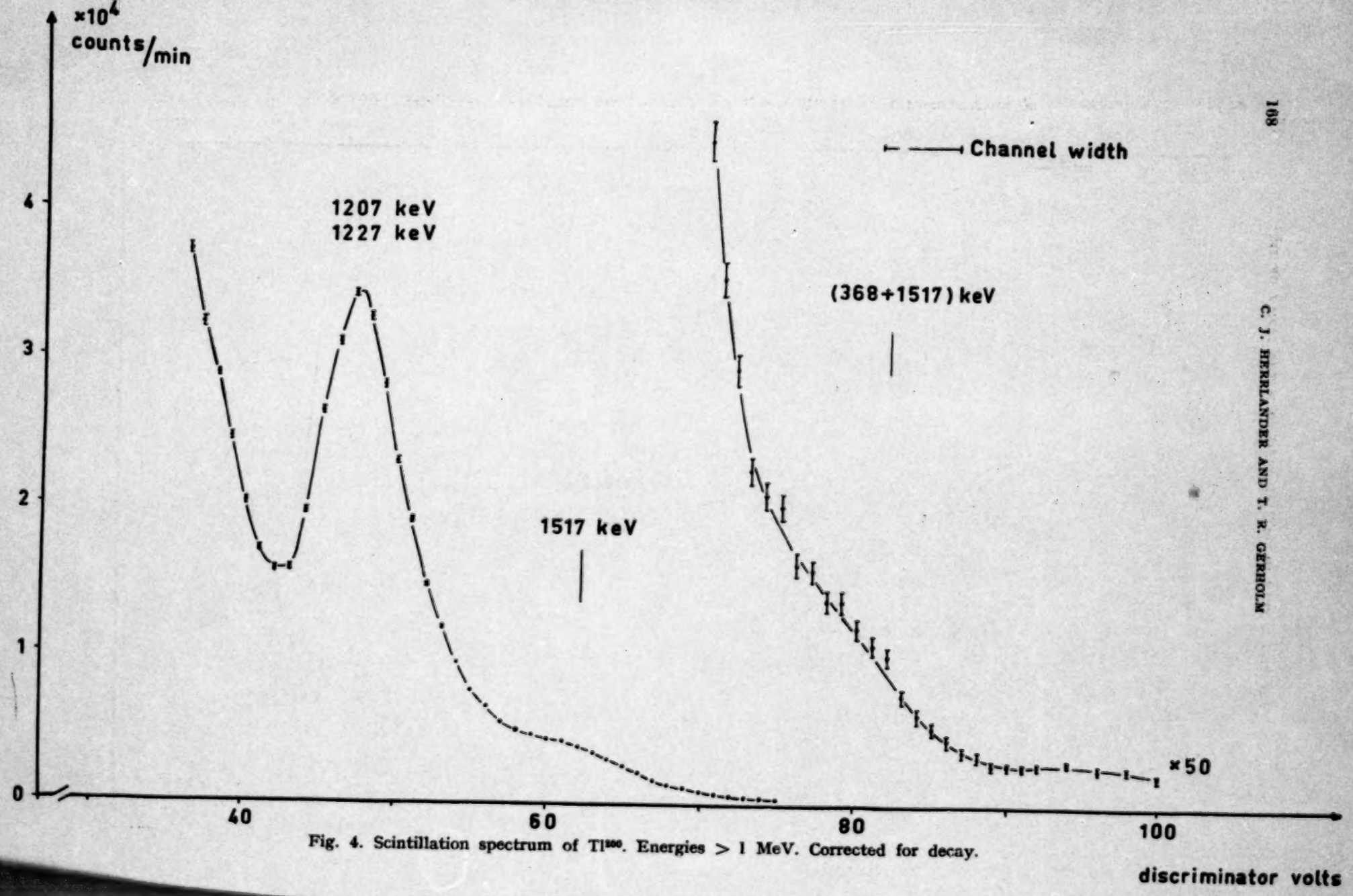

Fig. 4. Scintillation spectrum of Tl^{200}. Energies > 1 MeV. Corrected for decay.

of the 368 keV transition. This must be a pure electric quadrupole, since it connects the 2+ and 0+ states. Hence the conversion coefficient is known theoretically. The spectra obtained in different energy regions are shown in figs. 2—4, and the measured gamma ray intensities are given in table II.

TABLE II

E_γ keV	rel. gamma intensity ($\gamma_{368} = 100$)
252.0	< 0.9
289.3	< 0.4
309.3	< 2
368.0	100
579.4	14
828.6	7
1206.8+1226.9	30
1516.7	≈ 2

In fig. 4 a search for a possible gamma ray of energy (368+1517) keV is shown. If such a gamma ray exists, its intensity must be

$$\gamma_{(368+1517)} < 0.1 \qquad (\gamma_{368} = 100).$$

This intensity limit also includes the sum up peak of the two cascading transitions.

3.4. COINCIDENCE MEASUREMENTS

The energy and intensity measurements do not give enough information. For the construction of an unambigous level-scheme both electron-electron and electron-gamma coincidence measurements were made. For the electron-gamma measurements a tantalum absorber was used to depress the X-ray peak in the scintillation channel.

The results of the electron-electron coincidence measurements are given in table III. Generally the K-lines of the two transitions were focused in each channel (the relative half-width was 2.5 %). The genuine, as well as the accidental coincidence counting rates were measured. A variable delay was introduced into one of the channels to obtain the accidental coincidence background.

As the spectrometer cannot resolve the two K-lines of the 1207 and 1227 keV transitions, the whole coincidence lines for the two pairs of 309—1207 keV and 289—1227 keV K-conversion lines were measured (cf. fig. 5). From fig. 5a it can be seen that the 289 keV transition is in coincidence with the 1227 keV transition but not with the 1207 keV transition, whereas fig. 5b shows only that the 309 keV transition is in coincidence with the 1207 keV transition, but does not exclude a coincidence coupling between

the transitions of 309 and 1227 keV. However, this possibility is excluded from the following transition energy relations:

$$289.3+1226.9 = 1516.2$$
$$309.3+1206.8 = 1516.1 \quad \text{(cf. energy of cross-over} = 1516.2 \text{ keV)}$$

A level-scheme which is consistent with the electron-electron coincidence measurements is shown in fig. 10 (page 179). Several difficulties, however,

TABLE III

Measured electron-electron coincidences

E_γ (channel 1)	E_γ (channel 2)	coinc/min
368	252	33.1±3.5
368	289	30.4±3.6
368	309	17.8±2.2
368	579	60.7±4.6
368	829	46.3±5.3
368	1207−27	41.2±5.2
368	1364	4.1±1.7
368	1517	2.4±0.6
579	252	−0.4±0.8
579	629	0.2±0.4
579	712	0.7±0.35
579	787	2.1±0.6
579	829	12.0±1.6
252	289	1.3±0.6
252	309	−0.7±0.7
252	787	−0.2±0.4
252	829	−0.1±0.8
252	1207—27	0.1±1.1
252	1364	0.4±0.3
252	1517	0.2±0.4
289	1207	see fig. 5a
289	1227	
309	829	0.1±0.4
309	1207	see fig. 5b
309	1227	
787	829	−0.1±0.4

are connected with the 252 keV transition. For that reason, electron-gamma coincidences were measured between the 252 keV K-line and gamma rays with energies > 1 MeV.

From fig. 6 it is seen that the 252 keV transition is in coincidence with the most predominant transitions of energies > 1 MeV. Therefore, the most probable position of this transition is that shown in fig. 10 (page 179). This is not in disagreement with the electron-electron coincidence results (table III), since, for the most predominant case, 252—309, the electron-

electron coincidence effect can be estimated to be too small to be observed in our measurements.

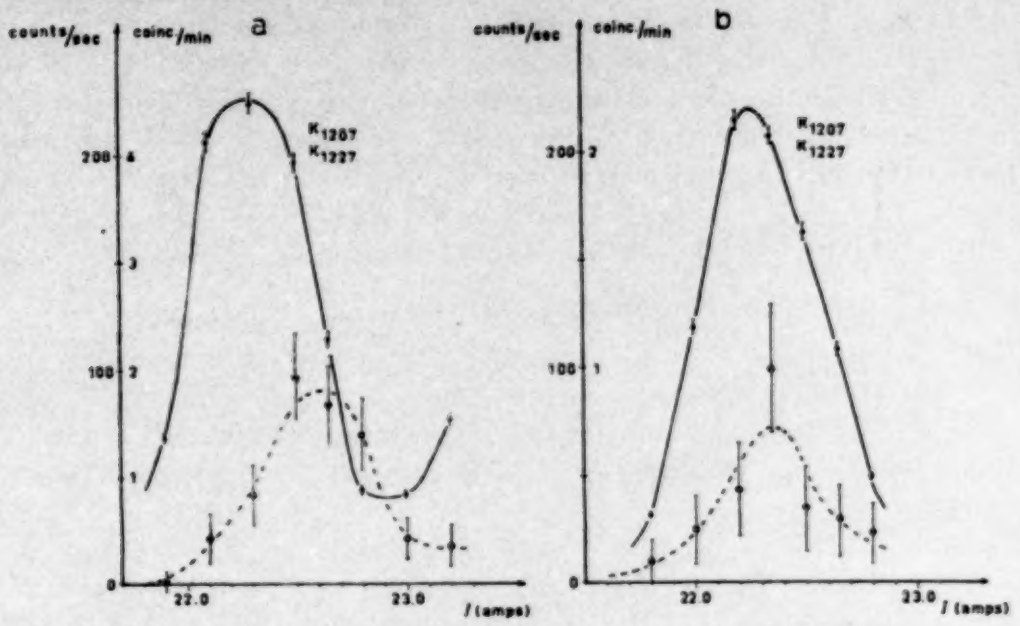

Fig. 5. $e^- - e^-$ coincidences (dotted line) between a) K_{289} or b) K_{309} and the unresolved K-lines of the 1207 and 1227 keV transitions (continuous line). Corrected for decay and accidental coincidences.

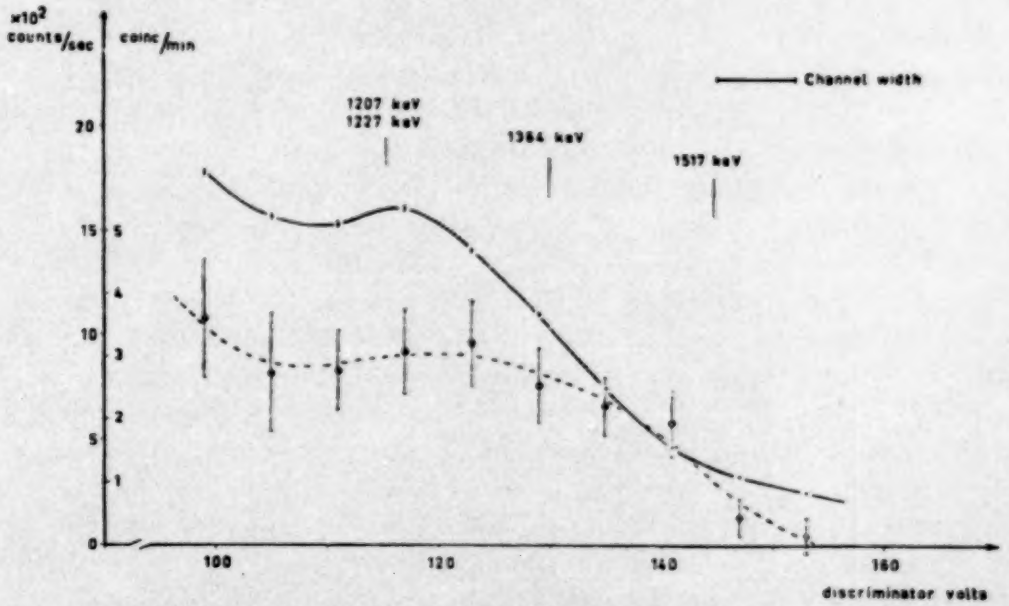

Fig. 6. $e^- - \gamma$ coincidences (dotted line) between K_{252} and gamma rays of energies > 1 MeV. The continuous line shows the counting rate of the gamma channel. Corrected for decay and accidental coincidences.

From coincidence measurements it is possible to calculate conversion probabilities ($\varkappa_i = \alpha_i/(1+\alpha_{tot})$) provided the branching ratios between

competing transitions are known [17]). The 368 keV K-line is shown to be in coincidence with eight other lines. For seven of these coincidences the product $\varkappa_{K368}\omega$ (ω is the transmission of the actual spectrometer channel) was found to be the same within the statistical errors: $(11\pm1)\times10^{-4}$. As the 368 keV transition is known to be a pure E2 transition this value can be used to calculate the effective transmission of the spectrometer. The theoretical K-conversion coefficient for an E2 transition of this energy is 3.91×10^{-2} (Sliv *et al.* [18]), which corresponds to a K-conversion probability of 3.69×10^{-2}. The transmission is then found to be

$$\omega = (3.0\pm0.3)\%.$$

(With the spectrometer adjustments used in these measurements the transmission is the same in both spectrometer channels).

Using this value of the transmission, we can calculate K-conversion probabilities of the 579 and 1227 keV transitions. The values obtained are given in table IV.

TABLE IV

E_γ	$\varkappa_K\omega$	$\varkappa_K$
579	$(3.0\pm0.3)\times10^{-4}$	$(1.0\pm0.2)\times10^{-2}$
1227	$(1.3\pm0.3)\times10^{-4}$	$(4\pm1)\times10^{-3}$

As mentioned above, only seven of the eight K-lines, shown to be in coincidence with the 368 K-line, will give the same value of $\varkappa_K\omega$. The missing one is the 252 K-line. For this coincidence combination the product of $\varkappa_K\omega$ was found to be more than a factor of two lower than for the other seven combinations. The discrepancy could be explained by an isomeric lifetime of the same order as the resolving time of the coincidence circuit ($2\tau \approx 0.15$ μs), but no delayed coincidences corresponding to this lifetime were found. Alternatively one could understand the reduced coincidence effect by assuming a cross-over from the 1885 keV level directly to the ground state. The intensity of such a transition should be comparable with the intensity of the 1517 keV transition. This, however, is in contradiction to scintillation spectrometer measurements, as the gamma intensity of the cross-over is found to be < 5 per cent of the intensity of the 1517 keV transition (page 169). Moreover, no K-line to this cross-over was observed (intensity limit. < 0.03 ($K_{368} = 100$)). Another possibility is to assume a transition taking place by internal pair-formation.

3.5. POSITON SPECTRUM

As the energy difference between the groundstates in Tl^{200} and Hg^{200} is of the order of 2 MeV (see fig. 10, page 179), one would expect to find positons in the decay of Tl^{200}, if the transitions to the lower levels in Hg^{200}

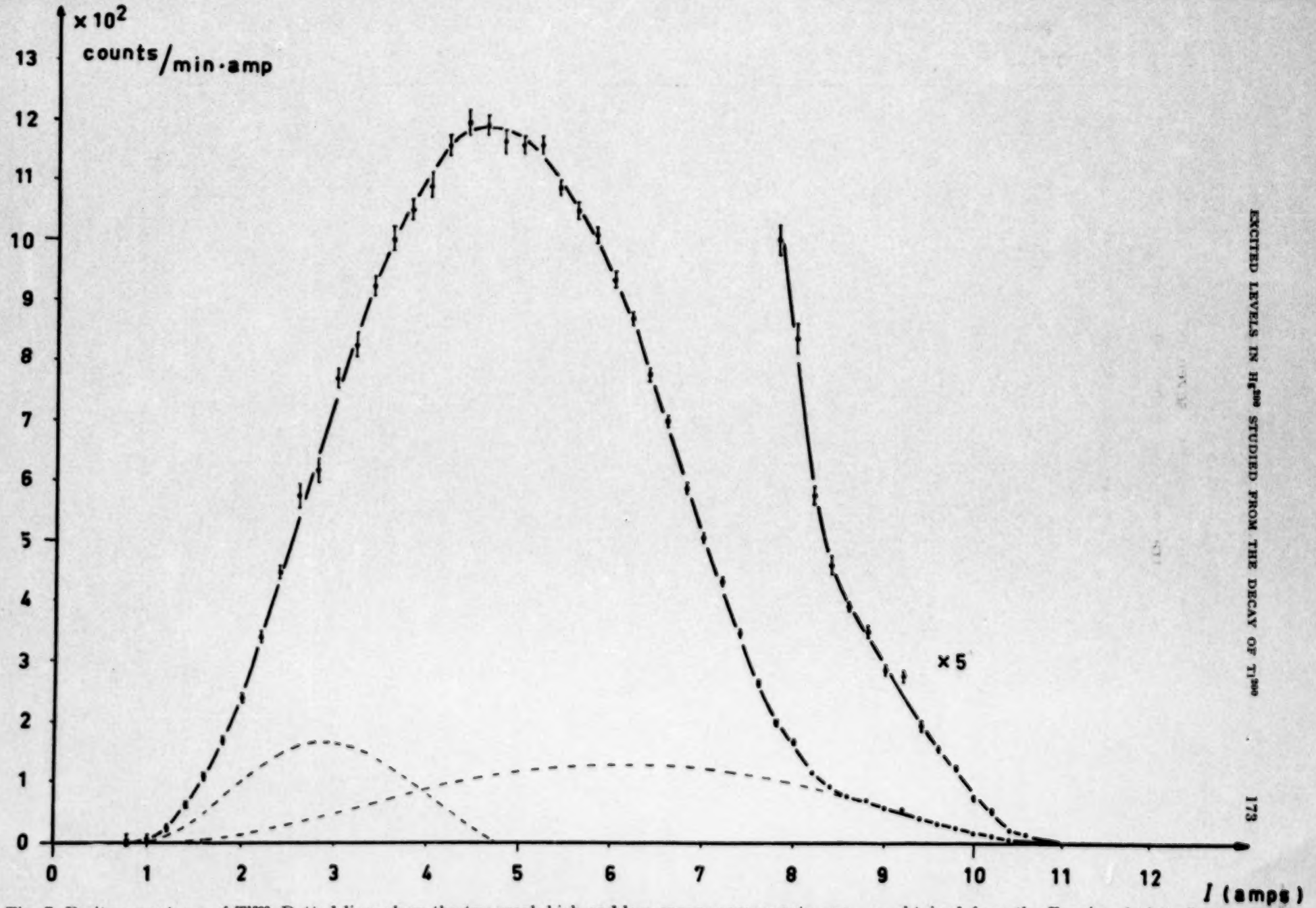

Fig. 7. Positon spectrum of Tl^{200}. Dotted lines show the two weak high and low energy components resp., as obtained from the Fermi-analysis in fig. 9a and 9b.

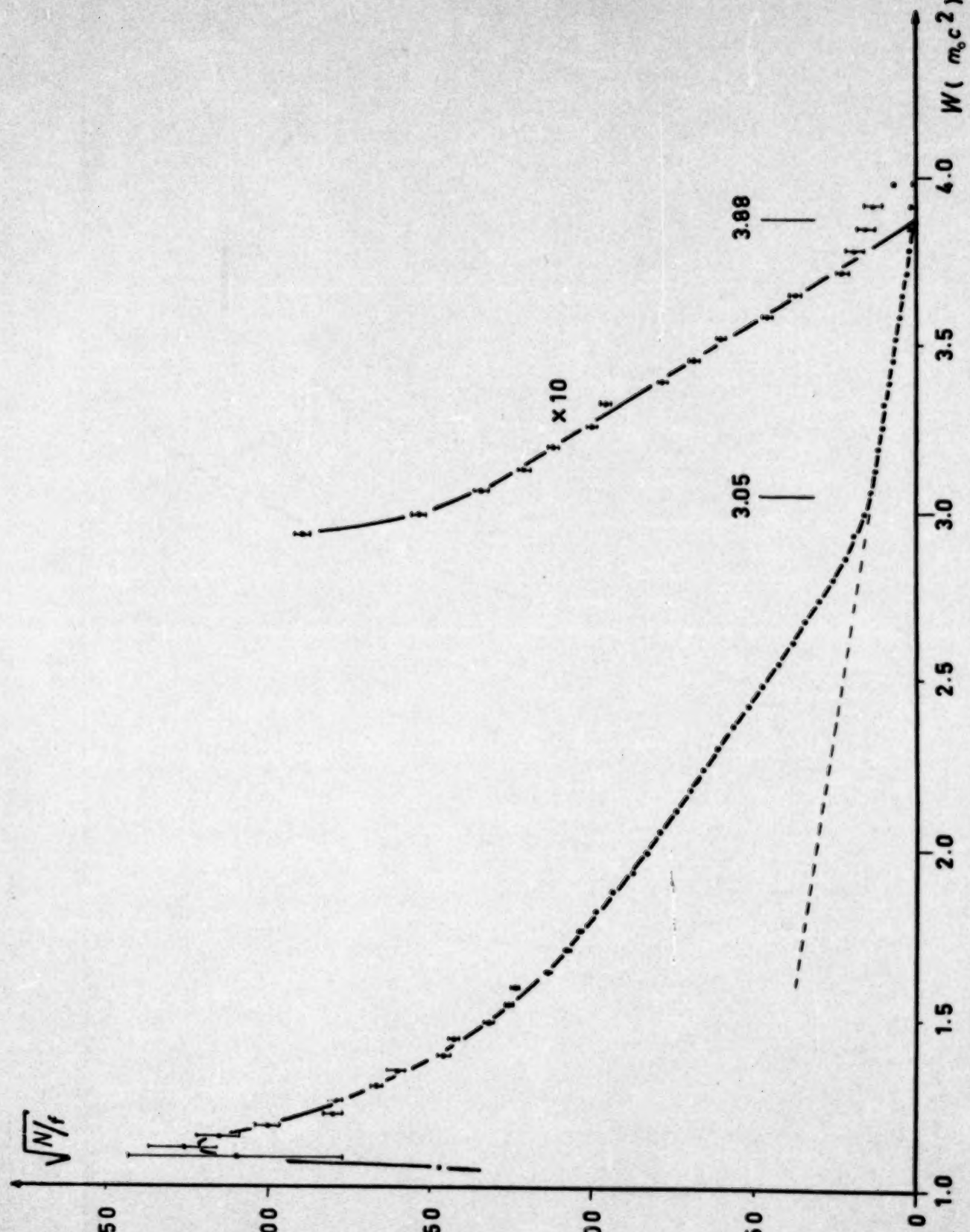

Fig. 8. Fermi-analysis of the positon spectrum of Tl^{200}. Corrected for screening. Allowed shape assumed.

are not highly forbidden. As Tl^{200} ground state is assumed to be a 2— state (cf. page 182) the transitions to the ground state (0+) and first excited state (2+) in Hg^{200} would be of the first forbidden type with log *ft*-values about 9—10 (*l*-forbidden) and about 7 respectively. This suggests partial half-lives of the order of 10^9 and 10^7 sec. Since the half-life of Tl^{200} is 10^5 sec (26.1 h), it would be possible to detect the positons in a spectrometer with sufficiently high transmission.

For that purpose a source was prepared for the intermediate image spectrometer. The instrument was supplied with a helical baffle to prevent the negative electrons from being detected. The positon spectrum obtained (cf. fig. 7) was calibrated both in energy and intensity against the K-lines of the 579 and 829 keV transitions. From the known relative electron intensities, the intensity relative to the K_{368}-line was calculated. The following intensity relation was found:

$$\frac{K_{368}}{\Sigma\beta^+} = 11.$$

A Fermi-analysis shows that the spectrum is a mixture of three components. Fig. 8 gives the Fermi-plot of the spectrum if it is supposed to have an allowed shape. In that case the energy difference between the two most energetic components is found to be (424±20) keV, which is too far from the expected value of 368 keV. If one assumes, however, a unique first forbidden shape for the high energy component, the energy difference between the two highest components is (384±20) keV, which is in better agreement with the energy of the first excited state (fig. 9a). The assumption that the high energy component really has such a unique shape is in agreement with the proposed spin and parity of Tl^{200} (2—) and the log *ft*-value (see table V) for this transition. The shape correction factor [19]) used is $S = (W^2-1)+(W_0-W)^2$. Fig. 9a also shows the Fermi-analysis of the second component assumed to have an allowed shape.

The remaining part of the Fermi-plot, after the two components have been subtracted, is shown in fig. 9b. There is very probably a third component, but it seems difficult to make the points lie on a straight line, even if corrections for unique shape are made. Due to these difficulties, the energy and the intensity of this component are very uncertain.

The energies and intensities of the three components are given in table V (cf also fig. 9 and 7). In table V the log *ft*-values are given, computed from the values of the ratio between K-capture and positon emission for allowed transitions given by Feenberg and Trigg [20]). These two log *ft*-values are consistent with first forbidden transitions, of which the one of higher energy has a spin change $\Delta I = 2$.

The transition between the ground states is found to be a first forbidden

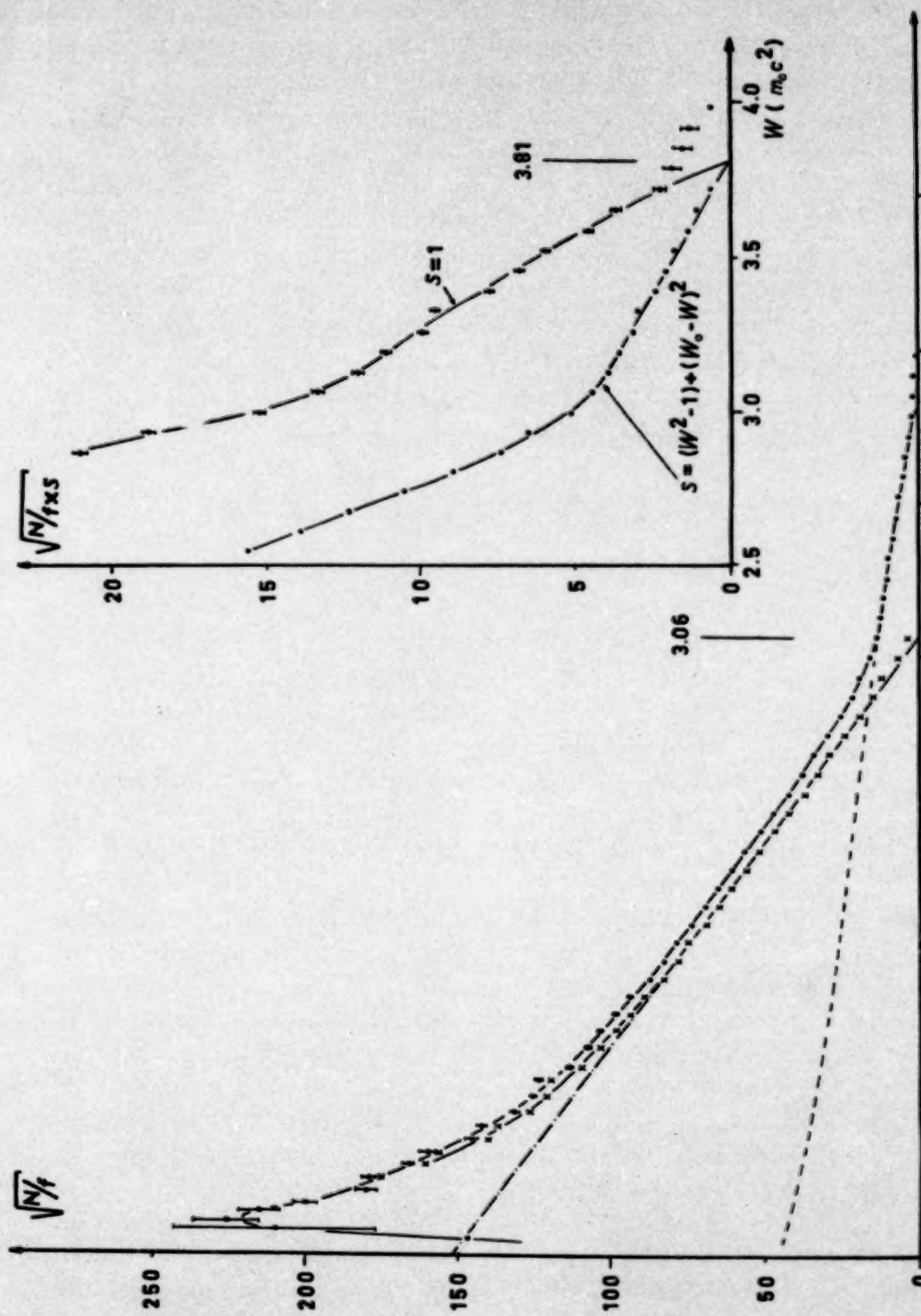

Fig. 9a. Fermi-analysis of the two most energetic components of the positon spectrum of Tl^{200}. Corrected for screening. The inset shows the high energy component with corrections for a unique first forbidden shape ($\Delta I = 2$, yes). This shape is then copied in the main fig. Allowed shape assumed for the second component.

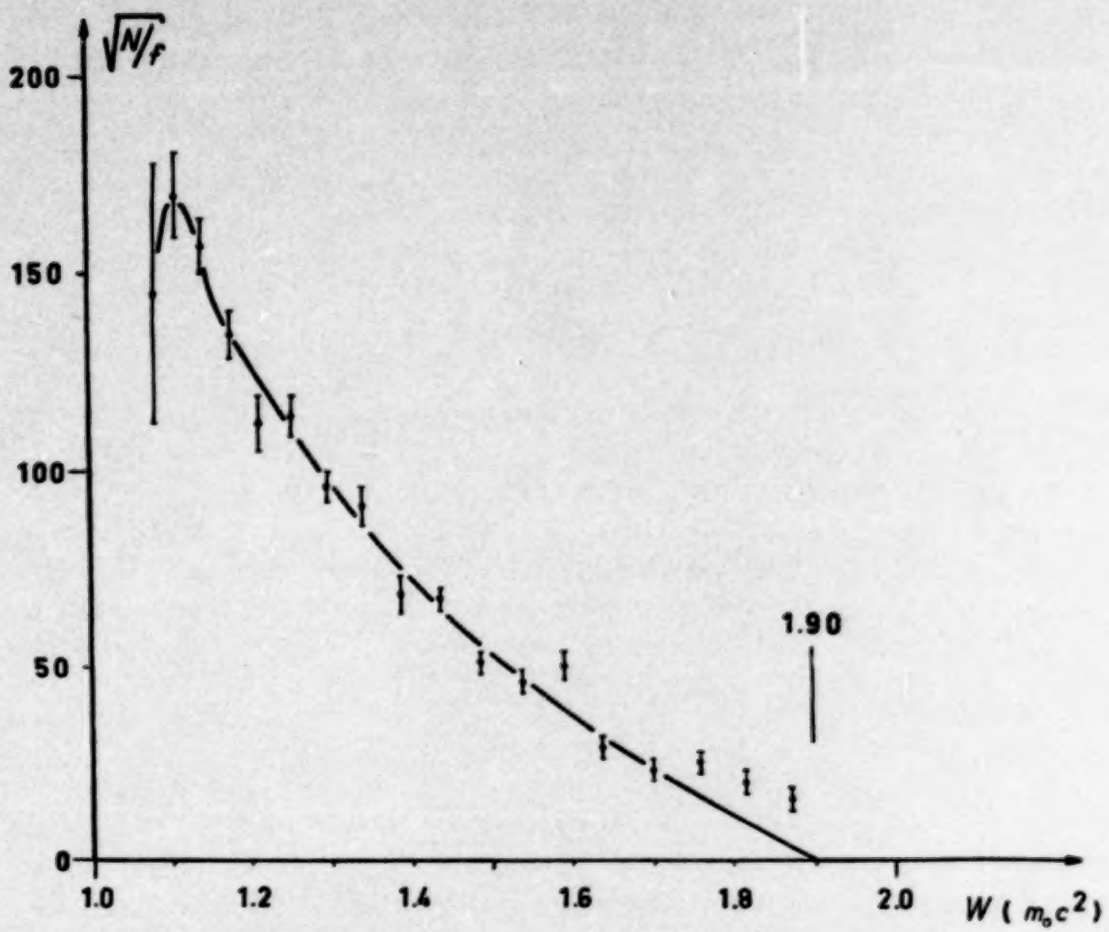

Fig. 9b. Fermi-analysis of the low energy component of the positon spectrum of Tl^{200} as obtained by subtracting the two other components (fig. 9a), the high energy component corrected for unique shape. Corrected for screening.

TABLE V

Transition	E_{max} (keV)	Intensity ($K_{368} = 100$)	log ($f_K/f_{\beta+}$)[20]	Tot. number of trans. ($K_{368} = 190$)	log ft
2− → 0+	1436±10	1.3	1.42	36(1.5 %)†	9.1
2− → 2+	1052±10	7.3	1.90	590(20 %)†	7.8
2− → 4+	460±25	0.6	3.2	1030	—

† Intensity in per cent of total number of disintegrations.

transition with $\Delta I = 2$. Moreover, the expression log $(W_0^2-1)ft$, which is about 10 for such transitions, is found to be 10.2. The spin and parity assignment of the ground state of Tl^{200} is thus 2−, arising from a coupling between the 81st proton and the 119th neutron. The 81st proton is found to be in a $s_{\frac{1}{2}}$ state in both Tl^{203} and Tl^{205} [21]) and this is accepted also for

the 81st proton in Tl^{200}. For the 119th neutron, different authors give different possibilities (see table VI). The only one of these possibilities which

TABLE VI

Proposed spin for the 119th neutron

Spin	proposed from measurements on	ref.
$p_{1/2}$	Au^{198}	22)
$p_{1/2}$	Hg^{199}	21)
$f_{5/2}$	Pb^{201}	23)

can combine with the spin ($s_{\frac{1}{2}}$) of the 81st proton to give a spin 2 is the $f_{5/2}$ assignment. The spins of the proton and neutron must then be antiparallel, in accordance with Nordheim's "strong" rule [24]).

It is possible to calculate the mass and binding energy of Tl^{200} with the aid of Wapstra's [25]) values for Hg^{200} and the energy difference between the ground-states in Hg^{200} and Tl^{200} as determined from the maximum positon energy:

Mass excess of Tl^{200} = (34550±3020) μ MU
Binding energy of Tl^{200} = (1 577 907±3020) keV.

4. Discussion of Multipolarity Assignments

The energies and level order of the decay-scheme given in fig. 10 are based on accurate energy measurements of the conversion lines and on coincidence measurements.

In order to get information on the multipolarities of the transitions and thus on the spins and parities of the levels, K/L-ratios and some conversion coefficients have been measured. The values are given in table VII. Most of the conversion coefficients are obtained by comparing scintillation and electron spectra intensities using the conversion coefficient of the 368 keV E2 transition as reference. These values should be considered only as rough estimates. For a few transitions, conversion coefficients were determined by the coincidence method. Due to the weak sources the errors in the K/L-ratios are relatively high, and for the same reason L-subshell-ratios were not measured.

The possible multipolarities, and spin and parity assignments are discussed below. The K/L-ratios are compared with theoretical values calculated from Rose *et al.* [26]), whereas the K-conversion coefficients are compared with Sliv's *et al.* [18]) theoretical values. Transition intensities are derived from the formulae

$$n = K\left(1+\frac{L+M+\dots}{K}+\frac{1}{\alpha_K}\right),$$

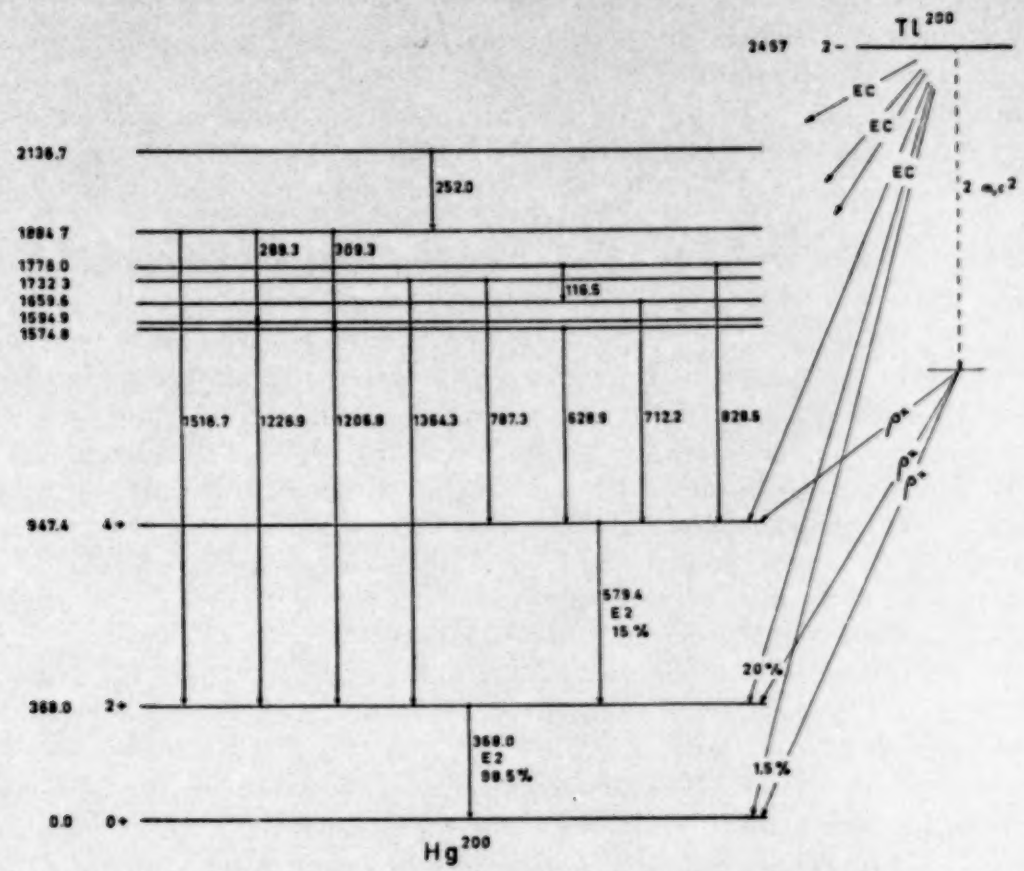

Fig. 10. Decay-scheme of Tl^{200}. For further information on multipolarities, spins and parities see section 4.

TABLE VII

E_γ	K/L	α_K
116.5	> 1.3	—
252.0	5.1±0.8	$> 2 \times 10^{-1}$
289.3	3.4±0.6	$> 5 \times 10^{-1}$
309.4	5.2±1.0	$> 3.4 \times 10^{-2}$
368.0	2.5±0.3	—
579.4	3.7±0.6	$(1.6 \pm 0.6) \times 10^{-2}$
		$(1.0 \pm 0.2) \times 10^{-2}$ †
628.9	6.4±1.0	—
712.2	> 5	—
787.3	> 5	—
828.6	4.8±0.7	$(3.5 \pm 1.0) \times 10^{-2}$
1206.8	3.8±0.7	—
1226.9	> 4.5	$(4 \pm 1) \times 10^{-2}$ †
1364.3	—	—
1516.7	—	$(1.0 \pm 0.5) \times 10^{-2}$

† From coincidence measurements.

where L/(M+N+ . . .) is assumed to be about 3 (this value is not critical). The number of transitions is given in per cent of the total number of disintegrations. Multipolarities of orders > M3 and E3 are left out, as all coincidences seem to be prompt, and no other indications for such transitions have been found.

4.1. THE 368 AND 579 keV TRANSITIONS

Earlier investigations [4, 5, 6]) have shown that the 368 keV transition is an E2 transition which goes to the ground state. Our K/L-ratio (2.5 ± 0.3) agrees well with the theoretical value of 2.44 for an E2 transition. The intensity of this transition accounts for 98.5 per cent of all disintegrations.

For the 579 keV transition, the measured K/L-ratio (3.7 ± 0.6) and K-conversion coefficient ($(1.6\pm0.6)\times10^{-2}$ and $(1.0\pm0.2)\times10^{-2}$) agree with an E2 transition (3.71 and 1.43 ± 10^{-2} resp.), although this does not fully exclude a small admixture of M1 radiation (6.1 and 5.13×10^{-2} resp.), and thus one cannot predict the spin of the second excited state.

In this connection it is interesting to make a comparison with the neighbouring nucleus Hg^{198}. Several investigations [27]) have shown that the levels in Hg^{198} are 0+ (0 keV), 2+ (411 keV), and 2+ (1087 keV). From the 411 and 1087 keV levels there are E2 transitions direct to the ground-state, while a 676 keV transition between the two 2+ states is a 60 % E2+40 % M1 mixture. If similar conditions hold for Hg^{200}, the 947 keV level should be 2+ and the 579 keV transition would be a mixture of E2 and M1. However, one would also expect a cross-over transition of electric quadrupole character to show up in the measurements, as is the case in Hg^{198}. The following gamma intensity relations have been found:

$$\text{in } Hg^{198}\text{: } \frac{\gamma_{1087}}{\gamma_{676}} = 3.7 \pm 0.9 \text{ [27]},$$

$$\text{in } Hg^{200}\text{: } \frac{\gamma_{947}}{\gamma_{579}} < 0.05.$$

In view of this fact it seems reasonable to assume 4+ for the second excited state in Hg^{200} and pure E2 character for the 579 keV transition. This assumption is confirmed by recent results from angular correlation measurements [28]). The relative intensity of this transition is calculated to be 15 per cent.

4.2. THE 252, 289, 309, 1207, 1227 AND 1517 keV TRANSITIONS

For these transitions it is not possible to decide multipolarities with certainty, as the information is not sufficient. For this reason, only pure transitions have been considered.

The K-conversion coefficient of the 1227 keV transition $(4\pm1)\times10^{-3}$ suggests an E2 transition ($\alpha_K = 3.35\times10^{-3}$). This is also consistent with

the measured K/L-ratio (> 4.5) compared with the theoretical value of 5.5. In spite of the fact that this E2 assignment is very doubtful, it will be accepted in the following discussion on multipolarities.

As the total gamma intensity of the two transitions of 1207 and 1227 keV is known (see table II), the K-conversion coefficient can then be calculated for the 1207 keV transition. It is found to be $(1.3\pm0.5)\times10^{-2}$. This indicates that the 1207 keV transition would be of M1($\alpha_K = 7.88\times10^{-3}$) M2($1.87\times10^{-2}$) or E3 ($7.14\times10^{-3}$) character with the following theoretical K/L-ratios. 6.3, 5.9 and 4.5 resp., none of which is in agreement with the experimental value (3.8 ± 0.7). The M1 assignment for this transition is in accordance with angular correlation measurements [28]).

For the 289 keV transition, the conversion coefficient ($> 5\times10^{-1}$) excludes electric radiation of multipolarities $<$ E4, and the K/L-ratio (3.4 ± 0.6) gives the best agreement with the theoretical value for M2 radiation (4.2). This is in accordance with a negative parity of the 1885 keV level, as the 1227 keV transition is supposed to be an E2 transition, and thus consistent with an allowed K-capture transition to this level. The fact that the 252 keV transition is very probably an M1 transition (see below), also supports the M2 assignment of the 289 keV transition. The parity of the 2137 keV level should then also be negative, giving possibilities for an allowed K-capture transition to this level.

The M1 assignment of the 252 keV transition is based on the K/L-ratio (5.1 ± 0.8) compared with the theoretical value (6.1) and conversion coefficient $> 2\times10^{-1}$ (theoretical value $= 4.4\times10^{-1}$). The total intensity of the 252 keV transition is found to be about 0.6 per cent, and the log *ft*-value for K-capture to the 2137 keV level = 6.5—7. The spins and parities of the two levels of 2137 and 1885 keV are supposed to be the same (2— or 3—), corresponding to allowed K-capture transitions. For these two states 1- can be excluded, as no transition is observed direct to the ground state from the 1885 keV level.

If the negative parity assignment of the 1885 keV level is accepted, the 1517 keV transition should be an E1, M2 or E3 transition. The relatively high conversion coefficient is rather uncertain, but excludes probably E1 radiation (theoretical conversion coefficient $= 9.22\times10^{-4}$). The experimental value ($(1.0\pm0.5)\times10^{-2}$) has then to be compared with theoretical values for M2 (1.01×10^{-2}) and E3 (4.37×10^{-3}).

For the 309 keV transition, the experimental conversion coefficient does not exclude any multipolarity with certainty, but the K/L-ratio (5.2 ± 1.0) indicates M1 (5.96), E1 (6.00) or M2 (4.26). The possible multipolarities of the 1207 keV transition that should be in cascade with the 309 keV transition and the above postulated negative parity of the 1885 keV level give the following four possibilities for the transitions of 309 and 1207 keV respectively:

309		1207
M1	———	M2
M1	———	E3
E1	———	M1
M2	———	M1

Transition intensities do not exclude any of these possibilities, and it seems impossible to predict anything about the intermediate state.

4.3. THE 629, 712, 787 AND 829 keV TRANSITIONS

The conversion coefficient of the 829 keV transition ($(3.5\pm1.0)\times10^{-2}$) is consistent with M1 (2.05×10^{-2}) or M2 (5.09×10^{-2}) radiation, but the K/L-ratio (4.8 ± 0.7) favours the M2 assignment. The theoretical K/L-ratios for M1 and M2 radiation of this energy are 6.07 and 5.28 resp. Angular correlation measurements [28]), however, favour the M1 assignment.

For the three transitions of 629, 712 and 787 keV one can point out only that the K/L-ratios indicate E1 or M1 transitions.

5. Discussion

Adyasevich *et al.* [9]) have, by neutron-capture experiments, measured a great number of transitions in Hg^{200}. The low energy levels found in these experiments are 0.37, 0.95, 1.10, 1.59, 1.73, 2.02, 2.10 and 2.40 MeV. All of these levels are fed directly from the 0— capture-state at 8.03, MeV, and all of them except the 0.95 MeV level, decay directly to the ground-state. Most of the levels are in agreement with levels given in fig. 10, but for some levels discrepancies exist. The levels at 1.10 and 2.02 MeV have not been observed in the decay of Tl^{200}, and some of the levels given in fig. 10 are not seen in the neutron-capture experiments. The most predominant difference is the transitions direct to the ground-state. Several of these transitions have not been observed from the corresponding levels found in the decay of Tl^{200}. Especially the transition from the 1.73 MeV level to the ground-state seems to be strange, as the transition from this level to the first excited state is not reported by Adyasevich *et al.*, whereas in the decay of Tl^{200} only the latter transition is observed.

In the neighbouring even-mass Hg isotopes, only the lowest excited states are known. In all nuclei with masses from 196 to 202 the energy of the first excited levels (2+) is about 400 keV [4]). The second excited state is hitherto known only in the two isotopes Hg^{198} [27]) and Hg^{200}. The energies are in both cases about 1 MeV above the ground-state, but the level assignments are, as already mentioned, different: 2+ in Hg^{198} and 4+ in Hg^{200}. The ground-state assignments of the neighbouring odd Tl isotopes seem to be 2— as in Tl^{200}. Tl^{204} is shown to be 2— [29]), and for

Tl^{202} the same assignment is very probable [30]). For Tl^{198}, the spin is found to be 2 [31]), but the negative parity is not experimentally confirmed.

The measurements on energy levels in Hg^{200} will continue in order to establish the spins and parities of the higher excited states in Hg^{200}. A search for an isomer in Tl^{200} will also be carried out. Possibilities exist for the proton and neutron to couple to a high spin, thus giving possibilities for an isomeric state. Isomeric transitions are also found in Tl^{198} (M4) [4]), Tl^{202} (E3) and Tl^{204} (E3) [30 32]). In Tl^{200}, however, no isomeric state with a half-life > 3 min has been observed neither in alpha-bombarded gold, nor the decay of Pb^{200}.

Thanks are due to Professor Manne Siegbahn and to our collegues at the Nobel Institute. In particular we should like to thank Dr. I. Bergström for his kind interest and many valuable discussions. We should also like to thank Professor Kai Siegbahn, Institute of Physics at the University of Uppsala. Finally we are much indebted to Dr. H. Atterling and Ing. Å. Svanheden and to the members of their cyclotron staffs for several in bombardments.

Note added in proof: In a recent investigation of the decay of Tl^{198}, Fisher and Knapp[33]) have reported two gamma rays of energy 637 and 588 keV in Hg^{198}, of which one probably connects a 4+ state with the 411 keV 2+ state. The 947 keV 4+ level in Hg^{200} should be compared with this new 4+ level in Hg^{198} rather than with the 2+ level at 1087 keV.

References

1) K. E. Bergkvist, I. Bergström, C. J. Herrlander, S. Hultberg, H. Slätis, E. Sokolowski, A. H. Wapstra and T. Wiedling, Phil. Mag. **46**(1955) 65
2) D. A. Orth, L. Marquez, W. J. Heiman and D. H. Templeton, Phys. Rev. **75** (1949) 1100
3) H. I. Israel and R. G. Wilkinson, Phys. Rev. **83** (1951) 1051
4) I. Bergström, R. D. Hill and G. de Pasquali, Phys. Rev. **92** (1953) 918
5) R. H. Davis, A. S. Divatia, R. D. Moffat and D. A. Lind, Phys. Rev. **100** (1955) 1266
6) R. Barloutaud, T. Grjebine and M. Riou, Compt. rend. **242** (1956) 1284
7) F. D. S. Butement and R. Shillito, Proc. Phys. Soc. **65** A (1952) 945
8) B. B. Kinsey and G. A. Bartholomew, Can. J. Phys. **31** (1953) 1051
9) B. P. Adyasevich, L. V. Groshev and A. N. Demidov, Conf. Acad. Sci. USSR on Peaceful Use of Atomic Energy, Phys. Math. Sci. July (1955) p. 270; Consultants Bureau Trans. p. 195
10) C. J. Herrlander, R. Stockendal, J. A. McDonnel and I. Bergström ,Nuclear Physics **1** (1956) 643
11) R. Stockendal and K. E. Bergkvist, Nuclear Instruments **1** (1957) 53
12) A. Hedgran, N. Svartholm, and K. Siegbahn, Proc. Phys. Soc. A **63** (1950) 960
13) H. de Waard, Nucleonics **13 : 7** (1955) 36
14) H. Slätis and K. Siegbahn, Arkiv. f. Fysik **1** (1949) 339
15) T. R. Gerholm, Rev. Sci. Instr. **26** (1955) 1069
16) M. C. Michel and D. H. Templeton, Phys. Rev. **93** (1954) 1422
17) T. R. Gerholm, Arkiv f. Fysik **11** (1956) 55
18) L. Sliv *et al.*, privately circulated tables.
19) C. S. Wu, Beta and Gamma ray Spectroscopy, Ed. Kai Siegbahn (North-Holland Publishing Co., Amsterdam, 1955) Chapter XI

20) E. Feenberg and G. Trigg, Rev. Mod. Phys. **22** (1950) 399
21) P. F. A. Klinkenberg, Rev. Mod. Phys. **24** (1952) 63
22) J. B. Reinolds, R. L. Christensen, D. R. Hamilton, A. Lemonick, F. M. Pipkin and H. H. Stroke, Phys. Rev. **99** (1955) 613A
23) R. Stockendal, J. A. McDonell, M. Schmorak and I. Bergström, Arkiv f. Fysik **11** (1956) 165
24) L. W. Nordheim, Phys. Rev. **78** (1950) 294; Rev. Mod. Phys. **23** (1951) 322
25) A. H. Wapstra, Physica **21** (1955) 385
26) M. E. Rose, (G. M. Goertzel and C. Swift), privately circulated tables.
27) L. G. Elliott and J. L. Wolfson, Phys. Rev. **82** (1951) 333
C. D. Schrader, E. B. Nelson and J. A. Jacobs, Phys. Rev. **90** (1953) 159
D. Schiff and F. R. Metzger, Phys. Rev. **90** (1953) 849
28) T. Lindqvist, private communication
29) T. Yuasa, J. Laberrigue-Frolow and L. Feuvrais, J. Phys. Radium **16** (1955) 39; Compt. Rend. **238** (1954) 1500
30) I. Bergström, private communication
31) G. T. Seaborg, private communication
32) S. H. Vegors Jr. and P. Axel, Phys. Rev. **101** (1956) 1067
33) P. S. Fisher and V. Knapp, Proc. Phys. Soc. A **69** (1956) 541

Nuclear Physics **3** (1957) 185—192; *North-Holland Publishing Co., Amsterdam*

THE POLARIZATION OF 155 MeV PROTONS ELASTICALLY AND INELASTICALLY SCATTERED FROM CARBON

R. ALPHONCE, A. JOHANSSON AND G. TIBELL

The Gustaf Werner Institute for Nuclear Chemistry, University of Uppsala

Received 7 December 1956

Abstract: The polarization of 155 MeV protons elastically and inelastically (4.43 MeV level) scattered from carbon has been measured for angles up to 35° (lab. system). The energy spread of the protons was small enough to allow separation of energy levels by absorbers in a range telescope. The asymmetries were determined for two absorber settings, one corresponding to elastically scattered protons, and the other to elastically plus inelastically scattered protons. The elastic polarization rises from zero at 2° to a maximum of 99.5 % at 21°, then goes through a minimum of −18 % at 32°.5 and reaches 28.4 % at 35°. The inelastic polarization appears to increase from 59 % to 96 % in the angular region 16°.2 to 27.°4 and then to decrease to 2 % at 35°.

1. Introduction

Since the first publication of results from experiments with beams of polarized high energy protons in 1953 [1]) extensive studies of polarization effects have been performed at a number of laboratories. A recent report of work done at Berkeley [2]) includes a full list of references.

In earlier experiments it has been difficult to sort out the elastically scattered protons for angles larger than a certain value where the contribution from inelastic scattering becomes appreciable. Because of the small energy spread of the external proton beam of the Uppsala synchrocyclotron it has been possible to determine the elastic polarization as well as the inelastic polarization (4.43 MeV level) for protons scattered from carbon.

2. Experimental Arrangements

Figure 1 gives a general view of the geometry of the experiment. Both scatterings took place outside the cyclotron tank. The internal beam has been extracted by the regenerative method [3, 4]). At this institute the fringing field of the cyclotron magnet is used as a peeler.

The external proton beam passed through two quadrupole lenses before reaching the first target, situated 14 m from the cyclotron. At this point the beam intensity was approximately 10^{10} protons per second within a nearly rectangular area, 3 mm wide and 11 mm high. The energy of the beam was 185 MeV. The energy spread of the protons has been determined with

a magnetic analyser [5]) and found to be not greater than 1 MeV. An estimation based on the measured range straggling confirmed this result.

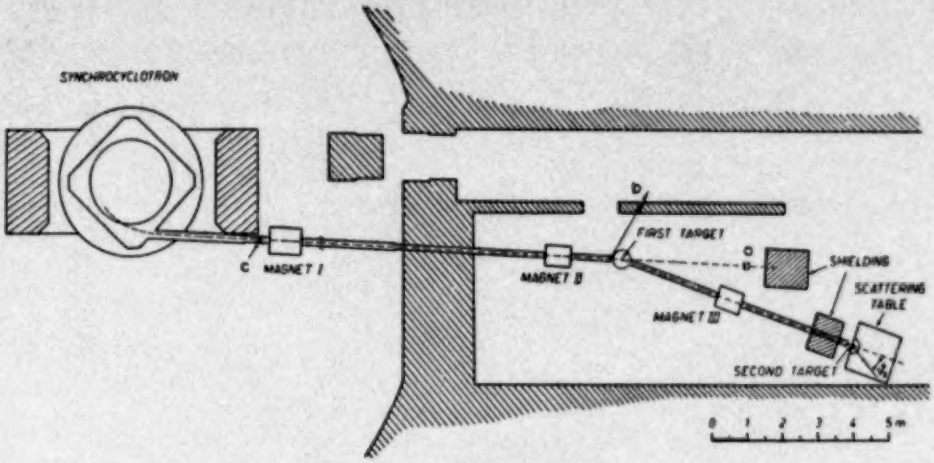

Fig. 1. General view of the experimental arrangements.

As first target a 24 MeV thick carbon disc was used. For geometrical reasons the first scattering angle had to be as large as 16°.2.

The angular spread of the once scattered beam was 0°.76 where the geometrical divergence of the beam contributed 0°.18. A third quadrupole lens placed half way between first and second targets focused the protons on the second scatterer. Here the intensity of the beam was approximately 10^5 protons per second over an area 6 mm wide and 35 mm high. A collimator with a rectangular slit 39 mm high was placed 10 cm in front of the second scattering target. The slit was 10 mm wide for angles larger than 5° and 4 mm in the small angle region. The background resulting from scattering in air was eliminated by placing the target in an evacuated chamber. Three different targets were used, and they are listed in table I together with the r.m.s. angular resolution for each case.

TABLE I

Angular resolution for the different scattering angles

ϑ_2°	Target thickness (g/cm²)	R.m.s. angular resolution (°)		
		geom.	mult. scatt.	total
2, 2.5	0.30	0.34	0.17	0.38
3, 4	0.79	0.34	0.29	0.45
6–27.4	2.09	0.55	0.49	0.74
30–35	2.09	1.11	0.49	1.21

The protons were detected in a triple coincidence telescope (resolution time 10^{-8} sec) with plastic scintillation crystals and EMI 6260 photomultipliers. The details of the telescope are shown in figure 2. The first

crystal defined the solid angle accepted by the telescope, and it was placed 50 cm from the second target for angles up to 27°. 4. For the three largest angles the telescope was moved 30 cm closer to the second target. For these angles the scattering chamber had to be removed, and the target was placed in air.

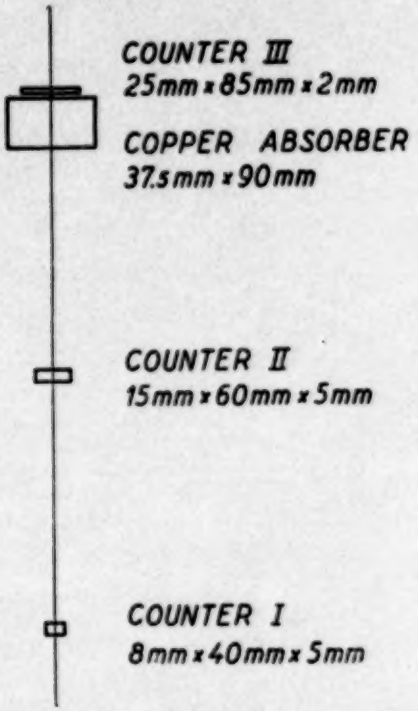

Fig. 2. Scale drawing of the triple coincidence telescope

The coincidence telescope was rigidly mounted on a scattering table which could be rotated about a horizontal axis. The alignment of the table was made with X-ray films which were scanned with a photometer after exposure. The distance between the two films was 110 cm. With this method it was possible to measure a misalignment as small as approximately 0.15 mm at the front and 0.3 mm at the back of the scattering table resulting in a possible angular error of 0°.02.

The beam was monitored by three independent monitors (a, b, and c in fig. 1):

a) A Faraday cup placed in the primary beam about four metres from the first target.

b) A double coincidence telescope which received protons scattered at 60° from the end window of the first vacuum system. The telescope counters were placed behind a concrete wall. Plastic scintillation crystals and EMI 5311 photomultipliers were used.

c) An ionization chamber filled with dry air located in the vacuum tube about three metres from the cyclotron tank.

The three monitors gave a reasonably constant counting ratio during the measurement of the asymmetry for any one angle.

3. Experimental Procedure

A range curve was determined with the telescope set at an angle of 3°. Copper absorbers were placed immediately before the last crystal. To compensate for the fact that the proton path was slightly longer in the outer parts of the absorber an aluminium plate of a special profile was inserted during the determination of the range curve. This plate was made to correspond to 1 mm of copper in the middle of its profile and thinner towards the edges. The range curve was used to determine the proper absorber thicknesses.

The asymmetries in the scattering from the second target were determined in the usual way by measuring the counting rate in one direction and then rotating the table through 180°. The second scattering plane made an angle of approximately 3° to the plane of the first scattering. The fact that the scattering had to be studied in this plane was due to a 3° inclination of the rectangular beam profile on the second scatterer. The effect of this inclination on the measured asymmetries was negligible.

For each angle two asymmetries were determined with two different absorber settings, one (A) chosen in such a way that the triple coincidence telescope accepted only those protons which had been elastically scattered in both targets. The other (B) was such that the energy threshold was lowered by an amount equal to the first excited level in carbon (4.43 MeV).

4. Auxiliary Experiment

For the treatment of the results of the asymmetry measurements it was necessary to know the contribution to the scattering from the ground and the various excited levels of carbon. For this reason the ratio of cross sections

TABLE II

Peak height ratios for protons scattered from carbon

$\vartheta°$	$i(4.43)/e$	$i(9.61)/e$
15	0.07	0.02
18	0.18	0.06
21	0.36	0.13
24.5	0.77	0.32
28	1.34	0.75
30	1.72	0.99
32.5	2.35	1.57
35	2.52	1.84
40	1.78	1.61

for elastically and inelastically scattered protons from carbon was measured with a magnetic analyser. The measurements were made at nine angles covering the energy range from 0 to 9.6 MeV excitation. The cross section

ratios were computed from the peak heights, and they are listed in table II where e denotes the height of the elastic peak, i (4.43) and i (9.61) the heights of the inelastic peaks corresponding to the 4.43 and 9.61 MeV levels respectively. The inelastic peak at 7.65 MeV was found to be negligible.

5. Treatment of Results

In the calculation of the polarizations from the measured asymmetries it has been assumed that the relation

$$\varepsilon = P_1 P_2 \tag{1}$$

is valid for the elastic as well as the inelastic scattering events. In eq. (1) ε and P denote asymmetry and polarization as conventionally defined. For pure elastic scattering eq. (1) has been proved on the basis of invariance considerations. In a following paper [6]) it is shown that in the first Born approximation eq. (1) is also correct for collective excitations. If in the future eq. (1) would be shown invalid for inelastic scattering, the "polarizations" calculated here are to be considered as asymmetries obtained with a 100 % polarized proton beam. Then the validity of eq. (1) is important only for the determination of the polarization of the protons scattered inelastically at the first target. The number of these is small compared to the number of protons scattered elastically. (See table II.) Eq. (3) below shows that the resulting uncertainty in P_{1i} only affects the determination of P_{2i} and only at angles where ν_1 and ν_2 are of comparable size. These angles lie well within the region of validity for the approximation used in the paper just referred to, and there is good reason to believe that the 4.43 MeV level in carbon is due to collective excitation [7]). Therefore no appreciable errors are introduced by the use of eq. (1).

Thus, assuming eq. (1) to hold for the two types of scattering studied here one obtains

$$\varepsilon_A = P_{1e} P_{2e} \tag{2}$$

$$\varepsilon_B = \frac{P_{1e} P_{2e} + \nu_1 P_{1i} P_{2e} + \nu_2 P_{1e} P_{2i}}{1 + \nu_1 + \nu_2} \tag{3}$$

where

indices 1 and 2 refer to the first and second scatterer respectively,

indices e and i refer to elastic and inelastic events respectively,

ν_1 is the mean number of protons (case B) scattered inelastically from the first target and elastically from the second divided by the number of protons scattered elastically from both targets,

ν_2 refers to the protons scattered first elastically and then inelastically.

In the derivation of these formulae it was assumed that no inelastic events were recorded in case A, and that in case B no inelastic events corresponding to a total energy loss in both scatterings of more than 4.43

MeV were detected. In this case the values of r_1 and r_2 could be determined directly from the first column of table II. In columns 1—4 of table III are given the measured asymmetries and the polarization values calculated from formulae (2) and (3).

TABLE III

$\vartheta_2°$	ε_A %	ε_B %	Uncorrected		Corrected	
			P_e %	P_1 %	P_e %	P_1 %
2	−3.7±5.8		−4.4±6.9			
2.5	8.1±6.8		9.6±8.1			
3	−0.5±4.2		−0.6±5.0			
4	32.3±7.0		38.4±8.3			
6	37.7±1.4		44.8±1.7			
8	40.8±2.1		48.5±2.5			
10	45.6±2.2		54.2±2.6			
11	50.2±2.2		59.6±2.6			
12	50.7±3.0		60.2±3.6			
13	54.5±3.8		64.7±4.5			
15	64.4±1.0		76.5±1.2			
16.2	70.9±1.4	68.0±1.5	84.2±0.8	64.5±12.3	84.3±0.8	59.0±18.5
18	76.3±2.2	72.7±1.4	90.6±2.6	72.8±20.9	91.4±2.8	71.8±23.4
20	81.9±1.4	77.8±1.5	97.3±1.7	82.2±11.8	98.7±1.9	74.9±12.6
22.5	79.8±2.2	74.5±2.1	94.8±2.6	79.5±10.1	96.7±3.2	74.7±11.5
25	54.0±3.4	60.5±2.8	64.1±4.0	83.9±9.4	61.2±5.0	90.5±10.9
27.4	22.6±6.1	46.7±5.4	26.8±7.2	81.5±13.7	16.0±9.3	96.2±16.1
30	16.8±4.8	28.6±3.8	20.0±5.7	43.0±8.1	9.8±8.8	51.1±9.6
32.5	−7.3±5.6	19.9±4.7	−8.7±6.8	38.8±8.8	−26.1±9.6	51.5±10.1
35	18.2±6.0	9.2±4.1	21.6±7.1	6.4±7.7	28.4±10.2	2.3±8.8

However, straggling introduces some overlapping of the peaks. In columns 5 and 6 of table III corrections for these overlappings have been applied resulting in shifts in the values of the polarization. In the application of these corrections the cross section ratios and the straggling determined from the range curve were used to calculate the amount of overlapping. The effect of the inelastic peak at 7.65 MeV was negligible. The resulting formula for case A was equal to the one given above for case B with r_1 and $r_2 \ll 1$. For case B the formula was generalized to include contamination from scattering events where the protons had suffered an energy loss up to 9.61 MeV (third excited level of carbon). The errors quoted in columns 5 and 6 of table III include estimated uncertainties of the corrections. All other errors are due to counting statistics only.

As a check on the correction method the experimentally found ratio between the counting rates for the two absorber settings was compared at each of the angles with that calculated from the results obtained with the magnetic analyser. They agreed fairly well.

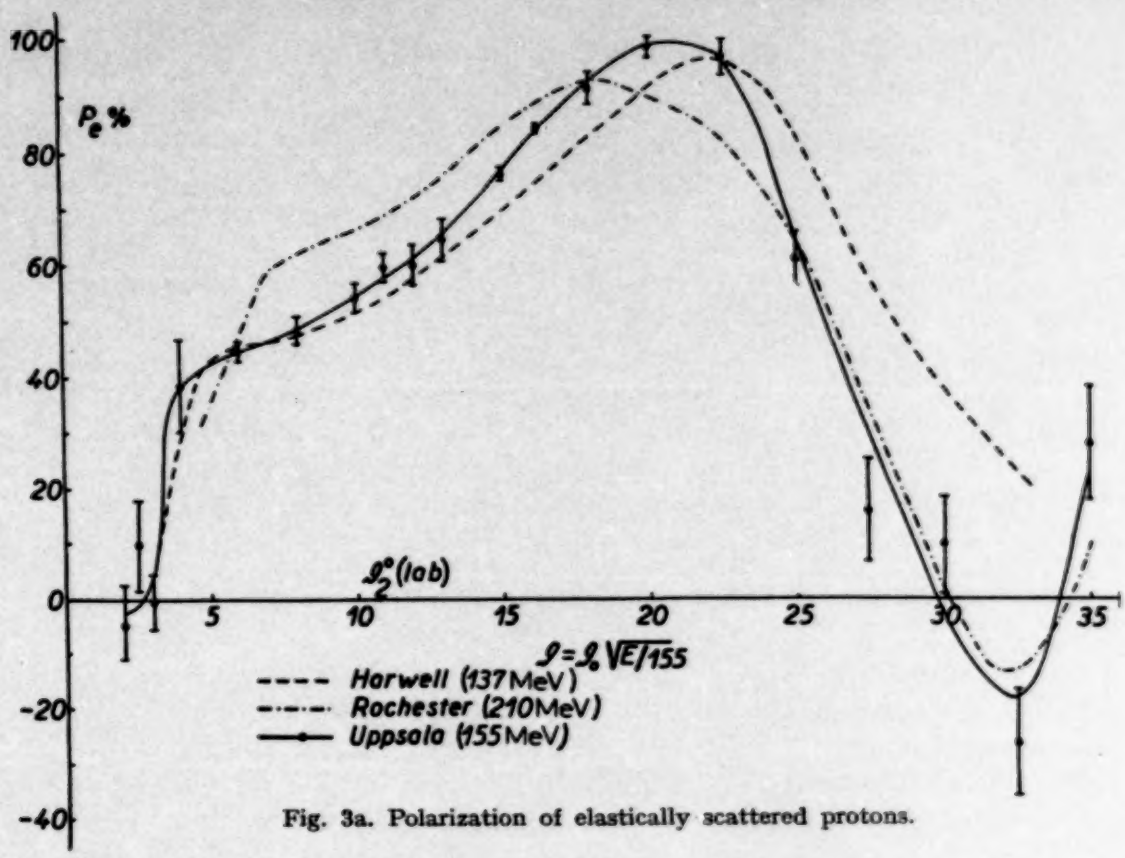

Fig. 3a. Polarization of elastically scattered protons.

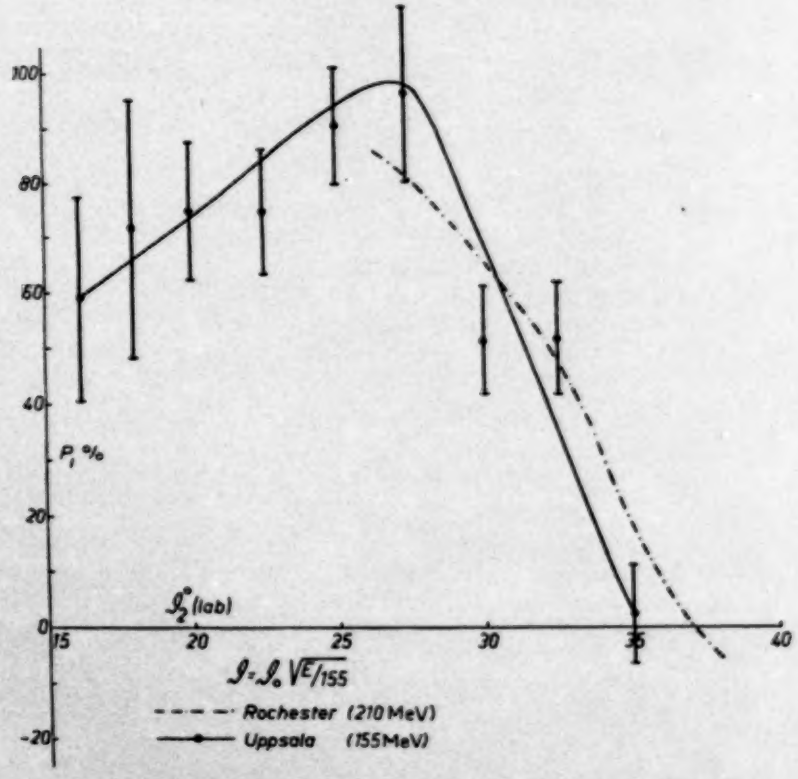

Fig. 3b. Polarization of inelastically scattered protons.

6. Concluding Remarks

The values of the elastic polarization obtained in the present experiment are also given in fig. 3a together with similar results from Harwell [8]) and Rochester [9]). The angular scale has been transformed according to the formula

$$\vartheta = \vartheta_0 \sqrt{\frac{E}{155}}.$$

As is seen from table III and fig. 3b the polarization of the inelastically scattered protons from carbon (4.43 MeV level) is positive and rather high for angles between 16° and 32°. These results can explain the difference between the curves obtained at Harwell and Rochester. In the latter experiment purely elastic events were separated whereas in the former the energy spread of the proton beam was too large for a complete separation.

The authors wish to thank Professors T. Svedberg and P. Ohlin for their great interest in this work, Dr. H. Tyrén for active encouragement during the whole experiment and especially for making the magnetic analyser available, Drs. W. J. Swiatecki, Th. Maris, and P. Hillman for stimulating discussions. Thanks are also due to Mr. Å. Svanheden for his successful work with the extraction of the beam, and to his cyclotron crew for assistance. The work has been supported by the Swedish Atomic Energy Commission.

References

1) C. L. Oxley, W. F. Cartwright, J. Rouvina, E. Baskir, D. Klein, J. Ring and W. Skillman, Phys. Rev. **91** (1953) 419
2) O. Chamberlain, E. Segrè, R. D. Tripp, C. Wiegand and T. Ypsilantis, Phys. Rev. **102** (1956) 1659
3) K. J. Le Couteur, Proc. Roy. Soc. A **232** (1955) 236
4) A. V. Crewe and J. W. G. Gregory, Proc. Roy. Soc. A **232** (1955) 242
5) A. Lovati and H. Tyrén, Journ. Sci. Instr. **33** (1956) 151
6) Th. A. J. Maris, Nuclear Physics **3** (1957) 213
7) Th. A. J. Maris and H. Tyrén, Nuclear Physics **3** (1957) 35
8) J. M. Dickson and D. C. Salter, reported at the Amsterdam Conference (1956)
9) W. G. Chesnut, E. M. Hafner and A. Roberts, Phys. Rev. **104** (1956) 449

Nuclear Physics **3** (1957) 193—196; *North-Holland Publishing Co., Amsterdam*

NIVEAUX DE ROTATION DE NOYAUX SANS AXE DE SYMETRIE

C. MARTY

Laboratoire de Physique et Chimie Nucléaires du Collège de France, Paris

Reçu le 10 Novembre 1956

Si un noyau atomique est représenté par N nucléons couplés à un core C, son hamiltonien, dans un modèle hydrodynamique peut s'écrire [1])

$$H = \mathscr{H} + \sum_\mu (I_\mu - J_\mu)^2 / \mathscr{I}_\mu = H_0 + \sum_\mu I_\mu^2 / \mathscr{I}_\mu - 2 \sum_\mu I_\mu J_\mu / \mathscr{I}_\mu. \qquad (1)$$

Dans (1) $\mathscr{H}$ ou H_0 ne contient que les variables intrinsèques du système (c'est-à-dire celles qui sont définies dans un système d'axes mobile lié au core C). I_μ, J_μ sont respectivement les composantes du moment angulaire total du système et du moment angulaire total des N nucléons, dans les axes mobiles. $\mathscr{I}_\mu$ est le moment d'inertie du système par rapport à l'axe mobile μ.

Lorsque la déformation est grande. il est possible d'étudier, par une méthode de perturbation [2]), l'effet des termes

$$H_1 = \sum_\mu I_\mu^2 / \mathscr{I}_\mu - 2 \sum_\mu I_\mu J_\mu / \mathscr{I}_\mu \qquad (2)$$

sur l'hamiltonien intrinsèque H_0. Si l'un des moments d'inertie est nul ou petit, le noyau a un axe de symétrie et on a le spectre de rotation habituel de Bohr-Mottelson.

Si les trois moments d'inertie sont du même ordre de grandeur, on a un noyau sans axe de symétrie; c'est ce cas qui est étudié ici.

H_0 commutant avec I_μ, l'approximation d'ordre zéro possède pour une énergie donnée E_0, les nombres quantiques usuels I et M de moment angulaire et un nombre quantique supplémentaire K, valeur propre de I_3, par exemple. Si $H_0 G = E_0 G$, la fonction d'onde d'ordre zéro contiendra des termes de la forme $D^I_{MK} G$ où les D^I_{MK} sont les représentations de rang $2I+1$ du groupe des rotations. En imposant à cette fonction d'onde d'être invariante par rapport aux transformations R_1, R_2, R_3 introduites par A. Bohr [1]), on peut déterminer les propriétés générales de l'approximation d'ordre zéro. En particulier lorsqu'il s'agit de noyaux pairs, les niveaux $I = 0, 2, 4, \ldots$ ont des fonctions d'onde de la forme

$$\psi_0(E_0, I, M, K) = \sqrt{(2I+1)/16\pi^2 (1+\delta_{0K})}\, \{D^I_{MK} + D^I_{M-K}\} G \quad (K = 0, 2, 4, 6 \ldots).$$

Les éléments de matrice de H_1, non nuls, sont

$$\begin{aligned}&\langle E_0 IMK\,|H_1|E_0 IMK\rangle = aI(I+1)+bK^2\\&\langle E_0 IMK+2|H_1|E_0 IMK\rangle = \{c(1+\delta_{0K})^{\frac{1}{2}}/2\}\, f_I(K+1) f_I(K)\end{aligned} \tag{3}$$

où

$$f_I(K) = [I(I+1)-K(K+1)]^{\frac{1}{2}},$$

$$a = \langle \mathcal{I}_1^{-1}+\mathcal{I}_2^{-1}\rangle/2, \qquad b = \langle \mathcal{I}_3^{-1}\rangle - a, \qquad c = \langle \mathcal{I}_1^{-1}-\mathcal{I}_2^{-1}\rangle/2$$

avec

$$\langle X\rangle = (G,\ XG).$$

En diagonalisant la matrice (3), on trouve les valeurs de l'énergie de

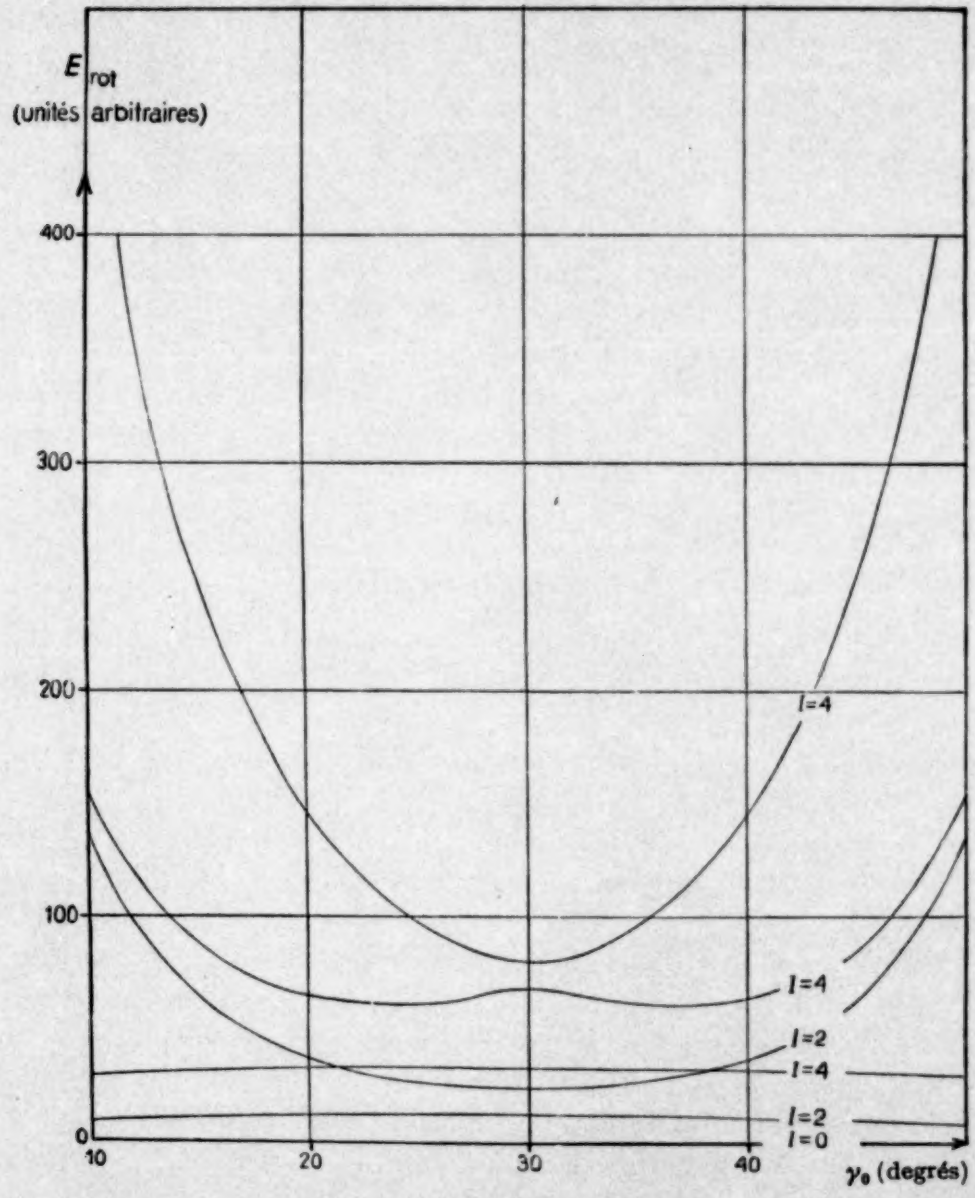

rotation E_{rot} du noyau. Sur la fig. 1, on a porté E_{rot} pour les niveaux $I = 0, 2, 4$, en fonction d'un paramètre angulaire γ_0, lié dans le modèle

initial de A. Bohr à la valeur d'équilibre des moments d'inertie: $\mathcal{I}_\mu \propto \sin^2(\gamma_0 - \mu \cdot 120°)$. Pour des raisons de symétrie, il est suffisant de faire varier γ_0 entre 0 et 60°; de plus la courbe représentative de E_{rot} est symétrique par rapport à 30° dans cet intervalle.

On remarque que pour $20° < \gamma_0 < 40°$, zône où l'approximation développée ici s'applique, il y a croisement d'un niveau $I = 4$ avec un niveau $I = 2$. A 30° la succession des niveaux est $I = 0, 2, 2$, au lieu de la suite habituelle $I = 0, 2, 4$; le rapport des énergies de rotation des deux niveaux $I = 2$ est alors exactement 2. En extrapolant ces résultats vers 0° et 60°, on retrouve l'ordre habituel des niveaux de rotation d'un noyau à symétrie axiale. Dans tous les cas les énergies de rotation des premiers niveaux 0, 2, 4 sont peu différentes de celles d'un noyau à axe de symétrie.

Si nous appelons f le niveau fondamental $I = 0$, a le niveau $I = 2$ le plus bas (pour $\gamma_0 = 30°$), b le niveau $I = 2$ le plus haut, on a pour fonctions d'ondes

$$\psi_f = \psi_0(E_0\,000), \qquad \psi_{\substack{a\\b}} = A_{\substack{a\\b}}\psi_0(E_0\,2M0) + B_{\substack{a\\b}}\psi_0(E_0\,2M2).$$

Le rapport des intensités de transition b → f à a → f, sous l'action d'un opérateur tensoriel T^k est fonction de

$$X = \langle b||T^k||f\rangle / \langle a||T^k||f\rangle = (A_b + B_b\varrho)/(A_a + B_a\varrho). \tag{4}$$

Pour des transitions quadrupolaires $\varrho = 2^{-\frac{1}{2}}\{\langle T_2^2\rangle + \langle T_{-2}^2\rangle\}/\langle T_0^2\rangle$.

Les coefficients A, B sont déterminés par le calcul de perturbations, mais ϱ est une fonction compliquée dépendant de la structure intrinsèque du noyau. Pour $\gamma_0 = 30°$, $X = 0.51\ (1-2.2\varrho)(1+0.71\varrho)^{-1}$.

On voit donc que le schéma des niveaux de rotation d'un noyau pair sans axe de symétrie est très différent de la suite habituelle deBohr-Mottelson La comparaison avec les données expérimentales montre que la plupart des noyaux fortement déformés ont un axe de symétrie, mais en se reportant à la figure 1, il est clair que d'assez larges variations par rapport à la symétrie axiale ne changent pas beaucoup les énergies de rotation des premiers niveaux $I = 0, 2, 4$. La famille de niveaux $I = 0, 2, 4$(K pair) n'est pas la seule possible; il existe, par exemple une bande $I = 3, 5 \ldots$ (K pair), mais possédant une fonction d'onde intrinsèque G' différente de G.

La suite $I = 0, 2, 2 \ldots$ que l'on obtient près de $\gamma_0 = 30°$ présente les caractéristiques de certains niveaux de noyaux intermédiaires (cf. ref. [3])) entre les noyaux magiques et ceux qui sont fortement déformés.

Pour savoir si ces noyaux intermédiaires relèvent du modèle décrit ici, il faudrait comparer la valeur de X donnée par (4) pour une transition E2 à la valeur expérimentale. Ceci n'est pas possible avec exactitude à cause du facteur inconnu ϱ.

Bibliographie

1) A. Bohr, Mat. Fys. Medd. Dan. Vid. Selsk **27** (1952) no. 14
2) C. Marty, Nuclear Physics **1** (1956) 85
3) L. Wilets et M. Jean, Phys. Rev. **102** (1956) 788

Nuclear Physics **3** (1957) 197—206; *North-Holland Publishing Co., Amsterdam*

CONCERNING LIFETIMES OF LOW ENERGY E1 GAMMA TRANSITIONS IN ODD MASS SPHEROIDAL NUCLEI

DONALD STROMINGER AND JOHN O. RASMUSSEN

Radiation Laboratory and Department of Chemistry and Chemical Engineering University of California, Berkeley

Received 11 December 1956

Abstract: A compilation of lifetime measurement data on low energy E1 transitions in odd-proton nuclei of the actinide region is given, and comparison is made with the single-particle lifetime formula. The comparison often shows a retardation of several orders of magnitude. Theoretical E1 matrix elements are calculated using Nilsson's spheroidal-well nucleon wave functions. The results show without exception a large retardation from the single-particle matrix elements. The selection rules in both the N, l, j, Ω representation and the N, n_z, Λ, Ω representation are considered. Quite generally in either representation selection rules forbid the combination of the large components of the wave functions with one another, and the various contributions of the small components to the E1 matrix element tend to cancel one another.

1. Experimental Information for Odd-Proton Nuclei

Over the past few years a large number of electric dipole transitions have been identified between low-lying states of odd-mass nuclei in the regions of spheroidal nuclei. Many of these have been found in the region of the actinide elements ($Z > 88$), and the present paper will be principally concerned with this region.

Table I lists the available data for electric dipole transitions of odd-proton nuclei in the actinide region. Most of these are of measured lifetime, and some have lifetimes shorter than the limits of detection. It is customary to compare gamma-transition rates with estimates from a "single-proton transition" formula. For the comparisons in table I we have employed the simplified formula of Moszkowski [1]):

$$\text{Transition probability} = \frac{0.693}{\text{half-life (sec)}} = 1.5 \cdot 10^{14} A^{2/3} E_\gamma^{\,3} S, \qquad (1)$$

where A is the mass number, E_γ is the gamma energy in MeV, and S is a statistical factor depending on initial and final proton state l and j values. We assume S equal to unity for these comparisons.

It is evident from table I that a large, though erratic, retardation of transition probability from the single-proton formula is the general rule.

TABLE I

Experimental E1 transition lifetimes for odd-proton nuclei in the actinide region.

Daughter nucleus	Energy of photon (MeV)	Half life of parent level (sec)	Partial half life of photon (sec)	Retardation factor from single proton formula	Ref.
$^{148}_{95}Am^{243}$	0.084	$< 4 \times 10^{-9}$	$< 5 \times 10^{-9}$	$< 2.5 \times 10^{4}$	a, b
$^{146}_{93}Np^{239}$	0.0756	$< 1.6 \times 10^{-9}$	$< 2 \times 10^{-9}$	$< 1.1 \times 10^{4}$	c, d
$^{144}_{93}Np^{237}$	0.0596	6.3×10^{-8}	1.6×10^{-7}	2.8×10^{5}	e
$^{144}_{93}Np^{237}$	0.0264	6.3×10^{-8}	$2.2_5 \times 10^{-6}$	3.5×10^{5}	e
$^{142}_{93}Np^{235}$	0.048	—	—	—	f
$^{142}_{91}Pa^{233}$	0.0869	3.7×10^{-8}	1.5×10^{-7}	8.2×10^{5}	f, g
$^{142}_{91}Pa^{233}$	0.0301	3.7×10^{-8}	2.2×10^{-7}	5.0×10^{4}	f, g
$^{140}_{91}Pa^{231}$	0.084	4.1×10^{-8}	1.4×10^{-7}	6.7×10^{5}	f, h
$^{140}_{91}Pa^{231}$	0.0255	4.1×10^{-8}	1.5×10^{-7}	2.0×10^{4}	f, h
$^{138}_{89}Ac^{227}$	0.027	4×10^{-8}	3.6×10^{-7}	5.7×10^{4}	i
$^{136}_{89}Ac^{225}$	0.040	$< 2 \times 10^{-9}$	$< 4.2 \times 10^{-9}$	$< 2.2 \times 10^{3}$	f

a. Engelkemeir, Fields and Huizenga, Phys. Rev. **90** (1953) 6
b. R. W. Hoff and L. Mann, unpublished data, 1955
c. F. Asaro and I. Perlman, Phys. Rev. **93** (1954) 1423
d. D. Strominger, Ph. D. Thesis, University of California (1956) (Radiation Laboratory Unclassified Report UCRL—3374) unpublished
e. Beling, Newton and Rose, Phys. Rev. **87** (1952) 670
f. F. S. Stephens, Ph. D. Thesis, University of California (1955) (Radiation Laboratory Unclassified Report UCRL—2970) unpublished
g. D. Engelkemeir and L. B. Magnusson, Phys. Rev. **94** (1954) 1395
h. D. Strominger and J. O. Rasmussen, Phys. Rev. **100** (1955) 844
i. Teillac, Rious and Desneiges, Compt. Rend. **237** (1953) 41

2. Nuclear Model Considerations

It should be noted again here that the mere existence of low-lying E1 transitions in odd-mass nuclei is not explainable in terms of transitions between states of lowest seniority (all nucleons paired except the odd one) in the spherical well model, since the required parity change and the spin change of one or zero is not to be found between orbitals within a given shell of the spherical well model. On the other hand, the explanation of these transitions is a simple and natural one in the spheroidal well model, where the ground state spin of an odd mass nucleus will in general be equal

to the *projection* of the total angular momentum of the odd nucleon on the principal symmetry axis.

Figure 1 is a reproduction of part of the level diagram of Nilsson [2]) for nucleons in a spheroidal well. In the encircled region are the near-lying

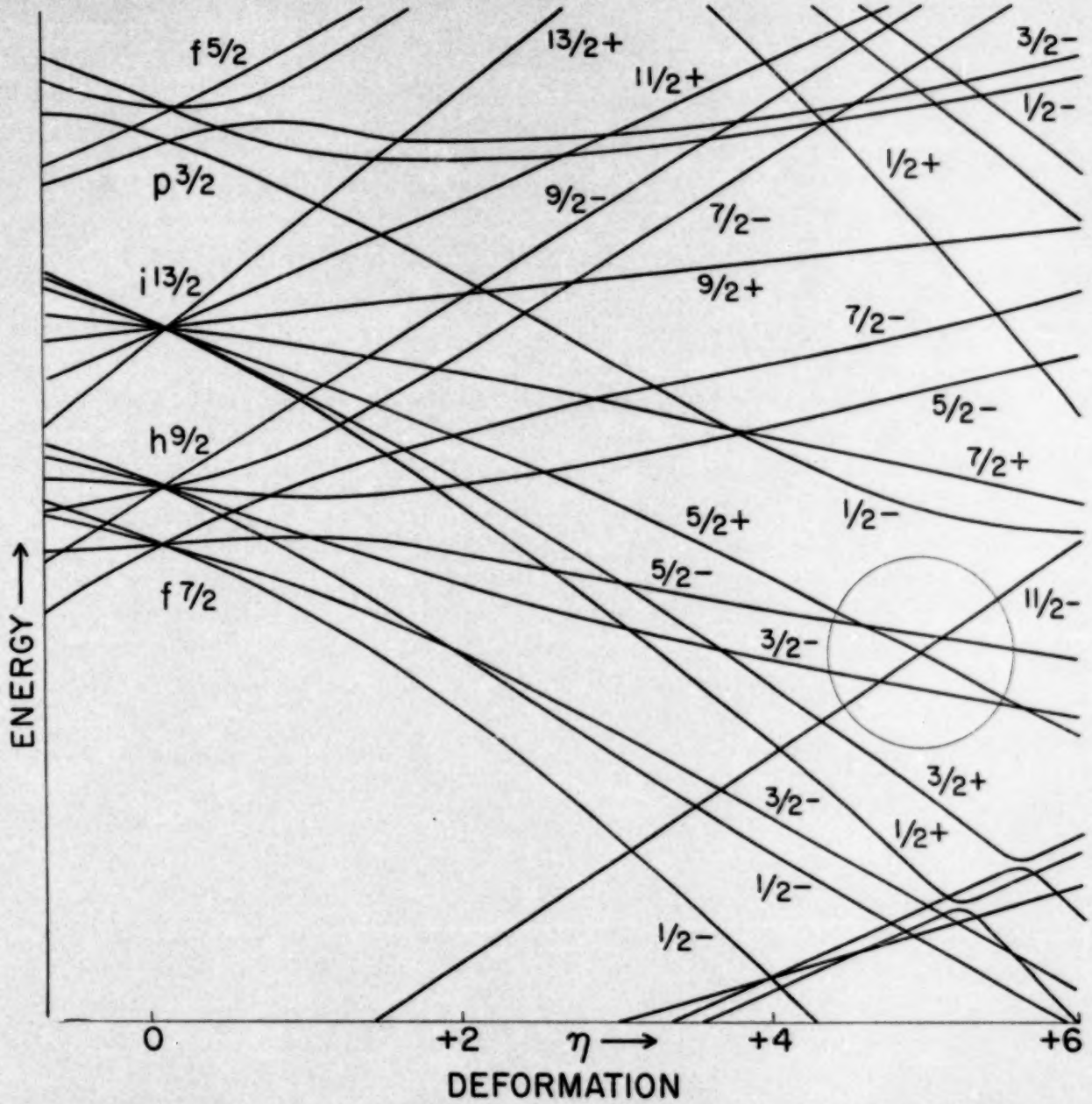

Fig. 1. A section of Nilsson's energy level diagram for nucleons in a spheroidal-well potential. The region encircled corresponds to low-lying and ground states of Np^{237}. The deformation parameter η is approximately twenty times as large as the deformation parameter $\delta = (R_{major} - R_{minor})/R_{average}$.

5/2+ and 5/2− levels which are believed to correspond to the ground and 59.6-keV states in Np^{237}, between which occurs a much-studied delayed E1 gamma transition. One also sees in this general vicinity many other

pairs of close-lying levels which could be connected by E1 gamma transitions.

As the properties of a particular nuclear state depend essentially on the deformation we must determine this quantity before we can consider detailed properties of intrinsic structure. An estimate of the deformation parameter η can be obtained from the empirically determined quadrupole moment. Nilsson [2]) has given the following approximate relationship:

$$Q_0 \approx 0.8ZR^2\delta(1+\tfrac{2}{3}\delta),$$

where Q_0 is the intrinsic quadrupole moment, Z is the atomic number of the nucleide, and R is the radius of charge of the nucleus ($\approx 1.2\times 10^{-13}A^{1/3}$ cm). η is approximately twenty times as large as δ.

Newton [3]) has determined the intrinsic quadrupole moment of Np^{237} from coulomb excitation experiments. From his value of $Q_0 \approx 11$ barns we obtain a value of $\eta \approx 5$.

The question of the highly retarded E1 transition rates has been an intriguing one. The spectacularly hindered (factor of 10^{15}) E1 isomer of 5.5 h half-life in Hf^{180} finds good qualitative explanation [4]) in terms of K-forbiddenness. However, for all the cases of table I except those in actinium, where state assignments are uncertain, we have no K-forbiddenness, the K-change never exceeding one. Some authors [5, 6]) have discussed the likelihood of neutron motion being generally admixed into a single-proton transition so as to effect a reduction from the single-proton estimate of equation (1).

In an early application [7]) of the Bohr-Mottelson spheroidal-well nuclear model to interpret levels of Np^{237} it was pointed out that a change in l (the odd-proton orbital angular momentum) exceeding one for the large components of the odd-proton wave function might be responsible for the retardation of the transition. It might be added here that a change in j exceeding one would likewise be a source of retardation if j were a fairly good quantum number. As soon as the Nilsson [2]) eigenfunctions in a spheroidal well were available, it was evident that the simple arguments about Δl or Δj hindrance could not account for very much retardation, since at the estimated deformation of Np^{237} neither j nor l are very good quantum numbers. For example, the Nilsson eigenfunction (No. 55) we assign to the ground state (5/2+) of Np^{237} is composed at deformation $\eta = +6$ of about 84 % $i_{13/2}$, 14 % $g_{9/2}$, 1.3 % $i_{11/2}$, 0.4 % $d_{5/2}$, and 0.3 % $g_{7/2}$ character. The eigenfunction assigned to the 59.6-keV state is, at the same deformation, about 79 % $h_{9/2}$, 7.6 % $f_{7/2}$, 7.4 % $f_{5/2}$, and 6.1 % $h_{11/2}$. There seem to be ample admixtures of j-values other than the principal value to allow E1 transitions to occur. As was learned from exact calculations of transition probabilities using these eigenfunctions, the various contributions from the small parts of the wave function tend generally to cancel one another.

3. Numerical Calculations of E1 Transition Rates

Nilsson's paper [2]) giving the eigenfunctions also gives general formulas for applying them to calculate electromagnetic transition probabilities of any desired multipolarity. Using his formulas (29), (35), (35b), and (41) we have calculated theoretical odd-proton E1 transition probabilities for the three values of prolate deformation for which Nilsson gives eigenfunctions and for various pairs of eigenfunctions which could be connected by low energy E1 transitions in the 82—126 proton shell.

Since there is a dependence on gamma energy and on nuclear size (i.e.

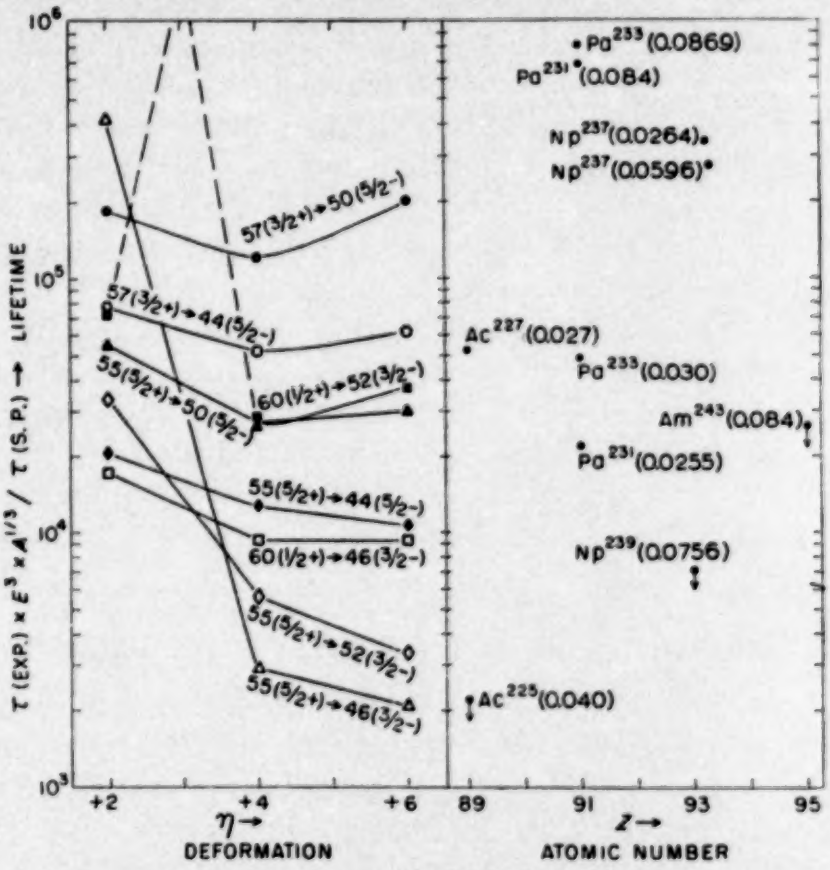

Fig. 2a. Calculated lifetimes as a function of deformation. Note that for purposes of comparison the calculated values are multiplied by $(E^3 \times A^{1/3})$ and divided by the value obtained from the single-proton formula. The deformation parameter η is approximately twenty times as large as the deformation parameter δ.

Fig. 2b. Experimental lifetimes as a function of atomic number for odd-proton nuclei in the actinide region. Note that a transition which proceeds as rapidly as predicted by the single-proton formula would have a value of unity on the ordinate scale of the figure.

on mass number), the results of the theoretical calculations of matrix elements will be here presented as a product $\tau\, E^3 A^{1/3}$ divided by the single-proton estimate, where τ is the mean-life in seconds for photon emission, E is the gamma energy in MeV, and A is the mass number. (The product $\tau\, E^3$ is inversely proportional to the so-called reduced transition probability

$B_e(1)$). Nilsson's formula [2]) for the transition probability of an E1 transition depends on mass number as the 1/3 power, whereas the simplified formula of Moszkowski [1]) (see eq. (1)), based on constant radial wave functions, gives a 2/3 power dependence on mass number.

Figure 2a shows the results of the theoretical calculations, and beside it with the same ordinate scale in fig. 2b are displayed the experimental life-time data. It is satisfying to note that the calculations always yield reduced transition probabilities lying within the same region as the experimental data.

Detailed agreement in individual cases is probably not to be expected. Quite generally the transitions are highly retarded and proceed by small parts of the wave function; hence, the transition probability will usually be quite sensitive to small details of the wave function and will strongly reflect small shortcomings of the model. We see, for example, that the calculation of transition 55—44 fails by a factor of 25 from agreeing with experiment in Np^{237}. For the 59.6 and 26.4-keV transitions in Np^{237} there is evidence [8]) from relative reduced transition probabilities that configuration mixing of states with $K \neq 5/2$ plays a significant role, a complication not taken into account in the theoretical calculations considered here.

A set of calculations was made earlier [9]) in which we calculated the radial integrals by the assumption of constant radial wave functions. The approximation in the case of these calculations proved to be a poor one, and results differed by as much as a factor of ten from those with correct harmonic-oscillator radial integrals.

4. E1 Selection Rules in Different Representations

The base vectors of the representation chosen by Nilsson [2]) for his calculations are eigenfunctions appropriate to the three-dimensional isotropic harmonic oscillator with no spin-orbit coupling. They are completely specified by the quantum numbers N, l, Λ, Σ; respectively, the principal oscillator quantum number, the orbital angular momentum, the orbital angular momentum component along the nuclear symmetry axis, and the intrinsic spin component along the symmetry axis. (The quantum number Ω is just the sum of Λ and Σ.) More appropriate in the spherical limit would be the ordinary spherical-shell model representation with base vectors specified by quantum numbers N, l, j, Ω. This representation is completely diagonal in the spherical limit.

For all the pairs of states taken for the calculations of E1 transition rates shown in fig. 2a one would find a vanishingly small transition probability as one approached the limit of no deformation. This forbiddenness could be correctly ascribed to violation of the selection rule $\Delta j = 0, \pm 1$ and in some cases to violation of the selection rule $\Delta l = \pm 1$.

For very large spheroidal deformation the above-mentioned representations may not be the most appropriate. Another useful representation takes the eigenfunctions in cylindrical coordinates of the anisotropic harmonic oscillator. Off-diagonal elements in the hamiltonian are contributed by the spin-orbit interaction and by deviations of the potential from harmonicity. Nilsson [2]) has discussed this representation in his appendix B. Eigenfunctions are specified by N, n_z, Λ, Ω; N and Ω having the same significance as before, n_z being the oscillator quantum number along the symmetry axis, and Λ the orbital angular momentum component along the symmetry axis.

Rassey and Moszkowski [10]) have obtained sets of eigenfunctions for a spheroidal well in the (N, n_z, Λ, Σ) representation. From their work at the deformation of about $\eta = +6$ the eigenfunction (No. 55) assigned to the ground state of Np^{237} is composed of 0.2 % (602), 1.3 % (613), 12 % (622), 17.4 % (633), and 69.2 % (642) where the quantum numbers in parentheses are N, n_z, and Λ respectively. The eigenfunction (No. 44) assigned to the 59.6-keV state is, at the same deformation, about 2.4 % (503), 2.1 % (512), 78.3 % (523), and 17.1 % (532). There seem to be ample admixtures to allow E1 transitions to occur. The detailed E1 calculations, however, show that contributions from small parts of the wave function tend to cancel one another.

Selection rules for E1 transitions in all the above representations can be derived. For the $|N, l, j, \Omega>$ functions we present the E1 selection rules in table II.

TABLE II

E1 Selection Rules in the N, l, j, Ω Representation.

ΔN	Δl	Δj	$\Delta\Omega$
± 1	$+1$	0, $+1$	0, ± 1
	-1	0, -1	

For the $|N, n_z, \Lambda, \Omega>$ functions we present the selection rules in table III.

TABLE III

E1 Selection Rules in the N, n_z, Λ, Ω Representation.

ΔN	Δn_z	$\Delta\Lambda$	$\Delta\Omega$
$+1$	$+1$	0	0
-1	-1	0	0
± 1	0	$+1$	$+1$
± 1	0	-1	-1

In table IV are given the appropriate quantum numbers for several of Nilsson's orbitals at large prolate deformation. Methods of assigning these quantum numbers have been discussed by Nilsson [2]).

TABLE IV

Spherical and Asymptotic Quantum Numbers for Nilsson's Orbitals

Nilsson's Orbital	N	Spherical Limit		Large Deformation Limit		Ω
		l	j	n_z	Λ	
44	5	3	7/2	2	3	5/2
46	5	3	7/2	3	2	3/2
50	5	5	9/2	1	2	5/2
52	5	5	9/2	2	1	3/2
55	6	6	13/2	4	2	5/2
57	6	6	13/2	5	1	3/2
60	6	6	13/2	6	0	1/2
36	5	5	11/2	3	2	5/2

By consulting table IV and figure 1 it it seen that no pairs of orbitals that can be associated with a low energy E1 transition can satisfy the selection rules of either table II or table III. Allowed transitions, such as that between orbital No. 55 to No. 36, occur between orbitals in different major shells and would generally involve several MeV energy difference.

Alaga [11]) has considered the role of the asymptotic quantum numbers in beta decay and has given beta selection rules in terms of them. Alaga has used these selection rules to classify many beta transitions in the region $150 < A < 190$. The comparisons of experimental data with Alaga's theoretical classifications indicate that these beta selection rules are very useful for explaining certain features of beta-decay transition rates in the regions of strongly deformed nuclei. Violation of selection rules in n_z or Λ in Alaga's study of beta decay resulted on the average in retardation of one order of magnitude.

The retardation of E1 gamma transitions from the single-proton formula, both the observed and the calculated, is generally several orders of magnitude, in contrast to the lesser effects in the beta decay studies. The reason for this difference is to be seen from a detailed examination of the small parts of the wave function in either the (N, l, j, Ω) or $(N, n_z, \Lambda, \Omega)$ representation. The small parts of the wave functions always give contributions to the E1 transition probability which tend to cancel one another. Thus, the low energy E1 transitions, being strictly forbidden in both the spherical limit and the large deformation limit, never acquire very large matrix elements at any deformation.

5. Odd-Neutron Actinide Nuclei and Nuclei in the Rare Earth Region

Our theoretical calculations have been confined to orbitals occurring in the odd-proton nuclei of the actinide region. More generally, low-lying

E1 transitions, many of measurable lifetime, are found for many odd mass nuclei in both major regions of stable spheroidal deformation ($150 < A < 190$ and $224 < A$). The theoretical basis for the retardation of E1 transitions in these other nuclei must be the same as that discussed in previous sections of this paper. Chase and Wilets [12]) have made calculations of E1 transition probabilities for Nilsson's orbitals appropriate to states of Lu^{175}, and they noted a theoretical retardation of about 10^4.

As a supplement to table I we have collected in table V the lifetime data on E1 transitions of odd-neutron actinide nuclei. In this case the transition life-times are compared with a "single-neutron transition formula." Some additional weak E1 transitions (316.1 keV and 334.5 keV) have also been observed [13]) branching from the 0.19 μsec state in Pu^{239}, and these transitions are more highly retarded than the other E1 transitions. The additional hindrance may be associated with the K-forbidden nature of these transitions ($\Delta K = -2$).

TABLE V

Experimental E1 Transition Lifetimes for Odd-Neutron Nuclei in the Actinide Region

Daughter nucleus	Energy of photon (MeV)	Half life of parent level (sec)	Partial half life of photon (sec)	Retardation factor from single-neutron formula	Ref.
$^{145}_{94}Pu^{239}$	0.106	1.9×10^{-7}	3.4×10^{-7}	5.2×10^{5}	a
$^{145}_{94}Pu^{239}$	0.0614	1.9×10^{-7}	1.9×10^{-6}	5.7×10^{5}	a
$^{141}_{90}Th^{231}$	0.185	$< 1.5\times10^{-9}$	$< 1.6\times10^{-9}$	$< 1.3\times10^{4}$	b, c
$^{141}_{90}Th^{231}$	0.143	$< 1.5\times10^{-9}$	$< 8.0\times10^{-9}$	$< 2.9\times10^{4}$	b, c
$^{135}_{88}Ra^{223}$	0.050	$< 2\times10^{-9}$	$< 3.2\times10^{-9}$	$< 4.8\times10^{2}$	c, d

a. D. Engelkemeir and L. B. Magnusson, Phys. Rev. **99** (1955) 135
b. F. S. Stephens, Ph. D. Thesis, University of California (1955), (Radiation Laboratory Unclassified Report UCRL—2970) unpublished.
c. D. Strominger, Ph. D. Thesis, University of California, (1956) (Radiation Laboratory Unclassified Report UCRL—3374) unpublished.
d. E. K. Hyde, Phys. Rev. **94** (1954) 1221

We are grateful to S. G. Nilsson for sending us his wave function calculations in advance of publication. We have gained much from stimulating discussions with Professor S. A. Moszkowski and are grateful to him and Mr. A. Rassey for sending us results of their very recent calculations. This work was performed under the auspices of the U. S. Atomic Energy Commission.

References

1) S. A. Moszkowski, Beta- and Gamma-Ray Spectroscopy, (Interscience, New York, 1955) pp. 373—395
2) S. G. Nilsson, Mat. Fys. Medd. Dan. Vid. Selsk **29** (1955) no. 16
3) J. O. Newton, private communication (1956)
4) Scharff-Goldhaber, McKeown, and Mihelich, Bull. Am. Phys. Soc. **1** No. 4 (1956) 206
5) J. M. Blatt and V. F. Weisskopf, Theoretical Nuclear Physics (Wiley, New York, 1952) pp. 624 sq
6) A. Bohr and B. R. Mottelson, Beta- and Gamma-Ray Spectroscopy (Interscience, New York, 1955) pp. 468—493
7) J. O. Rasmussen, Arkiv f. Fysik **7** (1953) 185
8) Hollander, Smith, and Rasmussen, Phys. Rev. **102** (1956) 1372
9) D. Strominger, Ph. D. Thesis, University of California (1956) (Radiation Laboratory Unclassified Report UCRL—3374) unpublished
10) A. Rassey and S. A. Moszkowski, unpublished calculations, 1956
11) G. Alaga, Phys. Rev. **100** (1955) 432
12) D. M. Chase and L. Wilets, Phys. Rev. **101** (1956) 1038
13) Hollander, Smith and Mihelich, Phys. Rev. **102** (1956) 740

Nuclear Physics **3** (1957) 207—212; *North-Holland Publishing Co., Amsterdam*

A NOTE ON THE CALCULATION OF COULOMB PENETRATION AND COULOMB WAVE FUNCTIONS

R. M. THALER and L. C. BIEDENHARN

University of California Los Alamos Scientific Laboratory †, *Los Alamos, New Mexico*

Received 17 November 1956

Abstract: The phase-amplitude method is applied to the calculation of Coulomb penetration and Coulomb wave functions. The methods discussed apply for $\eta = Z_1 Z_2 e^2/\hbar v > 1$.

1. Introduction

In the study of nuclear reactions with charged particles it is important, to know the penetrability of the Coulomb barrier ††. Under certain approximations, discussed in ref. [1]), for example, the barrier penetration factor for a state of angular momentum L may be written in terms of the Coulomb wave functions as

$$P_L = \varrho(F_L^2+G_L^2)^{-1}, \tag{1}$$

where $\varrho = kR$ and F_L and G_L are the regular and irregular Coulomb wave functions defined in the usual way.

It is readily apparent that the calculation of the penetration factor of ref. [1]) does not require a complete knowledge of the Coulomb wave function. In particular, the use of the amplitude-phase method for expressing the Coulomb functions immediately suggests itself, since the penetration depends only on the amplitude and not on the phase. According to this method the amplitude A_L is defined as

$$A_L = \sqrt{F_L^2+G_L^2}, \tag{2}$$

and the phase Φ_L is defined as

$$\Phi_L = \tan^{-1} F_L/G_L. \tag{3}$$

The Coulomb wave functions are thus expressed in terms of the amplitude and phase as

$$\begin{matrix} F_L \\ G_L \end{matrix} = A_L \begin{matrix} \sin \\ \cos \end{matrix} \Phi_L. \tag{4}$$

Wheeler [2]), using a method due to Milne [3]) has shown that the amplitude function A_L obeys a non-linear second order differential equation, viz.

† Work performed under the auspices of the U. S. Atomic Energy Commission.

†† For a discussion of this point, cf. R. G. Thomas [1]).

$$\frac{\mathrm{d}^2 A_L}{\mathrm{d}\varrho^2} + \left(1 - \frac{2\eta}{\varrho} - \frac{L(L+1)}{\varrho^2}\right) A_L - A_L^{-3} = 0, \tag{5}$$

where $\eta = Z_1 Z_2 e^2/\hbar v$. The amplitude is taken to satisfy the boundary conditions $A_L \to 1$ and $\mathrm{d}A_L/\mathrm{d}\varrho \to 0$ as $\varrho \to \infty$, in accordance with the usual definitions of the Coulomb functions. Various simple transformations of this differential equation are appropriate for calculation of the amplitude for different values of its arguments. Two similar transformations will be discussed below. Since recursion relations can easily be found to give values for higher angular momenta, only $L = 0$ will be considered below.

2. The W.K.B. Approximation

If the change of variable $x \equiv 2\eta/\varrho$ is made in equation (5), with L taken to be zero, one obtains the differential equation

$$(2\eta)^{-2} \frac{\mathrm{d}^2 \psi}{\mathrm{d}x^2} = \psi^{-3} - \psi x^{-4}(1-x), \tag{6}$$

where $\psi = xA_0$. At $x = 0$, it is clear that $\psi = 0$, $\mathrm{d}\psi/\mathrm{d}x = 1$, and $\mathrm{d}^2\psi/\mathrm{d}x^2 = 0$. Thus near $x = 0$ a good approximation to ψ may be obtained by setting the left hand side of eq. (6) equal to zero and solving the resulting algebraic equation. This gives

$$\psi = xA_0 = x(1-x)^{-\frac{1}{4}}. \tag{7}$$

This is obviously the W.K.B. approximation for the amplitude. Equation (6) now suggests the possibility of an expansion of ψ in decreasing even powers of η, of which the W.K.B. approximation is the zeroth order term. Thus, writing ψ as

$$\psi = x(1-x)^{-\frac{1}{4}} \left[1 + \sum_{n=1} \eta^{-2n} a_n(x)\right], \tag{8}$$

one may solve eq. (6) for the coefficients $a_n(x)$. This series is an asymptotic series, which, however, yields accurate values for $\eta \gg 1$, $x \ll 1$. The first few coefficients $a_n(x)$ are

$$a_1 = 2^{-8} \frac{x^3}{(1-x)^3} (3x-8), \tag{9.1}$$

$$a_2 = 2^{-17} \frac{x^5}{(1-x)^6} (-99x^3 + 528x^2 - 1216x + 3072), \tag{9.2}$$

$$a_3 = 2^{-25} \frac{x^7}{(1-x)^9} (6597x^5 - 52826x^4 - 185480x^3 - 361260x^2 + 6344x - 1474610), \tag{9.3}$$

$$a_4 = 2^{-35} \frac{x^9}{(1-x)^{12}} (-4057965x^7 + 43298560x^6 - 208751424x^5 + 597538732x^4 - 1134344192x^3 + 3538142400x + 5285002240). \tag{9.4}$$

The coefficients $a_1(x), \ldots a_4(x)$ are tabulated below for $0 < x < 0.5$ at intervals of 0.1. The coefficients are all equal to zero at $x = 0$. Tabular entries are presented as six digit numbers followed by the powers of ten which multiply them.

x	0.1	0.2	0.3	0.4	0.5
a_1	−4.12594 (−5)	−4.51660 (−4)	−2.18317 (−3)	−7.87037 (−3)	−2.53906 (−2)
a_2	1.73795 (−8)	1.08687 (−6)	1.77633 (−5)	1.82698 (−4)	1.61477 (−3)
a_3	−2.38340(−10)	−8.85943 (−8)	−5.08919 (−6)	−1.54371 (−4)	−3.85416 (−3)
a_4	6.26293(−12)	1.41434 (−8)	2.89888 (−6)	2.63500 (−4)	1.87673 (−2)

It is readily seen that this series converges very rapidly for small x or large η. For example, for $x = 0.3$, $\eta = 3$, inclusion of the term in η^{-2} gives six figure accuracy; inclusion of terms through η^{-4} gives eight figure accuracy. Similarly for $x = 0.5$, $\eta = 3$, inclusion of the η^{-2} term gives four figure accuracy; inclusion of terms through η^{-6} gives five figure accuracy.

3. The Amplitude in the Vicinity of the Turning Point

The series discussed above is of use for $\varrho > 2\eta$, that is beyond the classical turning point. In the vicinity of the turning point the differential equation eqs. (5) or (6), has no singularities and is easily integrated, provided one has accurate starting values at the turning point. Asymptotic expansions for F_0, $\mathrm{d}F_0/\mathrm{d}\varrho$, G_0, $\mathrm{d}G_0/\mathrm{d}\varrho$ at the turning point have already been published [4]). It is thus necessary merely to obtain A_0 and $\mathrm{d}A_0/\mathrm{d}\varrho$ by using these expansions and to integrate the differential equation. The asymptotic series obtained for the Coulomb functions at the turning point yield an accurate value very quickly for $\eta \gg 1$. Performing the change of variable $z = (2\eta/\varrho) - 1$, gives the differential equation

$$\frac{1}{(2\eta)^2}\frac{\mathrm{d}^2\psi}{\mathrm{d}z^2} = \psi^{-3} + \psi z(1-z)^{-4}. \tag{10}$$

The starting values at the turning point ($z = 0$) are

$$\psi(z=0) = \sqrt{F_0^2(\varrho = 2\eta) + G_0^2(\varrho = 2\eta)} \tag{11.1}$$

and

$$\left(\frac{\mathrm{d}\psi}{\mathrm{d}z}\right)_{z=0} = \frac{\psi^2(z=0) - 2\eta\left[F_0(\varrho=2\eta)\dfrac{\mathrm{d}F_0(\varrho=2\eta)}{\mathrm{d}\varrho} + G_0(\varrho=2\eta)\dfrac{\mathrm{d}G_0}{\mathrm{d}\varrho}(\varrho=2\eta)\right]}{\psi(z=0),}, \tag{11.2}$$

where the Coulomb functions at the turning point are as given in ref. [4]).

This integration has been coded for the IBM 704 and has proved most feasible in actual practice.

4. Recurrence Relations

The amplitude function obeys the following recurrence relations:

$$\frac{df_L}{d\varrho} = \frac{1}{L}\left(\frac{L^2}{\varrho}+\eta\right)(f_{L-1}-f_L) - \frac{2}{L}\sqrt{f_L f_{L-1}(L^2+\eta^2)-L^2}, \tag{12}$$

$$\frac{df_L}{d\varrho} = \frac{1}{L+1}\left(\frac{[L+1]^2}{\varrho}+\eta\right)(f_L-f_{L+1}) + \frac{2}{L+1}\sqrt{f_L f_{L+1}([L+1]^2+\eta^2)-[L+1]^2}, \tag{13}$$

$$\frac{1}{L}\left(\frac{L^2}{\varrho}+\eta\right)f_{L-1} - (2L+1)\left(\frac{1}{\varrho}+\frac{2}{L(L+1)}\right)f_L + \frac{1}{L+1}\left(\frac{[L+1]^2}{\varrho}+\eta\right)f_{L+1}$$
$$= \frac{2}{L}\sqrt{f_L f_{L-1}(L^2+\eta^2)-L^2} + \frac{2}{L+1}\sqrt{f_L f_{L+1}([L+1]^2+\eta^2)-[L+1]^2}, \tag{14}$$

where $f_L \equiv (A_L)^2$.

While these recurrence relations are somewhat more complicated than the relations for the Coulomb functions themselves, they have the advantage that the numerical accuracy for the amplitude increases as one recurs from small to large L. Thus it is sufficient to calculate the amplitude (A_0) for $L = 0$ by the methods discussed above and to obtain the values for higher values of L by recurrence.

5. Coulomb Functions

The Coulomb functions themselves may likewise be calculated by the above method if one also obtains the phase Φ_L. From the Wronskian relation
$(dF_L/d\varrho)G_L - (dG_L/d\varrho)F_L = 1$, one obtains

$$\frac{d\Phi_L}{d\varrho} = A_L^{-2}. \tag{15}$$

This equation together with the boundary condition

$$\frac{\Phi_L}{(\varrho\to\infty)} \to \varrho - \eta\log 2\varrho - \frac{L\pi}{2} + \sigma_L, \tag{16}$$

where $\sigma_L = \arg\Gamma(L+1+i\eta)$ serves to define the phase. The phase obeys the recurrence relation

$$\Phi_L = \Phi_{L-1} + \tan^{-1}\frac{L}{\sqrt{f_L f_{L-1}(L^2+\eta^2)-L^2}}. \tag{17}$$

The expansion for the phase which corresponds to the W.K.B. expansion for the amplitude A_0, eqs. (8)–(9), is

$$\Phi_0 = 2\eta\frac{\sqrt{1-x}}{x}\left[1-\sum_{n=1}\eta^{-2n}\alpha_n(x)\right] - \eta\log\eta\,\frac{1+\sqrt{1-x}}{1-\sqrt{1-x}}. \tag{18}$$

The W.K.B. approximation to the phase Φ_0 consists in neglecting terms of the order η^{-2} in eq. (18).

The first few coefficients $\alpha_n(x)$ are

$$\alpha_1 = \frac{x}{3 \cdot 2^6 y^2}[9y^2-6y+5], \tag{19.1}$$

$$\alpha_2 = \frac{x}{45 \cdot 2^{14} y^5}[1395y^6-1890y^5+1395y^4-12300y^3 + 25191y^2-19890y+5525], \tag{19.2}$$

$$\alpha_3 = \frac{x}{45 \cdot 2^{22} y^8}[34182y^{10}-113565y^9+131805y^8-154530y^7 + 3414450y^6-16774173y^5+39043215y^4-50520880y^3 + 37424430y^2-14968500y+2484750], \tag{19.3}$$

$$\alpha_4 = \frac{x}{2^{31} y^{11}}\left[-\frac{1086966}{7}y^{14}+723874y^{13}-\frac{3925592}{3}y^{12}+1195493y^{11} - 1624235y^{10}+\frac{214100941}{3}y^9-\frac{3047826369}{5}y^8+\frac{17956951270}{7}y^7 - \frac{58131159472}{9}y^6+\frac{115727117640}{11}y^5-\frac{148498132722}{13}y^4+ \frac{41237688533}{5}y^3-\frac{64855506427}{17}y^2+\frac{19486879125}{19}y-\frac{2564063045}{21}\right], \tag{19.4}$$

where $y = 1-x$.

The coefficients $\alpha_1(x)-\alpha_4(x)$ are tabulated below for $0 < x < 0.5$ at intervals of 0.1. The coefficients are all equal to zero at $x = 0$. Tabular entres are presented as six digit numbers followed by the powers of ten which multiply them.

x	0.1	0.2	0.3	0.4	0.5
α_1	4.43030 (−3)	9.70052 (−3)	1.66135 (−2)	2.68519 (−2)	4.427081(−2)
α_2	−2.62943 (−3)	−9.35014 (−3)	−2.69748 (−2)	−7.63856 (−2)	−2.31333 (−1)
α_3	3.41733 (−5)	7.35543 (−5)	1.68492 (−4)	1.49272 (−3)	2.71101 (−2)
α_4	3.15729 (−5)	6.67827 (−5)	6.51684 (−5)	−3.05478 (−3)	−1.84854 (−1)

The derivatives of the Coulomb wave functions are also of interest in some problems. To obtain these it is necessary to know the derivative of the amplitude and phase. The derivative of the phase is given immediately by eq. (15). In the case where the amplitude is obtained through integration of eq. (10), the derivative of the amplitude is obtained automatically. An asymptotic series in decreasing powers of η for the derivative of the amplitude function is obtained by differentiation of eqs. (8)—(9).

The authors are grateful for the valuable assistance rendered by Mr. Glenn Carter, who cheerfully undertook the tedious algebraic task of obtaining the coefficients of the expansion in η^{-2}.

References

1) R. G. Thomas, to be published
2) J. A. Wheeler, Phys. Rev. **52** (1937) 1123
3) W. E. Milne, Phys. Rev. **35** (1930) 864
4) Biedenharn, Gluckstern, Hull and Breit, Phys. Rev. **97** (1955) 542

Nuclear Physics **3** (1957) 213—216; *North-Holland Publishing Co., Amsterdam*

POLARIZATION OF HIGH ENERGY NUCLEONS EXCITING A COLLECTIVE LEVEL

TH. A. J. MARIS

The Gustaf Werner Institute for Nuclear Chemistry, Uppsala

Received 7 December 1956

Abstract: For a spin-orbit coupling of the form $[\Delta V \times \mathbf{P}] \cdot \boldsymbol{\sigma}$, which reduces to the usual $(1/r)(\mathrm{d}V/\mathrm{d}r)\mathbf{l} \cdot \boldsymbol{\sigma}$ term for a spherical nuclear potential, it is shown that the polarization properties of neutrons scattered on nuclei are in the first Born approximation equal for elastic scattering and all collective excitations, and independent of the potential shape.

The lowest 2+ levels in spherical light nuclei have been interpreted as representing the first quadrupole vibration of the nuclear surface [1]. Such an interpretation is not in disagreement with the angular distribution of the scattered 180 MeV protons exciting the 4.4 MeV level in C^{12} [2].

In connection with measurements done at this laboratory concerning the polarization properties of inelastically scattered protons exciting the 4.4 MeV level in Carbon [3], we have calculated in first Born approximation the scattering matrix in spin space [4] for inelastically scattered high energy neutrons exciting a collective nuclear state.

We denote by

$\mathbf{R}$, α_μ and $\hbar\mathbf{K}$ — the center of mass and collective coordinates and the momentum of the nucleus,

n_μ — the quantum number corresponding to the variable α_μ,

X — all other nuclear coordinates which may be coupled to the α_μ's by the unperturbed Hamiltonian,

$\psi(n_\mu, X)$ — the nuclear wave-function,

$\mathbf{r}$, $\mathbf{p}$ $(= \hbar\mathbf{k})$, $\boldsymbol{\sigma}$ and m — the space coordinates, momentum, spin and mass of the bombarding neutron,

s — the spin wave function of the bombarding neutron,

the indices f and i — the final and initial states.

The initial wave function is

$$(2\pi)^{-3}\, \mathrm{e}^{\mathrm{i}\mathbf{k}_\mathrm{i}\cdot\mathbf{r}}\, s_\mathrm{i}\psi_\mathrm{i}(n_\mu, X).$$

The final wave function is

$$(2\pi)^{-3}\, \mathrm{e}^{\mathrm{i}\mathbf{k}_\mathrm{f}\cdot\mathbf{r}}\, s_\mathrm{f}\, \mathrm{e}^{\mathrm{i}\mathbf{K}_\mathrm{f}\cdot\mathbf{R}}\, \psi_\mathrm{f}(n_\mu, X).$$

For the collective potential we take

$$H'(\alpha_\mu, \mathbf{r}-\mathbf{R}, \boldsymbol{\sigma}) = (1+i\beta)V(\alpha_\mu, \mathbf{r}-\mathbf{R}) - a(1+i\gamma)[\nabla V(\alpha_\mu, \mathbf{r}-\mathbf{R}) \times \mathbf{P}]\cdot\boldsymbol{\sigma}; \quad (1)$$

$V(\alpha_\mu, \mathbf{r}-\mathbf{R})$ represents the nuclear potential well, which is now also dependent on the collective coordinates which describe the collective excitations. We have taken a more general form of the spin-orbit coupling [5]) which reduces to the well known $(1/r)(\mathrm{d}V/\mathrm{d}r)\mathbf{l}\cdot\boldsymbol{\sigma}$ term for the case of a spherical potential with no collective degrees of freedom. β, a and γ are real coupling constants which are taken to be independent of the nuclear variables. For nuclei with non-zero ground state spin a possible dependence of the interaction on the nuclear spin orientation is neglected.

The cross section for the transition of the initial into the final state is

$$\sigma(\mathbf{k}_f, s_f, \psi_f; \mathbf{k}_1, s_1, \psi_1) = \frac{k_f}{k_1}\left(\frac{m}{2\pi\hbar^2}\right)^2 |H'_{fi}|^2 \tag{2}$$

with

$$\begin{aligned}
H'_{fi} &= (2\pi)^{-3}\langle\psi_f \mathrm{e}^{i\mathbf{K}_f\cdot\mathbf{R}}\mathrm{e}^{i\mathbf{k}_f\cdot\mathbf{r}} s_f|H'(\alpha_\mu, \mathbf{r}-\mathbf{R}, \boldsymbol{\sigma})|\mathrm{e}^{i\mathbf{k}_1\cdot\mathbf{r}} s_1\psi_1\rangle \\
&= \delta(\mathbf{K}_f+\mathbf{k}_f-\mathbf{k}_1)\langle\psi_f \mathrm{e}^{i\mathbf{k}_f\cdot\mathbf{r}} s_f|H'(\alpha_\mu, \mathbf{r}, \boldsymbol{\sigma})|\mathrm{e}^{i\mathbf{k}_1\cdot\mathbf{r}} s_1\psi_1\rangle \\
&= \delta(\mathbf{K}_f+\mathbf{k}_f-\mathbf{k}_1)\langle\psi_f \mathrm{e}^{i\mathbf{k}_f\cdot\mathbf{r}} s_f|(1+i\beta)V(\alpha_\mu,\mathbf{r})-a(1+i\gamma)[\boldsymbol{\nabla}V(\alpha_\mu,\mathbf{r})\times\mathbf{P}] \\
&\qquad\qquad \cdot\boldsymbol{\sigma}|\,\mathrm{e}^{i\mathbf{k}_1\cdot\mathbf{r}} s_1\psi_1\rangle \\
&= \delta(\mathbf{K}_f+\mathbf{k}_f-\mathbf{k}_1)\{\langle\psi_f \mathrm{e}^{i\mathbf{k}_f\cdot\mathbf{r}}|V(\alpha_\mu, \mathbf{r})|\mathrm{e}^{i\mathbf{k}_1\cdot\mathbf{r}}\psi_1\rangle(1+i\beta)\langle s_f/s_1\rangle \\
&- \langle\psi_f \mathrm{e}^{i\mathbf{k}_f\cdot\mathbf{r}}|[\boldsymbol{\nabla}V(\alpha_\mu, \mathbf{r})\times\hbar\mathbf{k}_1]|\mathrm{e}^{i\mathbf{k}_1\cdot\mathbf{r}}\psi_1\rangle a(1+i\gamma)\cdot\langle s_f|\boldsymbol{\sigma}|s_1\rangle \\
&= \delta(\mathbf{K}_f+\mathbf{k}_f-\mathbf{k}_1)\langle\psi_f \mathrm{e}^{i\mathbf{k}_f\cdot\mathbf{r}}|V(\alpha_\mu, \mathbf{r})|\mathrm{e}^{i\mathbf{k}_1\cdot\mathbf{r}}\psi_1\rangle \\
&\times\langle s_f|1+i\beta-i\hbar a(1+i\gamma)[\mathbf{k}_f\times\mathbf{k}_1]\cdot\boldsymbol{\sigma}|s_1\rangle.
\end{aligned} \tag{3}$$

Neglecting the very slight energy dependence of k_f, H'_{fi} differs for different collective excitations in first Born approximation only by a multiplicative function which is independent of the initial and final spin of the bombarding particle.

From this fact the following conclusions may be drawn:

a) For *elastic* scattering, which is contained in eq. (3) as the special case for which ψ_f is identical to ψ_1, the polarization is, in the first Born approximation with the interaction (1), determined by eq. (3) and therefore independent of the chosen nuclear potential. This is a generalization of the statement of Heckrotte [6]) and Malenka [7]) which is valid for a spherical potential.

b) For *inelastic* scattering the polarization is in the same approximation also independent of the excited nuclear state as long as this is a collective one and the interaction (1) is valid.

c) The well known relation for pure elastic scattering between asymmetry and polarization is in first Born approximation still valid for collective inelastic scattering. This is not obvious in general for inelastic scattering because the proof for that relation is based on the invariance of the physical scattering process under time reversal [4]).

Experimental verification of these conclusions and of eq. (3) may not be expected at large scattering angles, at which even exact calculations for the elastic scattering do not qualitatively agree with experimental results †. This fact just demonstrates a failure of the interaction (1). Furthermore the Born approximation limits us to angles at which the cross section is relatively large (otherwise the higher order terms become important). Eq. (3) will also be valid for protons in an angular region in which the Coulomb scattering is negligible.

Taking these restrictions and the general trend of the collective cross sections [2]) into account, one may hope, in the case of 150 MeV proton scattering on carbon, to find a qualitative agreement of the experimental results with formula (3) for angles between 10 and 30 degrees for collective inelastic excitations and between 10 and 20 degrees for elastic scattering. In this case all polarizations and asymmetries for collective and elastic scattering should therefore roughly be equal for angles between 10 and 20 degrees.

From (3) it follows for the polarization P and asymmetry for the scattering of a 100 % polarized beam ε that [8])

$$P = \varepsilon = \frac{a\hbar^2 k^2(\beta-\gamma)\sin\theta}{1+\beta^2+\dfrac{a^2\hbar^4 k^4}{4}(1+\gamma^2)\sin^2\theta}. \tag{4}$$

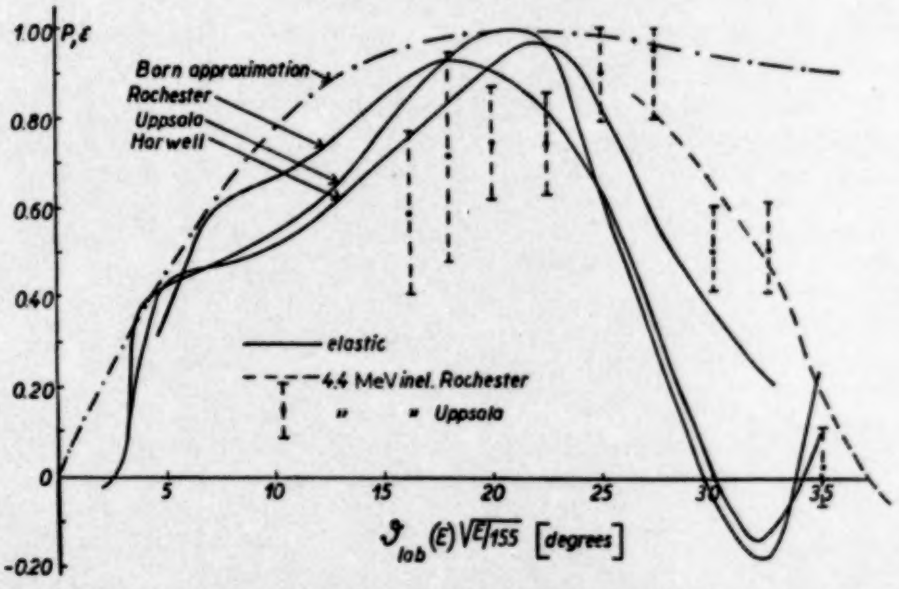

Fig. 1. The polarization and asymmetry of elastic and collective inelastic scattering for C^{12} in first Born approximation, which may give qualitatively correct results between 10 and 20 degrees for elastic and between 10 and 30 degrees for collective inelastic scattering. Experimental results are shown for comparison.

† The author thanks S. Köhler and T. Berggren for showing him preliminary results on phase shift calculations with different parameter values.

In fig. 1 we have plotted this function for 155 MeV bombarding energy and the parameter values: $\beta = 0.8$, $\gamma = -1.0$, $a\hbar^2k^2 = 5.0$. Experimental results at 155 MeV [3]), 137 MeV [10]) and 210 MeV [9]) for elastic scattering and scattering of protons exciting the 4.4 MeV level in C^{12} are shown for comparison. In these experiments essentially the values of ε have been measured. In the angular region indicated the agreement between the theoretical curve and the experimental results is as good as one could expect for the present approximation and supports the interpretation of the 4.4 MeV level in C^{12} as a collective excitation.

As long as it is not clear that ε equals P for every scattering process, it seems interesting to perform direct measurements of P. Such measurements are at present being done at this laboratory and a comparison of their results with eq. (4) could mean an additional test of the collective interpretation of the 4.4 MeV level.

The author is indebted to Prof. Th. Svedberg for the hospitality of his Institute. Thanks are due to R. Alphonce, P. Hillman, A. Johansson, G. Tibell and H. Tyrén for stimulating comments and for keeping the author continuously informed of their results. A discussion with Prof. M. Goeppert-Mayer and one with Prof. O. Chamberlain have been helpful. The author has received a grant of the Swedish Atomic Energy Commission.

Note added in proof: Dr. K. Nishimura kindly directed the attention of the author to the following abstracts [11, 12]) which have appeared in Bulletins of the American Physical Society, mentioning the equality of elastic and collective polarization in the Born approximation.

References

1) A. Bohr and B. R. Mottelson, Mat. Fys. Medd. Dan. Vid. Selsk **27** (1953) no. 16
2) Th. A. J. Maris and H. Tyrén, Nuclear Physics **3** (1957) 35
3) R. Alphonce, A. Johansson and G. Tibell, Nuclear Physics **3** (1957) 185
4) L. Wolfenstein and J. Ashkin, Phys. Rev. **85** (1952) 947
5) W. Heisenberg, Theorie des Atomkerns, Lecture notes by W. Macke, Max-Planck-Institut für Physik, Göttingen (1951)
6) W. Heckrotte, Phys. Rev. **94** (1954) 1797
7) B. J. Malenka, Phys. Rev. **95** (1954) 522
8) E. Fermi, Nuovo Cimento **11** (1954) 407
9) W. G. Chesnut, E. M. Hafner and A. Roberts, NYO 7672 (1956)
10) J. M. Dickson and D. C. Salter, private communication
11) M. Ruderman, Phys, Rev. **98** (1955) 267
12) K. Nishimura and M. Ruderman, Bull. Am. Phys. Soc. Series II Vol. 1 no. 8 (1956) 383

Nuclear Physics **3** (1957) 217—220; *North-Holland Publishing Co., Amsterdam*

ALPHA-ALPHA SCATTERING AT 38.5 MeV

W. E. BURCHAM
Department of Physics, University of Birmingham
W. M. GIBSON
Department of Physics, Queen's University of Belfast
D. J. PROWSE
H. H. Wills Physics Laboratory, University of Bristol
and
J. ROTBLAT
Physics Department, Medical College of St. Bartholomew's Hospital, London

Received 3 December 1956

Abstract: A measurement of the angular distribution of the scattering of alpha-particles by helium at 38.5 MeV is described. The c.m.s. cross-section is 110 mb/steradian at 90°, falling to a very sharp minimum of about 0.5 mb/steradian at 64°. Approximate calculations of the phase shifts show that δ_0 and δ_2 are large and δ_4 small: these results are in agreement with other evidence for levels of spin 4 at about 11 MeV and of spin 0 and 2 near to 19 MeV.

The scattering of alpha particles by helium has been studied in detail for incident energies up to 23 MeV. The experimental results and their theoretical interpretation are discussed by Steigert and Sampson [1]) and by Russell, Phillips and Reich [2]), who plot the nuclear phase shifts for s, d and g waves as a function of energy. The variation of these phase shifts with energy exhibits the influence of the 2+ level of the compound nucleus Be^8 at 2.9 MeV, and of a level of spin 4+ at about 11 MeV. Broad levels of spin 0+ and 2+ at an excitation energy near 19 MeV in Be^8 have also been suggested (Inglis [3])) to account for the variation of the angular distribution of alpha particles from the Li^7 (p, α) reaction with energy. The present paper reports on a preliminary study of the alpha-alpha scattering at an energy (38.5 MeV) at which evidence for these levels might be found. The only other published study of this scattering process for energies above 23 MeV is the work of Graves [4]), who obtained nuclear phase shifts for an energy of 30 MeV.

In the present work the 38.5 MeV alpha-particle beam from the Birmingham cyclotron was used. Previous publications (e.g. Burcham *et al.* [5]), Freemantle *et al.* [6])) have given results obtained with the 9.5 MeV proton beam and the 19 MeV deuteron beam in a scattering camera originally described by Burrows, Powell and Rotblat [7]). Several modifications which have been made to this camera, principally to improve the accuracy of the

geometrical arrangements and to allow the absolute measurement of the beam intensity, will be described in a future paper.

Gaseous targets of helium were used in two separate exposures at pressures of 15 and 30 cm of mercury; the alpha-particle beam carried a total charge of about 5 microcoulombs in each case. The particles leaving the target were recorded in Ilford C2 nuclear research plates.

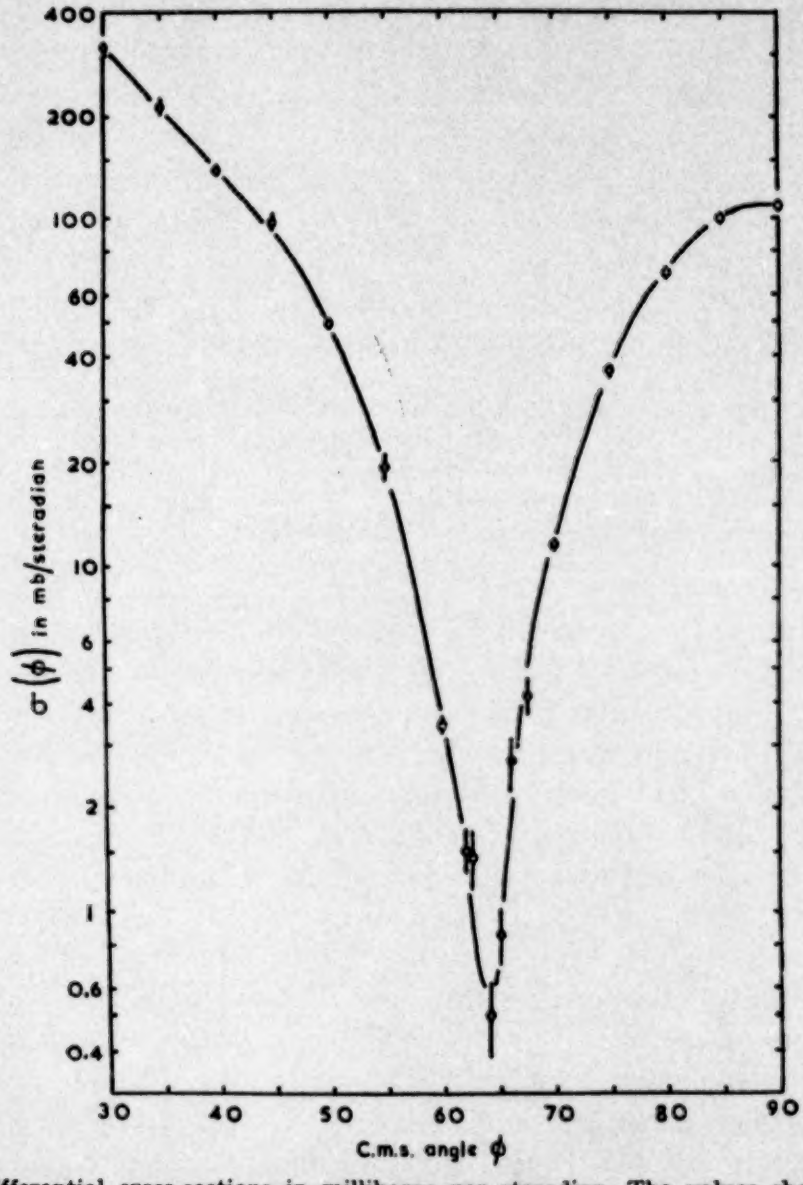

Fig. 1. Differential cross-sections in millibarns per steradian. The values shown for 70°, 80° and 85° are the means of those obtained at laboratory angles 35° and 55°, 40° and 50°, and 42.5° and 47.5° respectively.

When the plates were examined, separate distributions of range were plotted at each angle for the tracks of alpha-particles and protons, which were distinguished by their grain density. The mean ranges of the elastically scattered alpha-particles at several angles, corrected for the loss of energy

in the gas, gave a beam energy of 38.5±0.2 MeV. The range distributions showed that the contamination of the helium by other gases and the contamination of the bombarding beam by deuterons or protons were both less than 1 %. At several angles there were two well-defined groups of protons, which from their variation of range with angle were identified as due to the reaction $He^4(\alpha, p)Li^7$, with Li^7 being formed in its ground state and 0.477 MeV excited sate.

Detailed measurements of the number of elastically scattered alpha-particles were made at angles from 15° to 55° in the laboratory system, and differential cross-sections in the centre-of-mass system were calculated. The results from the two exposures were in good agreement: they are combined in the angular distribution shown in fig. 1 and table I.

TABLE I

ϕ	30	35	40	45	50	55	60	62	62.5	64	65	66	67.5	70	75	80	85	90
$\sigma(\phi)$	314	212	140	97	49	19.3	3.45	1.52	1.45	0.50	0.86	2.7	4.2	11.6	36.4	69.1	100	110
$\Delta\sigma(\phi)$	14	11	5	5	2	1.8	0.21	0.23	0.27	0.12	0.16	0.5	0.5	0.4	1.6	2.5	4	4

The outstanding feature of the angular distribution is the very sharp minimum at 64°, on each side of which the intensity rises by a factor 10 in $4\frac{1}{2}$°. There is no evidence that the true distribution does not drop to even lower values: the angular resolution of the apparatus is limited by the size of the scattering volume, which under these conditions gave a spread of $\frac{1}{2}$° in laboratory angles, and hence 1° in centre-of-mass angles. It would therefore hardly be possible without modifying the apparatus to observe a minimum sharper than that shown in fig. 1.

Particularly careful measurements were made across the minimum in each set of plates, to ensure that each result was genuine. At each point on the curve the uncertainty shown is the statistical one resulting from the number of tracks on which the cross-section is based: there is also an uncertainty in the absolute scale of these cross-sections which amounts to a further 5 %.

An approximate analysis in terms of real phase shifts shows that δ_0 and δ_2 are large, while δ_4, δ_6 and δ_8 are small. The small value of δ_4 indicates that the g-wave is not near resonance at 38.5 MeV. Since δ_4 is rising fairly rapidly at a bombarding energy 23 MeV this result is consistent with the existence of a level of spin 4+ in Be^8 at either 10.8 MeV (Steigert and Sampson) or 11.6 MeV (Nilson and Jentschke, quoted by Russell, Phillips and Reich). The s- and d-waves seem to be nearer to resonance at the bombarding energy of this experiment, in agreement with the existence of the levels postulated by Inglis. A large part of these phase shifts may however

be due to potential scattering. In order to join the present values of δ_0 and δ_2 to those available at 30 MeV and below 23 MeV, further observations at intermediate energies are required; these are being attempted. A detailed investigation of the reaction He^4 (α, p) Li^7 is also in progress, and the results will be used in a more accurate analysis of the alpha-alpha interaction in terms of complex phase shifts.

The authors wish to thank Dr R. McKeague for assistance in making the exposures, Mrs D. E. Anderson, Mrs S. E. Baker and Miss M. Pearce for the microscope work, Mr J. B. A. England and Mr D. Bredin for some of the calculations, and Mr G. McCauley for the calculation of the phase-shifts and discussion of the problem.

References

1) F. E. Steigert and M. B. Sampson, Phys. Rev. **92** (1953) 660
2) J. L. Russell Jr., G. C. Phillips and C. W. Reich, Phys. Rev. **104** (1956) 135
3) D. R. Inglis, Phys. Rev. **74** (1948) 21
4) E. Graves, Phys. Rev. **84** (1951) 1250
5) W. E. Burcham, W. M. Gibson, A. Hossain and J. Rotblat, Phys. Rev. **92** (1953) 1266
6) R. G. Freemantle, W. M. Gibson, D. J. Prowse and J. Rotblat, Phys. Rev. **92** (1953) 1268
7) H. B. Burrows, C. F. Powell, and J. Rotblat, Proc. Roy. Soc. A **209** (1951) 461

Nuclear Physics **3** (1957) 221—236; *North-Holland Publishing Co., Amsterdam*

A NEW METHOD OF MEASUREMENT OF NEUTRON POLARIZATION AND n—He^4 PHASE ANALYSIS

I. I. LEVINTOV, A. V. MILLER and V. N. SHAMSHEV
Institute of Chemical Physics, USSR Academy of Sciences, Moscow

Received 9 November 1956

Abstract: A helium analyzer for measurement of neutron polarization in the 1—18 MeV energy region is described. The efficiency of the analyzer in this region approaches 100 %. The sensitivity of the instrument is approximately 20 cpm for a neutron flux of 10^5 neut./cm^2 · sec. The instrument operates practically without any background. The azimuthal asymmetry of 2.45 and 3.4 MeV (D+D) neutrons scattered on He^4 has been measured. Analysis of the result confirms the experimental phase shift values obtained by Seagrave and contradicts the phase shift values mentioned by Huber and Baldinger.

1. Introduction

Partial polarization of nucleons in nuclear reactions is apparently a general property of most reactions and reflects the strong dependence of the interaction on the spin-orbit orientation which is so characteristic of nuclear forces. A systematic study of polarization in nuclear reactions seems to be very promising from the viewpoint of obtaining new information on transitions as well as of discovering new sources of highly polarized particles.

Presently available data on neutron polarization are sparse and are confined to the D (d, n) ($E_d = 600$ keV) and Li (p, n) ($E_p = 2.262$ MeV) reactions. Difficulties inherent in existing methods [1, 2, 3, 4]), which employ C^{12} and O^{16} analyzers, are the reason that more extensive investigations have not been conducted.

For systematic study of neutron polarization an analyzer is required which yields an appreciable and accurately calculable neutron polarization in a broad energy range. In the 1—20 MeV neutron energy range, C^{13} and O^{17} nuclei possess a sufficiently developed level structure whose width in most cases is ≈ 100 keV. The polarization of neutrons scattered on C^{12} or O^{16} is therefore a significantly non monotonic function of neutron energy and, due to the large number of levels and diversity of states, accurate phase analysis is made difficult. Thus, application of C^{12} or O^{16} nuclei as neutron analyzers in a broad energy range does not appear to be feasible and, at any rate for each separate range, a special and very cumbersome phase shift investigation would be required.

Another important shortcoming of these methods is the appreciable

neutron background due to neutrons which impinge on the detector without striking the analyzer. Even if very careful shielding and collimation are used the background comprises $\approx 80\,\%$ of the effect and, moreover, the shielding apparently hinders measurement of the angular dependence of polarization.

In the present paper we describe a method of measurement of neutron polarization which is approximately 100 % efficient in the 1—20 MeV energy range and is practically free of background difficulties. †

A by-product of the investigation was refinement of the n—He^4 phase shift analysis and measurement of the polarization of (D+D) neutrons from thick and thin targets in the $E_d = 400$—1800 keV energy region ††.

He^4 was used as scatterer in our analyzer. Let us consider in greater detail the polarization properies of this nucleus. Due to the special closed properties of this nycleus the He^4 levels, if such exist, lie above 25 MeV and hence, up to neutron energies of 20 MeV, scattering on He^4 takes place without excitation of internal degrees of freedom of the α-particle. At these energies, therefore, the states of the He^5 system are, in a good approximation, determined by the motion of the neutron in the effective field of an unexcited α-particle, this being equivalent to a potential well of depth $V_{eff} \approx 40$ MeV and width $r \approx 2 \times 10^{-13}$ cm, the effective depth being significantly dependent on the spin-orbit orientation [5, 17]). As is well known, an interaction of this type yields a very smooth dependence of the scattering phases on energy. On the other hand, the small radius of the system restricts the orbital momentum of scattered waves to P states at $E_n \leqq 10$ MeV and to D states at $E_n \leqq 20$ MeV.

The small number of phases and their regular dependence on energy facilitate accurate phase analysis ††† and the strong spin-orbital splitting of the potential leads to a large polarization which smoothly depends on energy and which is close to unity at convenient scattering angles throughout the 1—20 MeV energy region.

The second advantage of using He^4 as an analyzer is that helium recoil nuclei can be directly counted instead of the scattered neutrons. As a result one can completely avoid the background involved in previous methods.

Thin proportional counters filled with helium were used (fig. 1). The apparatus registered He^4 recoil nuclei moving at an angle φ_α with respect to the neutron beam which corresponded to maximum azimuthal asymmetry in scattering of polarized neutrons of a given energy on He^4. For

† The principle of the method and some preliminary results on refined n—He^4 scattering phase shift determinations are also presented in a paper by I. I. Levintov, A. V. Miller and V. N. Shamshev in the Doklady Akad. Nauk (1955).

†† See the following paper by Levintov, Miller, Tarumov and Shamshev in this journal.

††† Phase analysis of the n—He^4 system is also made easier by the possibility of comparing the results with the precisely measured p—He^4 phases [6, 7, 8]).

this purpose the counters were fixed in the direction defined by φ_α and the helium pressure and discriminator bias were chosen in such a manner as to record only recoil nuclei moving approximately parallel to the counter

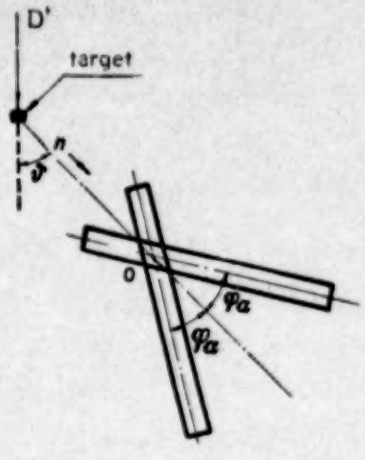

Fig. 1. Scheme of experiment.

axis. The azimuthal asymmetry R was measured by comparing the counting rate I_1 for the counters directed along φ_α with the counting rate I_2 corresponding to the angle φ_α

$$R = \frac{I_1}{I_2} = \frac{1+\overline{P}_x \cdot \overline{P}_{He}}{1-\overline{P}_x \cdot \overline{P}_{He}}$$

where $\overline{P}_x$ is the neutron polarization averaged over the volume of the counter in which the He^4 recoil nuclei were produced (operating volume) and $\overline{P}_{He}$ is the polarization of neutrons scattered by He^4 and averaged over the recoil angles (for details see below).

In order to estimate $\overline{P}_x$ quantitatively one must thus know the n—He^4 scattering phases. The phase analysis carried out by Huber and Baldinger [9]) and Seagrave [6]) on basis of data on the n—He^4 scattering angular distribution are not concordant, especially as regards the $P_{\frac{1}{2}}$ phase. This disagreement is apparently related to the essential unreliability of an analysis of the spin-orbit phase splitting made on the basis of data on $\sigma(\theta)$. The point is that spin-orbit splitting enters the expression for $\sigma(\theta)$ only as an additional term proportional to $\sin^2(\delta_l^+ - \delta_l^-)$. As a result $\sigma(\theta)$ is frequently insensitive to variations of $\delta_l^+ - \delta_l^-$ when $(1+l)\delta_l^+ + l\delta_l^-$ remains constant.

The polarization is proportional to $\sin(\delta_l^+ - \delta_l^-)$ and hence very sensitive to the magnitude of the spin-orbit splitting. Thus, even if a not very strongly polarized neutron beam is available one may carry out accurate phase shift analysis by measuring the angular dependence of the axial asymmetry in n—He^4 scattering by means of the method described above.

The (D+D) reaction was used as the source of polarized neutrons. This is a non resonance reaction and hence it could be expected that P_n should

vary smoothly with the deuteron energy. This circumstance renders the neutrons from the (D+D) reaction especially convenient for n—He^4 phase analysis. The fact that the (D+D) neutron polarization was known for only a single deuteron energy (E_d = 600 keV) was of no consequence since by measuring the azimuthal asymmetry at various n—He^4 scattering angles it was possible to determine simultaneously with greater precision the n—He^4 scattering phases and to determine the magnitude of the (D+D) neutron polarization.

2. Measurement of n—He^4 Azimuthal Scattering Asymmetry

The design of the measuring apparatus is illustrated in fig. 2. Seven copper tubes of 7 mm internal diameter were soldered together and placed in a vacuum tight container. The diameter of the tungsten counter wires

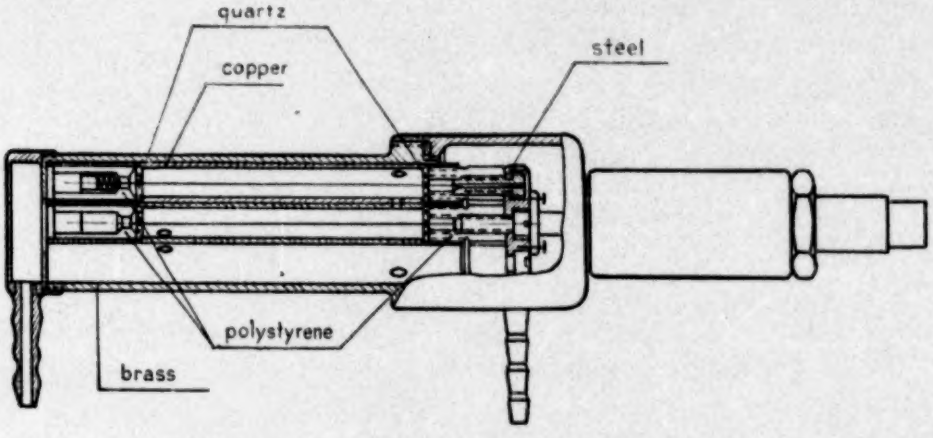

Fig. 2. Construction of proportional counters.

was 0.07 mm. The wires were centered by means of brass screws and holes drilled in polystyrene insulators. The high tension from dry batteries was applied simultaneously to each of the counter wires. Quartz washers were used to shield the operating volume of the counters from recoil protons ejected from the polystyrene insulators.

Eccentricity of the wires centered in the manner described above did not exceed 150μ, and the spread of the counter amplification factor was less than ± 1 %.

A general view of the measuring apparatus is shown in fig. 3. Two counter sets located on both sides of the target were used. The counter supports could move along a light brass ring whose centre coincided with that of the target. Revolving counter holders and limbs for setting the angle of rotation of the counters, φ_α, were mounted on the supports. The direction of ejection of the neutrons was read on a scale inscribed on the brass ring.

The geometry of the experiment required rigorous constancy of the position of the neutron source. For this purpose two electrodes coupled to a

galvanometer in a null circuit were placed in the target tube. With this device and small correcting magnets it was possible to fix the position of the ion beam striking the target with an accruracy of 0.2 mm.

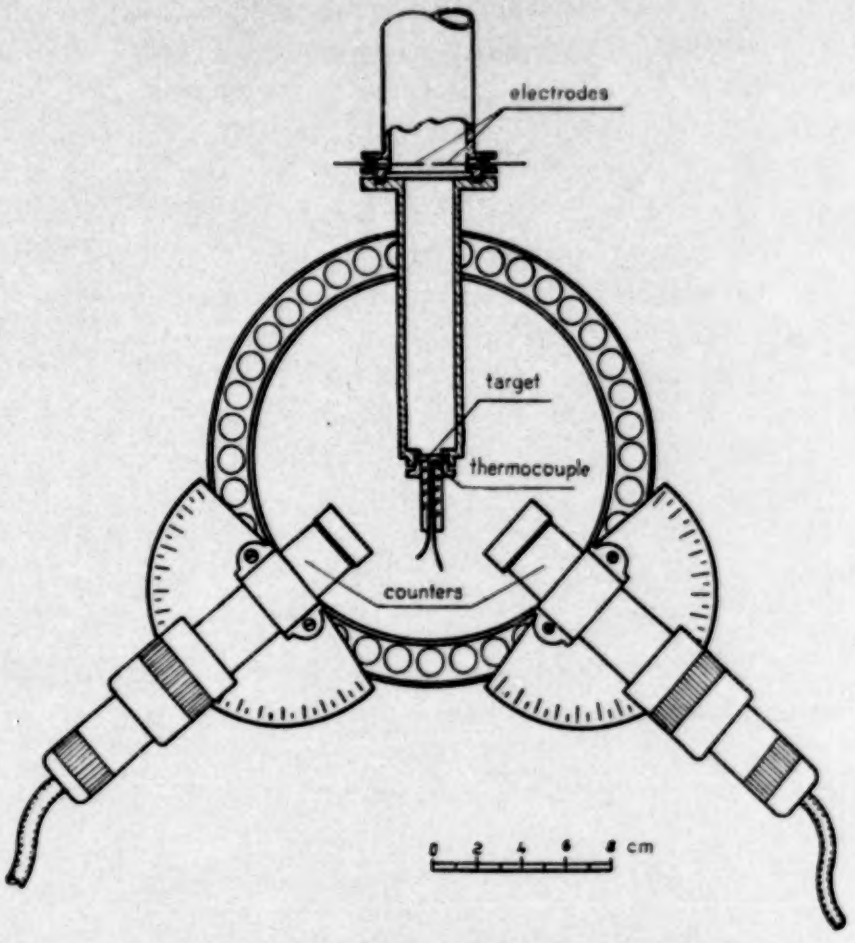

Fig. 3. General view of experimental arrangement.

Thick and thin zirconium targets saturated with deuterium were used in the measurements. The target temperature was measured with a thermocouple and kept constant at about 200° C. In this way it was possible to avoid the formation of a carbon film on the target as a result of decomposition of the absorbed oil layer under the action of the beam.

A uranium fission chamber located 10 cm from the target was used as monitor. The fraction of neutrons produced outside of the target (in the diaphragm, electrodes, etc.) and recorded by the chamber was less than1% for this arrangement.

In all of the experiments the helium pressure was such that the range of the He^4 recoil nuclei moving along the counter axis was 44 mm. The energy of these recoil nuclei was $E_\alpha = 0.64\ E_n \cos^2 \varphi_\alpha$ where E_n is the neutron energy. Data on the α-particle stopping power in helim were taken from ref. [16]).

The solid angle in which the recorded recoil helium nuclei were confined depended on the discriminator bias and varied between 10° and 18° depending on the counting rate in the particular experiment.

A continuous flow of helium through the counters was employed to ensure constant composition of the gas. The velocity of the flow was 30—40 cm³/min and was measured by a rheometer located at the terminal of the gas train. The helium pressure, which strongly influences the counter amplification factor, was chosen in accord with the prevailing atmospheric pressure. A special automatic regulator kept the pressure constant to within 0.1 %.

"DB"-type linear amplifiers were used, 5 channel integral discriminators being connected to their outputs. The discriminator scale was calibrated as follows. The counters were arranged in position $\varphi_\alpha = 0°$ and the momentum spectrum was measured near the upper limit. The largest momenta in this case were produced by recoil nuclei in head-on n—He^4 collisions. With help of the 5 discriminator channels it was possible to determine the position of the spectrum cut off to within 2 % and thus to establish a correspondence between the discriminator scale and energy of the helium recoil nuclei † (fig. 4).

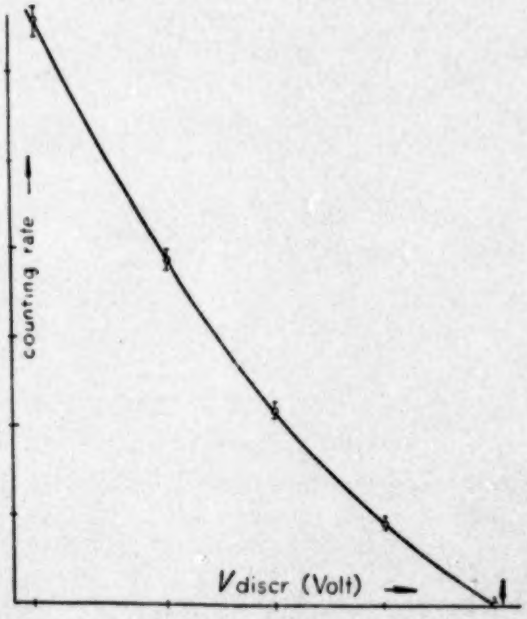

Fig. 4. Momentum spectrum of He^4 recoil nuclei produced in the counter in position $\varphi_\alpha = 0°$. The solid line corresponds to a spectrum computed from geometrical considerations and data on $\sigma_{n-\alpha}(\theta)$.

The following characteristics of the experimental arrangement were investigated:

† In the following, unity of the discriminator bias scale is taken to be the bias corresponding to head-on collision momenta.

1. Linearity of electronic circuit gain and gas amplification factor.
2. Sensitivity of the instrument to the background of scattered neutrons.
3. Influence of neutron scattering in the counter walls on the measured scattering asymmetry.
4. Effect of pressure and velocity of helium flow on counter gas amplification.
5. Possible distortion of results due to superposition of momenta.

Linearity of amplification was checked by comparing the momentum spectrum in the counter with the spectrum computed on basis of $\sigma_{n-\alpha}(\theta)$ data and [6]) geometrical considerations. Satisfactory agreement between these spectra (fig. 4) signifies that no appreciable deviations of the amplification from linearity were present.

Sensitivity of the apparatus to the background of scattered neutrons was assessed by placing in the immediate vicinity of the counters (at a distance of 20 cm) a massive (70 kg) lead scatterer. No appreciable change in the intensity of recorded neutrons was detected in this case.

The effect of neutron scattering in the counter walls on the measured asymmetry was assessed by tripling the wall thickness, lead jackets placed over the counters being used for this purpose. This only slightly reduced the counting rate ($\approx 10\ \%$) and within the statistical accuracy of the measurements ($\approx 3\ \%$) did not influence the magnitude of the asymmetry.

The gas amplification factor strongly depends on the pressure and presence of impurities in helium. The He gas used in the experiments was 99.8 % pure. The dependence of the amplification on pressure can be characterized by the coefficient 0.017 mm Hg^{-1} (the amplification factor at a pressure of 1100 mm Hg being considered to equal unity). The effect of the helium flow (which ensured constancy of the gas composition) on the gas amplification factor was especially large at flow velocities below 10 cm^3/min. Variation of the gas amplification with velocity was insignificant at velocities > 30 cm^3/min.

No distortion of the results of the measurements was detected which could be attributed to superposition of the momenta at intensities corresponding to full loading of the counters (1500 cps, which was the highest value encountered in the experiments). The asymmetry measurements were reproducible to 3 % for ion currents of 20 and 5 μA.

The neutron efficiency of the instrument can be characterized by the following figures: for a neutron flux of 3×10^5 neutr./$cm^2\cdot$sec ($E_n = 3.5$ MeV) and angles $\varphi_\alpha = 22°$, the counting rates in the discriminator channels biased at 0.4, 0.5, 0.6, 0.7 and 0.8 were respectively 180, 125, 75, 35 and 17 cpm.

3. Refinement of n—He^4 Scattering Phase Analysis

Due to the relatively "poor" geometry of the analyzer it would be difficult to perform a complete phase analysis on the basis of the asymmetry data. We therefore restricted our investigation to only two points of the most uncertain phase, δ_1^-, assuming that the remaining phases, δ_0 and δ_1^+, were known with sufficient accuracy.

This procedure was adopted on basis of the following considerations:

1. The experimental results of Huber and Baldinger [9]) and Seagrave [6]) pertaining to the δ_0 and δ_1^+ phases are in satisfactory agreement, whereas those pertaining to the δ_1^- phase are very different (see fig. 5).

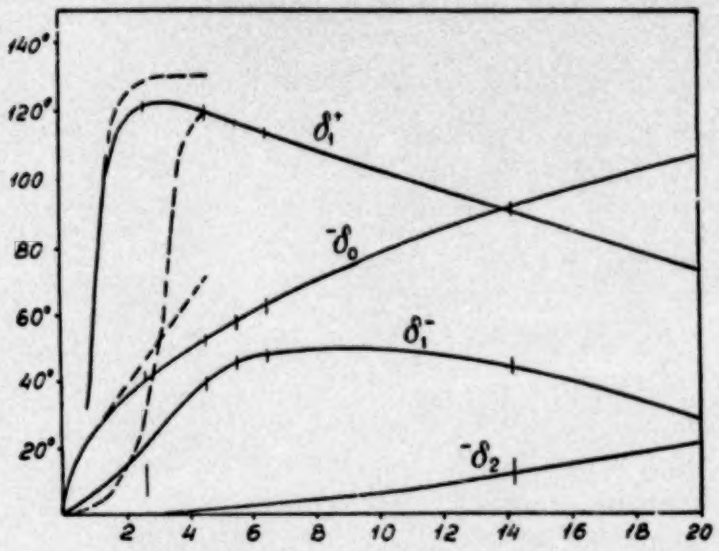

Fig. 5. Dependence of phase shifts in n—He^4 scattering on neutron energy E_n. Dotted line-data of Huber and Baldinger [5]); solid line-result of recalculation of phases from phase analysis of p—He^4 scattering; Seagrave's data [6]) are presented as experimental points.

2. Due to interaction charge symmetry a definite relation between the n—He^4 and p—He^4 phases exsits. The p—He^4 phases have been measured with much greater accuracy than the n—He^4 phases and analysis of the proton data therefore yields independent information on the n—He^4 phases. An approximate recalculation of the phases based on the Wigner-Eisenbud formalism was carried out by Adair [7]) and Dodder and Gammel [8]). The results for the δ_0 and δ_1^+ phases are in satisfactory agreement with experiment (fig. 5). Variation of the δ_1^- phase deduced from analysis of the p—He^4 interaction is significantly different from that obtained from Huber's data. Seagrave's data on δ_1^- are in better agreement but the point at $E_n = 2.61$ MeV greatly differs from the proton estimate †.

3. A large peak in the total cross section related to the $P_{3/2}$ He^5 nuclear

† The significance of this discrepancy was pointed out to us by Seagrave (private communication).

level was observed in the $E_n = 1$ MeV neutron energy range. As the contribution of the $P_{3/2}$ state to the cross section is $\approx 90\ \%$ in this energy range it is possible to deduce Γ and E_{res} from the shape of the peak and hence $\delta_1 = \text{arctg}\ \Gamma/(E_{res}-E_n)$. The value for δ_1^+ obtained in this manner agrees with results of analysis of $\sigma(\theta)$ for n—He^4 scattering.

Measurements of δ_1^- were carried out at neutron energies of 2.45 and 3.4 MeV. The 3.4 MeV point is of interest in that the δ_1^- phase, according to the data of Huber and Baldinger, passes through $\frac{1}{2}\pi$ at this energy.

3.1 $E_n = 3.4$ MeV

This neutron energy was obtained at $E_d = 800$ keV and a neutron emission angle $\theta_n = 49°$. The scattering asymmetry was measured at seven counter rotation angles $\varphi_\alpha = 22.5°$, 27.5°, 32.5°, 39°, 45°, 50° and 56°. Results of the measurements are presented in table I.

TABLE 1

Angle of rotation of the counters	22.5°	27.5°	32.5°	39°	45°	50°	56°
Helium pressure (atm)	1.340	1.213	1.100	0.935	0.790	0.680	0.540
Discriminator setting	0.75	0.67	0.60	0.49	0.40	0.33	0.25
Angular divergence $\Delta\Omega$	10°25′	10°35′	10°40′	11°05′	11°30′	12°00′	12°35′
Measured asymmetry	1.259± ±0.037	1.250 ±0.039	1.105 ±0.033	1.033 ±0.042	0.835 ±0.020	0.807 ±0.032	0.780 ±0.022

In order to obtain information relating to the quantities $P_{n-\alpha}$ and P(d, n) several corrections to account for the poor geometry must be applied.

The measured asymmetry can be expressed by the formula

$$R = \frac{\int \sigma_{DD}\, \sigma_{n-\alpha}\, \Delta\Omega r^{-2} (1+P_x \cdot P_{n-\alpha})\mathrm{dv}}{\int \sigma_{DD}\, \sigma_{n-\alpha}\, \Delta\Omega r^{-2} (1-P_x\, P_{n-\alpha})\mathrm{dv}} \qquad (1)$$

where σ_{DD} is the differential cross section for the (D+D) reaction,

$\sigma_{n-\alpha}$ is the scattering cross section,
P_x the neutron polarization,
$P_{n-\alpha}$ the polarization of neutrons scattered on helium,
$\Delta\Omega$ the solid angle containing the recorded tracks of the recoil helium nuclei,
r the distance between the target and an element of counter volume.

In our case P_x and $P_{n-\alpha}$ can be considered as known functions of P_{max} and δ_1^-, where P_{max} is the maximal D(d, n) polarization for a given E_d:

$$P_x = P_{max} \frac{\sin 2\theta}{\sigma(\theta)} K(Ed)$$

where $K(E_d)$ is a normalization factor. The relation between $P_{n-\alpha}$ and the phase δ_1^- is given by the Lepore formulae [11]). Equation (1) thus reduces to an equation with two unknowns

$$R = f(\delta_1^-, P_{max}).$$

Choosing a definite value of the phase δ_1^- one can compute P_{max} for each of the seven measured values of R. The calculation was performed graphically: two values of P_{max} were chosen in such a way as to make $f(\delta_1^-, P_{max})$ somewhat larger and somewhat smaller than the measured asymmetry R. Furthermore, a value of P_{max} was found by interpolation which corresponded to the measured asymmetry and its errors. $f(\delta_1^-, P_{max})$ was calculated by numerical integration; for this purpose the operating volume of each counter was divided into 20 parts.

Ultimately, determination of the phase δ_1^- reduced to the following:

1) Measurement of asymmetry for seven rotation angles of the counters φ_α (table 1).

2) Calculation, for each angle φ_α, of the maximum neutron polarization from the (D+D) reaction, the phase $\delta_1^- = 30°$ (after Seagrave) being used in one case and $\delta_1^- = 90°$ (after Huber and Baldinger) in the other.

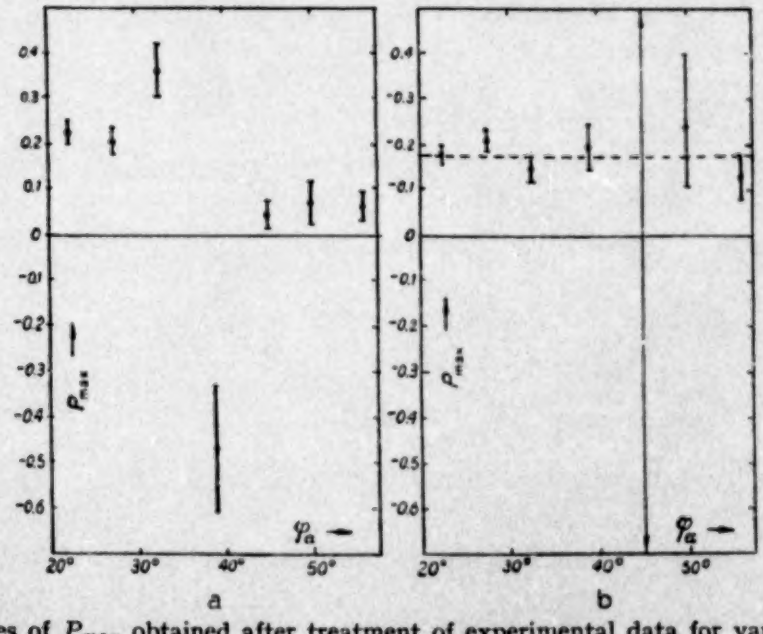

Fig. 6. Values of P_{max} obtained after treatment of experimental data for various rotation angles of counter φ_α.

a) Calculations employing phase shift values of Gruber and Baldinger [5])

b) Calculations employing phase shift values of Seagrave.

3) Comparison of the values of P_{max} determined by this method in each variant of the calculation. Good agreement of the values of P_{max} for each of the seven angles of rotation of the counters, φ_α, should testify to the correctness of the value of the phase δ_1^- employed in the calculations.

The results of calculation of P_{max} for each of the variants are presented in fig. 6. Evidently, the use of $\delta_1^- = 90°$ (after Huber and Baldinger) leads to a large spread of the values of P_{max} which considerably exceeds the experimental errors. On the other hand, if Seagrave's value, $\delta_1^- = 30°$, is employed in the calculations, values of P_{max} are obtained which within the limits of the errors, are in good agreement.

In this case one obtains for the polarization of (D+D) neutrons a value $P_{max} = 0.17$.

3.2 $E_n = 2.45$ MeV

δ_1^- was determined by comparing the experimental asymmetry of scattered neutrons possessing a known polarization with the asymmetry

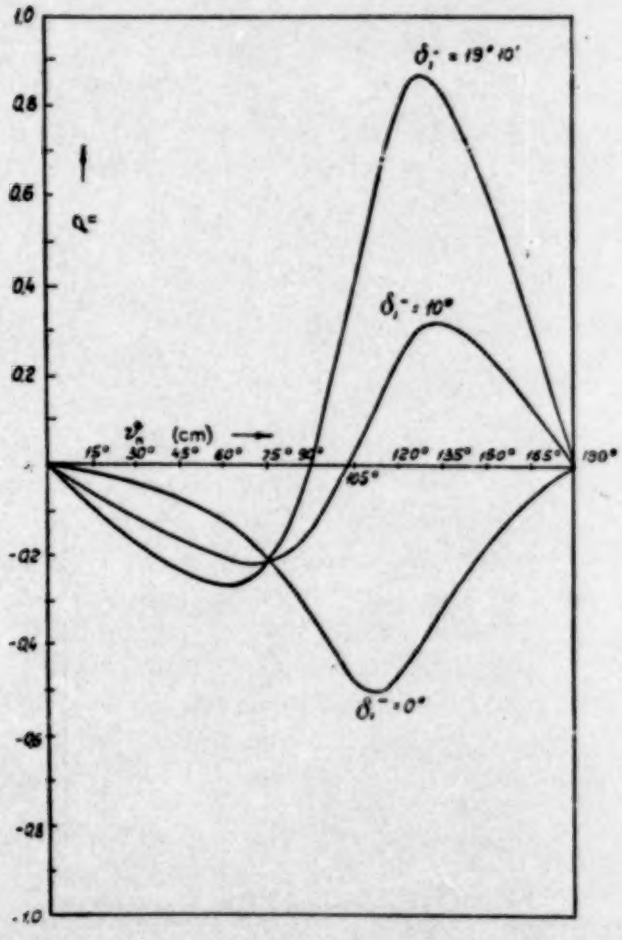

Fig. 7. Polarization of $E_n = 2.45$ MeV neutrons scattered on He^4; the calculations were performed for three phases: $\delta_1^- = 0°$; 10° and 19°10′ ($\delta_0 = -39°10'$; $\delta_1^+ = 121°10'$).

computed for various values of δ_1^-. Such measurements are very critical with respect to the magnitude of the phase δ_1^-. This can be seen from fig. 7 which represents the angular dependence of polarization in n—He^4 scattering calculated for $E_n = 2.45$ MeV on basis of the Seagrave phases δ° and δ_1^+ and for three values of $\delta_1^- = 0°$, 10°, 19°10′.

2.45 MeV neutrons can be obtained with $E_d = 1800$ keV and an emission angle $\theta_n = 106°$ (121° c.m.s.). The polarization angle of the (D+D) neutrons is then very close to the maximal value. Due to identity of particles in the (D+D) reaction, $\mathbf{P}(\pi-\theta$ c.m.s.$) = -\mathbf{P}(\theta$ c.m.s.$)$; thus, polarization of neutrons moving "backwards" at an angle θ_n (c.m.) = 121° can be directly determined from data on scattering asymmetry of neutrons moving "forward" at an angle θ_n (c.m.) = 59°, since for these neutrons one can accept Seagrave's phase δ_1^-. As a matter of fact, the energy of neutrons moving "forward" was 4.11 MeV, that is, close to the region in which our measurements confirmed Seagrave's analysis. Moreover, for this energy there is complete agreement between Seagrave's phases and the proton values.

Measurements of the scattering asymmetry of neutrons moving forward were performed for $E_d = 1800$ keV and θ_n (c.m.) = 59° with a thin (150 keV) target (for details see p. 237 of this journal); a value of $P_{max} = 0.170+0.010$ for the neutron polarization was obtained. Asymmetry measurements of neutrons moving "backwards" were performed with the same target and a counter rotation angle $\varphi_\alpha = 26°$. For a discriminator bias of 0.4 and helium

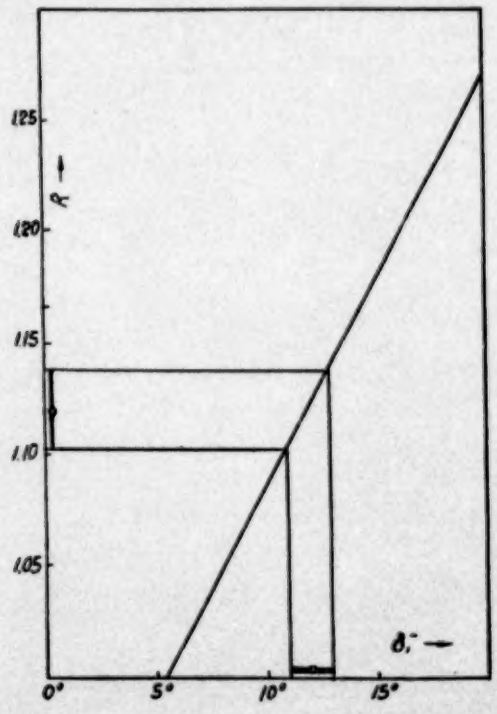

Fig. 8. Dependence of expected asymmetry R in $E_n = 2.45$ MeV experiments on magnitude of phase δ_1^-. A phase shift $\delta_1^- = 12° \pm 1°$ corresponds to the measured value $R = 1.120 \pm 0.018$.

pressure $p = 0.87$ atm the asymmetry was found to equal 1.120 ± 0.018. The dependence of the expected asymmetry in these measurements on phase δ_1^- is shown in fig. 8. This curve was calculated in the same way as for the experiment with $E_n = 3.5$ MeV. It follows from fig. 8 that the measured value of the asymmetry corresponds to a value $\delta_1^- = 12 \pm 1°$, which considerably differs from the proton estimate and agrees with the experimental data of Seagrave.

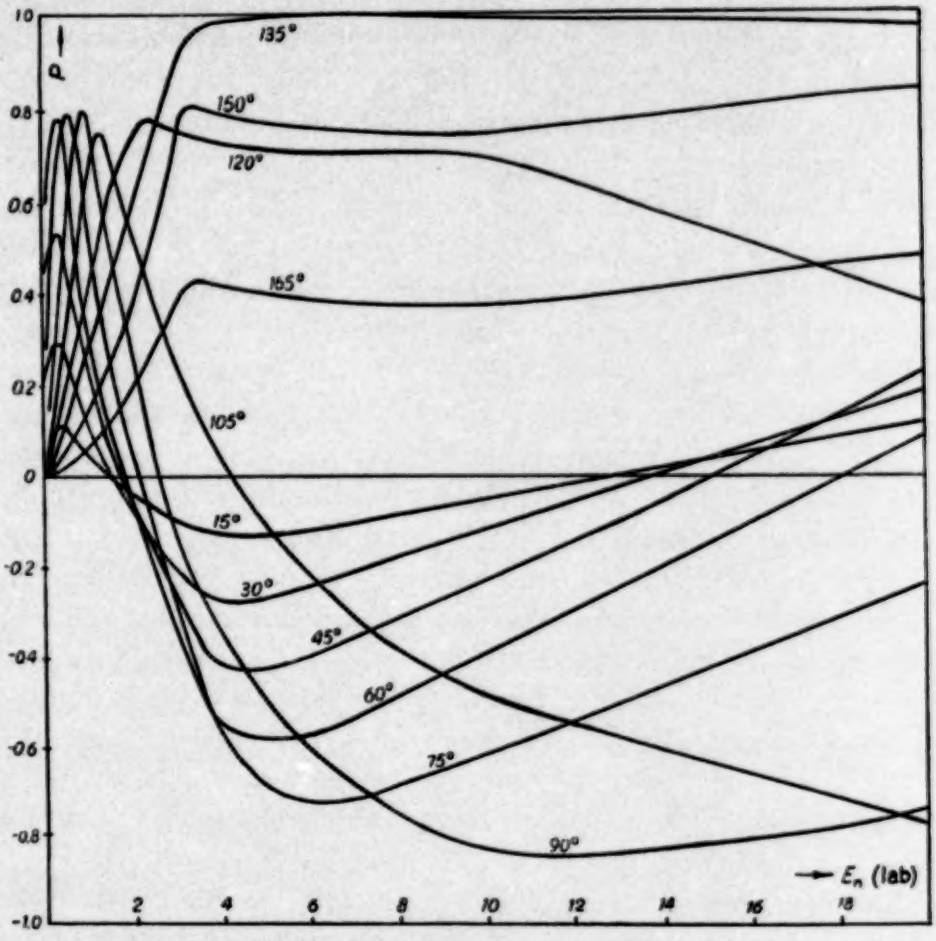

Fig. 9. Dependence of polarization of neutrons scattered by He^4 on neutron energy E_n for various scattering angles θ_n in the centre of mass system. The curves were computed from Seagrave's phase shifts [6]). The recoil angle of He^4 in the laboratory system $\varphi_\alpha = (\pi - \theta_n)/2$.

Our confirmation of Seagrave's phases means that helium can be used as a convenient and reliably calibrated analyser of polarized neutrons. The energy dependence of the polarization of neutrons scattered in helium is shown in fig. 9 for various scattering angles in the centre of mass system.

4. Theoretical Considerations

The energy dependence of the Seagrave phases is a natural consequence of the assumption that in a first approximation the n—He^4 and p—He^4

interaction is determined by the motion of the nucleon in the effective field of the unperturbed α-particle,

$$H(r) = -\frac{2 \cdot e^2}{r} + A_1 \cdot \varrho_1(r) + A_2 \cdot \frac{1}{r}\frac{d\varrho_2}{dr}(\mathbf{l} \cdot \boldsymbol{\sigma}) \qquad (2)$$

where A_1 and A_2 are evidently real for the energies under consideration and $\varrho_{1,2}$ are functions similar to the nucleon density distribution function in He^4 ($\varrho_1(0) = 1$).

The gradient shape of the spin-orbit interaction follows from general considerations, but ϱ_1 and ϱ_2, generally speaking, may be different. A satisfactory description of the P phase has been obtained in ref. [5]) † for $\varrho_1 = \varrho_2 = \exp[-(r/2.3)^2]$; $A_1 = 47$ MeV; $A_2/A_1 = 3.3 \times 10^{-27}$ cm^2. The slow growth of δ_1^- with energy and the absence of a distinct $P_{\frac{1}{2}}$ resonance are directly related to the decrease of the effective depth of the well in the $P_{\frac{1}{2}}$ state. The absence of $P_{\frac{1}{2}}$ resonance agrees with the results of ref. [12]) in which the (He^3+D) reaction was studied.

Description of the n—He^4 and p—He^4 interaction with aid of (2) permits one to compare the low and high energy interaction parameters; this, of course, cannot be done within the framework of the more general Wigner-Eisenbud method. Since, with the high energy data, one can obtain more detailed information pertaining to the shape of ϱ_1 and ϱ_2 this type of comparison, besides being of considerable physical interest (especially as regards the possibility of ascertaining the velocity dependence of the interaction range) is necessary for a correct estimation of the low energy parameters. The point here is that an energy interval of ≈ 10 MeV is not sufficient to yield reliable estimates of $\varrho(r)$ and the parameters A_1 and A_2 from the phase data. The phase variation can be approximately reproduced by employing various expressions for $\varrho(r)$, but the parameters are then found to be significantly at variance [5]).

We shall now present some preliminary conclusions which can be derived from the data of Chamberlain and Segrè [13]) on p—He^4 polarization and elastic scattering at 315 MeV (fig. 10). Since the He^4 radius is small at $E_p = 300$ MeV the Born approximation should be valid. In this case

$$P(\theta) \cdot \sigma(\theta) = 2 \cdot \mathrm{Im}\,(g) \cdot \mathrm{Re}\,(h); \qquad \sigma(\theta) = |g|^2 + |h|^2$$

where

$$g = A_1 \int j_0\left(2kr \cdot \sin\frac{\theta}{2}\right) \varrho_1 \cdot r^2\,dr; \qquad h = iA_2 k^2 \sin\theta \int j_0\left(2kr \cdot \sin\frac{\theta}{2}\right) \varrho_2 r^2\,dr.$$

If $\varrho_1 = \varrho_2$ one gets $h = g(A_2/A_1)ik^2 \sin\theta$, and $P(\theta)$, in general, will be independent of the shape of ϱ and will be determined by a single-maximum formula

† Cf. also ref. [17]).

$$P(\theta) = i\left|\frac{A_2}{A_1} - \frac{A_2^*}{A_1^*}\right| \cdot \sin\theta \cdot \left(1 + k^4 \cdot \left|\frac{A_2}{A_1}\right|^2 \cdot (\sin\theta)^2\right)^{-1}. \qquad (3)$$

Hence

$$\left|\frac{A_2}{A_1}\right| = \frac{1}{k^2 \cdot \theta_m},$$

where θ_m is the angle of maximum polarization. The peak on the Chamberlain-Segrè curve yields $A_2/A_1 = 3.3 \times 10^{-27}$ cm^2 in accord with the value of A_2/A_1 at low energies [5]). However, at $\theta \gtrapprox 20°$ the polarization dependence is essentially different from that which eq. (3) yields as the polarization changes its sign (fig. 10). This means that h is not exactly proportional to $g \cdot \sin\theta$ and that at $\theta \approx 27°$, g or h passes through zero.

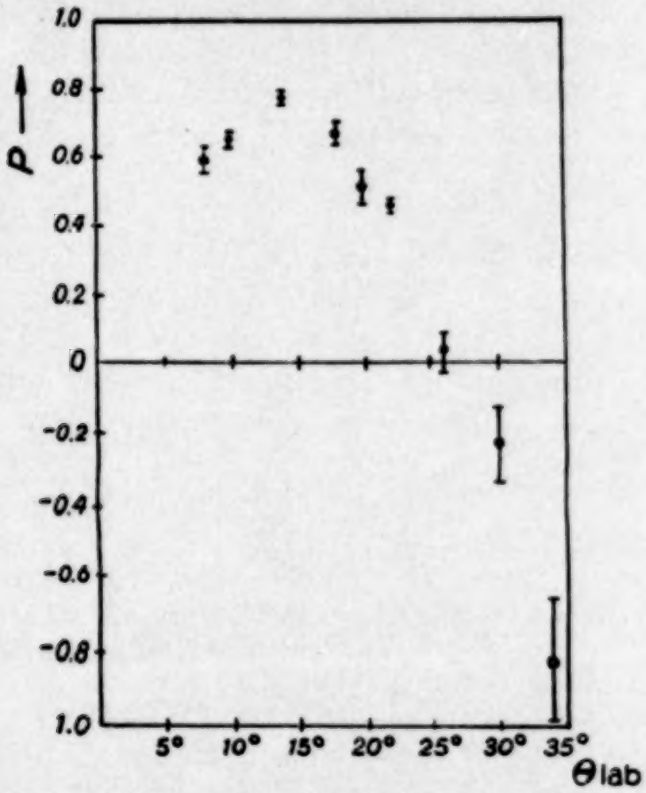

Fig. 10. Dependence of polarization of $E_p = 315$ MeV protons scattered by He^4 on the scattering angle in the laboratory system (measurements of Segrè and Chamberlain [13])).

We shall assume that h goes through zero at 27° although triple scattering experiments will be required to definitely settle this point [14]).

The following can thus be concluded:

1. The radial dependence of the imaginary part of potential ϱ_1 differs from the radial dependence of the spin-orbit potential ϱ_2.

2. ϱ_2 cannot be a Gaussian function as in this case $h \propto \sin\theta \cdot \exp(-\sin^2 \frac{1}{2}\theta)$ and hence does not go through 0.

3. If a second passage of $P(\theta)$ through 0 were observed at $\theta > 33°$ this

would signify that ϱ_1 were likewise a non-Gaussian function, ϱ_1 being shorter than ϱ_2.

The amplitude goes through zero in the case of a two parameter Wood-Saxon type potential [15])

$$\varrho = \frac{1}{1+e^{-(r-r_0)/a}} - \frac{1}{1+e^{(r+r_0)/a}}.$$

It would be interesting to derive the parameters for this type of potential from data on $\sigma(\theta)$ and $P(\theta)$ at low and high energies.

Our results confirm Seagrave's δ_1^- phase measurements at $E_n = 2.61$ MeV. The discrepancy between δ_1^- estimated from the proton data of Dodder and Gammel [8]) and the measured value should be ascribed to inadequacy of the Wigner-Eisenbud formalism in the considered case. Especially questionable is the assumption regarding the validity of the one-level approximation for such broad and overlapping levels.

It would be of interest to compare the neutron and proton phases expressed in terms of Hamiltonian (2).

The authors express their appreciation to the accelerator crew of the Institute of Chemical Physics and to A. N. Malishko and E. Z. Tarumov for assistance in carrying out the experiment, as well as to Ia. Smorodinsky and K. A. Ter-Martirosyan for helpful discussions on p, n—He^4 scattering. The authors are also indebted to A. I. Shalnikov for preparation of an important part of the apparatus.

References

1) R. W. Meier, R. Scherer and G. Trumpy, Helv. Phys. Acta **27** (1954) 577
2) R. K. Adair, S. Darden and R. E. Fields, Phys. Rev. **96** (1954) 503
3) R. Ricamo, Helv. Phys. Acta **26** (1953) 423
4) P. Huber and E. Baumgartner, Helv. Phys. Acta **26** (1953) 420
5) S. Schak, L. C. Biedenharn and A. Breit, Phys. Rev. **93** (1954) 321
6) J. D. Seagrave, Phys. Rev. **92** (1953) 1222
7) R. K. Adair, Phys. Rev. **86** (1952) 755
8) D. C. Dodder and J. L. Gammel, Phys. Rev. **88** (1952) 520
9) P. Huber and E. Baldinger, Helv. Phys. Acta **25** (1952) 435
10) R. J. Blin-Stoyle, Proc. Phys. Soc. A **65** (1951) 949
11) J. Lepore, Phys. Rev. **79** (1950) 137
12) G. F. Bogdanov, N. A. Vlasov *et al.*, JETP **30** (1956) 981
13) O. Chamberlain and E. Segrè, Phys. Rev. **96** (1954) 807
14) L. Wolfenstein, Phys. Rev. **96** (1954) 1654
15) M. A. Melkanoff, S. A. Mozkowski, J. Nodvik, D. S. Saxon, Phys. Rev. **101** (1956) 507
16) R. W. Gurney, Proc. Roy. Soc. A **107** (1926) 340
Editor's addition:
17) E. van der Spuy, Nuclear Physics **1** (1956) 381

Nuclear Physics **3** (1957) 237—239; *North-Holland Publishing Co., Amsterdam*

DEPENDENCE OF (D+D) NEUTRON POLARIZATION ON DEUTERON ENERGY

I. I. LEVINTOV, A. V. MILLER, E. Z. TARUMOV and V. N. SHAMSHEV
Institute of Chemical Physics, USSR Academy of Sciences, Moscow

Received 9 November 1956

Abstract: The polarization of (D+D) neutrons by thick and thin targets has been measured by a method described in the preceding paper for E_d lying between 0.6 and 1.8 MeV.

By applying the technique described in the preceding paper [1]) we have been able to measure the energy dependence of (D+D) neutron polarization. The ICP accelerating tube yielding deuterons of 1800 keV peak energy was employed.

Polarization measurements were performed with thick and thin zirconium targets. In all measurements the axes of rotation of the counters were located on a line which formed an angle of 49° with respect to the deuteron beam (see fig. 1 in the preceding paper), the angles of rotation, φ_α, being

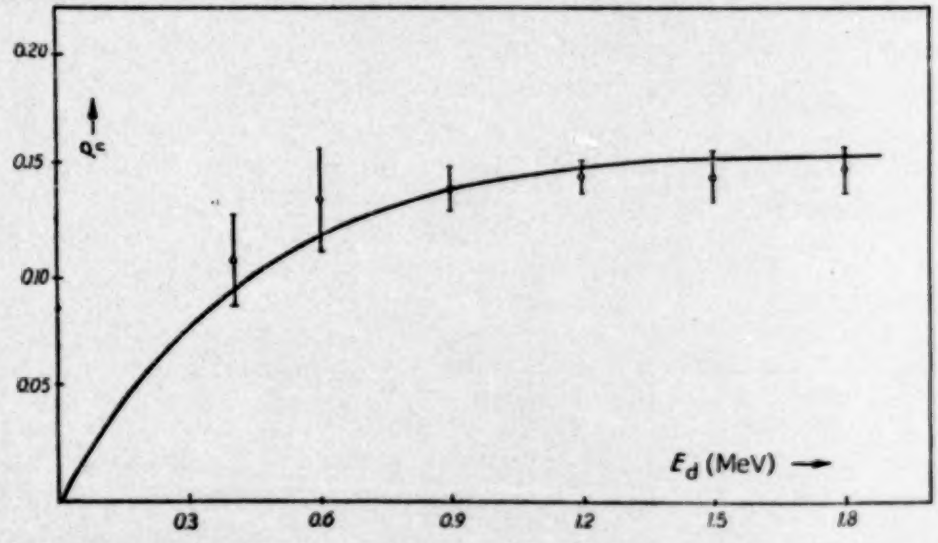

Fig. 1. (D+D) neutron polarization yield for angle Θ_n (lab) = 49°; obtained from thick target measurements at various deuteron energies E_d.

equal to 22°. The biases in the five discriminator channels were 0.4, 0.5, 0.6, 0.7 and 0.8. Computations of maximum polarization of the (D+D) neutrons were performed on basis of asymmetry data measured in the channels at 0.4 and 0.7. The discriminator channel with a 0.4 bias corresponded to the poorest geometry, the aperture of solid angle $\Delta\Omega$ (see eq. (1) in

our previous paper) being 19°. The aperture for the 0.7 channel was 11°. In all experiments the values of P_{max} obtained in both channels were in satisfactory agreement. In the further exposition we give the average value of P_{max} for the two channels; the experimental errors of P_{max} are merely the statistical errors of the measurements.

Results of measurement of the asymmetry with a thick target are presented in table I.

TABLE I

E_d (MeV)		0.4	0.6	0.9	1.2	1.5	1.8
Pressure in counters (atm)		1.034	1.143	1.263	1.380	1.449	1.566
Asymmetry R	0.4	1.119 ±0.029	1.170 ±0.028	1.141 ±0.016	1.119 ±0.011	1.125 ±0.013	1.106 ±0.011
	0.7	1.228 ±0.045	1.221 ±0.042	1.249 ±0.039	1.284 ±0.021	1.288 ±0.027	1.248 ±0.022

The maximal (D+D) neutron polarization, P_{max}, evaluated from these data is given in fig. 1. The calculations were carried out for an energy $\bar{E} = \frac{2}{3}E_d$, which corresponds to a linear dependence of the effective cross section of the reaction on deuteron energy. In this way it was possible to somewhat lower the uncertainty in the neutron energy (due to the presence of the thick target). The results presented in fig. 1 should thus be considered as the polarization "yield" from a thick target at the corresponding deuteron energies.

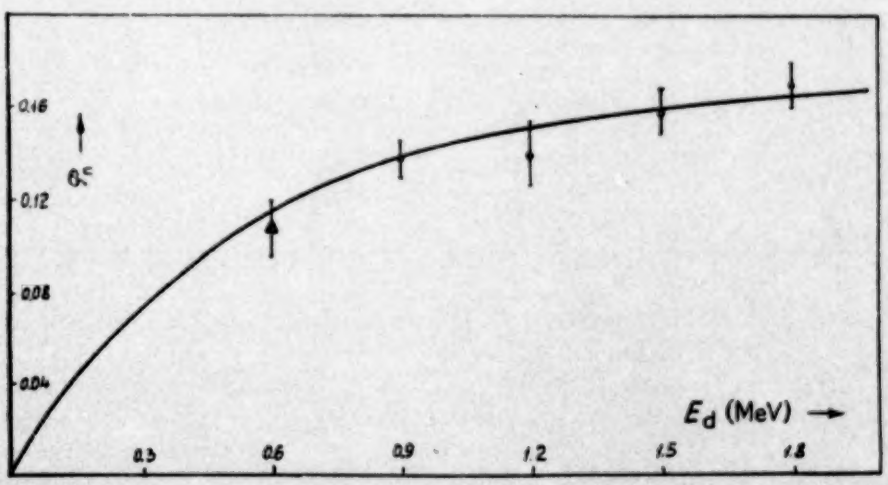

Fig. 2. (D+D) neutron polarization at angle Θ_n (lab) = 49°; obtained from thin target measurements at various deuteron energies E_d.
▲ result of measurements of Meier, Scherrer and Trumpy [3]).

A thin zirconium target 150 keV thick was used in the second set of measurements. On prolonged bombardment of the target with D ions the danger arises of a redistribution of the deuterium layer occurring, which may lead to an unpredictable change in the target thickness. The thin targets were therefore changed after every 20—30 hours of operation.

Results of asymmetry measurements in these experiments are given in table II; the values of P_{max} for (D+D) neutrons computed from these data are shown in fig. 2. The result of Meier, Scherrer and Trumpy [2]) for $E_d = 600$ keV (target thickness 70 keV) is presented in the same figure. Despite the large difference in the techniques employed our results are in good agreement with the data of this work which have heretofore been the only precise data on (D+D) neutron polarization.

TABLE II

E_d (MeV)		0.9	1.2	1.5	1.8
Pressure in counters (atm)		1.263	1.380	1.449	1.566
Asymmetry R	0.4	1.114 ±0.013	1.114 ±0.024	1.142 ±0.018	1.148 ±0.012
	0.7	1.261 ±0.024	1.253 ±0.049	1.273 ±0.037	1.348 ±0.027

Thus, the results presented in fig. 2 significantly extend our information concerning neutron polarization in this reaction. They indicate that up to $E_d = 1.8$ MeV the (D+D) neutron polarization monotonously depends on deuteron energy. This monotonous variation and the good precision of the values of P_{max} determined by us render the (D+D) reaction a convenient neutron source with a calibrated polarization.

We take the opportunity to express our thanks to the ICP accelerating tube group for help in carrying out the experiment.

References

1) I. I. Levintov, A. V. Miller and V. N. Shamshev, Nuclear Physics **3** (1957) 221
2) R. W. Meier, R. Scherer and G. Trumpy, Helv. Phys. Acta **27** (1954) 577

Nuclear Physics **3** (1957) 240—254; *North-Holland Publishing Co., Amsterdam*

A NOTE ON ROTATIONAL ENERGY LEVELS IN NUCLEI

F. VILLARS

CERN, *Geneva* †

Received 17 December 1956

Abstract: It is shown that the kinetic energy T of any system of interacting particles may be written in a "canonical form", which displays the dependence of T on the total angular momentum. A formula is given for the zero order moments of inertia associated with collective rotation of the system. The formalism is applied to nuclei, and, for purposes of comparison, to molecules.

In addition, it is shown that an unsymmetric formulation of the many particle problem, in which only the nucleons of a "core" participate in the definition of the body fixed axes, leads to a Hamiltonian which is related by a simple averaging process with the "unified" model of Bohr and Mottelson.

Finally, a connection is established between the "unified" model of Bohr-Mottelson and the "cranking model" of Inglis.

1. Introduction

The rotational spectra in molecules and in nuclei are experimentally characterized by a simple dependence of the energy eigen-values on the total angular momentum. This suggests that the kinetic energy operator itself, if written in terms of the total angular momentum and other suitable variables, should assume an especially simple form. This fact is well known for molecules [1]), but it seems to be less generally known that the kinetic energy of *any* system of particles may be written in a similar fashion. This "canonical form" of the kinetic energy is always based on the introduction of a "body-fixed" coordinate system. In molecules, the existence of well defined equilibrium positions of the particles provides a body fixed frame in a natural way. It is easily realized, however, that the existence of such equilibrium positions is by no means necessary for the possibility of introducing a "body fixed" frame. For any system of at least 3 particles, there exists an infinite variety of possibilities of defining such a frame in terms of the coordinates of the particles.

The "canonical form" thus appears as a result of a canonical transformation, in which the original particle coordinates and momenta are replaced by the following new variables:

a) the centre of mass $\mathbf{X}$, and total momentum $\mathbf{P}$,

b) the Euler angles θ_s ($s = 1, 2, 3$), describing the orientation of the body

† On leave of absence from Dept. of Physics, Mass. Inst. of Technology, Cambridge, Mass.

fixed frame in space, and their conjugate momenta Π_α, which are linear functions of the total angular momentum components † L_A,

c) $(3N-6)$ intrinsic variables ξ_σ, which need not be specified at this stage, and their conjugate momenta π_σ.

In terms of these new variables, the canonical form of the kinetic energy for a system of N particles of mass M reads ††

$$T = \frac{\mathbf{P}^2}{2MN} + T_{\text{int}}(\pi_\sigma, \xi_\sigma) + \tfrac{1}{2}\sum_{A,B} Q_{AB}(\xi_\sigma)(L_{\hat{A}} - L'_{\hat{A}})(L_{\hat{B}} - L'_{\hat{B}}) \qquad (1)$$

The L_A are the body fixed components of the *total* angular momentum; L'_A is an intrinsic angular momentum: $L'_A = L'_A(\xi_\sigma, \pi_\sigma)$, and Q_{AB} a reciprocal inertia tensor and a function of the intrinsic variables ξ_σ.

Now obviously not all systems do have rotational spectra. Their actual occurrence is therefore tied to certain specific conditions to be satisfied by the last term of (1). Roughly speaking, these conditions may be formulated as follows: It must be possible to introduce a body fixed system in such a way that

a) the differences $Q_{AB} - \overline{Q}_A \delta_{AB}$ stay small compared with the suitably chosen constants $\overline{Q}_A$.

b) the Coriolis-term in (1), $-\Sigma_{AB} Q_{AB} L_{\hat{A}} L'_{\hat{B}}$ is sufficiently small to be considered as a perturbation.

The possibility of satisfying such conditions depends of course on the intrinsic dynamics, governed by

$$H_{\text{int}} = T_{\text{int}}(\pi_\sigma, \xi_\sigma) + V(\xi_\sigma).$$

In section 2 the canonical form (1) of T shall be derived. This will also furnish an explicit expression for the inertia tensor Q_{AB}. In section 3, the results of sect. 2 are applied first, for the purpose of illustration, to molecules, then to nuclei. In section 4 the wave function is introduced. In section 5 the connection with the "unified model" is established; finally the Inglis "cranking" model is shown to be a semi-classical approximation of the unified model.

NOTATION

We shall use indices $\alpha, \beta, \gamma, \ldots$ to indicate vector components with respect to a space fixed (inertial) coordinate system. Projections of a vector on the body fixed axes will carry the subscripts $A, B, C, \ldots$. We shall also use the summation convention for vector and tensor components, wherever suitable.

† For the notation see below.

†† The equality of the masses is of course not essential, and is assumed here only for simplicity and in view of the application of the formalism to nuclei.

The relation between space and body fixed components of a vector is expressed through an orthogonal matrix $R_{A\alpha}$:

$$v_A = R_{A\alpha} v_\alpha ,$$
$$v_\alpha = R_{A\alpha} v_A .$$

We shall generally use double index notation for angular momenta, e.g.

$$L_{\alpha\beta} = x_\alpha p_\beta - x_\beta p_\alpha ;$$

wherever a one-index notation is more convenient, we characterize an axial vector by a $\hat{}$ over the subscript, e.g.

$$L_{\alpha\beta} \equiv L_{\hat{\gamma}} .$$

The subscripts $i, k, \ldots$ will be used to number the particles. A prime (e.g. x'_{iA}) is used to characterize quantities subject to some condition of constraint.

2. The Canonical Form of the Kinetic Energy

We think of a system of N identical particles with mass M. The starting point for our procedure is the observation that in any system of at least 3 particles the relative position of the particles in space can be used to define, in some arbitrary fashion, a "body fixed" coordinate system. Let then ξ_σ be a set of $(3N-6)$ independent variables, locating the particles with respect to that body frame. Calling $x_{i\alpha}$ the Cartesian components of the absolute position vector of the i^{th} particle, we can write

$$x_{i\alpha} = X_\alpha + R_{A\alpha}(\theta_s) x'_{iA}(\xi_\sigma) . \tag{2}$$

In this expression, X_α are the components of the centre of mass; $R_{A\alpha}$ is a 3-dimensional rotation matrix relating the space fixed to the body fixed frame in terms of 3 Euler angles θ_s; the x'_{iA} are the components of the vector $(\mathbf{x}_i - \mathbf{X})$ in the body fixed system, and as such expressible in terms of the ξ_σ. The set of x'_{iA} clearly satisfies

$$\sum x'_{iA} \equiv 0 \tag{3}$$

and 3 additional conditions which specify the particular choice of the body fixed system.

We now proceed to write the momentum $p_{i\alpha}$ in terms of π_σ (conjugate to ξ_σ), P_α (conjugate to X_α), and Π_s (conjugate to θ_s).
Clearly

$$p_{i\alpha} = \frac{1}{N} P_\alpha + \sum_\sigma \frac{\partial \xi_\sigma}{\partial x_{i\alpha}} \pi_\sigma + \sum_s \frac{\partial \theta_s}{\partial x_{i\alpha}} \Pi_s . \tag{4}$$

By taking the derivative of (2) with respect to $x_{k\beta}$, and solving for $(\partial \xi_\sigma / \partial x_{k\beta})$, we find another expression for the intrinsic momentum:

$$\sum_{\sigma} \frac{\partial \xi_\sigma}{\partial x_{i\alpha}} \pi_\sigma = \sum_{\sigma\tau} \frac{\partial x_{i\alpha}}{\partial \xi_\sigma} C^{-1}_{\sigma\tau} \pi_\tau - \sum_{s} \frac{\partial \theta_s}{\partial x_{i\alpha}} \sum_{A<B} A_{s,AB} L'_{AB}, \tag{5}$$

where the following definitions enter:

$$C_{\sigma\tau} = \sum_{i\alpha} \frac{\partial x_{i\alpha}}{\partial \xi_\sigma} \frac{\partial x_{i\alpha}}{\partial \xi_\tau}, \tag{6}$$

$$A_{s,AB} = -A_{s,BA} = \frac{\partial R_{A\alpha}}{\partial \theta_s} R_{B\alpha} \tag{7}$$

and

$$\begin{aligned} L'_{AB} &= \sum_i (x'_{iA} p'_{iB} - x'_{iB} p'_{iA}), \\ p'_{iA} &\equiv \sum_{\sigma\tau} \frac{\partial x'_{iA}}{\partial \xi_\sigma} C^{-1}_{\sigma\tau} \pi_\tau. \end{aligned} \tag{8}$$

L'_{AB} has the structure of an angular momentum, and will be called *intrinsic* angular momentum, since it is expressible in terms of the ξ_σ and π_σ alone. It is important to realize however that the x'_{iA} are not independent variables, nor are the p'_{iA} the momenta conjugate to the x'_{iA}.

The next step consists in expressing the momenta Π_s in terms of the total angular momentum with respect to the center of mass,

$$L_{\alpha\beta} = \sum_i (x_{i\alpha} p_{i\beta} - x_{i\beta} p_{i\alpha}) - (X_\alpha P_\beta - X_\beta P_\alpha).$$

Using (4) and (5), it follows that

$$\begin{aligned} L_{AB} &\equiv R_{A\alpha} R_{B\beta} L_{\alpha\beta} \\ &= L'_{AB} + \sum_s \Theta_{s,AB} (\Pi_s - \sum_{C<D} A_{s,CD} L'_{CD}), \end{aligned}$$

where

$$\Theta_{s,AB} = -\Theta_{s,BA} = \sum_i \left(x'_{iA} \frac{\partial \theta_s}{\partial x_{i\alpha}} R_{B\alpha} - x'_{iB} \frac{\partial \theta_s}{\partial x_{i\alpha}} R_{A\alpha} \right). \tag{9}$$

It follows from the general orthogonality relations for canonical variables, in this case from

$$\sum_{i\alpha} \frac{\partial \theta_s}{\partial x_{i\alpha}} \frac{\partial x_{i\alpha}}{\partial \theta_t} = \delta_{st},$$

that the two matrices (7) and (9) are orthogonal:

$$\sum_s A_{s,AB} \Theta_{s,CD} = \delta_{AC} \delta_{BD} - \delta_{BC} \delta_{AD}.$$

As a consequence of this, the total angular momentum, projected on the body fixed axes, reduces to

$$L_{AB} = \sum_s \Theta_{s,AB} \Pi_s. \tag{10a}$$

This relation may be inverted:

$$\Pi_s = \sum_{A<B} A_{s,AB} L_{AB}. \tag{10b}$$

Inserting (10b) and (5) into (4), we get the final expression for the momentum $p_{i\alpha}$ in terms of the new variables:

$$p_{i\alpha} = \frac{1}{N} P_\alpha + \sum_{\sigma\tau} \frac{\partial x_{i\alpha}}{\partial \xi_\sigma} C^{-1}_{\sigma\tau} \pi_\tau + \sum_{A<B} M_{i\alpha,AB}(L_{AB} - L'_{AB}). \tag{11}$$

As additional abbreviation, we introduced the important quantity

$$M_{i\alpha,AB} \equiv \sum_s \frac{\partial \theta_s}{\partial x_{i\alpha}} A_{s,AB} = \frac{\partial R_{A\gamma}}{\partial x_{i\alpha}} R_{B\gamma}. \tag{12}$$

Squaring (11) and summing over i and α, *all* cross terms are seen to vanish. For the cross term between the second and the third of (11), this is again due to a general orthogonality relation, in this case $\Sigma_{i\alpha}(\partial\theta_s/\partial x_{i\alpha})(\partial x_{i\alpha}/\partial\xi_\sigma) = 0$. For the kinetic energy, we therefore find as simple result the "canonical" form

$$T = \frac{1}{2MN} \sum_\alpha P_\alpha^2 + \frac{1}{2M} \sum_{\sigma\tau} C^{-1}_{\sigma\tau} \pi_\sigma \pi_\tau + \tfrac{1}{2} \sum_{A,B} Q^A_B (L_{\hat{A}} - L'_{\hat{A}})(L_{\hat{B}} - L'_{\hat{B}}), \tag{13}$$

where the inertial term Q_{AB} is given by

$$Q_{AB} = \frac{1}{M} \sum_{i\alpha} M_{i\alpha,\hat{A}} M_{i\alpha,\hat{B}}. \tag{14}$$

With this, we have established the canonical form (1) as an *exact* result, and in addition found an explicit expression for the tensor Q_{AB}. It becomes amply clear, from the definition of the $M_{i\alpha,AB}$, that the values of the elements of the inertia tensor directly depend on the way the Euler angles θ_s are defined in terms of the particle positions $x_{i\alpha}$.

3. The Zero Order Momenta of Inertia

It will be instructive to apply the results of the preceding section to both molecules and nuclei. The problem is then to specify the 3 additional conditions to be imposed on the x'_{iA}.

In molecules the situation is characterized by the existence of well defined equilibrium positions x^0_{iA}, about which the nuclei perform small amplitude oscillations:

$$x'_{iA} = x^0_{iA} + \delta x'_{iA}(\xi_\sigma). \tag{15}$$

The equilibrium positions define a quasi rigid frame, to which the body fixed system may be attached. In that case, the nuclei have zero angular momentum with respect to the "body fixed" frame, when in their equilibrium position. We therefore set up the 3 conditions

$$\sum_i (x^0_{iA}\,\delta x'_{iB} - x^0_{iB}\,\delta x'_{iA}) \equiv 0. \tag{16}$$

This is to hold identically in ξ_σ. This equation allows us to express the Euler angles θ_s in terms of the particle positions $x_{i\alpha}$. In fact, by (2), (16) is equivalent to the statement

$$\sum_i (x^0_{iA}\,R_{B\gamma}(\theta_s)x_{i\gamma} - x^0_{iB}\,R_{A\gamma}(\theta_s)x_{i\gamma}) \equiv 0,$$

which now has to hold identically in $x_{i\alpha}$, thus defining $\theta_s(x_{i\alpha})$. Taking derivatives, we find for the quantity $M_{i\alpha,\,AB}$, which determines the moment of inertia:

$$M_{i\alpha,\,AB} \approx \frac{1}{I^0_B + I^0_A}\,(x^0_{iA}\,R_{B\alpha} - x^0_{iB}\,R_{A\alpha}). \tag{17}$$

The approximation stems from the neglect of $\delta\mathbf{x}'$ compared to $\mathbf{x}^0$ in solving for $M_{i\alpha,\,AB}$. The $I_A{}^0$ are the principal moments of inertia

$$I^0_A = \sum_i (x^0_{iA})^2.$$

The off diagonal elements I^0_{AB} may of course be assumed to be zero, by suitable choice of axes. The actual mass tensor I_{AB} differs then only by terms of order $\delta\mathbf{x}'$ from $I^0_A\,\delta_{AB}$. With (17) the tensor Q_{AB} is diagonal. From (17) and (14) it follows that the zero order principal momenta are

$$\frac{1}{Q_{AA}} \approx M(I^0_B + I^0_C), \tag{18}$$

as expected for rigid rotation.

Equilibrium positions, as in (15), can clearly not be attributed to nucleons in nuclei. On the contrary, the wave function of each nucleon is assumed to extend over the entire nuclear volume, and for a given nucleon it is not so much the exact positions of the others that matter, but rather the general "distribution" of positions. It is this *distribution* which determines the effective potential, in which a given nucleon moves. The main point is then to realize that such a distribution may be stationary (apart from certain fluctuations) in a suitable frame of reference, and thus generate a potential which is stationary in that same frame. We thus see that the ideas associated with the independent particle picture, namely an effective potential determined by the "macroparameters" of the distribution of nucleons rather than by the details of their positions, momenta, etc., naturally suggest a description which isolates these features. Whereas for a long time the only macroparameters introduced have been size and depth of the effective (spherical) potential well, more recent in sight has shown the necessity of introducing shape (anistotopy) and orientation of the potential well. But clearly orientation is a dynamical variable rather than a para-

meter (contrary to shape) and the methods presented here allow to take care of this feature.

A distribution of positions may be characterized by suitable momenta, the lowest of which is

$$\sum_i w(i)(x_{i\alpha}-X_\alpha)(x_{i\beta}-X_\beta) \tag{19}$$

with $w(i)$ a suitable weight factor, e.g. some function of $\mathbf{x}_i^2$, etc. The principal axes of the tensor (19) conveniently furnish a set of body fixed axes, with respect to which the distribution characterized by the weight factor $w(i)$ is stationary.

Clearly any choice of $w(i)$ gives a possible definition of a body fixed system, and we shall have to develop criteria for a best choice. As an introduction to that subject, let us follow the way of least resistance and take $w(i) = 1$. In that case the body fixed system is characterized by

$$\sum_i x'_{iA} x'_{iB} \equiv 0 \qquad (A \neq B), \tag{20}$$

this equation holding identically in ξ_σ, so that the body system is, at all times, *exactly* given by the principal axes of the tensor (19), with $w = 1$. With (2) it follows that condition (20) is equivalent to

$$R_{A\alpha}(\theta_s)R_{B\beta}(\theta_s)\sum_i (x_{i\alpha}-X_\alpha)(x_{i\beta}-X_\beta) \equiv 0 \qquad (A \neq B),$$

a condition which again has to hold identically in the $x_{i\alpha}$ and thus defines the $\theta_s(x_{i\alpha})$. We easily find that now

$$M_{i\alpha,\,AB} = \frac{1}{I_A-I_B}(x'_{iA}R_{B\alpha}+x'_{iB}R_{A\alpha}), \tag{21}$$

where

$$I_A = \sum_i (x'_{iA})^2.$$

It is interesting to compare this expression with (17), the corresponding expression for molecules. As in that case, Q_{AB} becomes diagonal, with

$$\frac{1}{Q_{AA}} = M\frac{(I_B-I_C)^2}{I_B+I_C}. \tag{22}$$

This value is exactly equivalent to the hydrodynamic value obtained in the irrotational liquid drop model [2]). We shall therefore briefly refer to (22) as the "hydrodynamic" value of Q_{AA}^{-1}, and to (18) as the "rigid-body" value. Characteristic of the hydrodynamic Q_{AA}^{-1} is its zero value for a spherical distribution, and its increase with the square of the deformation.

At this point one may speculate about the consequences of applying definition (20) to molecules. This does not seem unnatural at least for non spherical molecules. In fact, at first sight, the difference, for the case of

such molecules, between definition (16) and (20) seems to be slight, since (20) holds "almost" (to order $\delta\mathbf{x}'$) as a consequence of (16). But the results are quite different and coincide only in the limit of extremely elongated molecules. The large difference in the values of Q_{AA} for the two definitions stems from the fact, that by (16) the intrinsic angular momentum is exactly zero in lowest order, and therefore the Coriolis effects are minimized; on the contrary, by (20), L'_{AB} is non zero even with the nuclei in their equilibrium positions; there results a large Coriolis correction to the rotational energy; the effective momenta of inertia, defined by the coefficients of $I(I+1)$ in the energy eigen-values (cf. subsection 5.4), must be identical in both cases. Definition (20), as applied to molecules, appears then simply as a possible, but not very clever choice of a body fixed system.

For nuclei, we have no choice but to take a definition similar to (20) (possibly with $w(i) \neq 1$). We realize, however, that this choice does nothing to minimize the Coriolis effect, and we must also be prepared to find it quite large, as the above discussion of molecules shows. In the light of this analysis it no longer appears too much of a puzzle to observe rotational spectra in nuclei with effective momenta of inertia differing appreciably from the hydrodynamic value (22) †.

4. Wave Functions; Spin ††

The angular momentum operators L_{AB} introduced in (10a), satisfy the well known relations [4, 5])

$$\begin{aligned} &[L_{AB},\ L_{AC}] = -i\hbar L_{BC}, \\ &[L_{\alpha\beta},\ L_{\alpha\gamma}] = +i\hbar L_{\beta\gamma}; \end{aligned} \tag{23a}$$

$$\begin{aligned} &[L_{AB},\ L_{\alpha\beta}] = 0, \\ &[L^2,\ L_{AB}] = [L^2,\ L_{\alpha\beta}] = 0. \end{aligned} \tag{23b}$$

The transformation (2) from a system of axes $\alpha\beta\gamma$ to axes ABC:

$$v_\alpha = R_{A\alpha}(\theta_s)v_A,$$

defines a transformation of angular momentum eigenstates ψ_{jm} and $\tilde{\psi}_{j\mu}$ in the two systems:

$$\psi_{jm} = \sum_\mu \mathscr{D}^{(j)}_{\mu m}(\theta_s)\tilde{\psi}_{j\mu} \tag{24}$$

The $\mathscr{D}^{(j)}_{\mu m}$, as functions of θ_s, are eigenfunctions of the operators L^2, L_z and L_3 to eigenvalues $\hbar^2 j(j+1)$, $\hbar m$ and $\hbar\mu$ respectively †††. From (23a, b) it follows that the Hamiltonian

† For comparison with experiment, see ref. [3]).

†† No originality is claimed for the substance of this section, which is mainly presented for the sake of completeness.

††† The z-axis is space fixed; the 3-axis body fixed.

$$H = T+V(\xi) \tag{25}$$

T being given by the canonical form (13), commutes with L^2 and L_z, but not generally with L_3. The eigenfunctions of H therefore have the structure

$$\psi_{nIM} = \sum_K \mathscr{D}^{(I)}_{KM}(\theta_\sigma)\ \phi_{nK}(\xi_\sigma) \tag{26}$$

corresponding to eigenvalues $\hbar^2 I(I+1)$ and $\hbar M$ of L^2 and L_z.

These results are easily generalized such as to include spin. As an intrinsic variable, we want to describe it in the body fixed system, that is, choose a representation in which s_3 rather than s_z is diagonal. By (24) it follows that the probability amplitudes a_m for s_z are connected with the probability amplitudes $\tilde{a}_\mu$ for s_3 by

$$a_m = \sum_\mu \mathscr{D}^{\dagger(\frac{1}{2})}_{m\mu}\tilde{a}_\mu. \tag{27}$$

The change of representation therefore defines a transformed Hamiltonian

$$\tilde{H} = \prod_i \mathscr{D}^{(\frac{1}{2})}(i) H \prod_i \mathscr{D}^{\dagger(\frac{1}{2})}(i).$$

From the symmetry property [6])

$$\mathscr{D}^{\dagger(j)}_{m\mu}(\theta) = (-1)^{m-\mu}\mathscr{D}^{(j)}_{-\mu_1-m}(\theta)$$

we derive that

$$\sum_m \mathscr{D}^{(j)}_{\mu m} L_{AB} \mathscr{D}^{\dagger(j)}_{m\mu'} = L_{AB}\delta_{\mu\mu'} - (j\mu/j_{AB}/j\mu'). \tag{28}$$

It follows that $\tilde{H}$ differs from H by the substitution

$$(L_{AB}-L'_{AB}) \to (L_{AB}-L'_{AB}-\tfrac{1}{2}\sum_i \sigma_{iAB}) = (L_{AB}-J'_{AB}). \tag{29}$$

Thus the total intrinsic angular momentum $\mathbf{J}'$ appears now in $\tilde{H}$; this is accompanied by a change in the physical interpretation of L_{AB}, which now represents the total angular momentum (including spin) of the system. The form (26) of the wave function, with $\phi(\xi_\sigma)$ replaced by $\phi(\xi, s_{i3})$, still holds, except that now I may take integer or half integer values, depending on whether the number of nucleons is even or odd.

We might add a word here concerning the symmetry properties of the wave function. A complete discussion of this subject is however rather tedious, due to the unspecified nature of the intrinsic variables, and we shall give, in the next section, a somewhat limited formulation of that problem, in connection with the choice of a simple trial function for ϕ, (26).

5. Discussion of Results

5.1. THE PROBLEM OF THE CONSTRAINED INTRINSIC MOTION

In order to combine the results of section 4 with an independent particle treatment of at least some of the nucleons, one may be tempted to choose

the corresponding x'_{iA} and p'_{iA} as independent pairs of canonical variables. Such a procedure would be inconsistent. To see this, we recall that the x'_{iA} are assumed to satisfy eq. (20) identically in the independent variables†; it follows that

$$[L'_{AB}, \sum_i x'_{iA} x'_{iC}] \equiv 0 \qquad (A \neq C). \tag{30}$$

The commutation relations of x'_{iA} with the intrinsic angular momentum cannot therefore be those of a vector; in fact, from a simple, but somewhat lengthy calculation one finds

$$\frac{i}{\hbar}[L'_{AB}, x'_{iC}] = \frac{2I_B}{I_A+I_B} x'_{iA}\delta_{BC} - \frac{2I_A}{I_A+I_B} x'_{iB}\delta_{AC}. \tag{31}$$

This relation guarantees the validity of (30). It must be realized that (31) holds *independently* of any specific choice of the (ξ_σ, π_σ); this proves in particular that none of the pairs (x'_{iA}, p'_{iA}) may be taken as independent variables, since in that case the usual relations

$$\frac{i}{\hbar}[L'_{AB}, x'_{iC}] = x'_{iA}\delta_{BC} - x'_{iB}\delta_{AC}$$

must hold, which are incompatible with (31). We may add that the commutators

$$[L'_{AB}, p'_{iC}] \quad \text{and} \quad [L'_{AB}, L'_{AC}]$$

cannot be evaluated without a specific choice for the ξ_σ; in particular the intrinsic angular momenta do *not* satisfy the simple angular momentum commutation relations.

5.2. CONSTRUCTION OF AN UNSYMMETRIC HAMILTONIAN

A completely different situation arises if we define the collective coordinates in an unsymmetric way, separating the N nucleons into a part N' forming a "core", and $(N-N')$ "valence"-nucleons, and applying transformation (2) and condition (20) to $\mathbf{x}_1 \ldots \mathbf{x}_{N'}$ only. It is then possible to describe the motion of the $(N-N')$ last nucleons in the body fixed frame of the other particles; in this case the variables

$$x_{rA} = R_{A\alpha} x_{r\alpha} \qquad (r = N'+1, \ldots, N)$$
$$p_{rA} = R_{A\alpha} p_{r\alpha}$$

are independent canonical pairs; if the spin of these particles is also referred to the body fixed axes, the methods outlined in section 4 lead to an unsymmetric, but *exact*, Hamiltonian (apart from the centre of mass adjust-

† *Editor's note:* For the treatment of relations of the type (20) as auxiliary conditions, see R. S. Nataf [7]).

ment corrections, which are small if $N-N' \ll N'$) of the following type:

$$H = H_{\text{int}}(\pi_\sigma, \xi_\sigma) + \frac{1}{2M}\sum_{rA} \mathbf{p}_{rA}^2 + \tfrac{1}{2}\sum_{r,s}' V(\mathbf{x}_r - \mathbf{x}_s)$$
$$+ \sum_{r=N'+1}^{N}\sum_{i=1}^{N'} V(\mathbf{x}_r - \mathbf{x}_i'(\xi_\sigma)) \tag{32}$$
$$+ \tfrac{1}{2}\sum_{A,B} Q_{AB}(L_{\hat{A}} - J'_{\hat{A}} - \sum_r j_{r\hat{A}})(L_{\hat{B}} - J'_{\hat{B}} - \sum_r j_{r\hat{B}}).$$

In (32) the "valence nucleons" do *not* participate in the definition of the inertia tensor Q_{AB}; this is the price to pay in order to be able to consider their positions and momenta (referred to be body fixed axes) as independent variables.

The structure (32) suggests a simple way of averaging over the intrinsic motion. We may introduce a normalized trial function $\phi(\xi; \beta_A)$, containing 3 variational parameters β_A in such a way as to have, with (22),

$$\langle Q_{AB}\rangle_\phi = \int d\tau_\xi \phi^* Q_{AB}\phi = \frac{\delta_{AB}}{\mathscr{I}_0 \beta_A{}^2}. \tag{33}$$

The β_A are thus identified as shape parameters. † It then follows that

$$\langle \sum_{i=1}^{N'} V(\mathbf{x}_r - \mathbf{x}_i'(\xi_\sigma)\rangle_\phi = U(\mathbf{x}_r;\ \beta) \tag{34}$$

represents a deformed single particle well. If N' is chosen in such a way as to allow a closed shell configuration for the core, we may assume that

$$\langle H_{\text{int}}\rangle_\phi = E_{00} + \tfrac{1}{2}C\sum_A \beta_A{}^2 + \dots \tag{35a}$$

and

$$J'_{\hat{A}}\phi = 0. \tag{35b}$$

It is not at all obvious that the relation (35b) should hold. It is interesting to see, however, that it takes such an assumption in order to establish the relation between (32) and the Hamiltonian of the "unified" model.

With (35a) and (35b) the ϕ-averaged Hamiltonian takes the simple form

$$\langle H\rangle_\phi = E_{00} + \tfrac{1}{2}C\sum_A \beta_A{}^2 + \sum_A \frac{1}{2\mathscr{I}_0\beta_A{}^2}(L_{\hat{A}} - \sum j_{r,\hat{A}})^2$$
$$+ \sum_r \left(\frac{\mathbf{p}_r{}^2}{2m} + U(\mathbf{x}_r,\ \beta)\right) + \tfrac{1}{2}\sum_{r,s}' V(\mathbf{x}_r - \mathbf{x}_s). \tag{36}$$

In the usually considered symmetric case,

$$\beta_3 = 0, \qquad \beta_1 = \beta_2 = \beta,$$

† There is of course the possibility to introduce the β_A as dynamical variables and to average over an invariant function of the residual intrinsic variables. The simpler method followed here is adequate for many purposes.

$\langle H\rangle_\phi$ is naturally split into 3 terms †:

$$\langle H\rangle_\phi = E_0(I,\ \beta)+H_{\text{part}}+H_{\text{cp}},$$

with

$$E_0(I,\ \beta) = E_{00}+C\beta^2+\frac{I(I+1)}{2\mathscr{I}_0\beta^2}, \tag{37a}$$

$$H_{\text{part}} = \sum_r\left(\frac{\mathbf{p}_r^{\,2}}{2m}+U(\mathbf{x}_r;\ \beta)+\frac{\mathbf{j}_r^{\,2}-2(\mathbf{L}\cdot\mathbf{j}_r)}{2\mathscr{I}_0\beta^2}\right), \tag{37b}$$

$$H_{\text{cp}} = \sum_{r,\,s}{}'\left(\tfrac{1}{2}V(\mathbf{x}_r-\mathbf{x}_s)+\frac{(\mathbf{j}_r\cdot\mathbf{j}_s)}{2\mathscr{I}_0\beta^2}\right); \tag{37c}$$

(37a) is a constant term; (37b) a sum of single particle Hamiltonians, whereas (37c) gives the interparticle couplings.

We may at this place take up the question of the choice of the body fixed system, which was temporarily settled by choosing 1 for the weight function $w(i)$ in (19). Clearly, if we had the means of solving eq. (32) properly, this would just be question of convenience. But in the light of the approximations made to get from (32) to (36), (37), especially assumption (35b), a different point of view must be taken: the problem is essentially to know *which* definition (19) for the body fixed axes is consistent with the assumption (35b) of a zero eigenvalue (not only expectation value!) of J'_{AB}. This is in fact the dynamical argument which must be applied to define $w(i)$. Once this is solved, then the Hamiltonian (36), (37), with appropriate zero order moments of inertia, may be considered established in a satisfactory way, and there remains the technical problem of finding a suitable solution of (37).

5.3. SYMMETRY PROPERTIES OF THE WAVE FUNCTION

The symmetry properties of the collective wave function have been studied by Bohr [8]) and for a somewhat more general situation by Marty [9]). It is seen that in our present formulation it is not possible to reproduce the results of Marty, since we cannot consider the x'_{iA} and p'_{iA} as independent variables. In connection with the approximate Hamiltonian (36) however, some statements can be made: if one assumes that the trial function $\phi(\xi;\ \beta_A)$ has the following simple transformation properties under the 3 basic symmetry operations R_1, R_2 R_3 considered by Bohr ††:

$$R_1\phi = \phi,$$
$$R_2\phi(\xi;\ \beta_1,\ \beta_2,\ \beta_3) = \phi(\xi;\ -\beta_2,\ -\beta_1,\ -\beta_3),$$
$$R_3\phi(\xi;\ \beta_1\beta_2\beta_3) = \phi(\xi;\ \beta_2\beta_3\beta_1),$$

† For $\beta_1=\beta_2$, $\Lambda = L_3-\Sigma j_{r,3}$ is a constant of the motion; if in addition $\beta_3=0$, Λ takes the value 0 only. This is implied in eq. (37).

†† R_1 is a reflexion of the 2 and 3 axes; R_2 a rotation of $\pi/2$ about the 3 axis, and R_3 a cyclic permutation (123 → 231) of the three axes.

then the same conclusions may be reached with regard to the symmetry structure of $\psi(\theta_s, \mathbf{x}_r)$:

$$\psi(\theta_s, \mathbf{x}_r) = \sum_K \left(\mathscr{D}^{(I)}_{KM}(\theta_s)\varphi_{JK}(\mathbf{x}_r) + (-1)^{I-J}\mathscr{D}^{(I)}_{-K,M}(\theta_s)\varphi_{J,-K}(\mathbf{x}_r)\right),$$

with the obvious generalizations if $\mathbf{J} = \Sigma_r \mathbf{j}_r$ is not a constant of the motion.

5.4 THE EFFECTIVE MOMENTS OF INERTIA

The single particle motion, governed by the Hamiltonian (37b), is disturbed by inertial forces. If this disturbance is weak enough, such as to permit a perturbation treatment, the single particle energy acquires a term $\approx I(I+1)$. On the basis of this effect, the deviations of the observed values of the moment of inertia from $\mathscr{I}_0\beta^2$ have been investigated by Kerman[10]) and Lüders [11]).

We shall give here a sketch of a Hartree-Fock solution of eqs. (37), for the case that $\mathbf{L}$ is considered as a *classical* vector. This will establish the relation of (37) with the "cranking model" of Inglis [12]) and Moszkowski [13]). We shall for that purpose also temporarily drop the interaction $V(\mathbf{x}_r - \mathbf{x}_s)$ between valence nucleons, and also drop their spin. As trial functions we choose a normalized determinant of single particle functions $\varphi_a(\mathbf{x}_r)$. With (37), dropping $E_{00} + C\beta^2$, we have †

$$\begin{aligned}\langle E\rangle = {} & \frac{\mathbf{L}_\perp{}^2}{2\mathscr{I}_0\beta^2} + \sum_a \left\langle \frac{\mathbf{p}^2}{2M} + U(\mathbf{x}_{t,\beta})\right\rangle_{a,a} \\ & + \frac{1}{2\mathscr{I}_0\beta^2}\Big\{\sum_a \langle \mathbf{I}_\perp{}^2\rangle_{a,a} - 2\mathbf{L}_\perp \cdot \sum_a \langle \mathbf{I}_\perp\rangle_{a,a} \\ & + \sum_{a,b}\left(\langle \mathbf{I}_\perp\rangle_{a,a}\cdot\langle \mathbf{I}_\perp\rangle_{b,b} - \langle \mathbf{I}_\perp\rangle_{a,b}\cdot\langle \mathbf{I}_\perp\rangle_{b,a}\right)\Big\}.\end{aligned} \tag{38}$$

Observing that

$$\langle \mathbf{I}_\perp{}^2\rangle_{a,a} = \sum_n \langle \mathbf{I}_\perp\rangle_{a,n}\cdot\langle \mathbf{I}_\perp\rangle_{n,a}$$

we can simplify (38) by dropping the terms

$$\sum_n{}' \sum_a \langle \mathbf{I}_\perp\rangle_{a,n}\cdot\langle \mathbf{I}_\perp\rangle_{n,a} \begin{pmatrix} a = \text{occupied} \\ n = \text{unoccupied}\end{pmatrix}.$$

This is presumably a bettter approximation than dropping the exchange terms altogether. There results from this approximation a very simple single particle equation:

$$\begin{aligned}&\left(\frac{\mathbf{p}^2}{2M} + U(\mathbf{x};\beta)\right)\varphi_a(\mathbf{x}) \\ &\quad - \frac{1}{\mathscr{I}_0\beta^2}\left(\mathbf{L}_\perp - \sum_b \langle \mathbf{I}_\perp\rangle_b\right)\cdot \mathbf{I}_\perp \varphi_a(\mathbf{x}) = E_a\varphi_a(\mathbf{x}).\end{aligned} \tag{39}$$

† The notation $\mathbf{L}_\perp$, $\mathbf{I}_\perp$ is used for the component of these vectors perpendicular to the 3-axis.

Anticipating an obvious effect, we write

$$\sum_b \langle \mathbf{l}_\perp \rangle_b = \varkappa \mathbf{L}_\perp \qquad (0 < \varkappa < 1). \tag{40}$$

Eq. (39) then reduces to

$$\left(\frac{\mathbf{p}^2}{2M} + U(\mathbf{x};\, \beta) - (\boldsymbol{\omega}_\perp \cdot \mathbf{l}_\perp) \right) \varphi_a(\mathbf{x}) = E_a \varphi_a(\mathbf{x}), \tag{41}$$

with $\boldsymbol{\omega}_\perp$ being defined as the angular velocity

$$\boldsymbol{\omega}_\perp = (1-\varkappa) \frac{\mathbf{L}_\perp}{\mathscr{I}_0 \beta^2}. \tag{41a}$$

We recognize in (41) the characteristic single particle equation of the Inglis model, in which a spheroidal potential rotates with constant angular velocity ω about an axis perpendicular to the symmetry axis of the spheroid. In this model, $\Sigma_a E_a$ is the total energy in the body fixed frame, and of the form

$$\sum_a E_a(\omega) = \sum_a E_a(0) - \tfrac{1}{2} \mathscr{I}_{\text{eff}} \omega^2, \tag{42a}$$

whereas the total average energy in the laboratory system is given by

$$\langle E \rangle = \sum_a E_a(0) + \tfrac{1}{2} \mathscr{I}_{\text{eff}} \omega^2. \tag{42b}$$

The relation between (42a) and (42b) is tied to the fact that in this model *all* nucleons are described by eq. (41).

We shall show that relations closely analogous to (42a, b) hold in the present case. Indeed, from (38) and (40) it follows that

$$\begin{aligned} \langle E \rangle &= \sum_a E_a + \frac{1}{2 \mathscr{I}_0 \beta^2} \left(\mathbf{L}_\perp^2 - \left(\sum_a \langle \mathbf{l}_\perp \rangle_a \right)^2 \right) \\ &= \sum_a E_a + \tfrac{1}{2} \frac{1+\varkappa}{1-\varkappa} \cdot \mathscr{I}_0 \beta^2 \cdot \omega^2 \end{aligned} \tag{43}$$

Now let us turn to E_a. The perturbation has the effect that

$$\langle \mathbf{l}_\perp \rangle_a = \langle \mathbf{l}_\perp \rangle_a (\omega = 0) + \eta_a \boldsymbol{\omega}_\perp. \tag{44}$$

It follows that $\varkappa$, as defined by (40), is determined by

$$\left(\sum_a \eta_a \right) \frac{1-\varkappa}{\mathscr{I}_0 \beta^2} = \varkappa. \tag{45}$$

With (43), (44) and (45), it is then easily seen that

$$\sum_a E_a(\omega) = \sum_a E_a(0) - \tfrac{1}{2} \mathscr{I}'_{\text{eff}} \omega^2, \tag{46a}$$

$$\langle E \rangle = \sum_a E_a(0) + \tfrac{1}{2} (\mathscr{I}_0 \beta^2 + \mathscr{I}'_{\text{eff}}) \omega^2, \tag{46b}$$

with

$$\mathscr{I}'_{\text{eff}} = \sum_a \eta_a.$$

We must now recognize that in the present method, the sum extends over the valence nucleons only, whereas the relations (42a, b) follow from summation over all nucleons. But it is well known that the Inglis model gives just $\mathcal{I}_0\beta^2$ for the contribution of the core-nucleons (or something very close to that), so that $(\mathcal{I}_0\beta^2+\mathcal{I}'_{\rm eff})$ is indeed the $\mathcal{I}_{\rm eff}$ of the cranking model.

We verify in addition that from (41a) and (45) it follows that

$$\omega_\perp = \frac{\mathbf{L}_\perp}{\mathcal{I}_0\beta^2+\mathcal{I}'_{\rm eff}} = \frac{\mathbf{L}_\perp}{2\,\mathcal{I}_{\rm eff}}$$

and hence

$$\langle E\rangle = \sum_a E_a(L=0)+\frac{\mathbf{L}_\perp{}^2}{\mathcal{I}_{\rm eff}}. \tag{47}$$

We have thus established — under certain restrictive assumptions — that the effective moment of inertia, derived from equations (37) in a classical approximation for the total angular momentum **L**, and defined by equation (47), is identical with the moment of inertia calculated from the Inglis model, and defined there by equation (42a) or (42b).

It remains to be shown to what extent such a classical approximation is meaningful. Lüders [11]) has given some thought to this question. Most important are probably the internucleon couplings of eq. (37c), as shown by Bohr and Mottelson [14]).

The author wishes to thank Professor Bakker for the hospitality extended to him at CERN, where this work was carried out.

References

1) H. H. Nielsen, Phys. Rev. **60** (1941) 794; Rev. Mod. Phys. **23** (1951) 90
2) A. Bohr, Rotational States in Atomic Nuclei (Thesis, Copenhagen, 1954)
3) G. M. Temmer and N. P. Heydenburg, Phys. Rev. **99** (1955) 1609
4) J. H. van Vleck, Rev. Mod. Phys. **23** (1951) 213
5) C. van Winter, Physica **20** (1954) 274
6) E. Wigner, Gruppentheorie und ihre Anwendung auf die Quantenmechanik der Atomspektren (Edwards Brothers Inc., Ann Arbor, 1944) especially Chapter 15
7) R. Nataf, Nuclear Physics **2** (1956/57) 497
8) A. Bohr, Mat. Fys. Medd. Dan. Vid. Selsk **27** (1952) no. 14
9) C. Marty, Nuclear Physics **1** (1956) 85
10) A. Kerman, Mat. Fys. Medd. Dan. Vid. Selsk **30** (1956) no. 15
11) G. Lüders, Zs. Naturf. **11a** (1956) 617
12) D. R. Inglis, Phys. Rev. **96** (1954) 1059
D. R. Inglis, Phys. Rev. **103** (1956) 1786
13) S. A. Moszkowski, Phys. Rev. **103** (1956) 1328
14) A. Bohr and B. Mottelson, Mat. Fys. Medd. Dan. Vid. Selsk **30** (1955) no. 1

Nuclear Physics **3** (1957) 255—261; *North-Holland Publishing Co., Amsterdam*

NUCLEAR SURFACES AND ZERO-ENERGY SCATTERING

D. C. PEASLEE

Purdue University, Lafayette, Indiana

Received 21 November 1956

Abstract: The assumption of a diffuse nuclear edge introduces computational difficulties in optical model calculations. The present note discusses an approximation procedure for this case, in which the diffuse edge is replaced by an infinitesimally thin "effective edge" with appropriate reflection and transmission coefficients. Illustration is made with zero-energy neutron scattering, where the parameters $\langle \Gamma_n/D \rangle$ and $\langle a-R \rangle$ are both multiplied by the same factor T for any shape of diffuse edge. The empirical value is $T \approx 2$, corresponding to a total edge "width" of order 2×10^{-13} cm.

1. Introduction

The assumption of anything but an ideal square edge for the nuclear optical potential introduces some difficulties of computation. The present note discusses an approximation procedure for this case, in which the effect of the potential edge on various phase shifts is expressed in terms of its reflection and transmission coefficients, s and t. An arbitrary edge is then represented as infinitesimally thin and located at a mean nuclear radius R, but with s and t peculiar to the special (non-square) features of the edge. The coefficients s and t may then be treated as phenomenological parameters, to be approximated by rough calculations or perhaps ultimately to be systematized by comparison with experiment.

This approach is illustrated for the simplest case of zero-energy (s-wave) neutron reactions. It shows quite generally that the effect of any edge modifications, whatever their detailed character, is to increase the scattering length by a factor T, which specifies the penetrability of the surface relative to that of a square edge. Available data suggest $T \approx 2$; this improves the agreement of observed and calculated $\langle \Gamma_n/D \rangle$ curves for $A \leqq 120$, with a fraction $\zeta \approx 0.04$ for the imaginary part of the optical potential.

2. Reflection and Transmission Coefficients

Suppose a barrier, centered at the origin, between two regions of asymptotically uniform potential. The wave functions far to the left and right are respectively $u_\pm \sim \exp(\pm iKx)$, $v_\pm \sim \exp(\pm ikx)$. An incident wave u_+ approaching the barrier from the left will produce a reflected wave s_+u_- and transmitted wave t_+v_+; this and the corresponding process for a wave incident from the right are symbolized by

$$\begin{aligned} u_+ + s_+ u_- &\longleftrightarrow t_+ v_+ \\ t_- u_- &\longleftrightarrow s_- v_+ + v_-. \end{aligned} \tag{1}$$

The subscripts on the coefficents s and t indicate the direction of the incident wave. The current conservation condition reads

$$|s_+|^2 + (k/K)|t_+|^2 = |s_-|^2 + (K/k)|t_-|^2 = \alpha^2 \leqq 1. \tag{2}$$

The possibility $\alpha^2 < 1$ is to allow for absorption in the barrier itself; absorptive (i.e., complex) parts of K and k are neglected. † By combining (1) with its complex conjugate (where $u_\pm{}^* = u_\mp$, $v_\pm{}^* = v_\mp$) and combining with (2), we obtain

$$k t_+ = K t_- \tag{3a}$$

$$s_+{}^*/s_- = -t_+{}^*/t_- = -t_-{}^*/t_+. \tag{3b}$$

Relations (3) are independent of barrier details. We may thus define parameters

$$\begin{aligned} (k/K)^{1/2} t_+ &= t e^{i\delta_t} = (K/k)^{1/2} t_- \\ s_+ &= s e^{2i\delta_s} = -s_-{}^* e^{2i\delta_t} \end{aligned} \tag{4}$$

where s, t are positive real numbers with

$$s^2 + t^2 = \alpha^2. \tag{5}$$

For application to $l = 0$ neutrons, let $x = r$ be the radial coordinate, and shift the position of the barrier to $r = R$. The region to the left of R is then the interior of the nucleus, and the connection to the external region is

$$u_+ - u_- \longleftrightarrow a v_+ + b v_-. \tag{6}$$

The combination $(u_+ - u_-)$ must occur on the left to assure a regular solution as $r \to 0$. The phase shift of the external solution is $\exp(2i\delta) = -(a/b)$, or by (1), (3), and (6)

$$e^{2i\delta} = \frac{1 + s_+{}^*}{1 + s_+} \cdot \frac{t_+}{t_+{}^*}. \tag{7}$$

In eq. (4) we must now account for shifting the barrier from the origin to R by putting $\delta_s \to \delta_s + \Delta$, $\delta_t \to \delta_t + \Delta - \delta_0$, where $\Delta = KR$, $\delta_0 = kR$. Then

$$e^{2i\delta} = \exp\{2i(\delta_t - \delta_s - \delta_0)\} \left[\frac{s + \exp\{2i(\delta_s + \Delta)\}}{1 + s \exp\{2i(\delta_s + \Delta)\}}\right]. \tag{8}$$

The corresponding cross section for compound nucleus formation in units of $\pi \lambda\!\!\!^{-2}$ is

† The changes introduced for complex K and k are minor. Only the real parts of K and k should appear in explicit velocity factors like those of eqs. (2)–(4). Also, for complex K we must take $u_-(K) = u_+(K^*)^*$ to keep a traveling wave damped in its direction of motion. This means that the complex conjugates of $s(K, k)$ and $t(K, k)$ should be understood throughout as $s^* = s(K^*, k^*)^*$ and $t^* = t(K^*, k^*)^*$.

$$\sigma_c = 1-|e^{2i\delta}|^2 = \frac{(1-s^2)\sinh 2\varepsilon}{\frac{1}{2}[e^{2\varepsilon}+s^2 e^{-2\varepsilon}]+s\cos 2\Delta_0} \tag{9}$$

where $\Delta_0 = \mathrm{Re}\,\Delta+\delta_s$, $\quad \varepsilon = \mathrm{Im}\,\Delta$.

3. Relation to the Scattering Length

The scattering length appears in the zero-energy limit of (8). In this limit we expect that s, $\alpha \to 1$ regardless of the edge shape; a zero-energy incident neutron will find any potential, however small, infinite in comparison to its own energy and will suffer total reflection. Denoting by a prime differentiation with respect to k evaluated at $k = 0$, we have by (4) and (5)

$$\begin{aligned} s' &= \frac{1}{s}\left[\alpha\alpha' - \frac{1}{2K}|t_+|^2\right] = \alpha' - \frac{1}{2K}|t_+|^2 \\ &= -2T/K. \end{aligned} \tag{10}$$

This defines a zero-energy surface penetration factor T having the value $T = 1$ for a sharp edge. The scattering length a is now defined as $k \to 0$ by

$$\begin{aligned} e^{2i\delta} &\to 1-2ika\ldots \\ &\to [1+2ik(\delta_t'-\delta_s'-R)\ldots][1-iks'\tan(\Delta_0+i\varepsilon)\ldots] \end{aligned} \tag{11}$$

where we may take $\delta_t-\delta_s = 0$ as $k \to 0$. Then

$$a - R_{\mathrm{eff}} = -T/K\tan(\Delta_0+i\varepsilon) \tag{12}$$

where $R_{\mathrm{eff}} = R-\delta_t'+\delta_s'$. The real part of (12) is the equation for an average scattering length; except over narrow intervals it is well approximated by setting $\varepsilon = 0$. The imaginary part of (12) is proportional to the zero-energy cross section for compound nucleus formation and hence to the corresponding average ratio of neutron width to level spacing, $\langle\Gamma_n/D\rangle$. Define an appropriate quantity γ by

$$\begin{aligned} \gamma &= \lim_{k\to 0}\left(\frac{K}{4k}\sigma_c\right) \approx 10^4\langle\Gamma_n(1\text{ eV})/D\rangle \\ &= \lim_{k\to 0}\left[\frac{K}{4k}(1-|1-2ika|^2)\right] = -K\,\mathrm{Im}\,\{a\} \\ &= T\left(\frac{\sinh 2\varepsilon}{\cosh 2\varepsilon+\cos 2\Delta_0}\right) = T\gamma_0. \end{aligned} \tag{13}$$

Here γ_0 is the function appropriate to a square well, where $T = 1$. Since the mean measured scattering length $\langle a-R_{\mathrm{eff}}\rangle$ and width-to-spacing ratio $\langle\Gamma_n/D\rangle$ are interpreted as real and imaginary parts of the complex eq. (12), the effect of the diffuse edge is to multiply both calculated functions by the same factor T, which expresses the penetrability of the diffuse edge.

Equation (12) satisfies general statements about the means and extrema[1]) of the real and imaginary parts of the reciprocal logarithmic derivative $\mathscr{R}$:

$$\begin{aligned} \mathscr{R}_{\mathrm{Im}} &\approx \gamma \approx \sinh 2\varepsilon/(\cosh 2\varepsilon+\cos 2\Delta_0) \\ \mathscr{R}_{\mathrm{Re}} &\approx \mathrm{Re}\,\{a-R_{\mathrm{eff}}\} \approx \sin 2\Delta_0/(\cosh 2\varepsilon+\cos 2\Delta_0). \end{aligned} \tag{14}$$

The extrema of $\mathscr{R}_{\mathrm{Im}}$ occur at $\cos 2\Delta_0 = 1$, with a mean value $\mathrm{M}_{\mathrm{Im}} = \coth 2\varepsilon$ and a mean-extreme deviation $\operatorname{csch} 2\varepsilon$. At these same points $\mathscr{R}_{\mathrm{Re}} = 0$. The extrema of $\mathscr{R}_{\mathrm{Re}}$ occur at $\cos 2\Delta_0 = -\operatorname{sech} 2\varepsilon$; their mean is $M_{\mathrm{Re}} = 0$, and the mean $-$ extreme deviation is again $\operatorname{csch} 2\varepsilon$. At these same points $\mathscr{R}_{\mathrm{Im}} = \coth 2\varepsilon = M_{\mathrm{Im}}$.

An explicit calculation has been performed (H. Amster, private communication) to test the conclusion that the principal effect of edge diffuseness is merely to multiply the γ_0 of a square well potential by a constant factor T. In this case the diffuse edge also contained an absorptive potential:

$$\begin{aligned} V &= -V_0(1+0.1i), \qquad r \leqq R_0 \\ V &= \frac{-V_0(1+0.1\,i)}{\exp\{K_0(r-R_0)\}-K_0(r-R_0)}, \qquad R_0 \leqq r < R_0+\frac{15}{K_0} \\ V &= 0, \qquad r > R_0+15/K_0. \end{aligned}$$

The Schroedinger equation with this potential and $k = 0$ in the external region was mechanically integrated outward from the origin, and a curve of γ vs. K_0R_0 obtained. Over the majority of its range this curve differed imperceptibly from one of the form (13) with $T = 2.2$ and an effective edge position at $[R_0+(1.55/K_0)]$. Where differences occurred, they were $< 5\,\%$.

4. Comparison with Experiment

We can try to determine an empirical value for T from data on γ and a. The maxima and minima in γ are given for small ε by

$$\gamma_{\max} \approx T/\varepsilon_{\max}, \qquad \gamma_{\min} \approx T\varepsilon_{\min}. \tag{15}$$

The value of ε varies amoung successive maxima and minima, since $\varepsilon \approx \frac{1}{2}\zeta\Delta_0$ for a uniform optical potential. The maximum at $A \approx 50$ corresponds to $\Delta_0 = (5/2)\pi$, the minimum at $A \approx 100$ to $\Delta_0 = 3\pi$. If we take the corresponding $\gamma_{\max} \approx 12$, $\gamma_{\min} \approx 0.4$,

$$\begin{aligned} T &= [\gamma_{\max}\gamma_{\min}\varepsilon_{\max}/\varepsilon_{\min}]^{1/2} \approx 2.0 \\ \zeta &= (2/\pi)\left(\frac{2\gamma_{\min}}{15\gamma_{\max}}\right)^{1/2} \approx 0.04. \end{aligned} \tag{16}$$

Figure 1 shows a plot of (13) with these parameters.

The optical model scattering length given by (12) is of course an average value and shows no fluctuations due to the vagaries of individual levels.

In order to compare with experiment, one must average the measured a for individual nuclei over a small region of A where Δ_0 can be assumed constant. These average $\langle a \rangle$ should then show the behaviour (12). Previous analyses of the scattering length are somewhat conflicting as regards T.

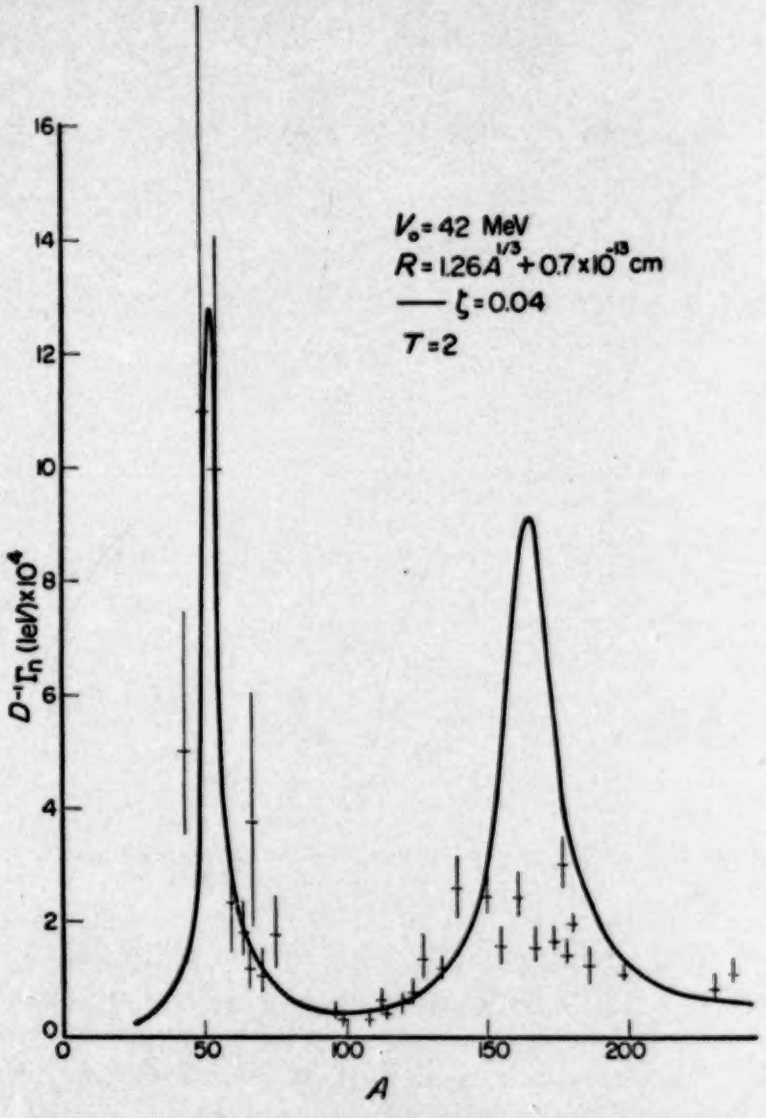

Fig. 1. Plot of γ vs. A. Experimental points from V. F. Weisskopf, Geneva Report No. 831 (1955).

Adair [2]) estimates a for individual nuclei by smooth extrapolation of the cross sections from higher energies; the resulting curve shows little indication of $T > 1$. Analysis of fluctuations in the scattering lengths of individual nuclei [3]) leads to $T \approx 2.4$; this analysis neglects the systematic variation of Δ_0 with A and is not certain to be consistent with the optical model. If we obtain $\langle a \rangle$ by averaging individual, low-energy scattering lengths

over groups of 4 or 5 neighbouring nuclei, the resulting plot † of $\langle a-R\rangle$ against $\Delta_0 \approx KR$ shows roughly the form (12). The best estimate of T is obtained from the minimum slope of the curve, which is $-T/K$ at $\Delta_0 = n\pi$. Only the positions $\Delta_0 = 2\pi$ and 3π are surrounded by enough empirical $\langle a\rangle$ values to make estimates of T feasible, yielding

$$\begin{aligned} T/K &\approx 1.3\times 10^{-13} \text{ cm} \\ T &\approx 1.9 \end{aligned} \tag{17}$$

for K corresponding to $V_0 = 42$ MeV. Fig. 2 shows a plot of (12) with

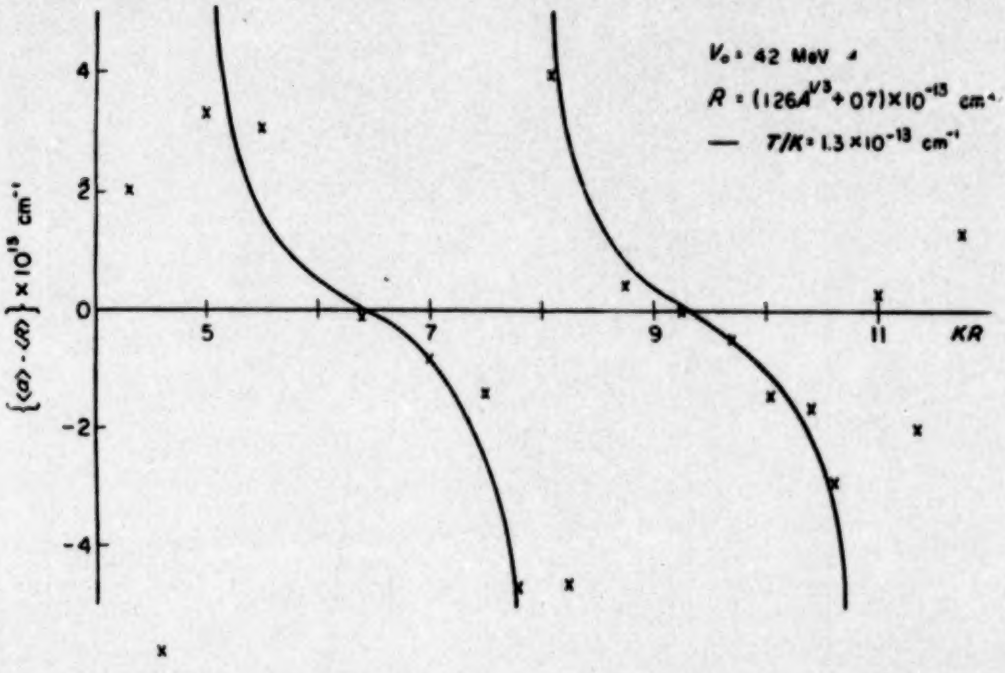

Fig. 2. Plot of $\langle a-R\rangle$ vs. KR; × = experimental point, averaged from D. J. Hughes and J. A. Harvey, U. S. Atomic Energy Commission Report BNL-325 (1955).

$\varepsilon = 0$ for the parameter (17), along with the empirical values of $\langle a-R\rangle$. The values (17) and (16) for T are consistent, although of course neither is very precise.

The factor $T \approx 2$ accentuates the well-known discrepancy between the calculated maximum of γ at $A \approx 160$ and the experimental points. Whatever the explanation of this disparity, it seems unlikely that the nuclear surface becomes substantially less diffuse and hence reduces T around $A = 160$. It is tempting to associate the reduction of γ with the marked deformations characteristic of these nuclei. One such possibility is to associate with the coordinate deformations some increase in irregularity of the nucleon momentum distribution in the nucleus. The Pauli principle then becomes

† Here we put $R_{eff} \approx R$; for an edge shape as described by (18) the error in dropping $\delta_s'-\delta_t'$ is $\lesssim 5$ % of R. In taking $\Delta_0 = KR$, we have neglected δ_s, which is only a few degrees for the edge shape specified in (18) as $k \to 0$.

less effective in restricting nucleon-nucleon collisions inside the nucleus, so that ζ increases. If ζ should increase in this way to a maximum of order 0.1 for the most deformed nuclei near $A = 160$, the calculated peak of γ in fig. 1 could be reduced by a factor of 2 or 3, bringing it closer to the experimental points. Since the increase in ζ would depend on the degree of deformation, the calculated peak of γ would also be made irregular in shape. Of course a corresponding increase in ζ should be observable for these nuclei at incident neutron energies of a few MeV; although no such effect has been reported, present calculations in this energy range may be inconclusive as regards ζ. In any case, no such simple increase in ζ can alone make the calculated curve of γ pass through the average of the experimental points in fig. 1.

5. Edge Width

The empirical value $T \approx 2$ provides an estimate of the edge width, if a specific shape is assumed and absorption in the edge is neglected. We conclude by giving width estimates for a couple of simple shapes. A popular form is the Eckart potential [4]) $V(r) = V_0[1+\exp\{(r-R)/d\}]^{-1}$, for which

$$\begin{aligned} s &= \frac{\sinh[\pi d(K-k)]}{\sinh[\pi d(K+k)]} \\ T &= -Ks'/2 = \pi Kd \coth(\pi Kd) \\ d &\approx 0.4\times 10^{-13} \text{ cm}. \end{aligned} \tag{18}$$

This value of d corresponds to $T \approx 2$, $V_0 = 42$ MeV, and is comparable to that obtained from analyses of proton [5]) and electron [6]) scattering experiments. For an edge of uniform slope (trapezoidal well), the half-width of the edge corresponding to $V_0 = 42$, $T \approx 2$ is [7]) $d' \approx 1.0\times 10^{-13}$ cm. This value of d' yields an edge very similar in appearance to the Eckart edge specified by (18), so that the effective "width" of the edge is about $2d' \approx 2\times 10^{-13}$ cm.

The author wishes to thank Drs H. J. Amster and W. S. Emmerich for helpful discussions.

References

1) H. Amster, Phys. Rev. (in press)
2) R. K. Adair, Phys. Rev. **94** (1954) 737
3) J. M. C. Scott, Phil. Mag. **45** (1954) 411, 751, 1322
4) C. Eckart, Phys. Rev. **35** (1930) 1303
5) D. S. Saxon *et al.*, Michigan Conference, June 1955.
6) Hahn, Ravenhall and Hofstadter, Phys. Rev. **101** (1956) 1131
7) Z. Jankovic, Phil. Mag. **46** (1955) 376

Nuclear Physics **3** (1957) 262—272; *North-Holland Publishing Co., Amsterdam*

THE FLUCTUATION PROBLEM IN μ-MESON BURSTS †

A. N. MITRA

Physics Department, Muslim University, Aligarh, U. P. (India)

Received 21 November 1956

Abstract: The effect of the fluctuation problem on the size-frequency distribution of large cosmic-ray bursts is investigated in some detail, assuming the μ-meson to be an ordinary Dirac particle. This is achieved with the help of a general distribution function called the Polyá distribution, which reduces to the previously investigated Poisson and Furry cases at appropriate limits. It is found that the fluctuation of the number of shower particles has a considerable influence on the size of cosmic ray bursts, and this result partially obscures any conclusion that may be made on the spin of the μ-meson with the help of burst-production data.

1. Introduction

The theory of cosmic ray bursts has perhaps been the most important tool for determining the spin of the μ-meson. As early as 1941, Christy and Kusaka [1]) found that the theoretical size-frequency distribution of large bursts produced by Bremsstrahlung of high-energy mesons was a fairly sensitive function of the "spin" assumed for the μ-meson. Thus by a comparison of their results with the experimental values of Schein and Gill [2]) they were able to conclude that μ-mesons were most likely to be ordinary Dirac particles (spin $-\frac{1}{2}$). This conclusion of Christy and Kusaka is generally accepted as the standard evidence for spin$-\frac{1}{2}$ of μ-mesons. Another notable work on this subject was done by Chakrabarty [3]) whose result did not, however, rule out the possibility of higher spin values for these particles. Recently there have been suggestions that these particles may have higher spin (notably 3/2), on the basis of Feynman's conjecture that the masses of various particles might be accounted for entirely in terms of their virtual interactions with other fields. This possibility was recently investigated and disproved by Mathews [4]) who found that the large Bremsstrahlung cross section for spin$-3/2$ particles would give rise to far more bursts at sea level than are actually observed and apparently well-accounted for on the spin$-\frac{1}{2}$ basis. The author, in a recent note [5]), has, however, given some qualitative arguments to show that such a conclusion would lose some strength if the fluctuation in the number of shower particles were considered in some detail. The purpose of this paper is to substantiate these arguments by presenting the actual calculations on the part played by the fluctuation problem in

† Based on part of a thesis submitted to Delhi University and approved by that institution for the award of Ph. D. degree, 1954.

influencing the size of cosmic ray bursts, assuming them for definiteness to be produced by μ-mesons of spin—$\frac{1}{2}$.

The calculation of the size-frequency distribution of large bursts involves knowledge of (1) the Cascade Theory of showers and (2) the theory of fluctuations. The most satisfactory work to date on the Cascade Theory is one due to Snyder [6]) † who gives the total average number $\overline{N}(t)$ of particles produced at a certain depth t in the form of an infinite series the first term of which accounts for more than 95 % of the whole. Snyder further gives numerical data for electron- and photon-initiated showers, of which clearly the latter are necessary for the present investigation since at sea level radiative bursts account for nearly 95 % of the whole. In this paper a simple expression for $\overline{N}(t)$ has been obtained by fitting Snyder's data with skew Gaussian functions which give a fairly accurate representation of his numerical values with an error well within the limits of Cascade Theory. These functions are used here to calculate the size-frequency distribution of μ-meson bursts.

As regards the theory of fluctuations the problem is much more difficult to solve since the distribution function giving the probability of obtaining more than N particles at a certain depth t has, in principle, to be obtained as the solution of an extremely unwieldy and complicated integro-differential equation. Attempts have therefore been made to obtain this distribution function either from general considerations or by considering simplified models. The earliest attempt in this direction was made by Bhabha and Heitler [7]) who postulated the Poisson distribution on the basis of genetical independence of the shower particles, an assumption which depends for its validity on the largeness of the number of these particles. A more promising attempt was made almost simultaneously by Furry [8]) who obtained a distribution as the solution of a differential equation based on the actual mechanism of the shower. A serious limitation of the Furry distribution is, however, that it was obtained by neglecting ionization losses and regarding electrons and photons as identical particles. This was the distribution used by Christy and Kusaka [1]) for calculating the number of bursts of different sizes. Chakrabarty [3]), on the other hand, used the Poisson distribution for the same purpose. Unfortunately very little is known about the fluctuation problem in the actual cosmic-ray case to decide between these alternatives, except that the mean square deviation of the number of particles from the average is too large for a Furry distribution and too small for a Poisson one. It is perhaps reasonable to assume that the actual distribution is such that the mean square deviation derived from it should lie somewhere between the above two extremes. Fortunately there exists a

† More recently Chakrabarty has given an equally satisfactory treatment of Cascade Theory. See ref. [6a]).

distribution, the so-called Polyá distribution [9]) which depends on a certain parameter b and reduces to the Poisson and Furry limits when $b = 0$ and $b = 1$ respectively. It is therefore useful to study the variation of the integral size-frequency distribution as a function of the parameter b. The simplest assumption is of course to regard b as a constant (independent of the thickness t of the material traversed and the energy of the photon initiating the shower), remembering that the Polyá distribution is at most a good empirical model and not any theoretically derived function (unlike Furry's).

The calculations in this paper are carried out using (1) the Bremsstrahlung formula (with complete screening) for spin—$\frac{1}{2}$ particles of mass 210 m_e, (2) the cascade Theory data given by Snyder and (3) the Polyá distribution for the fluctuations. (Knock-on showers are clearly negligible for primary energies $> 10^9$ eV). Section 2 summarizes the relevant properties of the Polyá distribution and contains a short derivation of the integral size-frequency distribution in the form of a Bromwich integral whose evaluation is discussed in the appendix. Section 3 is devoted to a brief discus- of the results.

2. The Integral Size-Frequency Distribution

We start with a discussion of the relevant properties of the Polyá distribution which gives the probability for a number N of particles to be produced at a depth t (radiation units) in the form

$$P(N,t) = \frac{1}{N!}\left(\frac{\lambda}{1+b\lambda}\right)^N [1 \,.\, (1+b) \ldots (1+(N-1)b)](1+b\lambda)^{-\frac{1}{b}}. \qquad (1)$$

Taking the limit $b = 0$ one obtains

$$P_1(N,t) = \frac{1}{N!}\lambda^N e^{-\lambda} \qquad (2)$$

which is clearly the Poisson distribution with λ playing the part of $\overline{N}$, the average number of particles. Setting $b = 1$ in (1) one gets

$$P_2(N,t) = \frac{1}{1+\lambda}\left(1-\frac{1}{1+\lambda}\right)^N \qquad (3)$$

which may be compared with Furry distribution

$$\frac{1}{\overline{N}}\left(1-\frac{1}{\overline{N}}\right)^N. \qquad (4)$$

The average number of particles in the general case is given by

$$\begin{aligned}\overline{N} &= \sum_0^\infty NP(N,t)\\ &= \sum_1^\infty \frac{1}{(N-1)!}\left(\frac{\lambda}{1+b\lambda}\right)^N [(1+b)\ldots(1+(N-1)b)](1+b\lambda)^{-\frac{1}{b}}\\ &= \frac{\lambda}{[1+b\lambda]^{\left(1+\frac{1}{b}\right)}}\left[1-\frac{b\lambda}{1+b\lambda}\right]^{-\left(1+\frac{1}{b}\right)} = \lambda.\end{aligned} \tag{5}$$

The second moment of the distribution is similarly given by

$$\begin{aligned}\langle N^2\rangle_{\text{Av}} &= \sum_0^\infty N^2 P(N,t)\\ &= \lambda+\lambda^2(1+b)\\ &= \overline{N}+(\overline{N})^2(1+b).\end{aligned} \tag{6}$$

Thus

$$\sigma^2 = \langle N^2\rangle_{\text{Av}} - (\overline{N})^2 = \overline{N}(1+b\overline{N}).$$

We shall regard b as a pure constant lying between 0 and 1, without specifying any fixed numerical value in advance.

Since we are more interested in the probability of finding more than N particles we must first find a suitable expression for the same. The generating function for $P(N, t)$ is easily verified to be

$$G(x) = \left(\frac{1}{1+b\lambda}\right)^{\frac{1}{b}}\left[1-\frac{b\lambda x}{1+b\lambda}\right]^{-\frac{1}{b}}, \tag{7}$$

since $P(N, t)$ is the coefficient of x^N in the expansion of (7). Using Maclaurin's theorem with remainder in integral form, we have

$$G(x) = \sum_0^N \frac{x^j}{j!}G^j(0) + \int_0^1 \frac{x^{N+1}}{N!}(1-y)^N G^{N+1}(xy)\,dy, \tag{8}$$

where

$$G^j(0) = (j!)P(j,t). \tag{9}$$

Putting $x = 1$ in (8) we have

$$\begin{aligned}1 = \sum_0^N P(j,t) + \int_0^1 dy\,\frac{(1-y)^N}{N!}\left(\frac{1}{1+b\lambda}\right)^{\frac{1}{b}}\left(\frac{\lambda}{1+b\lambda}\right)^N\\ \times[(1+b)\ldots(1+Nb)]\left(1-\frac{b\lambda y}{1+b\lambda}\right)^{-\left(N+1+\frac{1}{b}\right)}.\end{aligned} \tag{10}$$

Thus from (10) the probability of obtaining more than N particles at depth t is by definition given by

$$P(>N,t) = \frac{1}{(N!)}(\overline{N})^{N+1}[(1+b)\ldots(1+Nb)]\int_0^1 y^N\,dy[1+by\overline{N}]^{-\left(N+1+\frac{1}{b}\right)}, \tag{11}$$

where we have changed y to $1-y$ in (10) and used relation (5) for $\overline{N}$.

The values of $\overline{N}$ at different depths due to a primary photon of energy E_0 may be obtained from Snyder's paper [6]). By a process of curve fitting the numerical values of $\overline{N}$ given by Snyder for a photon-initiated shower have been found to be fairly accurately represented by the following expressions

$$\begin{aligned}\overline{N}(t) &= N_m \exp\left[-0.49\,(t_m-t)^2/t_m\right],\ t<t_m \\ &= N_m \exp\left[-0.25\,(t-t_m)^2/t_m\right],\ t>t_m\end{aligned} \tag{12}$$

where N_m is the maximum number of electrons produced at a depth t_m and is given by

$$N_m = \frac{0.325}{(y_0)^{\frac{1}{2}}}\,e^{y_0}, \qquad t_m = y_0, \qquad y_0 = \ln(E_0/\beta), \tag{13}$$

β being the "critical" energy for the material traversed. It may be noted that the expressions (12) satisfy the following necessary condition very closely:

$$\int_0^\infty \overline{N}(t)\mathrm{d}t = \frac{E_0}{\beta} = e^{y_0}. \tag{14}$$

Finally we require the Bremsstrahlung cross section (with complete screening) due to a Dirac particle of mass $M = 210\ m_e$. The extreme relativistic cross section for the production of a photon of energy between E_0 and $E_0+\mathrm{d}E_0$ by such a meson of energy W is given by [3])

$$Q(W, E_0)\mathrm{d}E_0 = \frac{16}{3}\,\frac{Z^2}{137}\left(\frac{e^2}{Mc^2}\right)^2\left(\frac{W-E_0}{E_0}+\frac{3E_0}{4W}\right)\frac{\mathrm{d}E_0}{W}\ln\left[183Z^{-\frac{1}{3}}\frac{M}{m}\right], \tag{15}$$

m being the mass of the electron.

We are now in a position to calculate the probability $P(N_>, W)$ for a meson of initial energy W being accompanied by more than N electrons after passing through a layer of thickness t. Following the procedure of Chakrabarty [3]) and neglecting small variations in the energy of the meson, we have

$$P(N_>, W) = lp\int_0^W Q(W, E_0)J_{N_>}(E_0)\,\mathrm{d}E_0, \tag{16}$$

where l is the characteristic length (one radiation unit) and p is the number of atoms per cm^3 of the substance, so that

$$(lp)^{-1} = \frac{4Z^2}{137}\left(\frac{e^2}{mc^2}\right)^2\ln(183Z^{-\frac{1}{3}}). \tag{17}$$

The quantity $J_{N_>}$ in (16) is defined as

$$J_{N_>}(E_0) = \int_0^t \mathrm{d}t'\,P(>N, t'), \tag{18}$$

in which the integration over t' arises from the possibility of the shower

being produced anywhere within the thickness t. Since we are concerned with burst production after the meson has traversed a sufficiently large thickness, the upper limit in (18) may be extended to ∞. Thus from (11) and (18) we have

$$J_{N>}(E_0) = \int_0^\infty \mathrm{d}t \int \frac{(\bar{N})^{N+1}}{(N!)} \cdot \frac{\Gamma\left(N+1+\frac{1}{b}\right)}{\Gamma\left(1+\frac{1}{b}\right)} \cdot b^N \int_0^1 \frac{y^N \mathrm{d}y}{(1+by\bar{N})^{N+1+\frac{1}{b}}}$$

$$= \frac{1}{(N!)} \int_0^1 \mathrm{d}y \int_0^\infty \mathrm{d}t \sum_{r=0}^{\infty} \frac{(-1)^r}{r!} (by)^{N+r} (\bar{N})^{N+r+1} \tag{19}$$

$$\times \left[\frac{\Gamma\left(N+\frac{1}{b}+1+r\right)}{\Gamma\left(1+\frac{1}{b}\right)}\right].$$

Substituting for $\bar{N}$ from (12) in (19) and integrating † term by term over t and y we have

$$J_{N>}(E_0) = \frac{3.04(t_m)^{\frac{1}{2}} N_m}{(N!)\Gamma\left(1+\frac{1}{b}\right)} \sum_{r=0}^{\infty} (-1)^r (N_m b)^{N+r} \frac{\Gamma\left(N+1+r+\frac{1}{b}\right)}{(r!)(N+1+r)^{3/2}}. \tag{20}$$

This series can be expressed as a Bromwich integral as follows. The function

$$f(Z) = \frac{\Gamma(Z)(N_m)^{N-Z+1} b^{N-Z} \Gamma(N+1+\frac{1}{b}-Z)}{(N+1-Z)^{3/2}} \tag{21}$$

has simple poles at the points $Z = 0, -1, -2, \ldots -r, \ldots$ because of the factor $\Gamma(Z)$, and all other points on the negative side of the imaginary axis are regular. The infinite series in (20) is just the sum of the residues at these poles. Thus we have

$$J_{N>}(E_0) = \frac{3.04(t_m)^{\frac{1}{2}}}{(N!)\Gamma\left(1+\frac{1}{b}\right)} \cdot \frac{1}{2\pi i} \int_{C-i\infty}^{C+i\infty} f(Z)\mathrm{d}Z, \tag{22}$$

where C is a real constant > 0, since the path of integration must lie to the right of all the poles. Further the line of integration can be shifted to any

† A typical integral over t is of the form

$$\int_0^\infty (\bar{N})^n \mathrm{d}t = \int_0^{t_m} (\bar{N})^n \mathrm{d}t + \int_{t_m}^\infty (\bar{N})^n \mathrm{d}t$$

$$\approx \int_{-\infty}^{t_m} (\bar{N}^n)\, \mathrm{d}t + \int_{t_m}^\infty (\bar{N})^n \mathrm{d}t$$

$$= \tfrac{1}{2}(t_m)^{\frac{1}{2}} (\pi)^{\frac{1}{2}} (N_m)^n [(0.49n)^{-\frac{1}{2}} + (0.25n)^{-\frac{1}{2}}] = 3.04 \left(\frac{t_m}{n}\right)^{\frac{1}{2}} (N_m)^n.$$

position on the right provided it does not cross the point $Z = N+1$ which is a singular point for $f(Z)$. The integral (22) can be evaluated by the method of saddle-points which must lie between 0 and $N+1$.

Now the quantity of more immediate interest from the experimental point of view is not $P(N_>, W)$ but its average value over the meson spectrum. Thus if $S(W)\mathrm{d}W$ is the number of mesons in the energy range W and $W+\mathrm{d}W$ incident on the top of the material under consideration, then the total probability of obtaining a shower of more than N particles below an infinitely thick layer of the material (irrespective of the meson energy) is from (16) given by

$$R(N) = lp \int_{W_{\min}}^{\infty} S(W)\mathrm{d}W \int_0^W \varphi(W, E_0)\mathrm{d}E_0 J_{N_>}(E_0). \tag{23}$$

For larger bursts with $N > 100$ we can take like Chakrabarty [3])

$$S(W)\mathrm{d}W = \delta I_0 (2\times 10^9 \text{ eV})^{\delta} \mathrm{d}W/W^{\delta+1}, \tag{24}$$

where

$$I_0 = 0.01 \text{ sec}^{-1} \cdot \text{cm}^{-2} \tag{25}$$

and

$$\delta = 1.87.$$

The lower limit of E_0 integration in (23) may be taken to be β since no shower production is possible below this value. Collecting the results contained in (13), (15), (17), (21)—(25) and interchanging the order of E_0 and W integrations in (23) we have finally

$$\begin{aligned} R(N) &= lp\, \delta I_0 (2\times 10^9)^{\delta} \int_{\beta}^{\infty} J_{N_>}(E_0)\mathrm{d}E_0 \int_{E_0}^{\infty} \frac{\mathrm{d}W}{W^{\delta+1}} Q(W, E_0) \\ &= \left[\frac{3.04\, lp\, \delta I_0 (2\times 10^9)^{\delta}}{\Gamma(N+1)\Gamma\left(1+\frac{1}{b}\right)}\right] \\ &\quad \times \frac{1}{2\pi i} \int_{C-i\infty}^{C+i\infty} \mathrm{d}Z \frac{\Gamma(Z)\Gamma\left(N+1+\frac{1}{b}-Z\right) b^{N-Z}}{(N+1-Z)^{3/2}} \\ &\quad \times \int_{\beta}^{\infty} \frac{(0.325)^{N+1-Z}\, e^{y_0(N+1-Z)}}{(y_0)^{\frac{N-Z}{2}}} \mathrm{d}E_0 \int_{E_0}^{\infty} \frac{Q(W, E_0)\mathrm{d}W}{W^{\delta+1}} \\ &= A\beta^{-\delta}\left[\frac{1}{\delta(\delta+1)} + \frac{3}{4(\delta+2)}\right] \frac{\phi(\delta, b)}{\Gamma(N+1)}, \end{aligned} \tag{26}$$

$$A = \frac{16}{3}\frac{Z^2}{137}\left(\frac{e^2}{Mc^2}\right)^2 lp\, \delta I_0 (2\times 10^9)^{\delta} (3.04) \ln\left[183 Z^{-1/3}\frac{M}{m}\right], \tag{27}$$

$$\phi(\delta, b) = \frac{1}{2\pi i}\int_{C-i\infty}^{C+i\infty} dZ \cdot \frac{\Gamma(Z)\Gamma\left(N+1+\frac{1}{b}-Z\right) b^{N-Z}}{(Z+\delta-N-1)^{\left(\frac{N}{2}+1\right)}} \times \frac{\Gamma\left(1+\frac{Z-N}{2}\right)(0.325)^{N+1-Z}}{(N+1-Z)^{3/2}}. \quad (28)$$

This integral is evaluated by the saddle-point method in the appendix By taking suitable approximations it has been found possible to obtain an analytical expression which is given below:

$$\frac{\phi(\delta, b)}{\Gamma(N+1)} = \frac{0.38}{(2\pi f_2)^{\frac{1}{2}}} \cdot \frac{\Gamma\left(1.79+\frac{1}{b}\right)}{\Gamma\left(1+\frac{1}{b}\right)} \cdot (b)^{0.79} (e f_1)^{\frac{1}{f_2}} N^{-\left(1.79+\frac{f_1}{f_2}\right)} (\ln N)^{\left(\frac{1}{f_2}-1\right)}, \quad (29)$$

where $f_1(b)$ and $f_2(b)$ are functions of b defined in the appendix.

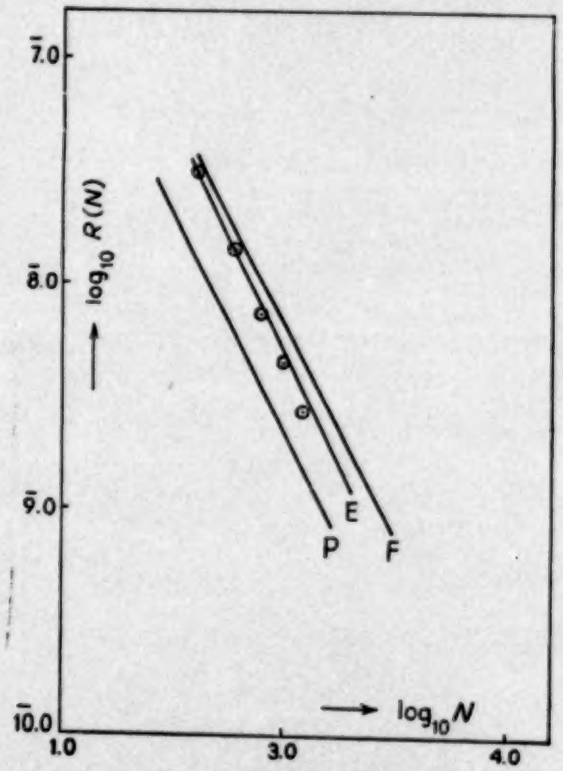

Fig. 1. Plots of log $R(N)$ vs. log N for lead. The circles denote the experimental points of Schein and Gill. P and F are the theoretical curves for the cases $b = 0$ and $b = 1$ respectively. E is the theoretical curve obtained by taking $b = 0.87$.

3. Discussion

The quantity $R(N)$ defined by (26) and (29) may now be compared with the experimental result of Schein and Gill [2]) for burst production in lead ($Z = 82$). Fig. 1 gives plots of $\log_{10} N$ vs. $\log_{10} R(N)$ (for different values

of b) alongside the experimental values of the same quantities. It is seen that the experimental curve lies between the theoretical ones with $b = 0$ and $b = 1$, being much nearer the latter than the former. By interpolation, the value $b = 0.87$ is found to be in agreement with experiment, indicating that the distribution is very close to Furry's, provided the spin of the μ-meson is assumed to be $\frac{1}{2}$. It is also seen from the curves that the two extreme distributions differ by almost a factor of 3, which indicates the amount of uncertainty which a lack of knowledge of the fluctuations would impose on any spin-determination of the μ-meson by this method.

As regards the bearing of this result on any higher spin hypothesis (integral spins must be ruled out from considerations of angular momentum conservation in the processes $\pi^{\pm} \to \mu^{\pm}+\nu$), the burst-production estimates given by Mathews [4]) on the spin$-3/2$ basis are rather qualitative, yet his conclusion does not appear to be so clear-cut if the observations in the last paragraph are taken into account. It is therefore, not irrelevant to make more accurate calculations of Bremsstahlung by spin$-3/2$ particles (preferably with effects of radiation damping included) before it is definitely possible to choose between the spin$-\frac{1}{2}$ and spin$-3/2$ alternatives. If even the improved calculations definitely exclude the spin$-3/2$ hypothesis, the result of this paper may be taken to have provided an experimental determination of the fluctuation parameter b.

This investigation was carried out while the author was a Ph. D. student in Delhi University, working under Professor R. C. Majumdar. The author is deeply indebted to Professor Majumdar for having suggested the investigation and giving constant guidance and encouragement throughout the work.

Appendix

We give here a derivation of the result contained in eq. (29) of the text.

Making the substitution $Z = N+S$, we may write (28) as follows

$$\phi(\delta, b) = \frac{1}{2\pi i}\int_{C-i\infty}^{C+i\infty} \mathrm{d}S \exp\left[\phi_1(S)\right] \tag{A1}$$

where

$$\begin{aligned}\phi_1(S) = {} & \ln \Gamma(N+S)+\ln \Gamma\left(1+\frac{1}{b}-S\right) + \ln \Gamma\left(1+\frac{S}{2}\right) \\ & - S \ln b+(1-S) \ln (0.325)-1.5 \ln (1-S) \\ & -\left(1+\frac{S}{2}\right) \ln (\delta+S-1)-\ln \Gamma\left(1+\frac{1}{b}\right).\end{aligned} \tag{A2}$$

The saddle-point S_0 is given by

$$\phi_1'(S_0) = 0 \tag{A3}$$

where

$$\phi_1'(S) = \psi(N+S)+\lambda(b, S) \tag{A4}$$

Here $\psi(x)$ is the digamma function defined by

$$\psi(x) = \frac{\mathrm{d}}{\mathrm{d}x} \ln \Gamma(x) \tag{A5}$$

and

$$\begin{aligned}\lambda(b, S) = {} & \tfrac{1}{2}\psi\left(1+\frac{S}{2}\right) - \ln (0.325) + \frac{1.5}{1-S} \\ & - \frac{\left(1+\frac{S}{2}\right)}{S+\delta-1} - \tfrac{1}{2} \ln (S+\delta-1) \\ & - \ln b - \psi\left(1+\frac{1}{b}-S\right).\end{aligned} \tag{A6}$$

The integration of (A1) by the saddle-point method gives, in the usual manner

$$\phi(\delta, b) = [2\pi\phi_1''(S_0)]^{-\frac{1}{2}} \exp [\phi_1(S_0)]. \tag{A7}$$

Eq. (A3) for S_0 may be solved approximately by first noting that $\psi(N+S)$ is practically independent of S since N is large and Re $(S) \approx \mathrm{O}(1)$, so that

$$\psi(N+S) \approx \ln N. \tag{A8}$$

Secondly, the largest and most rapidly varying part in (A6) is the term $1/(S+\delta-1)$ which indicates that S_0 must not differ much from $1-\delta$. Thus it is natural to express $\lambda(b, S)$ empirically as a function of the form $1/(A+BS)$ where A and B are functions of b. A numerical computation of the function $\lambda(b, S)$ for the different cases $b = 0$, 0.1, 0.2, 0.5 and 1.0 and over the range $-0.70 \geqq S \geqq -0.90$ for S shows that $\lambda(b, S)$ can indeed be expressed to an excellent approximation as

$$\lambda(b, S) = -\frac{1}{f_1(b)+\varepsilon f_2(b)} \tag{A9}$$

where

$$\varepsilon = S+0.79,$$

with an error $< 2\,\%$. The functions f_1 and f_2 are represented as follows

$$\begin{aligned} f_1(b) &= 0.197 - \frac{b}{20.1+15.2b}, \\ f_2(b) &= 3.10 - \frac{b}{0.69+0.77b}. \end{aligned} \tag{A10}$$

From (A6), (A8) and (A9) the saddle-point equation becomes simply

$$\ln N-(f_1+\varepsilon_0 f_2)^{-1} = 0, \qquad \varepsilon_0 = S_0+0.79,$$

giving

$$\varepsilon_0 = (f_2)^{-1}\,[(\ln N)^{-1} - f_1]. \tag{A11}$$

From (A5), (A6), (A9) and (A11) we have

$$\phi_1''(S_0) \approx \lambda'(b, S_0) = f_2[f_1 + \varepsilon_0 f_2]^{-2} = f_2(\ln N)^2. \tag{A12}$$

Finally, $\phi_1(S_0)$ can be simply evaluated using the following result

$$\phi_1(S_0) = \int_0^{\varepsilon_0} \frac{-\mathrm{d}\varepsilon}{f_1 + f_2\varepsilon} + \phi_1(-0.79) + \varepsilon_0(\ln N), \tag{A13}$$

remembering that ε_0 is a small quantity.

Using Stirling's approximation for the Γ-function which appears in $\phi_1(-0.79)$ and evaluating the purely constant terms numerically from the tables we obtain

$$\begin{aligned}\phi_1(-0.79) = {} & N \ln N - N - 1.29 \ln N + \tfrac{1}{2} \ln (2\pi) + 0.79 \ln b \\ & + \ln \Gamma\left(1.79 + \frac{1}{b}\right) - \ln \Gamma\left(1 + \frac{1}{b}\right) - 0.966.\end{aligned} \tag{A13'}$$

The other terms in (A13) can be evaluated directly by means of (A11). Collecting all these results and substituting in (A7) we finally obtain eq. (29) of the text.

References

1) R. F. Christy and S. Kusaka, Phys. Rev. **59** (1941) 414
2) M. Schein and P. S. Gill, Rev. Mod. Phys. **11** (1939) 267
3) S. K. Chakrabarty, Ind. J. Phys. **16** (1942) 377
4) J. Mathews, Phys. Rev. **102** (1956) 270
5) A. N. Mitra, Nuclear Physics **2** (1956/57) 283
6) H. S. Snyder, Phys. Rev. **76** (1949) 1563
6a) S. K. Chakrabarty and M. R. Gupta, Phys. Rev. **101** (1956) no. 2
7) H. J. Bhabha and W. Heitler, Proc. Roy. Soc. A **159** (1937) 432
8) W. H. Furry, Phys. Rev. **52** (1937) 569
9) N. Arley, Stochastic Processes and Cosmic Radiation (J. Wiley & Sons Inc, New York, 1948) p. 98

Nuclear Physics **3** (1957) 273—298; *North-Holland Publishing Co., Amsterdam*

A SCINTILLATION SPECTROMETER STUDY OF THE PHOTODISINTEGRATION of O^{16} †

N. L. SVANTESSON

Department of Physics, University of Lund, Sweden

Received 7 November 1956

Abstract: The nuclear reactions $O^{16}(\gamma, p\gamma')N^{15}$ and $O^{16}(\gamma, n\gamma')O^{15}$ were used to study the photodisintegration of O^{16}. Various bremsstrahlung spectra with peak energies ranging between 16 and 30 MeV were used to excite the target nuclei. The photons emitted in the two reactions were measured with a NaI(Tl) scintillation spectrometer covering photon energies from 2 to 11 MeV.

The results support the belief of the 6.1 and 6.3 MeV states in O^{15} and N^{15}, respectively, being $p_{3/2}^{-1}$ states. Transitions to these two states, 30 percent, are together with ground state transitions, 70 percent, the only ones observed between 20.0—22.5 MeV excitation energies. In the region between 22.5 and 25.0 MeV also transitions to 7, 9, and 10—11 MeV states were observed. Ground state transitions in this interval occurred in about 40 percent, while the transition probability to excited states was shared roughly equally between the 6.1—6.3 MeV states and all the other states, mainly the 7 MeV states. σ_{int} from 20—25 MeV amounted to about 0.1 MeV · barn. The ratio between σ_{int} for (γ, p) and (γ, n) reactions was about 3 : 2. The nuclear elastic scattering of photons was also measured and was used to determine the integrated cross section for photon absorption up to 40 MeV which was found to be 0.3 MeV · barn.

1. Introduction

The nuclear reactions $O^{16}(\gamma, n)O^{15}$ and $O^{16}(\gamma, p)N^{15}$ have been used by several authors to study the nuclear photon absorption in O^{16} for energies up to 25 MeV. The (γ, n) reaction was studied by detecting the neutrons emitted [1]), or the residual positron activity of O^{15} [2, 3, 4]) with BF_3 and Geiger counters, respectively. The (γ, p) reaction was studied in three different investigations with different bremsstrahlung peak energies: 18.7 [5]), 21.0 [6]), and 25.0 [7]) MeV. The first and the second of these three investigations were concerned with transitions to the ground state of N^{15} only. The proton spectrum measured in the investigation with the 25 MeV bremsstrahlung spectrum included also protons in transitions to excited states in N^{15}. In this case an unequivocal identification of the photoprotons with energies less than about 7 MeV was, however, not possible, since this

† The experimental part of this investigation was supported by the U.S. Air Force, through the Office of Scientific Research and Development Command. A preliminary report was given at the New York meeting of the American Physical Society, January 31, 1956. Bull. Am. Phys. Soc. Ser. II **1** (1956) 28. This report is based on experimental data obtained during a year's stay at the National Bureau of Standards, Washington, D.C. The final calculations and interpretations were performed at the University of Lund.

requires knowledge about the proton spectra at various bremsstrahlung peak energies.

Available investigations of the photoprotons give detailed information about the nuclear absorption leading to the ground state of N^{15} only, while the photoneutron work is concerned with the total nuclear absorption followed by neutron emission. The results do not give any information about the probability of transitions to the different excited states in the daughter nuclei. Therefore no conclusions can be made about the nature of the photodisintegration process.

This paper is concerned with a study of the photons emitted by an oxygen (water) target when irradiated with bremsstrahlung photons with different energies above the threshold for transitions to the excited states in the daughter nuclei, i.e. the nuclear reactions $O^{16}(\gamma, n\gamma')O^{15}$ and $O^{16}(\gamma,p\gamma')N^{15}$. The photons emitted by the target were detected by a

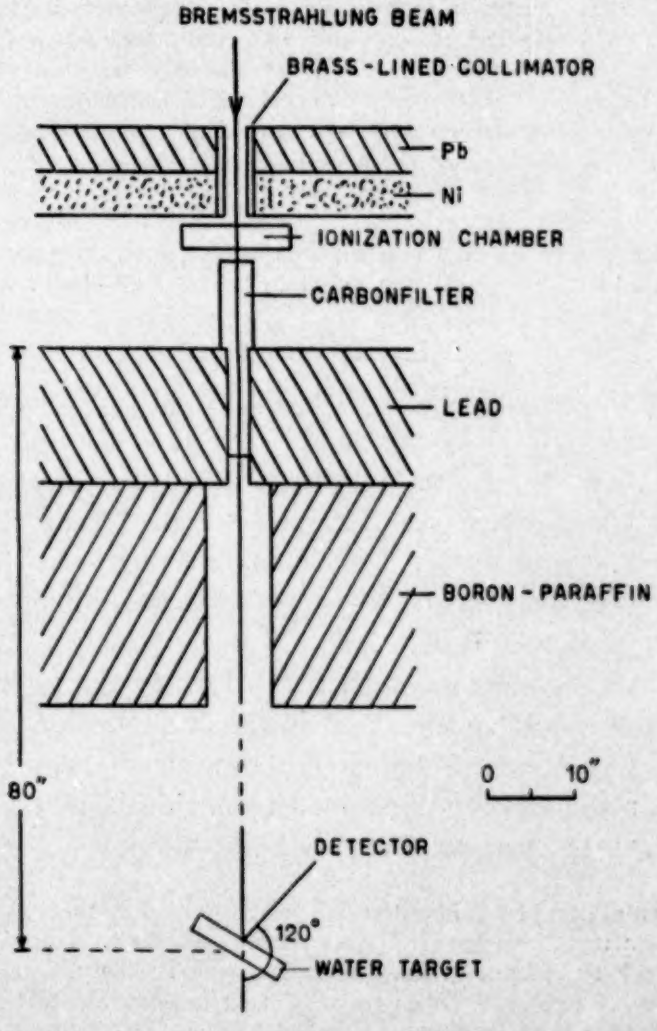

Fig. 1. The experimental arrangement.

scintillation spectrometer with a NaI(Tl) crystal of diameter 5″ and thickness 4″.

2. Experimental Procedure

The experimental arrangement, which was essentially the same as that used by Fuller and Hayward [6]), is shown in figs. 1 and 2. The bremsstrahlung

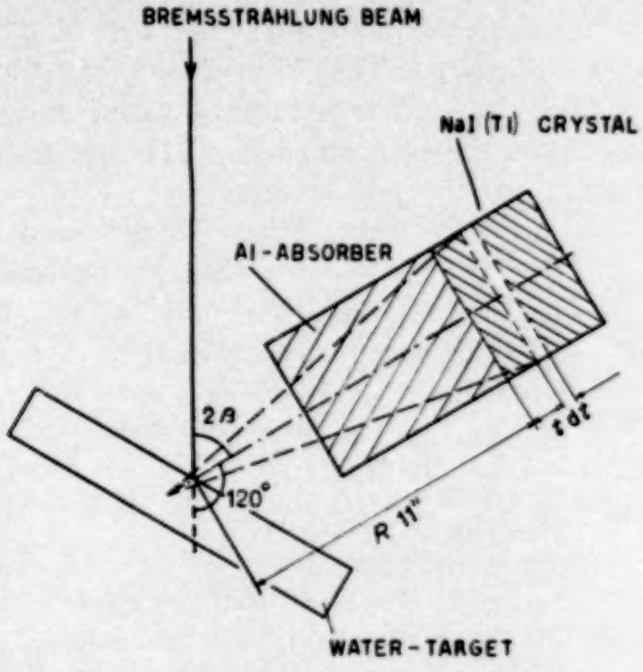

Fig. 2. The geometry.

beam from the NBS 50 MeV betatron was collimated by a brass-lined hole in the Pb+Ni shield. The beam diameter on the target was about 3½″. The beam intensity was monitored by a transmission ionization chamber made of Al. The charge collected on a condenser was measured with a vibrating reed electrometer. In order to absorb the low energy photons, 90 g/cm² carbon was placed in the collimated bremsstrahlung beam.

The detector was shielded from the betatron by a 16″ lead wall and was furthermore surrounded with at least 5″ of lead. Particular care was taken to minimize the background due to neutrons, otherwise contributing considerably to the background in the energy region under consideration. For this purpose, the detector was shielded from the betatron by about 25′ of a mixture of boric acid and paraffin. Outside the lead shield the detector house was surrounded by about 15″ of the same mixture.

The water used as a target was contained in a Lucite box with 1/16″ walls. Target thicknesses between ½″ and 4″ were studied. Sufficient intensity without undue disturbance from multiple processes was achieved with a 2″ target.

A NaI(Tl) crystal of diameter 5″ and thickness 4″, in conjunction with a 6364 DuMont photomultiplier was used to detect those photons emitted by the target at 120° from the direction of the bremsstrahlung beam. The distance from the intersection of the bremsstrahlung beam and the surface of the target to the crystal surface was 11″. A 7″ Al absorber was placed in front of the crystal to absorb electrons and low energy photons emitted by the target.

The pulses produced by the photomultiplier were amplified and then analysed in two ten-channel pulse height analysers, gated by a pulse from the betatron expansion circuit. The yield pulse varied in duration from 15 to 40 μsec, depending on the electron energy. The gate width was kept at about twice the length of the yield pulse.

Using the 1.28 and 4.43 MeV photons from a Na^{22} and a RaD-Be source respectively, the pulse height was found, within the experimental accuracy, to be proportional to the photon energy. The pulse heights measured for the two photon energies were then compared with the pulses produced by a precision pulser, used to determine the firing points of the analyser. The channel widths were determined with the pulser used as a sliding pulser. The variation of the channel width observed during the measurements was less than ± 2 percent. No changes in pulse height due to the different counting rates [9]) used in this experiment were observed. The counting rate was determined to give no pile up of pulses in the energy interval studied.

Pulse height distributions with the Lucite box empty and filled with water respectively, were measured immediately after each other for eight different bremsstrahlung spectra from 16 to 30 MeV. The pulse height distributions measured with the empty Lucite box in the beam were subtracted from the corresponding distributions observed with the box filled with water. The distributions thus determined for bremsstrahlung maximum energies 20.0, 22.5, and 27.5 MeV are presented in fig. 3. The contribution of the background to the total number of pulses for two different pulse height distributions, E^{max} 22.5 and 27.5 MeV, respectively, is given in table 1.

3. Interpretation of the Observed Pulse Height Distribution

3.1. PHOTONS IN THE ENERGY RANGE 6.1–6.3 MeV

At sufficiently high bremsstrahlung energies a peak appeared in the pulse height distribution at a pulse height corresponding to about 6 MeV.

To determine whether the peak might be due to a single γ-ray line of this energy, the pulse height distribution produced by bremsstrahlung with a maximum energy of 27.5 MeV was compared to different spectrometer response functions of about 6 MeV energy estimated from a pulse height distribution produced by the 4.43 MeV photons from a RaD-Be source.

When measuring the 4.43 MeV distribution the same experimental arrangement was used as in the measurements with the water target. In this measurement the background pulse height distribution was determined with two

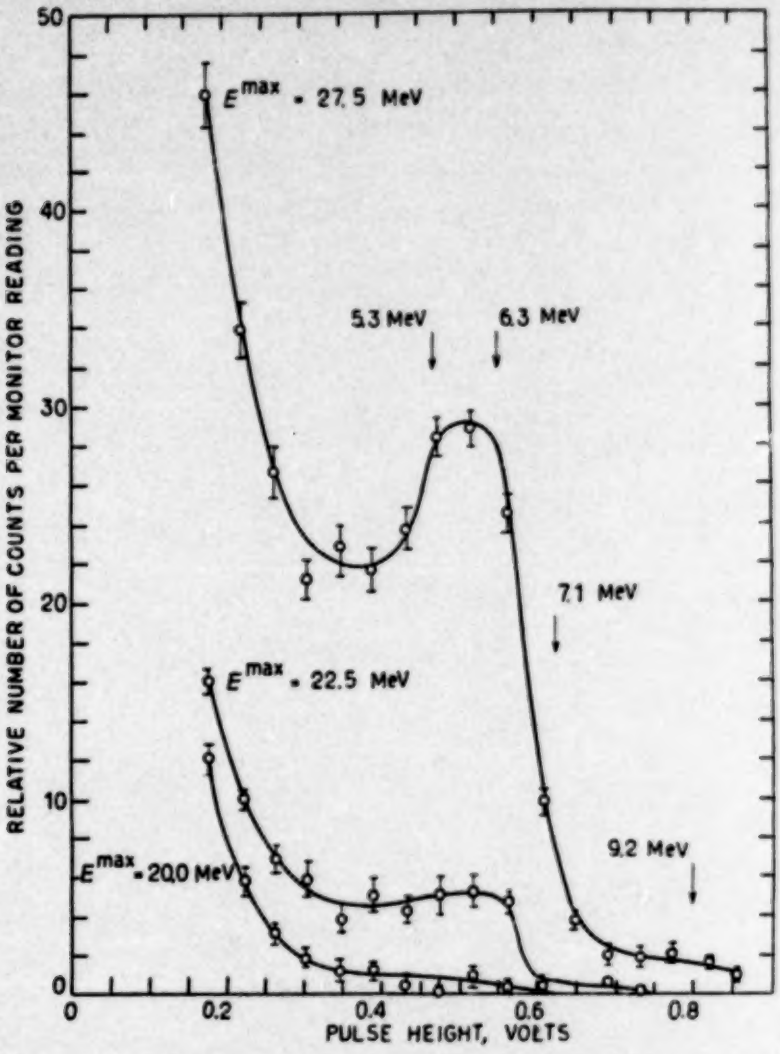

Fig. 3. Pulse height distributions measured when irradiating a 2″ water target with 20.0, 22.5, and 27.5 MeV bremsstrahlung spectra. The background distributions are subtracted.

TABLE 1

The ratio n_B/n_T between the number of background pulses (n_B) and the total number of pulses (n_T) measured at different pulse heights determined for two different bremsstrahlung spectra.

Pulse height		n_B/n_T	
		E^{max} (MeV)	
(Volt)	(MeV)	22.5	27.5
0.4	(4)	0.8	0.5
0.5	(5)	0.7	0.3
0.6	(7)	1.0	0.5
0.7–0.9	(8–10)	0.7	0.1

inches of lead in front of the crystal. The distribution for the 4.43 MeV photons measured in this way was then normalised to the same counting rate in the peak, as the distribution measured when irradiating the oxygen target. Then, by changing the energy scale, pulse height distributions for different photon energies at about 6 MeV were calculated. By trial and error it was found that the one calculated for a photon energy of $1.39 \times 4.43 = 6.16$ MeV gave the best agreement with the peak under investigation (fig. 4).

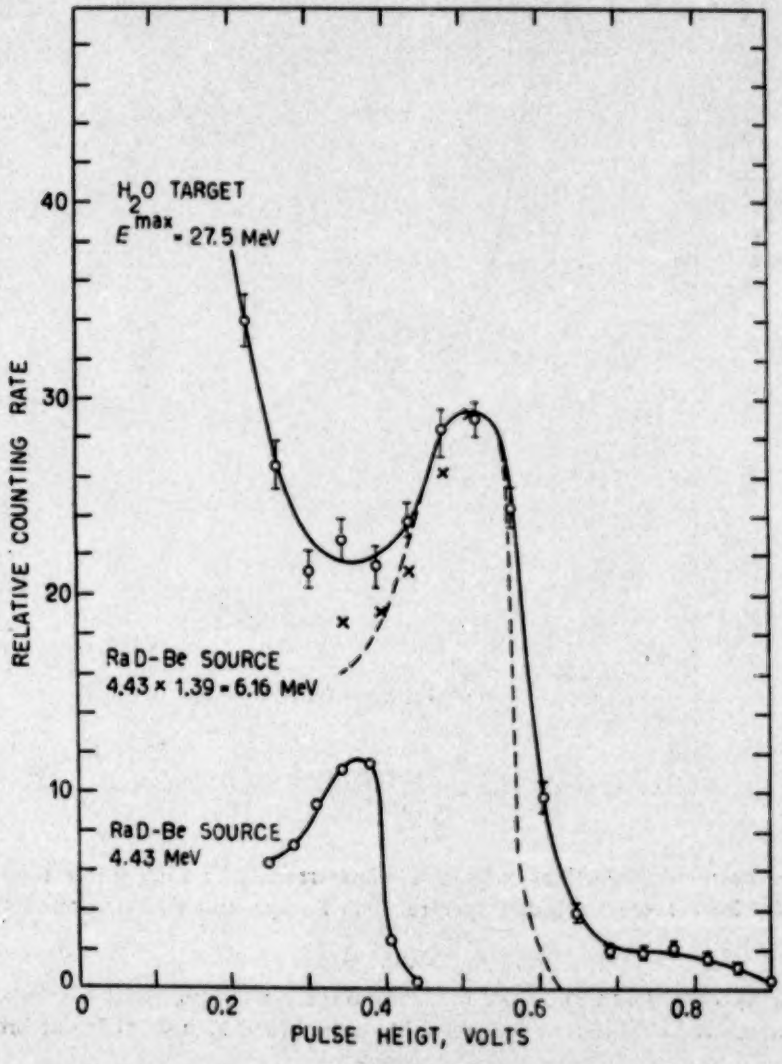

Fig. 4. The pulse height distribution measured when irradiating a water target with a 27.5 MeV bremsstrahlung spectrum. The points marked × indicate the pulse height distribution obtained after subtraction of a 5.3 MeV distribution, the peak height of which is 10 per cent of the total height of the 6.2 MeV peak. Also shown is a 6.2 MeV pulse height distribution estimated from a 4.43 MeV (RaD-Be) distribution.

The estimate of the 6.2 MeV response function by reducing the energy scale only means that the energy of the peak due to the escape of annihilation radiation is lowered by about 0.2 MeV in relation to the photopeak. However,

owing to the escape of bremsstrahlung photons from the crystal, in an accurate determination of the response function for 6 MeV photons some broadening of the combined photo and escape peak might be expected. In view of the inaccuracy in the determination of the width of the peak and the difficulties in fitting the two peaks, the error in the determination of the energy was estimated as ± 0.2 MeV. Absorption measurements were performed with 2″ of aluminium and $\frac{1}{2}$″ of lead in front of the crystal to make sure that the peak was produced by photons emitted by the target and not by capture γ-rays in the detector. The absorption calculated from the sum of the pulses in the four channels giving the peak was in both cases only slightly below the electronic absorption calculated for 6.2 MeV photons from the data of White [10]).

It was therefore concluded that the peak under consideration was due to photons with an energy of 6.2 ± 0.2 MeV. Only for bremsstrahlung

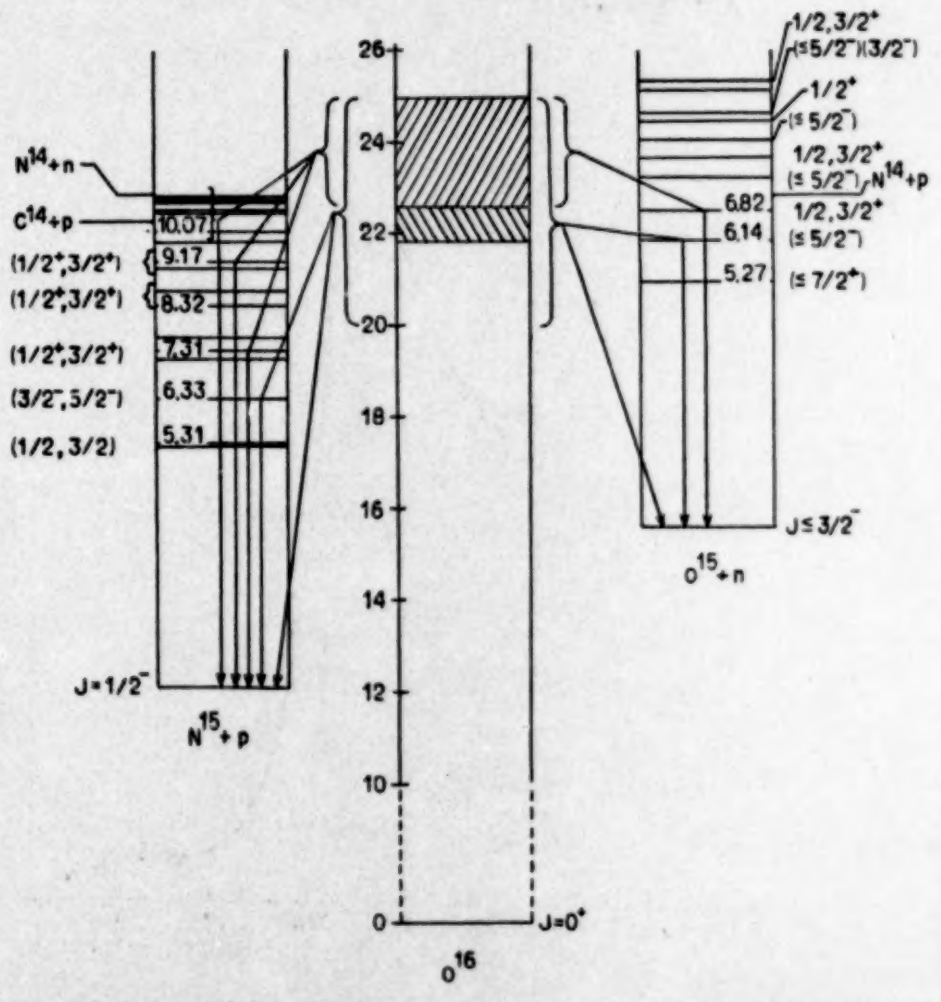

Fig. 5. Level schemes of O^{15} and N^{15} based on the data of Lauritzen and Ajzenberg [11]). The transitions from the excited states are those treated in this paper. The shaded region in O^{16} between 21.8 and 22.5 MeV corresponds to the peak in the cross section for ground state transitions observed by Stephens *et al.* [7]).

energies above 20 MeV did pulses appear with measurable intensity in the channels corresponding to the 6.2 MeV peak. The threshold for production of pulses corresponding to the peak, is then well above the threshold for the photodisintegration of O^{16}, fig. 5. The photons were therefore ascribed to transitions in the daughter nuclei. The measured photon energy is in good agreement with the energy, 6.1 and 6.3 MeV, of the second excited states in O^{15} and N^{15}, respectively [11]) (fig. 5). The threshold values for these reactions, $O^{16}(\gamma, n\gamma')O^{15}$ and $O^{16}(\gamma, p\gamma')N^{15}$, are 21.7 and 18.4 MeV (Coulomb barrier 2.7 MeV) which favour this interpretation. The energy difference between the two levels 6.3 and 6.1 should accordingly broaden the peak in the pulse height distribution to a corresponding degree.

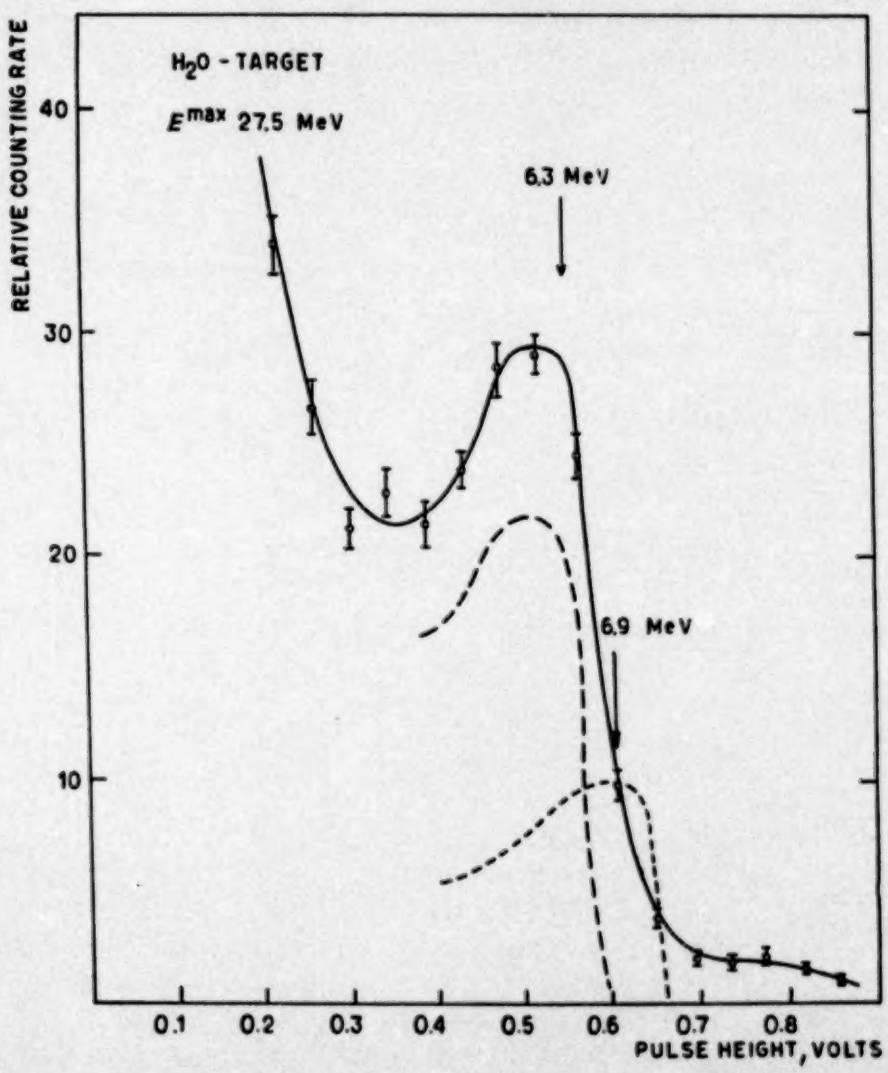

Fig. 6. The pulse height distribution measured when irradiating the target with a 27.5 MeV bremsstrahlung spectrum. The dashed curves represent respectively a 7.1 MeV pulse height distribution, normalised at the 6.9 MeV point and the distribution resulting from subtracting the 7.1 MeV distribution from the total.

3.2. OTHER PHOTONS

However, if the photopeak of the 6.3 MeV pulse height distribution is assumed to have a gaussian shape, it should not noticeably contribute with pulses at 6.9 MeV. The pulses at this and higher energies must therefore be produced by photons with energies, above 6.3 MeV. In fig. 6 a 7.1 MeV pulse height distribution, estimated in the same way as the 6.2 MeV distribution, has been normalised to the 6.9 MeV point on the pulse height distribution measured when irradiating the target with the 27.5 MeV bremsstrahlung spectrum. After subtraction of this distribution the peak in the residual distribution showed much better agreement with the estimated 6.2 MeV distribution. The photon energy 7.1 MeV thus obtained fits in well with the 7.3 MeV level in N^{15}. The 7.16 MeV state was excluded as it usually cascades to the 5.3 MeV level [12]) and no photons of this energy were observed in the present experiment. However, if transitions to the 7.3 MeV in N^{15} occurs, then also the corresponding state at 6.8 MeV in O^{15} should be produced. Owing to this energy difference, the channel in which the 7.3 MeV photopeak occurs, includes only part of the 6.8 MeV photopeak. Thus, a pulse height distribution normalised as described above might result in a loss of pulses. In view of the good agreement between the estimated 6.2 MeV distribution and the distribution obtained after subtraction of the 7.1 MeV distribution, it is felt that this loss of pulses is small. However, it has been estimated that this way of normalising the distribution of 7.3 and 6.8 MeV photons might cause a loss of as much as 25 per cent of the total number of pulses produced by these photons. They are in the following referred to as 7 MeV photons.

From fig. 3 it is obvious that there are also some photons with still higher energies. As the background decreases strongly at these pulse heights, it was possible to make an analysis of this part of the pulse height distribution in spite of the relatively low counting rate, fig. 7. The figure indicates a maximum at a pulse height corresponding to 9.0 ± 0.2 MeV. The data are not accurate enough to permit an unequivocal determination of the corresponding level in the residual nuclei. These photons will therefore below be referred to as 9 MeV photons. The distribution above about 9.5 MeV does not show any maximum. These pulses are most likely due to various photon energies between 10 and 11 MeV. They are referred to below as 10 MeV photons.

The amount of 5.3 MeV photons produced in transitions from the first excited states in O^{15} and N^{15} was estimated by subtracting from the measured pulse height distribution (E^{max} 27.5 MeV) 5.3 MeV pulse height distributions with different intensities, estimated from the 4.43 MeV distribution in the manner described above. The result of subtracting a 5.3 MeV distribution with a peak height 10 per cent of the total height of the 6.2 MeV peak

is shown in fig. 4. From a comparison with the estimated 6.2 MeV distribution it was concluded that there were probably no 5.3 MeV photons, but if any, they represented no more than 10 per cent of all other daughter photons.

The great number of pulses in the low energy part of the pulse height distribution was, at least to some extent, due to bremsstrahlung produced by compton electrons and electrons created in pair production, as deter-

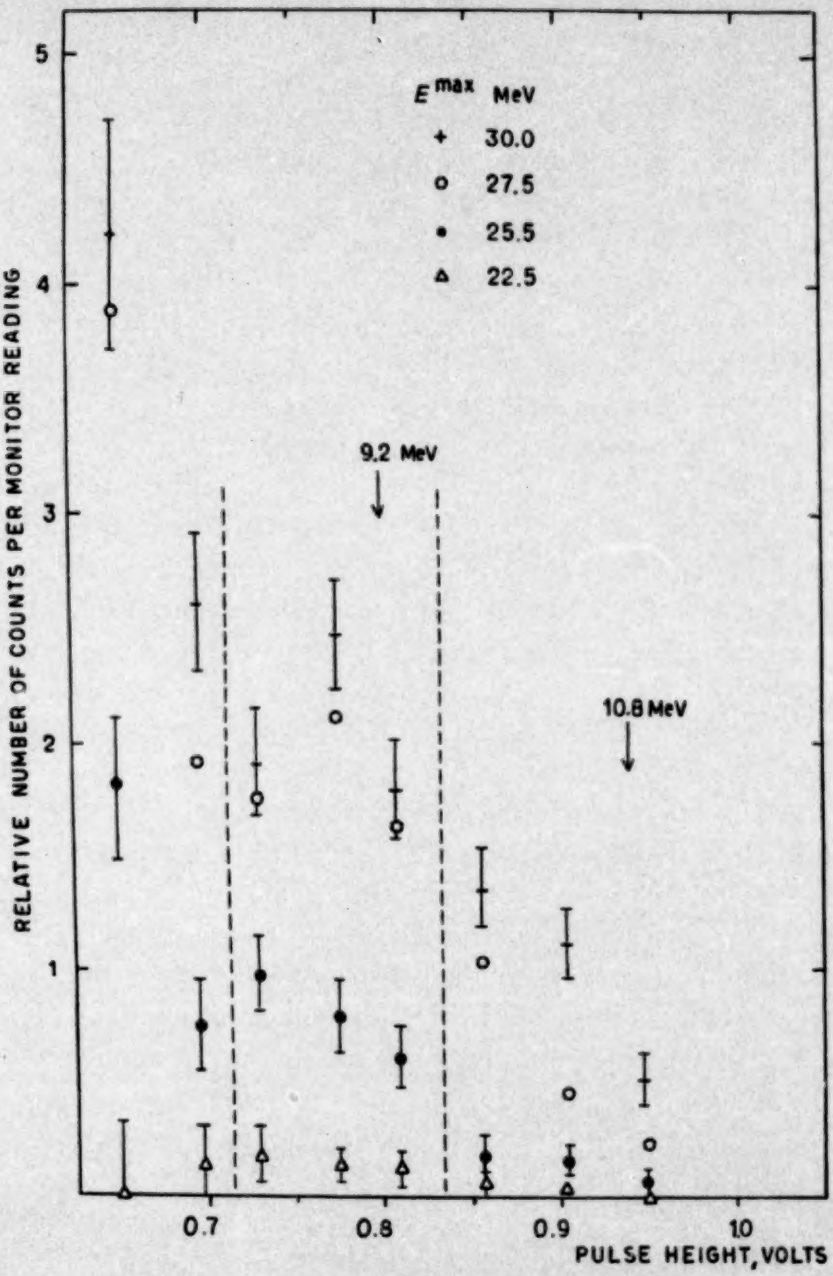

Fig. 7. The high energy part of the pulse height distributions measured when irradiating the water target with bremsstrahlung of different maximum energies. The errors in the distribution measured with E^{max} 27.5 MeV, not shown in the figure, are the same as for E^{max} 30.0 MeV. The dashed lines indicate the intervals used to calculate the cross section for the 9 and 10 MeV photons respectively.

mined in a comparison of pulse height distribution for different target thicknesses. The ratio between the number of pulses in corresponding channels in the two pulse height distributions measured with a 4″ and a ½″ water target is plotted in fig. 8. For pulse heights above those corre-

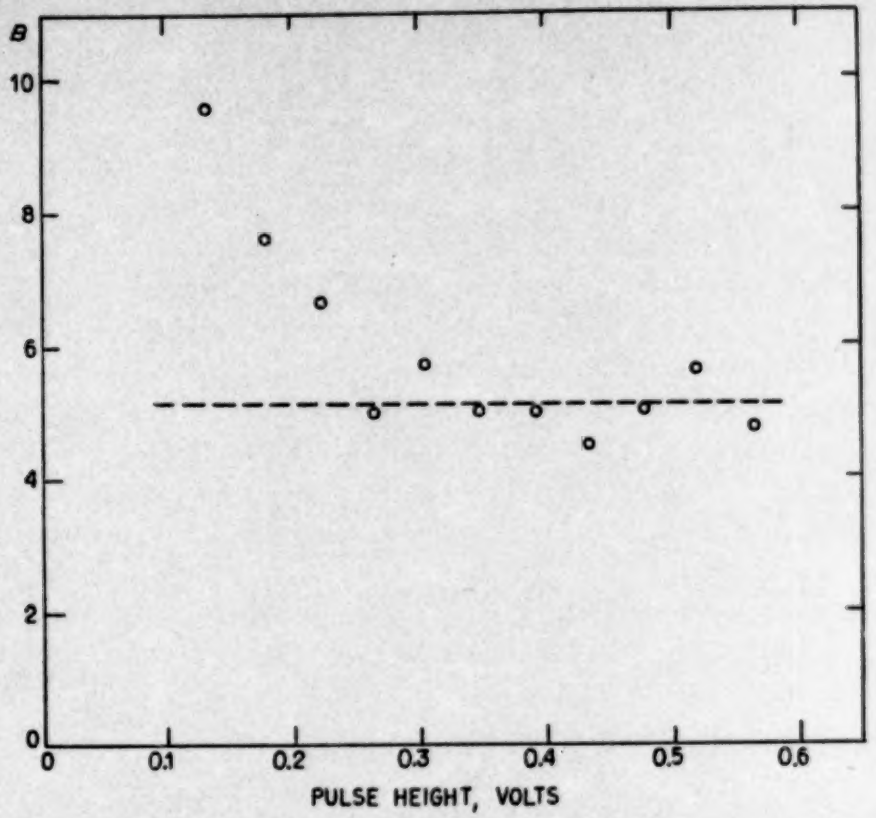

Fig. 8. The ratios between the number of pulses in corresponding channels observed with a 4″ and 1/2″ water target, respectively. The dotted line corresponds to the ratio expected from the change in electronic absorption with the target thickness.

sponding to about 2.5 MeV, good agreement was found between the experimental quotient 5.0, and the calculated, 5.2. At pulse heights less than those corresponding to about 2.5 MeV there was an increase of pulses from the 4″ target, which was ascribed to multiple processes in the target. The deviation between the estimated and the measured pulse height distributions at about 4 MeV (0.3—0.4 Volts) in fig. 4 might be due to photons of this energy. Owing to the way in which the background was determined, these pulses might be caused by neutrons produced in the water target. In view of the above, no interpretation of the pulse height distribution below about 5 MeV is possible.

3.3. THE POSSIBILITY OF CASCADES

In the discussion above the photons observed were interpreted as due to γ-ray transitions directly to the ground states in the daughter nuclei. One might however possibly imagine that they may also have been produced

in γ-ray cascades from higher levels. Since the present data do not exclude this possibility, it was considered useful to peruse reports on cascades in other investigations of γ-rays from excited O^{15} and N^{15} nuclei. Only the 6.1—6.3 MeV levels were considered, since only in this case, an unequivocal identification of the corresponding levels was found possible.

Cascade transitions from the 10.8 MeV state in N^{15} through the 6.3 MeV state have been reported by Kinsey *et al.* [13] and more recently by Campion and Bartholomew [14]). With a pair spectrometer they studied γ-rays with energies above 3 MeV produced by thermal neutron capture in N^{14}. According to these authors, the cascade transitions are accompanied by ground state transitions in roughly equal numbers. Owing to the low cross section for the production of 10 MeV photons observed in the present investigation, these cascade transitions could not appreciably contribute to the 6.1—6.3 MeV peak. Thompson [15]) observed in a study of the N^{14}+d reaction with a NaI(Tl) scintillation spectrometer 1.88 and 0.84 MeV γ-rays which were attributed to cascades from the 7.17 MeV state in N^{15} through the 5.3 and 6.3 MeV states, respectively. The cascade through the 5.3 MeV should, according to Thompson however, occur about 20 times as often as the one through the 6.1 MeV state. Since no 5.3 MeV photons were observed in the present investigation, it was concluded that the 7.17 MeV state in N^{15} is not produced in the photodisintegration of O^{16} or at least the cross section must be small.

Johnson *et al.* [16]) studied the γ-rays with energies above 0.5 MeV emitted in the reaction N^{14}(p, γ)O^{15} using a NaI(Tl) scintillation spectrometer. They reported a cascade 1.39+6.21 MeV but did not observe any corresponding ground state transition (7.60 MeV). The same radiative capture reaction was studied by Bashkin *et al.* [17]). They quoted the ratios 40 : 100 : 25 between the observed 6.65, 6.10, and 5.25 MeV γ-rays. The ground state transitions were found to be less than 5 per cent of those to the 6.1 MeV state. For the same reason as in the case of the 7.17 MeV state it was concluded that the 7.6 MeV state is not produced in the reaction studied in this investigation.

The discussion above cannot be considered as an exhaustive answer to the question whether or not cascades occur through the levels studied. All the data in the present paper are, however, based on the assumption that cascades do not occur, not only considering the 6.1—6.3 MeV states but also the 7, 9, and 10 MeV states.

4. The Cross Sections

4.1. THE YIELD CURVES

In order to study the yield of 6.1—6.3 MeV photons as a function of the maximum bremsstrahlung energy, the pulses in the four channels providing

the peak were used. Some of these pulses are, however, produced by photons with energies above 6.3 MeV. Owing to the shape of the response function of the spectrometer, this contribution influences the results appreciably. A cross section analysis therefore demands corrections for the tails of the pulse height distributions corresponding to the higher photon energies present. This is also true for the 7 and 9 MeV pulse height distributions. Knowledge about the response functions of the spectrometer for the geometry used is thus necessary. The available information is, however, restricted to the 4.43 MeV photons from a RaD-Be source and the 15 MeV photons elastically scattered by the C^{12} nucleus [18]). Since the shape of a

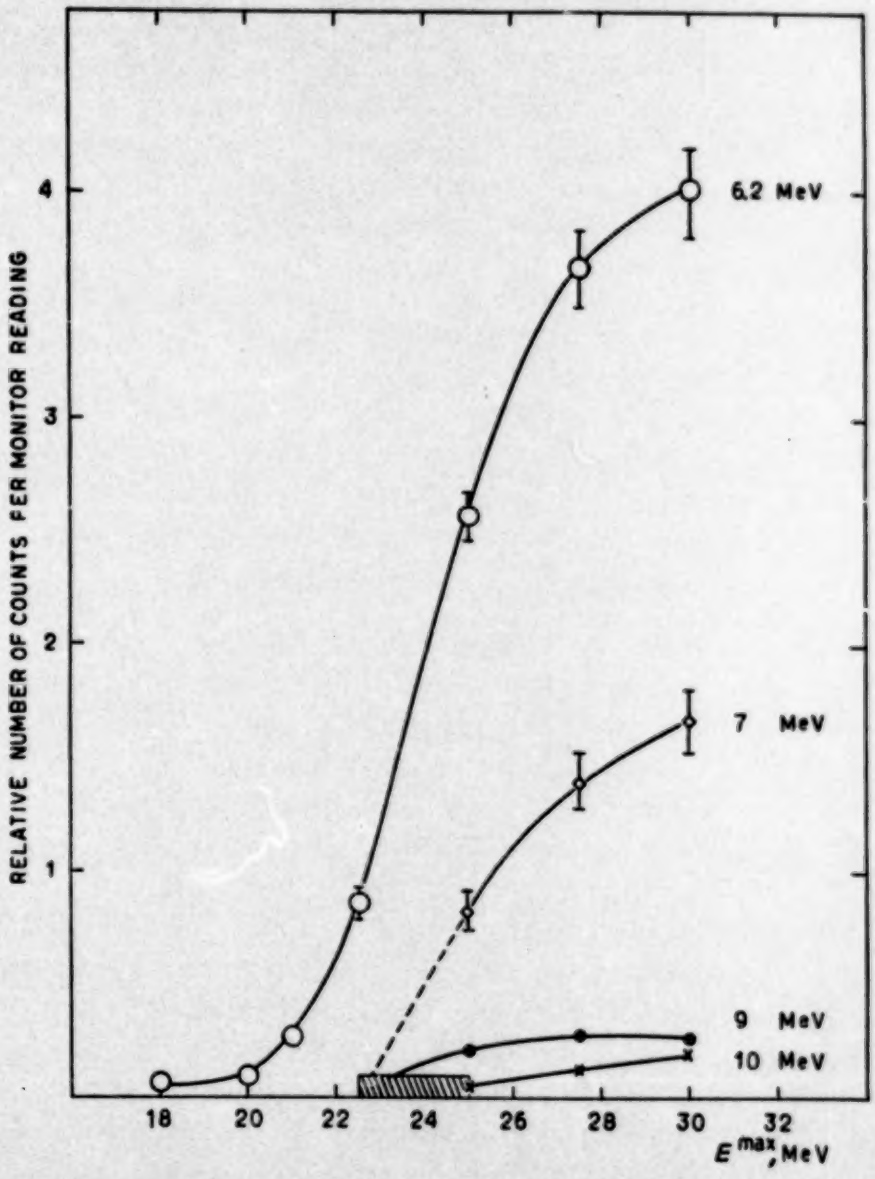

Fig. 9. The yield curves observed for the different daughter photon energies. The shaded area shows the energy interval in which the 7, 9, and 10 MeV photons are predominantly produced. When the statistical errors are not shown, they are within the symbols.

15 MeV pulse height distribution estimated from a 4.43 MeV distribution through changing the energy scale only agrees with the measured 15 MeV distribution within the experimental errors, it is felt that this way of estimating the response function for interjacent photon energies should be fairly accurate. The yield curves for the various daughter photons were determined in the following way. First, the yield curve for the 10 MeV photons was based upon the three channels marked in fig. 7. Using the average number of pulses in these channels for normalisation a pulse height distribution was calculated for this photon energy. After correction for the 10 MeV pulse height distribution the pulses in the three channels (fig. 7) forming the maximum at 9 MeV were treated in the same way. The yield curve for the 6.2 and 7 MeV photons was based on the pulse height distributions in fig. 6. Corrections were applied for all photons with higher energies. The yield curves thus determined are reproduced in fig. 9.

The threshold for observing the pulses corresponding to the 6.2 and 7 MeV is about 20 and 22.5 MeV, respectively, while in the case of the 9 and 10 MeV photons the corresponding thresholds are within the energy interval 22.5—25.0 MeV.

4.2. EVALUATION OF THE CROSS SECTIONS

1) *6.1 and 6.3 MeV Photons*

The cross section, $\sigma(E)$, for production of the 6.1—6.3 MeV photons as a function of the excitation energy, E, can be calculated from the yield curve in fig. 9 from the expression

$$n(E^{\max}) = k \cdot f(E^{\max}) \cdot \varepsilon \cdot e^{-\mu_{Al} \cdot l_{Al}} N(E^{\max}); \qquad (1)$$

$n(E^{\max})$ is the sum of number of pulses per monitor reading in the four channels providing the peak in the pulse height distribution measured for a bremsstrahlung spectrum with a maximum energy $E^{\max}$, and $N(E^{\max})$ the total number of 6.1—6.3 MeV photons emitted from the target per MeV incident bremsstrahlung energy and thus a function of $\sigma(E)$. $f(E^{\max})$ is the total bremsstrahlung energy (MeV) incident on the target per monitor reading for a bremsstrahlung spectrum $E^{\max}$, $\exp(-\mu_{Al} l_{Al})$ the attenuation in the Al absorber in front of the crystal, ε includes the crystal efficiency and the solid angle, and k the ratio between the number of pulses in the four channels, n, and the number of pulses determined by the complete response function.

The response function of the spectrometer was estimated from the 4.43 MeV pulse height distribution, as described in the interpretation of the pulse height distribution. In the present case, however, the 4.43 MeV distribution was measured without the 7″ Al absorber in front of the crystal. The large number of pulses due to multiple scattering in the absorber were

then excluded. The response function was then extra-polated to zero energy as shown in fig. 10. As proved experimentally at 4.43 MeV, the absorption

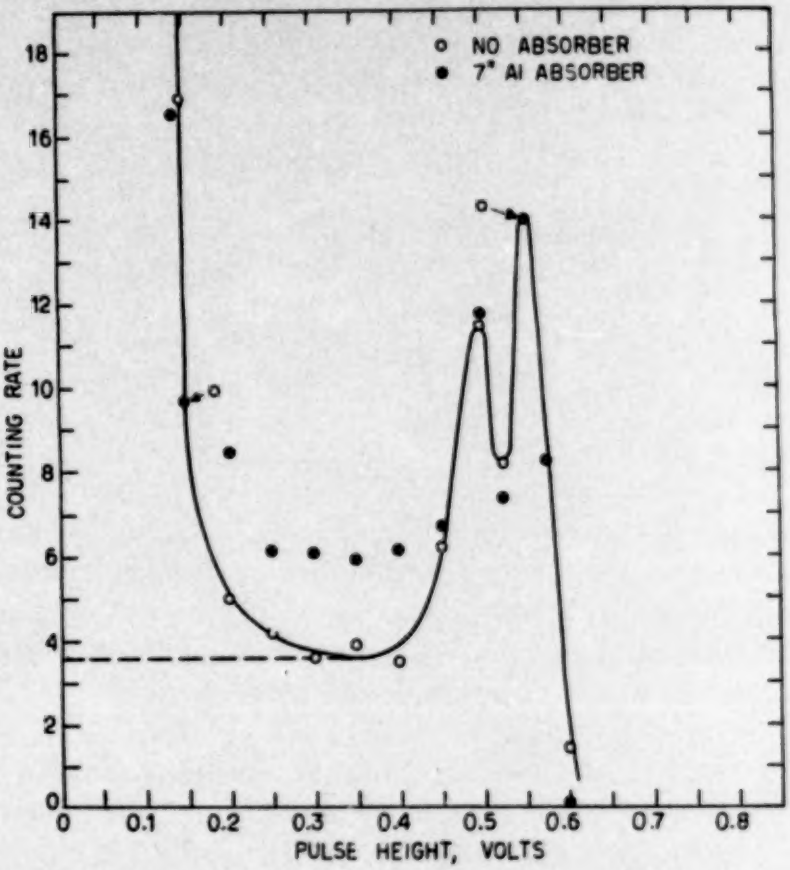

Fig. 10. Pulse height distribution for the 4.43 MeV photons form a RaD-Be source measured with an without 7" Al in front of the crystal. The two distributions were normalised at the peak value. Also shown is the extrapolation of the distribution to zero pulse height used to determine the 6.3 MeV response function.

coefficients [10]) for narrow beam geometry could then be used in calculating the attentnation in the absorber from the four channels giving the peak. $f(E)^{\max}$ was determined by comparing the monitor reading with the number of roentgens, as measured with a 25-r Victoreen thimble chamber in an 1/8" Pb cap at the position of the centre of the target. The bremsstrahlung energy incident on the target was then calculated from the number of measured roentgens [19]).

ε is the differential absorption multiplied by the corresponding solid angle, integrated through the whole target thickness:

$$\varepsilon = \int_0^T \frac{S}{(R+t)^2} \cdot e^{-\mu_{NaI} \cdot t} \cdot \mu_{NaI} \cdot dt \qquad (2)$$

where S is the crystal front area, R the distance between the centre of the target and the midpoint of the front surface of the crystal. T is the total

thickness of the crystal and t the distance between the disintegrating O^{16} atom and the front surface of the crystal measured along the crystal axis. μ_{NaI} is the linear absorption coefficient for 6.2 MeV photons in the crystal. The expression under the integral assumes that the angular aperture of the beam is small; the error caused by this assumption was found to be negligible. Calculations also showed that the solid angle calculated for the centre of the target could be considered a good average value for all points within the target.

The total number of 6.1—6.3 MeV photons emitted by the target is given by the expression

$$N(E^{max}) = \int_{E_{th}}^{E^{max}} \int_0^T \int_0^{4\pi} e^{-A(\sigma_n+\sigma_e'+\sigma_e'')\cdot x/\cos\beta} \cdot e^{\mu_c \cdot l_c} \cdot \eta(E, E^{max}) \cdot A \cdot \frac{d\sigma(E)}{d\Omega} \cdot dE \cdot \frac{dx}{\cos\beta} \cdot d\Omega; \quad (3)$$

A is the number of oxygen atoms (water molecules) per cm^3 in the target, σ_e' and σ_e'' the cross section for electronic absorption of the bremsstrahlung and the 6.1—6.3 MeV photons, respectively. σ_n, the nuclear absorption of the incident bremsstrahlung was neglected as no significant deviation from the calculated electronic absorption was observed when 19″ water was placed in the bremsstrahlung beam incident on the target. β is defined from the scattering angle $(180-2\beta)°$ (fig. 2), x as the distance between the disintegrating nucleus and the target surface, T as the total thickness of the target and E_{th} the observed energy threshold for this reaction. $\eta(E, E^{max})$ the number of photons per MeV incident bremsstrahlung energy with an energy between E and $E+dE$ in the unfiltered bremsstrahlung beam and $\exp(-\mu_c \cdot l_c)$ is the attenuation in the carbon absorber of the primary beam. $d\sigma(E)/d\Omega$ is the differential cross section for the production of the 6.1—6.3 MeV photons at the excitation energy E. Since the angular distribution of the photons were not measured and no theoretical calculations are available, the distribution of the 6.1—6.3 MeV photons, as well as all other photons considered in this paper, were assumed isotropic, *i.e.* the differential cross section will be replaced by $\sigma(E)/4\pi$.

After integration through the target thickness, (3) can be written as

$$N(E^{max}) = \int_{E_{th}}^{E^{max}} \frac{1-e^{-A(\sigma_e'+\sigma_e'')\cdot T/\cos\beta}}{\sigma_e'+\sigma_e''} \cdot e^{-\mu_c \cdot l_c} \cdot \eta(E, E^{max}) \cdot \frac{\sigma(E)}{4\pi} \cdot dE. \quad (4a)$$

The ratio

$$e^{-\mu_c \cdot l_c} \cdot (1-e^{-A(\sigma_e'+\sigma_e'')T/\cos\beta})/4\pi(\sigma_e'+\sigma_e'')$$

varies only slightly over the energy interval of interest so that a mean value C could be used. Furthermore, if $\eta(E, E^{max})$ is replaced by the in-

tensity $\mathcal{J}(E, E^{max})$ divided by the photon energy E, the expression simplifies to

$$N(E^{max}) = C\int_{E_{th}}^{E^{max}} \sigma(E) \cdot \frac{\mathcal{J}(E, E^{max})}{E}\, dE. \qquad (4b)$$

In evaluating this integral, the tables for cross section analysis computed by Penfold and Leiss [20]) from the Schiff integrated-over-angle bremsstrahlung intensity spectrum were used. Since the bin width used in this computation, 0.5 MeV, was much smaller than the experimental bins,

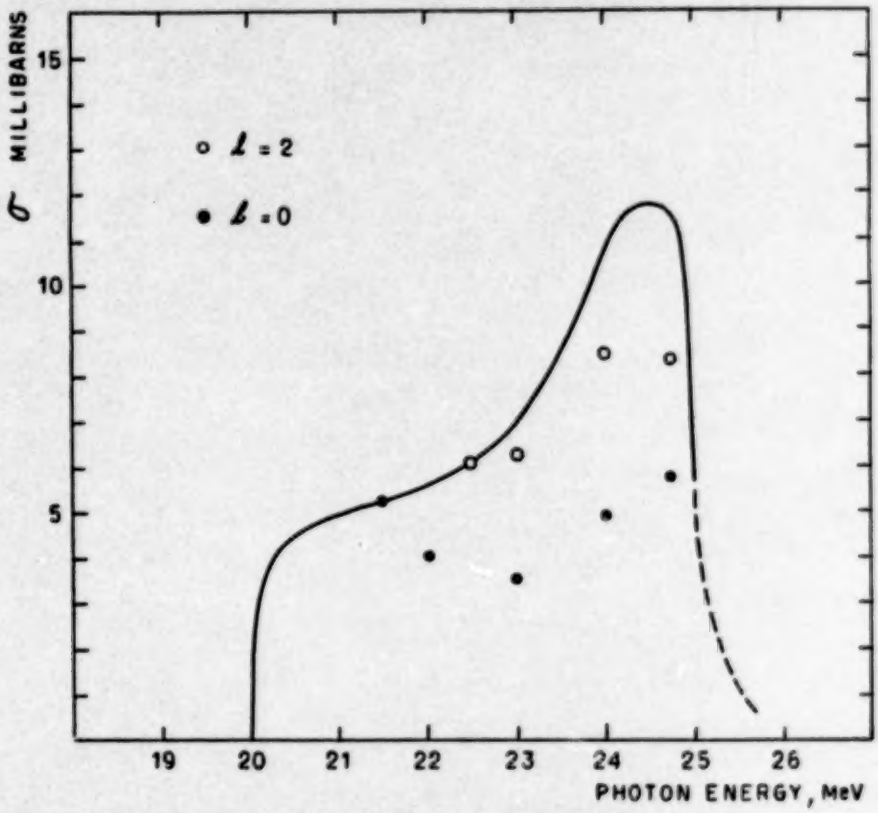

Fig. 11. The cross section curve calculated from the 6.2 MeV yield curve in fig. 9. The points were obtained by multiplying the cross section curve with $\sigma(\gamma, p)/[\sigma(\gamma, p)+\sigma(\gamma, n)]$ for $l = 0$ and $l = 2$, respectively. (fig. 13). Thus they indicate the contributions from the (γ, p) and the (γ, n) reactions to the total cross cection.

$N(E^{max})$ was taken from the smooth yield curve in fig. 9. The cross section curve for production of 6.2 MeV photons calculated in this way is reproduced in fig. 11.

2) *The 7, 9 and 10 MeV Photons*

In the case of the 7, 9 and 10 MeV photons the yield curves did not lend themselves to a determination of the cross section in the way described above for the 6.2 MeV photons. Therefore the integrated cross section was determined directly from a comparison of the yield curves with various

isochromates between 20 and 25 MeV. These were calculated from the Schiff integrated over angle spectra as tabulated by Penfold and Leiss [20]). The yield points for the 7 and 9 MeV photons determined when irradiating the target with 25.0, 27.5, and 30.0 MeV bremsstrahlung spectra fitted the 24 and 23 isochromats, respectively.

When calculating the cross section for the 7 MeV photons this way, all those photons possibly produced by bremsstrahlung below 24 MeV are

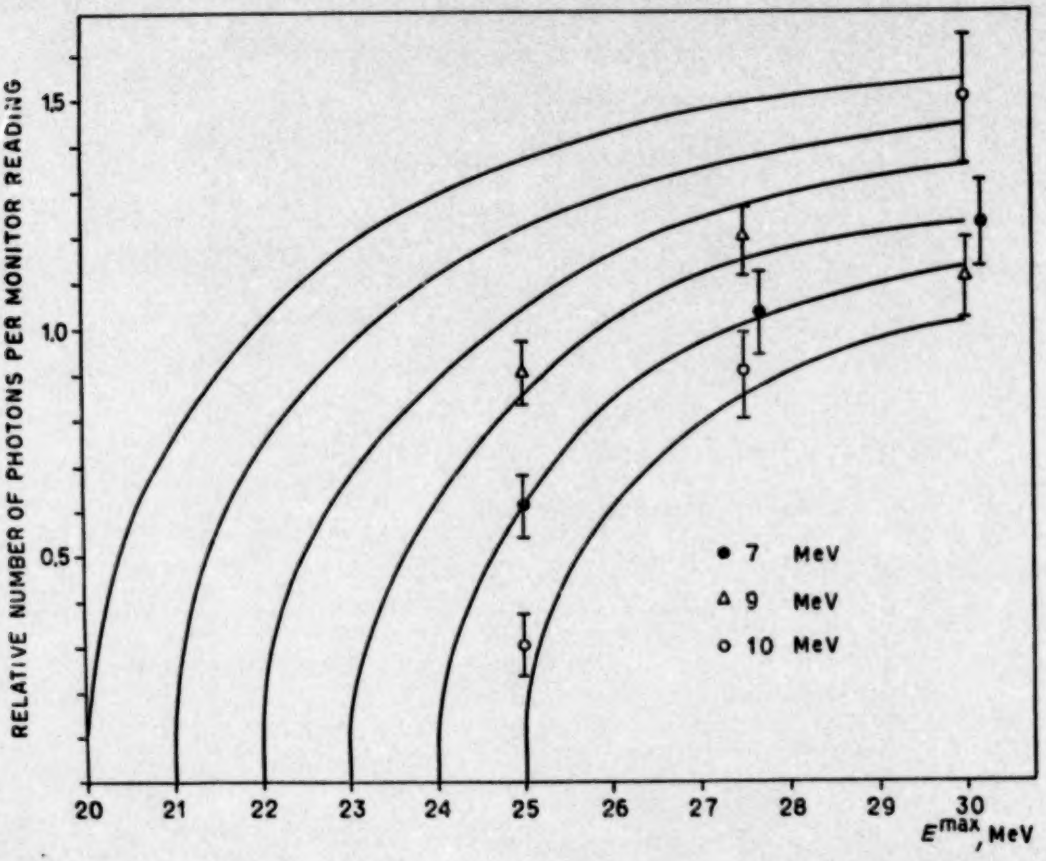

Fig. 12. Isochromats between 20 and 25 MeV calculated from the Schiff spectrum as tabulated by Penfold and Leiss [22]). The experimental yield points for the different daughter photons are also given. The errors given in the figure are the statistical errors only.

assumed to be fed from a 24 MeV level. In order to estimate the error thereby introduced, the integrated cross section was also calculated for a yield curve in which the points at 22.5 and 25.0 were connected with a straight line. This value deviated by less than 5 per cent from the value found above.

In the case of the 9 MeV photons the energy value of the corresponding isochromat, 23 MeV, coincides with the excitation energy at which the 9 MeV photons can be produced if the influence of the Coulomb barrier is considered. This together with the fairly accurate fit of the yield points

to the isochromat suggested that the cross section for production of these photons decreases rapidly above 23.0—23.5 MeV.

The yield points of the 10 MeV photons did not fit very well to any isochromat. The experimental data might well be interpreted as indicating a smooth (average) cross section between 24 and 30 MeV. The 25 MeV isochromat was used to calculate the cross section.

The integrated cross sections were calculated from eq. (1) and (4b). The ratio

$$(1-e^{-A(\sigma_e'+\sigma_e'')T/\cos\beta})/(\sigma_e'+\sigma_e'')$$

in eq. (4b) is not influenced by the variation of the daughter photon energy. In eq. (1) the variation of the attenuation in the aluminium absorber for the different photon energies, a few per cent, has to be considered. More important is the energy dependence of k, the ratio between the numer of pulses in the four channels providing the 6.2 MeV peak and the number of pulses determined by the complete response function (determined without the 7" Al absorber). In the calculations of the cross sections for production of the 7, 9, and 10 MeV photons this ratio was considered constant.

3) *Splitting of the Cross Section between O^{15} and N^{15}*

Transitions to excited states at 9 MeV in O^{15} have a calculated threshold 24.6 MeV, which is above the energy of the isochromat (23 MeV) to which the experimental data fit. All the observed photons of this energy must therefore originate from N^{15}. This also applies to the 10 MeV photons.

The 6.2 and 7 MeV photons could, however, be due to transitions to both the mirror nuclei, O^{15} and N^{15}. In order to split up the total cross section, the contributions from the $(\gamma, p\gamma')$ and the $(\gamma, n\gamma')$ reactions were calculated from a comparison between the barrier penetration coefficients for protons, $T_l(p)$, and neutrons, $T_l(n)$, at equal excitation energies. The reduced widths were assumed to be equal. As these incorporates properties of the interior of the nucleus only, the assumption may be justified by the complete symmetry between the two mirror nuclei †). The relative contribution from the $(\gamma, p\gamma')$ reaction is then

$$r(l, E) = \frac{\sigma(\gamma, p)}{\sigma(\gamma, p)+\sigma(\gamma, n)} = \frac{T_l(p)}{T_l(p)+T_l(n)}. \qquad (6)$$

† A breakdown of the isotopic spin selection rules in the energy region between 20 and 25 MeV as suggested by D. H. Wilkinson[21]) might influence the result of the splitting of the total cross section in this way. In this energy region the at present available experimental data do however not give positive evidence that this is the case. For instance, when comparing the (γ, p) and the (γ, n) data it is necessary to observe that Penfold and Spicer reported that they did not (carefully) study the energy region between 21.5 and 22.4 MeV. Furthermore, the present investigation shows that the giant resonance is much broader than assumed by Wilkinson, when discussing the (γ, α) reaction.

The ratio $r(l, E)$ calculated from the data of Penfold and Spicer [23]) for transitions to 6.2 MeV states and for $l = 0$, 1, and 2, respectively, is plotted in fig. 13. The excitation of the oxygen nucleus should be due to electric dipole photon absorption. Since the 6.1 and 6.3 MeV levels are assigned a total angular momentum $\leqq 5/2$ and 3/2, 5/2 in O^{15} and N^{15}, respectively,

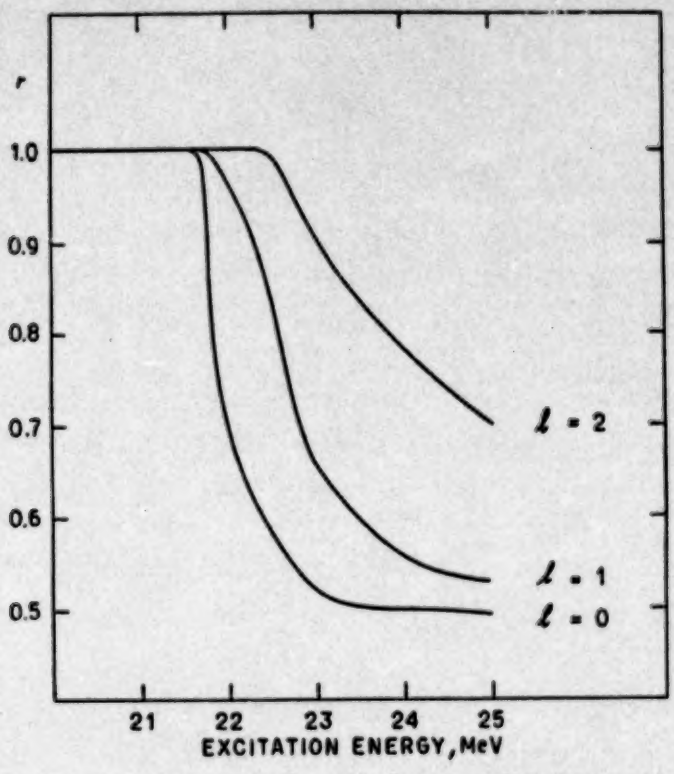

Fig. 13. The ratio $r = \sigma(\gamma, p)/[\sigma(\gamma, p)+\sigma(\gamma, n)]$ for $l = 0$, 1, and 2 respectively, for transitions to the 6.1—6.3 MeV states in O^{15} and N^{15} calculated from the transmission coefficients given by Penfold and Spicer [23]). The excitation energy refers to O^{16}.

and odd parity, the total angular momentum of the emitted nucleons must be either zero or two. In fig. 11 the cross section curve for the 6.1—6.3 MeV photons was multiplied by the ratio r for $l = 0$ and $l = 2$. The 7.3 MeV state in N^{15} is assigned even parity. If the observed photons are ascribed to transitions from this level, the photonucleons must have $l = 1$. The splitting of the cross section has been based on this assumption.

The integrated cross sections for the $(\gamma, p)+(\gamma, n)$ and for each of these two reactions calculated with the given assumptions are listed in table 2. In the same table also the integrated cross section for transitions to the ground state in N^{15} as calculated from fig. 2 in the paper of Stephens *et al.* [7]) is shown. The ratio between the transition to the ground state and to the excited states in the energy interval 20 to 25 MeV in table 2 agrees with the value determined from the photoproton spectrum of Stephens *et al.* [7]) if 1.2 mb is used as a mean value of the cross section for ground state transitions between 14 and 18 MeV. The transitions to the ground state in

TABLE 2

The integrated cross section (MeV.mb), together with the relative numbers, for the $O^{16}(\gamma, p)N^{15}$ and $O^{16}(\gamma, n)O^{15}$ reactions. The cross section for ground state transitions in the (γ, p) reactions was taken from Stephens *et al.* [7]) The same cross section was also used for ground state transitions in the (γ, n) reaction. In splitting the cross section for 6.2 MeV and 7 MeV photons into cross section for the two different reactions the photonucleons were assumed to have $l = 0$ and $l = 1$, respectively.

Excitation energy in O^{16} (MeV)	Reaction	Photodisintegration to										Total σ_{int}
		ground state		excited state (MeV)								
				6.2		7		9		10		
		(MeV·mb)	%	(MeV·mb)	%	(MeV·mb)	%	(MeV·mb)	%	(MeV·mb)	%	(MeV·mb)
20.0–21.0	γ, p	3	43	4	57							7
	γ, n	3	100									3
	$\gamma, p+\gamma, n$	6	60	4	40							10
21.0–22.5	γ, p	11	61	7	39							18
	γ, n	11	92	1	8							12
	$\gamma, p+\gamma, n$	22	73	8	27							30
22.5–25.0	γ, p	14	32	11	26	12	28	4	9	2	5	43
	γ, n	14	45	10	32	7	23					31
	$\gamma, p+\gamma, n$	28	38	21	28	19	26	4	5	2	3	74
20.0–25.0	γ, p	28	41	22	32	12	18	4	6	2	3	68
	γ, n	28	61	11	24	7	15					46
	$\gamma, p+\gamma, n$	56	49	33	29	19	17	4	3	2	2	114

the mirror nucleus O^{15} was assumed to have the same cross section as in the case of N^{15}.

The most important uncertainties in the data given in table 2 are, under the made assumptions, due to the lack of detailed knowledge about the spectrometer response functions for various photon energies between 6 and 11 MeV and the background produced in the target. Altogether, the data of the integrated cross section for 7, 9 and 10 MeV photons emitted in the $(\gamma, p\gamma')+(\gamma, n\gamma')$ reactions are not considered to have an accuracy better than $^{+25}_{-50}$ per cent.

5. The Total Photon Absorption

In order to investigate to what extent the present cross section data reproduced the giant resonance, an attempt was made to determine the total photon absorption cross section.

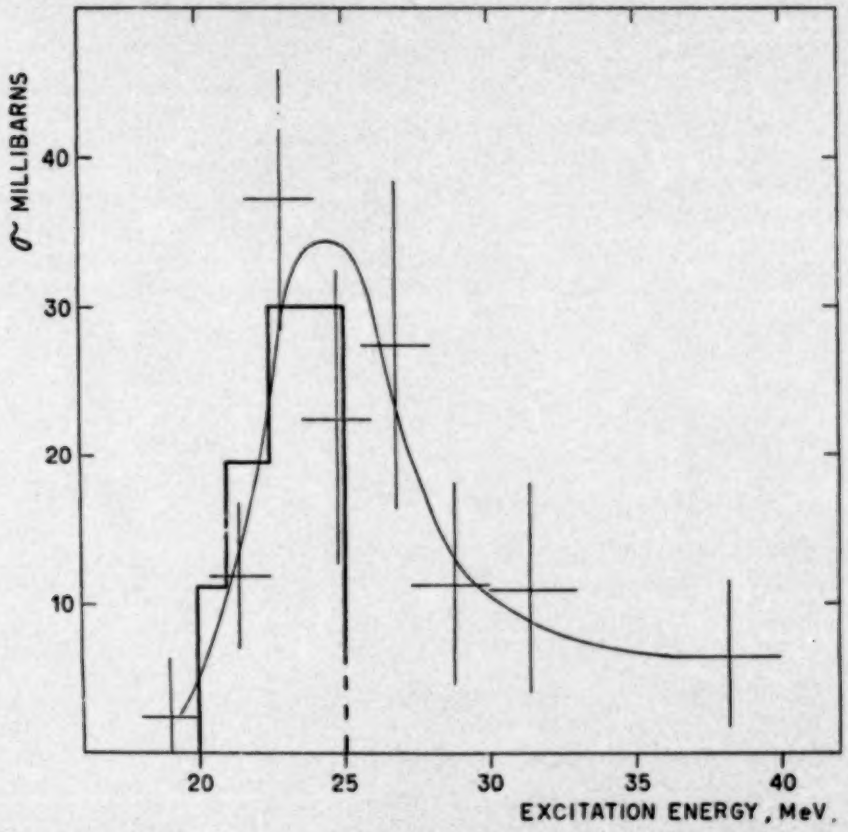

Fig. 14. The $(\gamma, p)+(\gamma, n)$ cross section histogram from table 2. The curve represents the total photon absorption. It is normalised by making the integrated cross section between 20 and 25 MeV equal to the value represented by the histogram. The experimental points refer to the mean value of the nuclear elastic scattering of photons in the energy intervals shown by the horizontal lines, multiplied by a normalisation factor 5.9×10^2. The vertical lines represent the statistical errors.

The average nuclear elastic scattering of photons in energy intervals a few MeV wide was measured using the method of Fuller and Hayward [8]).

The experimental data multiplied by a normalisation factor 590 is shown in fig. 14. The relation between the total elastic scattering, $\sigma_s(E)$, and the total nuclear absorption of photons, $\sigma_a(E)$ is given by the equation [8])

$$\sigma_s(E) = \frac{1}{6\pi\lambda^2}\left[\sigma_a^2(E) + \left(\frac{2E}{\pi}\,\mathrm{P}\int\frac{\sigma_a(E')\mathrm{d}E'}{E'^2-E^2}\right)^2\right] \qquad (7)$$

$$+\frac{8\pi}{3}D^2 + \frac{8}{3\pi}\frac{1}{\hbar c}DE^2\,\mathrm{P}\int\frac{\sigma_a(E')\mathrm{d}E'}{E'^2-E^2}$$

derived under the assumption of $E1$ transitions. The influence of Thomson (D) terms on the absorption curve is well within the experimental errors and was ignored.

The absorption, $\sigma_a(E)$, was deduced from the elastic scattering data in the following way. A smooth curve was drawn through the elastic scattering points. This curve peaked at about 24 MeV. When calculating $\sigma_a(E)$ at this energy, the integral in eq. (7) was negligible and the equation then simplifies to $\sigma_a^2 = 6\pi\lambda^2\sigma_s$. σ_a thus calculated at 24 MeV was 27 ± 6 mb. This value agrees within the total errors with the corresponding value in table 2, 30 mb.

The $\sigma_a(E)$ curve was then, as a guess, assumed to have the same shape as the elastic scattering curve. From the guessed $\sigma_a(E)$-curve, $\sigma_s(E)$ was calculated at several points. Agreement between the calculated and the experimental curves was then attained by trial and error. Only small corrections of the original guessed curve were necessary. The absorption curve thus determined was used to calculate the integrated cross section between 20 and 40 MeV. In this case the absorption curve was normalised (fig. 14) to give the same integrated cross section between 20 and 25 MeV as given in table 2. The value of σ_{int} from 20 to 40 MeV thus found was 290 MeV mb. If the Thomson scattering is considered, this figure will be slightly increased.

6. Discussion and Conclusions

6.1. THE 6.1 AND 6.3 MeV STATES IN O^{15} AND N^{15}

The most striking result of the present investigation is perhaps that the 6.1–6.3 MeV photons are produced in the whole region between 20 and 25 MeV with a high cross section, mean value about 5 mb, and that they are the only photons observed in the region 20 to 22.5 MeV. These facts together with the identification of the 6.1 and 6.3 MeV photons with gamma ray transitions from the states with the total angular momentum and parity assignments $\leqq 5/2^-$ in O^{15} and $3/2^-$ or $5/2^-$ in N^{15} favours strongly the belief that these states are single hole states [23]), $p_{1/2}^{-1}$.

6.2. THE GIANT RESONANCE IN O^{16}

Penfold and Spicer [4]) found in a study of the $O^{16}(\gamma, n)O^{15}$ reaction on the

basis of the radiative widths that the reaction below 19 MeV proceeds principally by $E2$ absorption and between 22 MeV and the upper limit of their investigation, 23 MeV, by E1 absorption. In the energy region between 20 and 21.5 MeV their results do not permit any conclusion. Their data indicate an increase in the cross section at about 20 MeV excitation energy. They conclude furthermore that all the absorption in the energy region studied takes place in levels with an energy spacing of the order of 10^5 eV.

In an investigation of the $O^{16}(\gamma, p)N^{15}$ reaction Stephens *et al.* [7]) report report weak peaks (a few millibarns) in the cross section for ground state transitions at 19.6 and 20.6 MeV. Between 21.8 and 22.5 MeV, *i.e.*, within the region of electric dipole photon absorption reported by Penfold and Spicer, they report a broad peak (about 12 mb) in the cross section. The results of these latter authors make it probable that this peak found in the study of the (γ, p) reaction is due to several unresolved levels.

The results of the present investigation indicate that in the energy region between about 20 MeV and 22.5 MeV, except for the ground state transitions reported by Stephens *et al.* [7], $p_{3/2}^{-1}$ states are the only ones produced. The cross section curve for production of the 6.1—6.3 MeV states in the daughter nuclei has a peak at about 24 MeV.

Furthermore the study of the gamma ray transitions in the daughter nuclei indicate a cross section for production of excited states other than the 6.1—6.3 MeV, rising from about 22.5 MeV, a peak at about 23.0 to 23.5 MeV, and then probably a small, fairly constant cross section between 25.0 and 30 MeV. The 7, 9, and 10 MeV photons occur as soon as they are energetically allowed.

A comparison between the total photon absorption curve and the cross section histogram from table 2 (fig. 14) indicates that from 20 to 25 MeV excitation of O^{16} the photodisintegration proceeds essentially to O^{15} and N^{15}, while above this energy, reactions like (γ, pn) and $(\gamma, 2p)$ (fig. 5) are probably predominant.

The integrated cross section for transitions to the excited states in the daughter nuclei obtained in this experiment under the made assumption, combined with the cross section for ground state transitions reported by Stephens *et al.* [7]), amounts to 0.11 MeV · barn. The integrated cross section between 20 and 40 MeV, as determined by the absorption curve in fig. 15, is 0.29 MeV · barn. This figure agrees within the errors with the value 0.34 MeV · barn calculated from the expression

$$\sigma_{\text{int}} = 0.015\, A\,(1+0.8x) \qquad (8)$$

derived by Levinger and Bethe [24]) for electric dipole excitation if $x = \frac{1}{2}$ is used as a measure of the strength of the neutron-proton exchange force. The value 0.29 MeV barn does not, however, include the E1 absorption

above 40 MeV, which from investigations of this [25]) and other [26]) elements is known not to be negligible. The results in the present investigation therefore indicate $\frac{1}{2} < x < 1$.

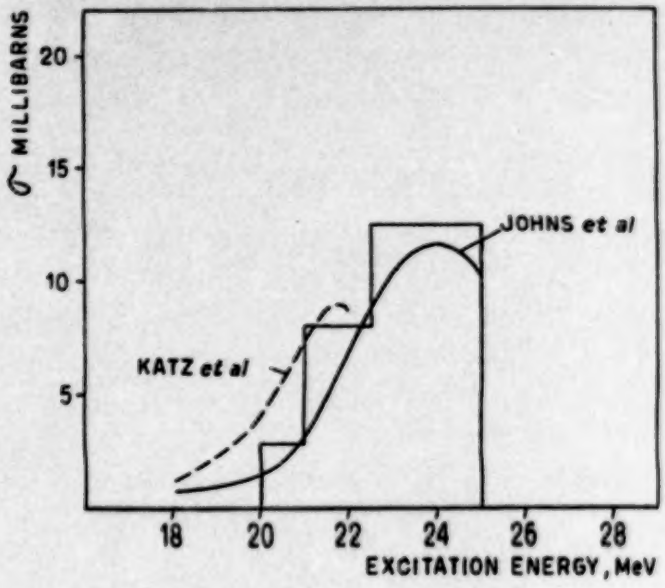

Fig. 15. The (γ, n) cross section histogram from Table 2, together with the experimental results of Katz *et al.* [2]) and Johns *et al.* [3]).

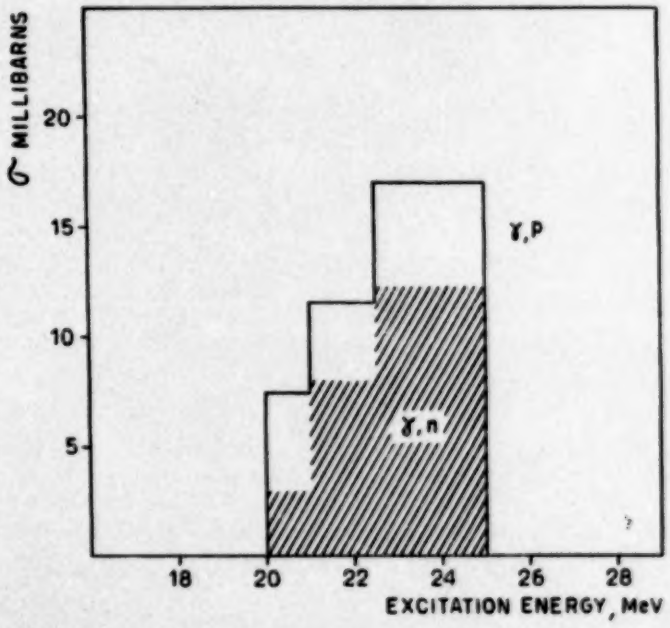

Fig. 16. The (γ, p) and (γ,n) cross section histograms from table 2.

The integrated cross section data for the (γ, n) reaction in table 2 were used to draw the cross section histogram in fig. 15 which agrees well with the results of Johns *et al.* [3]) and essentially also with those of Katz *et al.* [2])

The cross section histograms for both the (γ, p) and (γ, n) reactions are

plotted in fig. 16 from the data in table 2. The ratio between the integrated cross section curves is roughly 3 : 2. This higher value for the (γ, p) reaction originates from the difference in barrier penetration and from the fact that some of the transitions to levels with higher energies in O^{15} are energetically forbidden because of the difference in threshold for the (γ, p) and the (σ, n) reactions.

The experimental part of the present investigation as well as the preliminary treatment of the data were carried out during my stay as a guest worker at the Betatron Section of the National Bureau of Standards. I wish to express my sincere gratitude to the chief of that section, Dr. H. W. Koch, and to the staff members, especially to E. G. Fuller and E. Hayward for their collaboration in collecting the data and valuable suggestions. Thanks go to Drs. S. A. E. Johansson, Haru Morinaga, and N. Starfelt for valuable discussion and for commenting upon the manuscript. I also wish to acknowledge grants from Atomkommittén and Kungl. Fysiografiska Sällskapet, Sweden.

References

1) Montalbetti, Katz and Goldemberg, Phys. Rev. **91** (1953) 659
2) Katz, Haslam, Horsley, Cameron and Montalbetti, Phys. Rev. **95** (1954) 464
3) Johns, Horsley, Haslam and Quinton, Phys. Rev. **84** (1951) 856
4) A. S. Penfold and B. M. Spicer, Phys. Rev. **100** (1955) 1377
5) B. M. Spicer, Phys. Rev. **99** (1955) 33
6) S. A. E. Johansson and B. Forkman, Phys. Rev. **99** (1955) 1031
7) Stephens, Mann, Patton and Winhold, Phys. Rev. **98** (1955) 839
8) E. G. Fuller and E. Hayward, Phys. Rev. **101** (1956) 692
9) Bell, Davis and Bernstein, Rev. Sci. Instr. **26** (1955) 726
10) G. R. White, National Bureau of Standards Report 1003, May 1952, unpublished
11) E. Ajzenberg and T. Lauritsen, Rev. Mod. Phys. **27** (1955) 77
12) Bent, Bonner, McCrary, Ranken and Sippel, Phys. Rev. **99** (1955) 710
13) Kinsey, Bartholomew and Walker, Can. J. Phys. **29** (1951) 1
14) P. J. Campion and G. A. Bartholomew, Bull. Am. Phys. Soc. Ser. II, **1** (1956) 28 and private communication
15) L. C. Thompson, Phys. Rev. **96** (1954) 369
16) Johnson, Robinson and Moak, Phys. Rev. **85** (1952) 931
17) Bashkin, Carlson and Nelson, Phys. Rev. **99** (1955) 107
18) Fuller, Hayward and Svantesson, Bull. Am. Phys. Soc. Ser. II, **1** (1956) 21
19) National Bureau of Standards Handbook 55 (Febr. 1954) p. 33, unpublished
20) A. S. Penfold and J. E. Leiss, to be published
21) D. H. Wilkinson, Phil. Mag. **5** (1956) 379
22) Ref. [4]) and B. M. Spicer, private communication
23) D. R. Inglis, Rev. Mod. Phys. **25** (1953) 390
24) J. S. Levinger and H. A. Bethe, Phys. Rev. **78** (1950) 115
25) R. Sagane, Phys. Rev. **84** (1956) 587
26) L. W. Jones and K. M. Terwilliger, Phys. Rev. **91** (1953) 699

Nuclear Physics **3** (1957) 299—306; *North-Holland Publishing Co., Amsterdam*

ON THE INTERACTIONS OF FAST μ-MESONS

G. N. FOWLER †

Department of Theoretical Physics, University of Manchester

and

A. W. WOLFENDALE

Department of Physics, Durham Colleges in the University of Durham

Received 23 November 1956

Abstract: The experimental and theoretical aspects of the production of stars and showers by fast μ-mesons are reviewed. Difficulties are encountered in explaining the increase in cross section, with energy, for production of stars and showers with energy transfers of above about 400 MeV. These difficulties can be resolved if the Williams virtual photon method is assumed to be valid and if it is assumed that the photo-nuclear cross section has further resonances, above the π-meson resonance at about 300 MeV, corresponding to the production of heavy mesons or groups of π-mesons.

1. Introduction

Cosmic ray stars and showers produced in nuclear emulsions exposed underground were first attributed to the electromagnetic interactions of μ-mesons by George and Evans [1]). Later work with emulsions, Geiger counters and cloud chambers has apparently confirmed the existence and interpretation of these events. These authors have accounted for the events by Williams' procedure [2]) in which the meson is replaced by an equivalent beam of photons: this photon flux, when multiplied by the observed photo-nuclear cross section gives the nuclear interaction cross section of the μ-meson. Reasonable agreement is found between the observed and expected cross sections. However, since the behaviour of real photons has only been investigated up to the comparatively low energy of about 500 MeV rather uncertain extrapolation is necessary to find the effective photo-nuclear cross section at higher energies. George [3]) has assumed that the photo-nuclear cross section for star production, found by Miller [4]), that is

$$10^{-28}\ \text{cm}^2/\text{nucleon at 300 MeV},$$

remains the same at higher photon energies.

Another feature of the interaction proposed by George concerns the dynamical relation between the momentum of the μ-meson, its deflection, and the energy of the resultant star. George has assumed that the interaction takes place with a single nucleon and that the energy is transferred as kinetic energy of the struck nucleon. From the energy of the star (estimated from the number of tracks) and the deflection of the primary he has

† Now at the Physics Department, University of Bristol.

determined the energy spectrum of the underground μ-mesons. This spectrum appears to be consistent with that expected from an extrapolation of the accurately known sea-level spectrum (see, for example, ref. [3])). The variation of star-production cross section with depth can be calculated if the photo-nuclear cross section and the underground spectrum are known. At depths down to about 1000 m.w.e. the energy spectrum can be represented by

$$N(E)\mathrm{d}E = \frac{2E_0^2}{(E+E_0)^3}\mathrm{d}E, \tag{1}$$

where E_0 is the ionisation loss down to the depth considered. If ε is the minimum energy transfer, α the fine structure constant and $\sigma_{h\nu}$ the photo-nuclear cross section (assumed constant) then the cross section for star production is, following George[3]),

$$\sigma_\mu = \frac{0.9\alpha}{\pi}\,\sigma_{h\nu}\left\{\log\frac{E_0}{\varepsilon}\right\}^2. \tag{2}$$

In the following we will discuss recent experimental results with particular reference to the variation with depth of the cross section and the dynamics of the interaction.

2. The Experimental Results

In order of increasing energy of interaction, in which ionising particles are produced, we have the production of single protons, stars and showers.

2.1. PHOTO-PROTON PRODUCTION

Kaneko [5]) has observed events, in nuclear emulsions exposed underground, in which single protons are produced with a cross section of $(1.0\pm0.5)\times10^{-30}$ cm^2/nucleon. This value is not far from the theoretical value, 2.4×10^{-30} cm^2/nucleon, calculated on the assumption that the protons are produced by the equivalent beam of photons interacting through the 'giant-dipole' nuclear moment (energy transfer $\approx$ 20 MeV).

2.2. STAR PRODUCTION

Most of the evidence on star production comes from studies with nuclear emulsions. Stars having more than 3 prongs can be seen with high efficiency under the low magnification necessary for a fast scanning rate, and the cross sections for star production usually refer to stars having $\geqq 3$ prongs.

The variation, with depth, of the cross section for star production found by various workers is shown in fig. 1. The term star includes showers, i.e. events where secondary particles at near minimum ionisation are produced. Also shown is the expected variation according to equation (2) assuming a constant photo-nuclear cross section of 1.0×10^{-28} cm^2/nucleon and $\varepsilon = 150$ MeV.

2.3. SHOWER PRODUCTION

Events in which shower particles are produced have been investigated by emulsion, Geiger counter and cloud chamber techniques. Since the cross section for shower production is very low ($\approx 10^{-30}$ cm^2/nucleon) most of

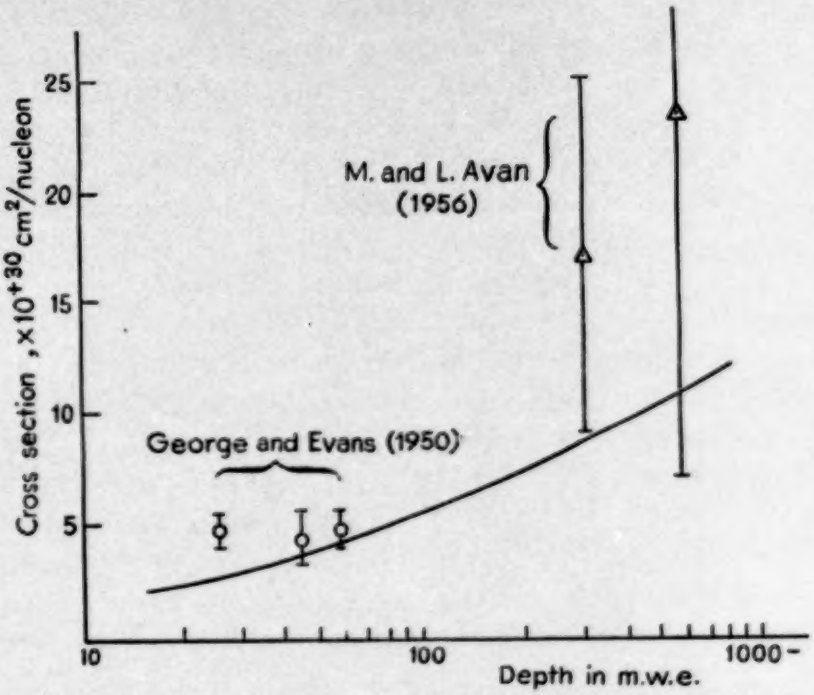

Fig. 1. Variation of cross section for star production with depth.

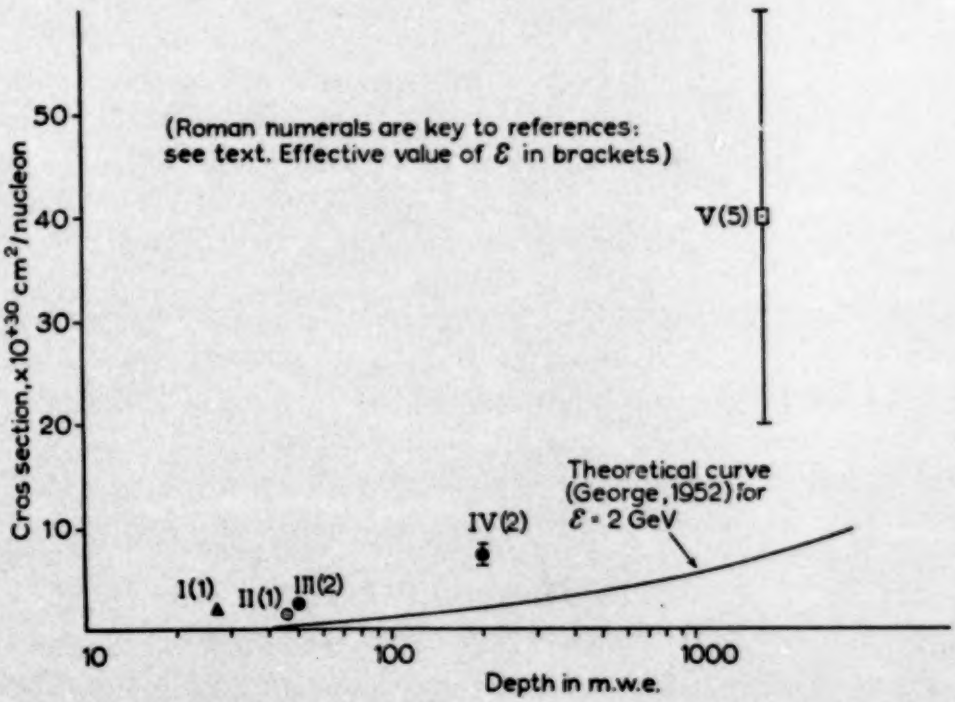

Fig. 2. Variation of cross section for shower production with depth.

the evidence comes from counter experiments. Figure 2 shows the experimental results for the variation of the cross section with depth. The diversity of techniques used has meant that the minimum shower energy differs for the various experiments: the minimum energies are indicated in the figure. These experiments will be considered in some detail. Point (I) gives the cross section found by Braddick and Leontic [6]) at a depth of 26 m.w.e. using a multiplate cloud chamber. The showers were produced either in the plates inside the chamber or in a lead absorber immediately above the chamber; in this way it was ensured that the shower particles were not electrons. The emulsion experiment of George and Evans [7]) gives the cross section denoted by (II). This is a mean value plotted at the mean of three relatively close depths. Points III and IV are for counter hodoscope experiments performed by Argan *et al.* [8]) at 50 and 200 m.w.e. On account of the difficulty in interpreting the counter records and the presence of a background of events due to the penetration of the counter array by electron showers, there is some doubt about the accuracy of these points. Point V gives the cross section found by Barrett *et al.* [9]) using a counter hodoscope array. Here the authors are confident that the events accepted as penetrating showers do not contain any appreciable fraction of electron showers. The cross section shown is a lower limit and the large error is due almost entirely to uncertainties in the effects of geometry and the lack of knowledge of the range of the secondaires.

Also plotted in fig. 2 is the expected variation (equation (2)) for a minimum shower energy, ε, of 2 GeV. Since ε enters only in the logarithm term the theoretical curve shown permits a rough comparison to be made between theory and experiment. It is evident that there is an increase in cross section with depth for both stars and showers of smaller magnitude than predicted.

With regard to the nature of the secondary particles, George and Evans[7]) and M. and L. Avan (private communication) have shown from scattering and minimum range measurements in the emulsion that some, at least, of the secondary particles are light mesons.

Barron *et al.* (to be published) have similarly identified light mesons — presumably π-mesons, — emerging from showers and have observed 2 cases in which the secondary particles produce further nuclear interactions in the emulsion. M. and L. Avan have also identified a K-meson among the secondaries of a shower and another K-meson entering the emulsion from the surrounding lead shield.

3. The Theoretical Aspect

If it is assumed that the interpretation of underground stars and showers given above is correct then obviously measurements on μ-mesons afford a good opportunity for examining electromagnetic effects (e.g. photo-

nuclear interactions) in nuclei at energies which are much greater than those available with more conventional methods. In principle differential cross sections can be measured for stars of different energies but in practice the number of stars found at any one depth is so small that integral cross sections only have any significance. A study of the variation of photo-nuclear cross section with photon energy is, therefore, complicated. If the experimental values of σ_μ, E_0 and ε are inserted in equation (2) and $\sigma_{h\nu}$ determined, it is found that $\sigma_{h\nu}$ is not in fact constant but increases with

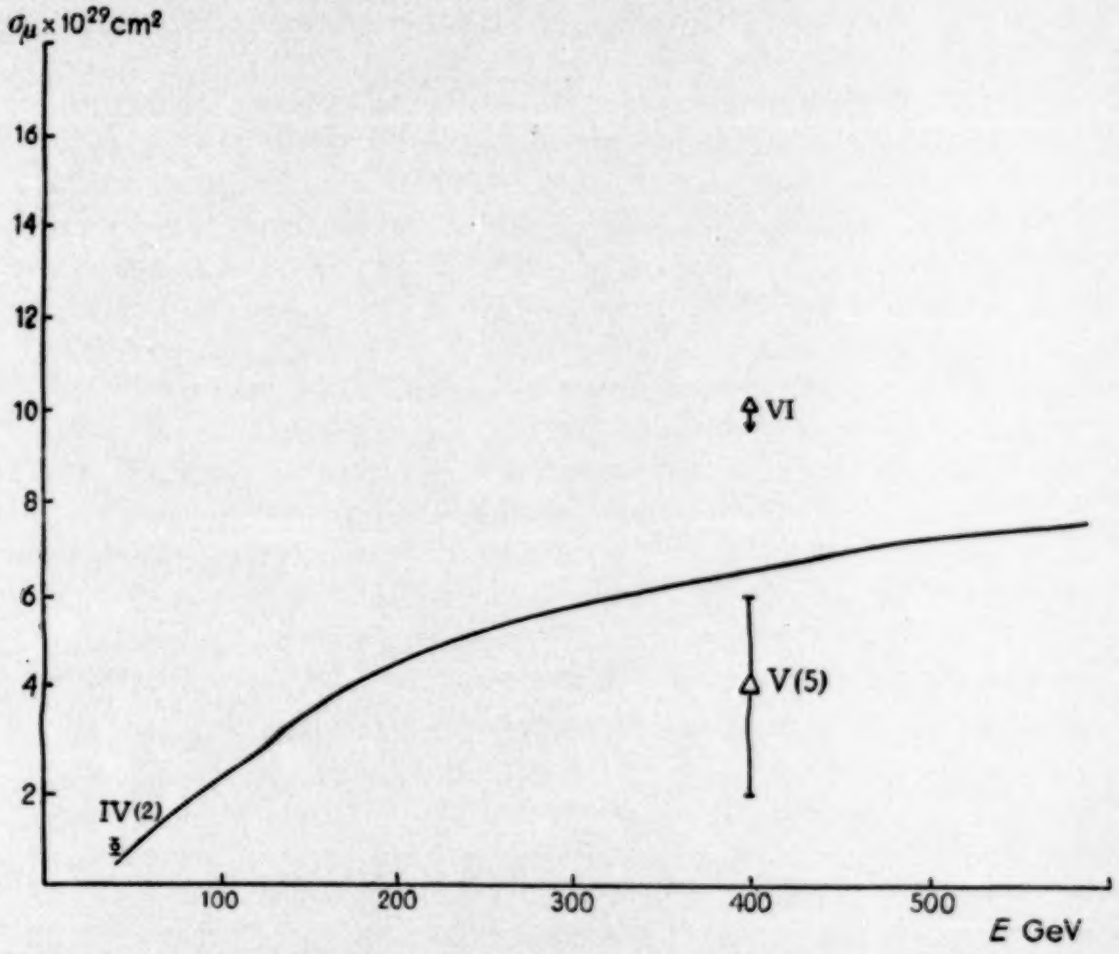

Fig. 3. Variation of theoretical cross section for shower production with energy (see text). Roman numerals are key to references: see text. Effective value of ε in GeV in brackets.

E_0 (for example Barrett *et al.* find $\approx 10^{-27}$ cm²/nucleon). An alternative method of investigating the variation of $\sigma_{h\nu}$ with energy is to study the range-energy relation for fast μ-mesons. This has been done by Rodgers *et al.* (to be published) where a comparison has been made of the sea-level μ-meson spectrum and the depth-intensity curve. These authors give a graph showing the dependence of $\sigma_{h\nu}$ on photon energy, $h\nu$, in the region $25 < h\nu < 300$ GeV. This is derived using the Williams method and in view of the experimental errors is to be regarded as having qualitative

significance only. From this curve, again using the Williams method, a qualitative result for the relation between σ_μ and E can be derived. This is shown in fig. 3 with $\varepsilon = 5$ GeV; the initial slope is much steeper than that predicted by assuming $\sigma_{h\nu}$ constant, and the slope at higher energies is substantially less, arising from a peak in the photo-nuclear cross section in the region of $h\nu = 50$ GeV. The values of σ_μ found by Argan *et al.* and Barrett *et al.* are shown in fig. 3, plotted at the mean energy corresponding to each depth, together with an upper limit found by the latter authors (point IV). It is apparent that the variation of σ_μ with energy, found from the underground shower measurements, is not inconsistent with that found by Rodgers *et al.*

It is necessary now to examine the basis of the theory applied to the underground interactions and, in particular, to decide whether the approximations underlying the Williams method are valid in these conditions. This question has been discussed by one of the authors [10]) and again by George [11]). In the first of these papers it is assumed that the energy is transferred as kinetic energy to a single nucleon regarded as free (see § 1) with production of a meson in a subsequent nucleon-nucleon collision. The result of this analysis is that it is not legitimate to apply the Williams' method to a process of this kind and that the theoretical cross section for star production by μ-mesons through an electromagnetic process should be an order of magnitude smaller than is observed experimentally. The essential point is that for the process described above the dimensions of the perturbed system are those of the nucleus so that, for an energy transfer $W > 150$ MeV, $qR/h \gg 1$, where q is the corresponding momentum transfer (assuming conservation of energy and momentum with a single nucleon) and R is the nuclear radius. In these circumstances the theoretical result should be much smaller than that given by the Williams method. However, the experiments of Panofsky *et al.* [12, 13]) on π-meson production by 600 MeV electrons on protons are very well interpreted by means of the Williams method, taking an individual nucleon as the perturbed system, i.e. assuming that the meson is produced in some kind of resonant process in the collision with a single nucleon. This is the point of view adopted by George [3, 11]), although it is inconsistent with an elastic collision between the meson and nucleon. The dimensions of the perturbed system, the individual nucleon, may be determined from the arguments of Watson *et al.* [14]) who find that the average distance from the centre of a proton at which the π-meson is produced by a photon is $\hbar/2m_\pi c$. The dimensions may also be found from the measurements of McAllister and Hofstadter [15]) who find for the proton radius $r_0 \approx 0.7 \times 10^{-13}$ cm, a value which is consistent with the estimate of Watson *et al.*

The Williams method in its original form is then applicable over a greater range of energy and momentum transfers. If p, p' are the momenta of the incident and final meson and q and W the momentum and energy transfers then for small scattering angles and relativistic particles

$$q^2 = (p-p')^2+p'p\theta^2,$$
$$W/c = p-p'.$$

Thus $q_{\min} = W/c$ so that with the above estimate of the nucleon dimensions we find that now the theoretical cross section for stars with $W \gg 400$ MeV should be considerably less than that predicted by the Williams method. In fact for a 10 GeV incident μ-meson taking $\hbar q_{\min}/2m_\pi c = 3\hbar$ ($W = 1$ GeV) the cross section is reduced by an order of magnitude. With regard to the experiments of Panofsky referred to above it is in fact found that the meson production occurs predominantly for small θ, i.e. $q \approx q_{\min}$, and the values W observed in this experiment are ≈ 250 MeV, for which $\hbar q_{\min}/2m_\pi c \approx \hbar$, so that significant deviations from the Williams result would not be expected.

Thus the use of the Williams method for energy transfers of the order of 1 GeV and beyond implies that higher energy resonances presumably involving heavy mesons and hyperons come into play and this is consistent with the apparent increase in the photo-nuclear cross section.

4. Conclusions

For low μ-meson energies, < 10 GeV, the production of protons by the electromagnetic field of the incident meson interacting with the nuclear 'giant' dipole seems to rest on a sound foundation. Here the energy transfer is $\lesssim 20$ MeV.

For high μ-meson energies, $\gtrsim 10$ GeV, the stars with energies $\lesssim 500$ MeV can be interpreted by means of the Williams method using the observed photo-nuclear cross section.

For stars (and showers) with energies $\gtrsim 500$ MeV it is apparent that the Williams method applied to single π-meson production is not valid. Experiments appear to indicate one or more further resonances in the photo-nuclear cross section; the production of hyperons, for example, in such resonances would mean a smaller perturbed system and hence an extension of the validity of the Williams method. It is important to note that even at a depth of 50 m.w.e., 90 % of the energy released in star production arises from energy transfers greater than about 400 MeV. Thus even here the effects of the higher resonances should be important.

In conclusion it can be remarked that there is wide scope for further measurements, particularly of the cross sections for star production at great depths and for a detailed study of the masses of the particles produced in the interactions.

The authors wish to thank Professors L. Rosenfeld and G. D. Rochester for helpful discussions and for reading the manuscript. A. L. Rodgers has assisted the authors considerably by making available his results and calculations on the sea-level spectrum and the intensity-depth relation, and they are particularly grateful to him.

Note added in proof: A recent communication from the Osaka group (T. Kitamura and M. Oda [16])) is relevant to the conclusions of this paper. These authors assume that the nuclear interaction of μ-mesons is similar to that of the nucleonic component and go on to show that a large fraction of the underground events should be due to π-mesons. They predict, for example, that about 40 % of the interactions at 32 m.w.e. with energy transfers above 1GeV are due to π-mesons, and that this fraction increases at lower energy transfers. This result is, however, inconsistent with the observations of George and Evans [7]), who show that the number of π-mesons of sufficient energy to produce characteristic stars is much smaller than the total number of stars. It is probable that the assumption, mentioned above, is responsible for the overestimate of Kitamura and Oda.

References

1) E. P. George and J. Evans, Proc. Phys. Soc. A **63** (1950) 1248
2) E. J. Williams, Mat. Fys. Medd. Dan. Vid. Selsk **13** (1935) no. 4
3) E. P. George, Progress in Cosmic Ray Physics Vol. I (North Holland Publ. Co., Amsterdam, 1952)
4) R. D. Miller, Phys. Rev. **82** (1951) 260
5) M. Kaneko, J. Phys. Soc. Japan **10** (1955) 600
6) H. J. J. Braddick and B. Leontic, Phil. Mag. **45** (1954) 1287
7) E. P. George and J. Evans, Proc. Phys. Soc. A **68** (1955) 829
8) P. E. Argan, A. Gigli and S. Sciuti, Nuovo Cimento **11** (1954) 532
9) P. M. Barrett, L. M. Bollinger, G. Cocconi, Y. Eisenberg and K. Greisen, Rev. Mod. Phys. **24** (1952) 133
10) G. N. Fowler, Proc. Phys. Soc. A **68** (1955) 482
11) E. P. George, Proc. Phys. Soc. A **69** (1956) 428
12) W. K. H. Panofsky, C. M. Newton and G. B. Yodh, Phys. Rev. **98** (1955) 751
13) W. K. H. Panofsky, W. M. Woodward and G. B. Yodh, Phys. Rev. **102** (1956) 1392
14) K. M. Watson, J. C. Keck, A. V. Tollestrup and R. L. Walker, Phys. Rev. **101** (1956) 1159
15) R. W. McAllister and R. Hofstadter, Phys. Rev. **102** (1956) 851
16) T. Kitamura and M. Oda, Prog. Th. Phys. **16** (1956) 252

Nuclear Physics **3** (1957) 307—313; *North-Holland Publishing Co., Amsterdam*

ETUDE DES ELECTRONS AUGER-K EMIS PAR LE ZINC 65

J. B. BELLICARD et A. MOUSSA

Institut de Physique Atomique, Faculté des Sciences de Lyon

et S. K. HAYNES

Laboratoire de l'Aimant Permanent, C.N.R.S., Bellevue †

Reçu le 10 Novembre 1956

Abstract: Using a double focusing magnetic spectrometer with ironless coils, the energies and relative intensities of the groups of Auger K lines of ^{65}Cu resulting from the decay of ^{65}Zn have been determined.

1. Introduction

Le ^{65}Zn se désintègre principalement par capture d'électrons, la conversion interne d'un quantum γ de 1.11 MeV produit un supplément de vacances K, en proportion d'ailleurs très faible. Le réarrangement des couches électroniques du ^{65}Cu ainsi formé s'accompagne de l'émission d'électrons Auger-K.

Le ^{65}Zn a déjà été étudié par l'un d'entre nous [1]), l'étude présente a eu pour but de préciser la structure des groupes d'électrons Auger-K au moyen du spectromètre à double focalisation et grand pouvoir séparateur installé à l'Institut de Physique Atomique de Lyon [2]).

2. Préparation des Sources

Le ^{65}Zn employé a été préparé à Oak Ridge par la réaction ^{65}Cu (d, 2n) ^{65}Zn, l'activité spécifique indiquée était 22 curies/g. Le chlorure de zinc a d'abord été déposé en solution dans une gouttière de tantale et séché à l'air, puis évaporé dans le vide pour être recueilli sur des films de formvar d'épaisseur 20 μg/cm^2, recouverts d'une couche d'aluminium de 5μg/cm^2. Les films de formvar ont été préparés suivant la technique décrite par Barreau, Léger, Moreau, et Prugne [3]). Ils étaient placés à une distance de l'évaporateur suffisante pour obtenir un dépôt sensiblement uniforme. L'emplacement de la source était délimité par un cache qui permettait d'obtenir des sources de longueur 20 mm et de largeur variant de 1 à 2 mm. Parmi les diverses sources préparées, trois ont été retenues:

Source	(a)	largeur	2 mm	activité	0.6 μC
,,	(b)	,,	2 mm	,,	1.8 μC
,,	(c)	,,	1 mm	,,	0.2 μC.

† Boursier Fulbright de l'Université Vanderbilt, Nashville, Tenn., U.S.A.

3. Réglages du Spectromètre

Les diaphragmes limitant le faisceau d'électrons ont été réglés de manière à assurer le meilleur compromis entre le pouvoir séparateur et le facteur de transmission pour une largeur de source donnée. Ainsi qu'on l'a montré dans un travail antérieur [2]), on peut alors adopter pour l'ouverture de la fente du compteur une largeur égale à celle de la source, et obtenir ainsi un pouvoir séparateur théorique égal à 0.325 S/R, où S est la largeur de la source et R le rayon de la trajectoire électronique moyenne (soit ici $R = 21$ cm.)

Pour les sources (a) et (b) le facteur de transmission est alors 6.2×10^{-3} et le pouvoir séparateur théorique $\Delta(B\varrho)/B\varrho = 3.1\times10^{-3}$. Pour la source (c) le facteur de transmission est 4.3×10^{-3} et le pouvoir séparateur théorique est 1.5×10^{-3}.

Le compteur G.M. du spectromètre était obturé par une fenêtre de formvar de 10 μg/cm^2, composée de trois films superposés, déposés sur une grille de lectromesh transparente à 50 %, et très légèrement aluminiée. Le cut-off de cette fenêtre, contrôlé au moyen du spectre continu du dépôt actif du thorium, se situait vers 1.2 keV, les corrections pour l'absorption de la fenêtre étaient donc négligeables. Le compteur était rempli d'un mélange à pressions partielles égales d'argon et d'éthanol, la pression totale étant 2 cm de mercure. La composante verticale du champ magnétique terrestre (normale au plan de la trajectoire électronique moyenne) a été compensée à moins de 1 % près au cours des mesures. La durée moyenne des comptages a été de 20 à 50 min par point pour la source (a) et de 60 à 120 min par point pour la source (c), le mouvement propre moyen étant de 25 à 30 c/min.

L'étalonnage en énergie a été fait au moyen des raies de conversion du thorium B+C. Les sources ont été préparées par évaporation dans le vide du dépôt actif, dans les mêmes conditions que pour les sources de ^{65}Zn. La reproductibilité de la géométrie du système permet de mesurer les produits $B\varrho$ à environ 5×10^{-4} près. Nous avons vérifié que le rapport $B\varrho/i$, où i est le courant dans les bobines, est le même pour les raies A, F, et I, les valeurs adoptées pour $B\varrho$ étant celles données par K. Siegbahn [4]).

4. Résultats Obtenus

La fig. 1 représente les groupes KLL, KLX, KXY, les deux premiers tels qu'ils ont été obtenus avec la source (a); le groupe KXY, très faible, a été compté avec la source (b) et reporté sur le graphique en le normalisant par rapport au groupe KLX. La forte activité spécifique de la substance et la faible activité totale déposée nous ont permis d'obtenir des sources assez minces pour que les trois groupes soient parfaitement séparés. Cependant la figure 2, qui représente le groupe KLL compté avec la source (b) montre déjà nettement un étalement vers les basses énergies, dû à l'épaisseur

plus grande de la source. On déduit des comptages effectués avec les sources (a) et (b) les intensités relatives suivantes:

$$KLL/KLX/KXY = 1.00/0.30\pm0.02/0.017\pm0.004.$$

Nous avons essayé, en utilisant la source (c), de séparer les six raies qui composent le groupe KLL. La figure 3 montre le résultat des comptages, l'erreur statistique est assez grande, malgré la durée des comptages, la cadence au sommet du groupe ne dépassant pas 15 c/min. Les raies ne sont pas séparées, il faudrait pour cela, soit une activité spécifique plus grande, soit un spectromètre de plus grandes dimensions permettant d'employer des sources de plus grande surface. Nous avons pu cependant déduire des graphiques 1 à 3 les intensités relatives des trois sous-groupes:

$$KL_IL_I/KL_IL_{II}+KL_IL_{III}/KL_{II}L_{II}+KL_{II}L_{III}+KL_{III}L_{III}$$
$$= 0.11\pm0.01/0.31\pm0.02/1.00.$$

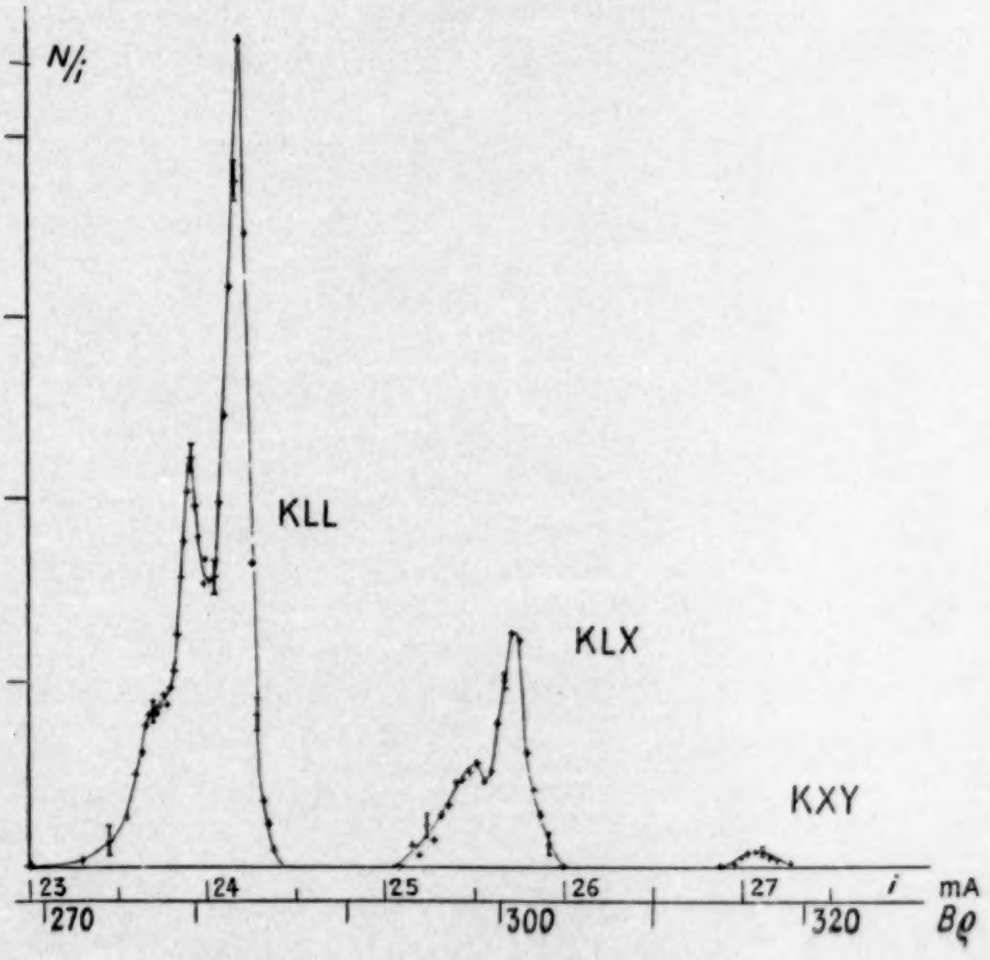

Fig. 1

Ces valeurs sont comparées dans le tableau I à celles obtenues expérimentalement par divers auteurs pour quelques valeurs de Z.

Nous avons déterminé d'autre part les énergies correspondant aux sous-groupes KLL, portées dans le tableau II.

On peut en déduire une estimation de l'énergie de liaison des électrons L dans l'atome de cuivre lorsqu'un électron L est manquant. On sait en effet que l'énergie de la raie Auger KL_mL_n peut s'écrire

$$E = E(K)_Z - E(L_m)_Z - E'(L_n)_Z;$$

$E(K)_Z$ et $E(L_m)_Z$ désignent les énergies de liaison des électrons K et L_m

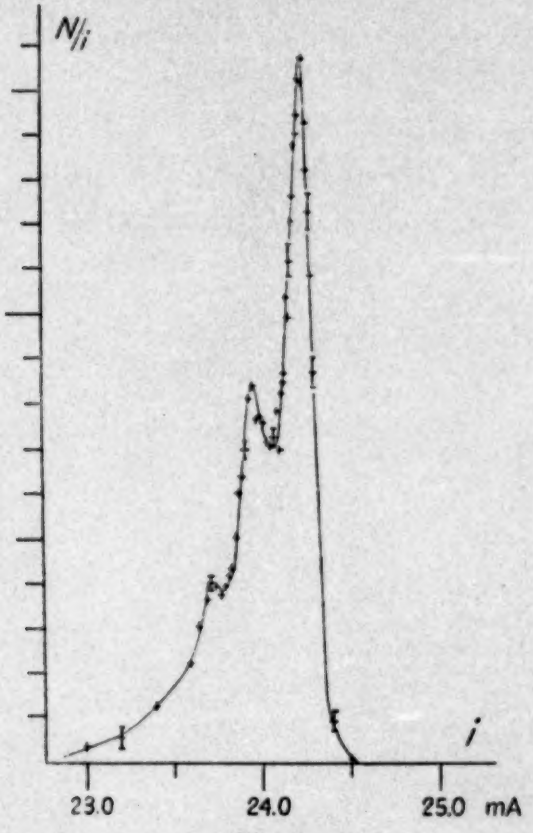

Fig. 2

TABLEAU I

Z	84	47	29	26
référence	[5])	[6])	présent travail	[7])
$KL_{II}L_{II} + KL_{II}L_{III} + KL_{III}L_{III}$	1.00	1.00	1.00	1.00
$KL_IL_{II} + KL_IL_{III}$	0.95	0.47	0.31	0.33
KL_IL_I	0.39	0.18	0.11	0.15

dans l'atome neutre de numéro atomique Z, et $E'(L_n)_Z$ l'énergie de liaison d'un électron L_n lorsqu'un électron est manquant en L_m. Comme Bergström

et Hill [8]), l'ont proposé, on peut définir un incrément de charge nucléaire ΔZ tel que

$$E'(L_n)_Z = E(L_n)_{Z+\Delta Z}$$

en admettant une variation linéaire de E avec Z, entre Z et $Z+1$. Le tableau II donne les énergies des raies Auger calculées par la formule ci-

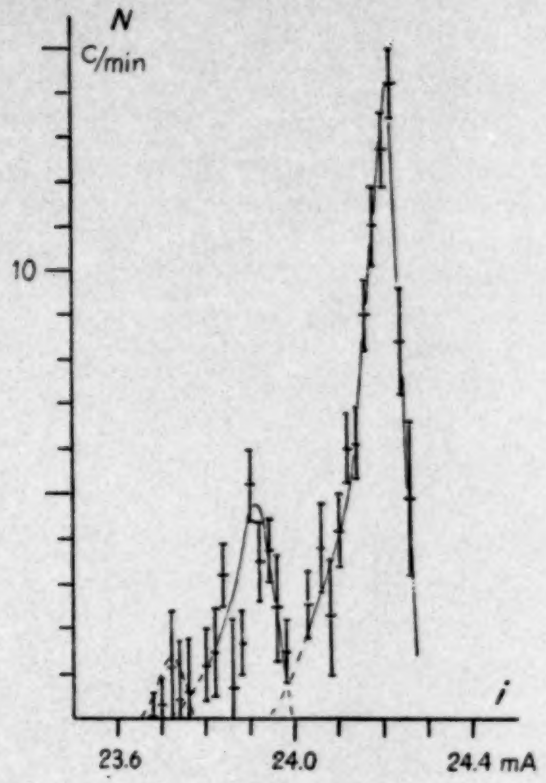

Fig. 3

TABLEAU II

Transition	Energie théorique (eV)		Energie expérimentale (eV)	ΔZ (exp)
	$\Delta Z = 0$	$\Delta Z = 1$		
$KL_I\ L_I$	6782	6682	6735	$\Delta Z(L_I) = 0.5$
$KL_I\ L_{II}$	6928	6835	6845	$\Delta Z(L_{II}) = 1$
$KL_I\ L_{III}$	6947	6858		$\Delta Z(L_{III}) = 1$
$KL_{II}\ L_{II}$	7074	6981	7015	
$KL_{II}\ L_{III}$	7093	7004		
$KL_{III}\ L_{III}$	7112	7023		

dessus, dans les deux hypothèses $\Delta Z = 0$ et $\Delta Z = 1$. On voit qu'on peut estimer $\Delta Z = 0.5$ pour L_I et $\Delta Z = 1$ pour L_{II} et L_{III}. La précision est assez faible puisque les raies ne sont pas séparées, cependant les valeurs

obtenues sont assez satisfaisantes si on les compare à celles données par divers auteurs pour des éléments plus lourds [9]).

Le groupe KLX est beaucoup plus complexe que le groupe KLL et donc encore plus difficile à résoudre en raies, cependant en se basant sur les positions théoriques de celles-ci on peut donner une idée de sa structure. On pourra ainsi comparer les intensités relatives à celles calculées par Pincherle [10]). On remarque deux sous-groupes: le premier ($B\varrho = 298.2$) correspond aux raies $KL_IM_{I\,à\,V}$ et KL_IN_I, le second ($B\varrho = 301.3$), nettement plus intense correspond aux raies $KL_{II}M_{I\,à\,V}$, $KL_{II}N_I$, $KL_{III}M_{I\,à\,V}$, $KL_{III}N_I$. Le tableau III permet de comparer les valeurs théoriques et expérimentales des énergies et intensités de ces transitions. Pour le calcul des énergies on a employé la formule rappelée plus haut et on a pris $\Delta Z = 1$ pour les couches M et N.

TABLEAU III

Transition	Energie (eV)		Intensité théorique (Pincherle)		Rapport expérimental d'intensité
	théorique	expér.le		rapport	
$KL_I\,M_I$	7745	7760	0.260	0.245 $\left(=\frac{0.851}{3.475}\right)$	0.54 ± 0.08
$KL_I\,M_{II,III}$	7791		0.520 (0.851)		
$KL_I\,M_{IV,V}$	7870		0.046		
$KL_I\,N_I$	7882		0.025		
$KL_{II,III}\,M_I$	7900	7925	0.375	1.00	1.00
$KL_{II,III}\,M_{II,III}$	7946		2.321 (3.475)		
$KL_{II,III}\,M_{IV,V}$	8025		0.752		
$KL_{II,III}\,N_I$	8037		0.027		

En ce qui concerne les énergies l'accord est assez satisfaisant, dans chaque sous-groupe, avec l'énergie moyenne des composantes les plus intenses prévues par Pincherle. Les raies n'étant pas séparées il existe une incertitude sur le point de référence à choisir sur le profil pour calculer l'énergie. Les sous-groupes étant plus étalés que dans le cas du groupe KLL, la précision est moins bonne et on peut estimer l'énergie connue à 15 ou 20 eV près. D'ailleurs la forme même des deux sous-groupes est en assez bon accord qualitatif avec les prévisions théoriques: le sous-groupe KL_IM présente un renforcement assez net du côté des faibles énergies, le sous-groupe $KL_{II,III}M$ présente au contraire un renforcement très net du côté des grandes énergies. Mais l'accord n'est pas satisfaisant au point de vue quantitatif et le rapport $KL_IM/KL_{II,III}M$ est trouvé nettement plus grand que la prévision théorique.

Il semblerait à priori que les calculs de Pincherle doivent être plus exacts pour les valeurs de Z voisines de 30 que pour les valeurs plus élevées. Cependant ils se trouvent en désaccord quantitatif avec nos mesures sur trois points, dont le premier a déjà été mis en évidence par les mesures d'autres auteurs [11]):

a) rapports KLL/KLX/KXY;

b) rapport $KL_IL_I/KL_IL_{II}+KL_IL_{III}$: valeur expérimentale 1/2.8 à comparer à la valeur théorique 1/3.52;

c) rapport $KL_IX/KL_{II,III}X$: valeur expérimentale 0.54 à comparer à la valeur théorique 0.245.

On peut en conclure que l'emploi de fonctions d'onde qui ne tiennent pas compte de l'effet d'écran ne permet pas de calculer avec précision les rapports d'intensité des diverses transitions Auger, même pour des éléments assez légers.

Nous remercions vivement le Dr S. Rosenblum qui a accueilli l'un de nous dans le laboratoire de l'Aimant Permanent à Bellevue, et a mis à notre disposition les moyens de préparation des sources. L'un de nous (J.B.B.) a bénéficié, pendant ce travail, d'une allocation du Centre National de la Recherche Scientifique, qui a également subventionné la construction du spectromètre.

Bibliographie

1) J. F. Perkins et S. K. Haynes, Phys. Rev. **92** (1953) 687
2) A. Moussa et J. B. Bellicard, J. Phys. Radium **15** (1954) 85A
3) P. Barreau, P. Léger, J. Moreau et P. Prugne, J. Phys. Radium **15** (1954) 4A
4) K. Siegbahn, Beta and Gamma-ray Spectroscopy (North Holland Publ. Company, Amsterdam, 1955) p. 920
5) Réf. [4]), p. 631
6) F. A. Johnson et J. S. Foster, Can. J. of Phys. **31** (1953) 469
7) J. B. Bellicard et A. Moussa, Comptes Rendus **241** (1955) 1202
8) I. Bergström et R. D. Hill, Ark. f. Fys. **8** no. 2 (1954) 21
9) Réf. [4]), p. 627
10) L. Pincherle, Nuovo Cimento **12** (1935) 81
11) Réf. [4]), p. 633

Nuclear Physics 3 (1957) 314—335; *North-Holland Publishing Co., Amsterdam*

STUDIES IN THE α-PARTICLE MODEL OF NUCLEI

IV. The Polarisation Forces between α-Clusters in Nuclei

A. HERZENBERG and A. S. ROBERTS †

Department of theoretical physics, University of Manchester

Received 11 October 1956

Abstract: The polarisation forces between α-particles are calculated for central forces between nucleons. There are two distinct possibilities to consider. The first is that the nuclear potential does not contain a direct part, when the polarisation energy is the only source of an attraction between α-particles. The Rosenfeld mixture is treated as an example of such a potential, and it is shown that the polarisation energy due to this potential is too small to account for the attraction required by the α-particle model. The second possibility to consider is that the nuclear potential does contain a direct part, which is assumed to be attractive, when there is a direct attraction between α-particles (analogous to the attraction between oppositely charged ions) which the polarisation forces supplement. The Serber potential is treated as an example of a potential with a direct part, and it is shown that the polarisation forces due to this potential cannot play more than a minor role in the attraction between α-particles; however, the magnitude of the polarisation energy is not negligible, and is of the order of the α-α binding energy per pair of nearest neighbours in the α-nuclei.

The distortion of α-particles to which polarisation gives rise may be interpreted as a tendency for the α-particles to dissolve. The probability of solution is estimated, and is shown to be small for $A \leqq 40$ even if polarisation does provide most of the attraction between α-particles, perhaps through the action of tensor forces.

1. Introduction

One of the basic needs of the α-particle model of nuclei is an attractive force between α-particles which acts when they do not overlap [1]). One way in which such a force can arise is through polarisation. Polarisation forces between α-particles have been discussed qualitatively by Heisenberg [2]) and Margenau [3]). The purpose of this paper is to treat them quantitatively.

Two polarisation processes are possible. The first exists if there is a direct tail in the nuclear potential, i.e. a tail independent of exchange operators. Such a tail gives rise to a field of force extending outside an α-particle; if two α-particles come within range of one another's field of force, then they will be distorted from being spherically symmetric in such a way as to minimise the energy. The energy is therefore lower than it would be in the absence of the polarisation, so that the latter produces an attraction. A second polarisation process arises from the part of the nuclear potential which depends on the spins and isobaric spins. If two α-particles approach one another, then

† Now at British Rayon Research Institute, Manchester.

their internal motions become correlated in such a way that nucleons whose spins and charges make them attract come closer than nucleons whose spins and charges make them repel. This correlation of the motions also leads to an attraction. The process is to some extent analogous to that underlying the Van der Waals forces between atoms.

It can be shown [4]) that if the overlap between α-particles is small enough for the exchange of nucleons between them to be negligible, then the energy associated with polarisation, which we shall denote by V_{POL}, is a static potential, i.e. a function of the distance of separation of the mass centres of the α-particles. This result holds if the kinetic energy of relative motion is not more than about 5 MeV.

We shall calculate V_{POL} for two α-particles in §§ 2 and 3, and take up the case of more than two α-particles in § 4. The method of calculation used (see § 2) is almost identical with that used in the calculation of intermolecular Van der Waals forces (see, e.g., [5]), and leads to the result that V_{POL} consists of two terms of the form $\langle 0|(V_{\alpha\alpha}-\langle 0|V_{\alpha\alpha}|0\rangle)^2|0\rangle/\Delta E$, where $V_{\alpha\alpha}$ is the interaction potential between the nucleons constituting the two α-particles, and ΔE is a measure of the energy of excitation in the virtual excited states which polarisation engenders in the internal motions. The symbols $\langle 0|\ldots|0\rangle$ imply the calculation of the expectation value with respect to the ground state of the internal motion in such a way that the distance of separation of the mass centres is fixed. The two separate terms are related to the two polarisation processes; in the one term, $V_{\alpha\alpha}$ is the direct part of the nuclear potential, and in the other the part depending on the spins and isobaric spins.

To calculate the contribution to V_{POL} from the two processes, we have made calculations with nuclear potentials of two exchange types: the Rosenfeld mixture, which does not have a direct part and therefore gives only the correlation type of polarisation, and the Serber potential, which does have a direct part and gives rise to both kinds of polarisation. Only central potentials are treated in this paper.

In our choice of the spatial dependence of the nuclear potential, we have been guided by the form of the expression for the polarisation energy. The appearance of $V_{\alpha\alpha}^2$ must favour a long-tailed potential if the distance of separation is large enough. On the other hand, the numerator $\langle 0|(V_{\alpha\alpha}-\langle 0|V_{\alpha\alpha}|0\rangle)^2|0\rangle$ is the mean square fluctuation of $V_{\alpha\alpha}$, and this feature might favour a more abruptly varying, or short-tailed, potential. We have therefore made calculations with both a Gaussian and a Yukawa potential. The results of the calculation for two α-particles are given in § 3.

In § 4 we consider non-additive effects which arise when there are more than two α-particles. Such non-additive effects arise only if the nuclear potential has a direct part. If there are three α-particles in a row, then the distortion of the middle one by the one on the left changes its energy

of interaction with the one on the right. We shall calculate the magnitude of the resulting non-additive energy for three α-particles.

The results are discussed in § 5. We shall deal with, among other points, the following difficulty of the α-particle model. It was pointed out by Heisenberg [2]) that polarisation implies a tendency of the α-particles to dissolve; this implies a breakdown of the α-particle model. We shall show that even if the attraction between α-particles were wholly due to polarisation, then the probability of the α-particles not being in the ground states of their internal motions would be small in nuclei in which the α-particles have only a small number of neighbours.

2. Theory

2.1. METHOD

A formalism for the interaction of two α-clusters has been developed in a previous paper [4]). The wavefunction is written in the form

$$\Psi^{(2\alpha)} = \sum_{\mathrm{P}} (\pm)\Phi(1234,\ 5678;\ \mathbf{X})F(\mathbf{X}), \tag{2.1}$$

where 1, 2, . . . 8, denote the co-ordinates of the eight nucleons, and $\mathbf{X}$ is the vector separation of the mass centres of the groups (1234) and (5678). The function Φ represents the internal motion of two α-clusters containing respectively nucleons (1234) and (5678); as a consequence of their interaction, the clusters are distorted in a way depending on $\mathbf{X}$. F describes the relative motion of the two clusters. One obtains a wave equation for F by inserting the expression (2.1) into the variational principle equivalent to the Schrödinger equation, and varying F. If one takes Φ to be real (see below) and normalised over the internal co-ordinates of the two α-clusters, one is led to the following equation (see ref. [4]), equation (3.36) †),

$$-\frac{\hbar^2}{2\mu}\nabla_X{}^2 F(\mathbf{X}) + \Delta K(\mathbf{X})F(\mathbf{X}) + E_{\mathrm{int}}(\mathbf{X})F(\mathbf{X}) + (V_{\mathrm{X}}F)(\mathbf{X}) = E'F(\mathbf{X}), \tag{2.2}$$

where

(i) μ is the reduced mass of the two α-particles,

(ii)
$$\Delta K(\mathbf{X}) = \frac{\hbar^2}{2\mu}\int \mathrm{dv_{int}}\, \nabla_{\mathrm{X}}\Phi \cdot \nabla_{\mathrm{X}}\Phi \tag{2.3}$$

(the integration $\int \mathrm{dv_{int}}$ extends over all co-ordinates left when $\mathbf{X}$ is held constant; the notation $\int \mathrm{dv_{int}}$ will be used whenever we have to integrate over the internal co-ordinates of the α-clusters: if only one α-cluster is involved, then the mass centre is to be held fixed; if two α-clusters are involved, then the vector separating the two mass centres is to be held fixed. If we wish to integrate only over the spatial internal co-ordinates, we shall use the notation $\int \mathrm{dv}^{(\mathrm{S})}_{\mathrm{int}}$),

† The term $V_{\mathrm{X}}F$ was denoted by $\int \mathrm{d}\boldsymbol{\xi}\, P(\mathbf{X}, \boldsymbol{\xi})F(\boldsymbol{\xi})$ in ref. [4]).

(iii) $V_X F$ is a term coming from the exchange integrals which arise when expectation values are calculated with the anti-symmetrised function (2.1);

(iv) E' is the expectation value of the energy calculated with the wave function given in (2.1).

The term $E_{\text{int}}(\mathbf{X})$ in (2.2) is defined as

$$E_{\text{int}}(\mathbf{X}) = \int \mathrm{d}v_{\text{int}} \Phi(1234,\ 5678; \mathbf{X})\ (H_{\text{int}}+V_{\alpha\alpha})\Phi(1234,\ 5678;\ \mathbf{X}), \qquad (2.4a)$$

where H_{int} is the internal energy of the two sets of nucleons (1234, 5678), and $V_{\alpha\alpha}$ is the interaction potential between them; (see ref. [4]), eqs. (3.18), (3.21), (3.24)). To calculate $E_{\text{int}}(\mathbf{X})$, one needs the detailed form of Φ, which is determined as follows: we assume that the nucleon-exchange term $V_X F$ in (2.2) has the effect of a strong short range repulsion which prevents the α-clusters from overlapping (ref. [1])). Then it follows from (2.2) that the mutual attraction of the α-clusters which the α-particle model requires must come from $E_{\text{int}}(\mathbf{X})$; (we shall later see that ΔK is negligible). According to Rayleigh's principle, the expectation value E' is a minimum in the ground state, and to achieve this minimum, we shall adjust Φ so as to make $E_{\text{int}}(\mathbf{X})$ negative and numerically as large as possible. This condition is satisfied if $E_{\text{int}}(\mathbf{X})$ is the lowest eigenvalue of the equation

$$[H_{\text{int}}+V_{\alpha\alpha}]\Phi = E_{\text{int}}(\mathbf{X})\Phi, \qquad (2.4b)$$

subject to the condition that Φ be square integrable over the internal co-ordinates of the two α-clusters. $\mathbf{X}$ is to be held constant in the solution of (2.4b).

In § 3 of ref. [4]) it was assumed that Φ is real. This assumption was made in order to eliminate a velocity dependent term in V_{POL} and is justified if the force between two nucleons is central, i.e. if $V_t = 0$ in eq. (2.2) of ref.[1]), because then $(H_{\text{int}}+V_{\alpha\alpha})$ is real, and one can choose Φ to be real. (Note that the tensor operator $(\boldsymbol{\sigma}_i \cdot \hat{\mathbf{r}}_{ij} \ldots)$ in eq. (2.2) of ref. [1]) is not real.) The calculations presented here are confined to central forces.

To solve (2.4b) approximately, we shall calculate the expectation value of the operator on the left of (2.4b) with the wave function

$$\Phi = N[1+A(V_{\alpha\alpha}-\langle 0|V_{\alpha\alpha}|0\rangle)]\Psi_0^{(\alpha)}(1234)\ \Psi_0^{(\alpha)}(5678); \qquad (2.5)$$

here A is a parameter, $\Psi_0^{(\alpha)}(1234)$ is a normalised approximate form for the ground state wave function of an α-particle, and N is a normalisation constant so that $\int \mathrm{d}v_{\text{int}}\Phi^2 = 1$. The parameter A is to be adjusted so as to minimise the expectation value of E_{int}. The term $A(V_{\alpha\alpha}-\langle 0|V_{\alpha\alpha}|0\rangle)$ in (2.5) takes account of polarisation. The reason for the form of the trial function (2.5) is that in the ground state solution of (2.4b) the wave function is concentrated near the (negative) maxima of $(V_{\text{int}}+V_{\alpha\alpha})$ to an extent

limited only by the kinetic energy and the exclusion principle. ($V_{\rm int}$ is the internal potential energy of the two α-clusters.) The ground state eigenfunction of (2.4b) is therefore an "out-of-focus image" of the potential energy.

With the aid of (2.5) we obtain

$$E_{\rm int} \approx \frac{\langle \Phi|(H_{\rm int}+V_{\alpha\alpha})|\Phi\rangle}{\langle \Phi|\Phi\rangle} = 2E_0^{(1)}+V_{\rm D}(\mathbf{X})+V'_{\rm POL}(\mathbf{X}), \tag{2.6}$$

where

$$2E_0^{(1)} \equiv \langle 0|H_{\rm int}|0\rangle, \qquad V_{\rm D}(\mathbf{X}) \equiv \langle 0|V_{\alpha\alpha}|0\rangle, \tag{2.7}$$

and

$$V'_{\rm POL}(\mathbf{X}) = \frac{(\langle 0|V_{\alpha\alpha}^2|0\rangle - \langle 0|V_{\alpha\alpha}|0\rangle^2)(2A+A^2\Delta E)}{1+A^2\langle 0|V_{\alpha\alpha}^2|0\rangle}. \tag{2.8}$$

The notation $\langle 0|$ operator $|0\rangle$ signifies $\int dv_{\rm int}\, \Psi_0^{(\alpha)}\Psi_0^{(\alpha)}$ operator $\Psi_0^{(\alpha)}\Psi_0^{(\alpha)}$. ΔE is defined by

$$\begin{aligned} \Delta E &= (\Delta E)^{(0)}+(\Delta E)^{(1)}, \\ (\Delta E)^{(0)} &= \langle \text{exc}\,|H_{\rm int}|\,\text{exc}\rangle - \langle 0|H_{\rm int}|0\rangle, \\ (\Delta E)^{(1)} &= \langle \text{exc}\,|V_{\alpha\alpha}|\text{exc}\rangle - \langle 0|V_{\alpha\alpha}|0\rangle, \end{aligned} \tag{2.9}$$

where the notation $\langle \text{exc}\,|\,\text{operator}\,|\,\text{exc}\rangle$ signifies

$$\frac{\langle 0|(V_{\alpha\alpha}-\langle 0|V_{\alpha\alpha}|0\rangle)\ \text{operator}\ (V_{\alpha\alpha}-\langle 0|V_{\alpha\alpha}|0\rangle)|0\rangle}{\langle 0|(V_{\alpha\alpha}-\langle 0|V_{\alpha\alpha}|0\rangle)^2|0\rangle},$$

i.e. an average over the mixture of excited states produced when $V_{\alpha\alpha}$ operates on $\Psi_0^{(\alpha)}\Psi_0^{(\alpha)}$. In deriving (2.8), we have made the approximation of replacing $H_{\rm int}$ by $\langle 0|H_{\rm int}|0\rangle$ wherever it operates on $\Psi_0^{(\alpha)}\Psi_0^{(\alpha)}$. A may be assumed to be real because we shall deal only with central forces for which the Hamiltonian is real.

If we insert (2.6) into (2.2), then we obtain the wave function for the relative motion with the different types of force $V_{\rm D}$, $V_{\rm POL}$, $V_{\rm X}$ showing explicitly (if we write $V_{\rm POL}=V'_{\rm POL}+\Delta K$); it is in this form that the equation is discussed in ref. [1]). In the calculations presented here, we shall at first neglect ΔK, and therefore drop the prime on $V'_{\rm POL}$. We shall show in § 3 that ΔK is negligible.

The argument which led us to adjust Φ so as to minimise $E_{\rm int}(\mathbf{X})$ works only in the ground state. We next show that the resulting polarisation energy is correct also for excited states. An alternative approach to the interaction of α-particles is obtained if one replaces the repulsive nucleon-exchange operator $V_{\rm X}$ in (2.2) by a phenomenological repulsive potential (ref. [4]), § 4). The exchange of nucleons between the α-clusters can then be neglected and $V_{\alpha\alpha}$ can be treated as a perturbation. If one does this, one

obtains again an equation of the form (2.2), with $E_{\rm int}$ replaced by $V_{\rm D}+V_{\rm POL}+2E_0^{(1)}$. Provided that the kinetic energy of relative motion is not too high (say not more than a few MeV), the polarisation energy turns out to be a static potential and is therefore independent of the state of excitation. Therefore the ground state value of the polarisation energy can be used also in low-lying excited states. (The perturbation method does not lend itself to an actual calculation of $V_{\rm POL}$ because it gives a formula of the form familiar in second-order perturbation theory which requires the wave functions and excitation energies of all states of the α-particle.)

2.2. NUCLEAR POTENTIAL

We assume a static central two-body potential of the form given in the first line of eq. (2.2) of ref. [1]). The coefficients a are normalised as in eq. (2.4) of ref. [1]).

The principle guiding the choice of potential shape has been explained in the introduction. The following potentials should cover most possibilities:

Gaussian:

$$V(r_{ij}) = V_{\rm G} \exp(-\varkappa r_{ij}^2) \tag{2.10}$$

with

$$V_{\rm G} = 43.7 \text{ MeV}, \quad \varkappa^{-\frac{1}{2}} = 1.9\times 10^{-13} \text{ cm}, \quad q = 0.62,$$

or

$$V_{\rm G} = 72 \text{ MeV}, \quad \varkappa^{-\frac{1}{2}} = 1.49\times 10^{-13} \text{ cm}, \quad q = 0.62; \tag{2.11}$$

Yukawa:

$$V(r_{ij}) = V_{\rm Y} \exp(-r_{ij}/\lambda)/(r_{ij}/\lambda), \tag{2.12}$$

$$V_{\rm Y} = 51.0 \text{ MeV}, \quad \lambda = 1.37\times 10^{-13} \text{ cm}, \quad q = 0.65. \tag{2.13}$$

The figures for the Yukawa potential and the first set of figures for the Gaussian potential were taken from ref. [6]), p. 131. The second set of figures for the Gaussian were taken from Blatt and Jackson [7]), so as to fit the n–p spin triplet scattering length and effective range, and the spin singlet scattering length.

The following two types of exchange dependence are considered:

Rosenfeld mixture:

$$a_0 = a_\sigma = 0, \quad a_\tau = \tfrac{1}{4}(1-q), \quad a_{\sigma\tau} = \tfrac{1}{12}(1+3q); \tag{2.14a}$$

Serber potential:

$$a_0 = -\tfrac{3}{16}(1+q), \quad a_\sigma = \tfrac{1}{16}(-1+3q), \tag{2.14b}$$

$$a_\tau = \tfrac{1}{16}(3-q), \quad a_{\sigma\tau} = \tfrac{1}{16}(1+q).$$

The Rosenfeld mixture potential satisfies the conditions imposed by the requirement that nuclear binding energies and densities should saturate as the number of nucleons in a nucleus becomes indefinitely large [6]). The

Serber potential is being investigated as an example of a potential which does not satisfy these saturation conditions (because $a_0 < 0$).

2.3. FORMULAE

With a potential of the form given in § 2.2, the function $\Psi_0^{(\alpha)}$ must be an eigenfunction with eigenvalues zero of the operators of total mechanical intrinsic spin and isobaric spin of the α-particle.
We take

$$\Psi_0^{(\alpha)} = \varphi_0^{(\alpha)}(1234)D(1234), \tag{2.15}$$

where $\varphi_0^{(\alpha)}$ is a normalised symmetric function of the spatial co-ordinates, and D is a normalised Slater determinant whose rows are constructed from the four spin-and-charge states of a nucleon.

For $\varphi_0^{(\alpha)}$ we take

$$\varphi_0^{(\alpha)}(1234) = \left(\frac{\pi}{4\beta}\right)^{-9/4} \exp\left(-\tfrac{1}{2}\beta \sum_{\substack{i,j=1 \\ 1>j}}^{4} r_{ij}^2\right). \tag{2.16}$$

The parameter β is related to the root-mean-square radius of the α-particle by

$$\varrho_\alpha = \left\{\int \mathrm{d}v_{\mathrm{int}}\, \Psi_0^{(\alpha)}(1234)[\mathbf{r}_1 - \tfrac{1}{4}(\mathbf{r}_1+\mathbf{r}_2+\mathbf{r}_3+\mathbf{r}_4)]^2 \Psi_0^{(\alpha)}\right\}^{\frac{1}{2}} = \frac{3}{4\sqrt{(2\beta)}} \tag{2.17}$$

With (2.15) we find

$$\langle 0|V_{\alpha\alpha}|0\rangle = 16a_0 \int \mathrm{d}v_{\mathrm{int}}^{(\mathrm{S})} |\varphi_0^{(\alpha)}(1234)|^2 |\varphi_0^{(\alpha)}(5678)|^2, \tag{2.18}$$

the integration $\int \mathrm{d}v_{\mathrm{int}}^{(\mathrm{S})}$ being over the spatial internal co-ordinate of the two α-clusters only while the vector $\mathbf{X}$ separating the mass centres is held constant. The a_σ, a_τ, and $a_{\sigma\tau}$ terms in the nuclear potential do not contribute to (2.18) because we have

$$\langle D(1234)|(\boldsymbol{\sigma}_i,\ \boldsymbol{\tau}_i,\ \text{or}\ \boldsymbol{\sigma}_i\boldsymbol{\tau}_j)|D(1234)\rangle = 0, \qquad (i, j = 1, 2, 3, 4), \tag{2.19}$$

because of the different properties of the $\boldsymbol{\sigma}(\boldsymbol{\tau})$ operators and the spin-and-charge functions D for rotations in ordinary (isobaric spin) space. Also with (2.15) we find

$$\begin{aligned}
&\langle 0|V_{\alpha\alpha}^2|0\rangle \\
&= 16a_0^2 \int \mathrm{d}v_{\mathrm{int}}^{(\mathrm{S})} |\varphi_0^{(\alpha)}(1234)|^2 |\varphi_0^{(\alpha)}(5678)|^2 [V(r_{15})^2 + 6V(r_{15})V(r_{16}) + 9V(r_{15})V(r_{26})] \\
&+ 48(a_\sigma^2 + a_\tau^2 + 3a_{\sigma\tau}^2) \\
&\int \mathrm{d}v_{\mathrm{int}}^{(\mathrm{S})} |\varphi_0^{(\alpha)}(1234)|^2 |\varphi_0^{(\alpha)}(5678)|^2 [V(r_{15})^2 - 2V(r_{15})V(r_{16}) + V(r_{15})V(r_{26})].
\end{aligned} \tag{2.20}$$

In (2.20) there are no cross terms like, for example, $a_\sigma a_\tau$, because of (2.19).

With (2.10), (2.11), and (2.15), we get

$$\begin{aligned} E_0^{(1)} &= \tfrac{1}{2}\langle 0|H_{\rm int}|0\rangle \\ &= 9\frac{\hbar^2}{m}\beta - 3(1+q)\int \mathrm{d}v_{\rm int}^{(S)}\,|\varphi_0^{(\alpha)}(1234)|^2 V(r_{12}) \\ &= 9\frac{\hbar^2}{m}\beta - 3(1+q)V_G\left(1+\frac{\varkappa}{2\beta}\right)^{-3/2}, \end{aligned} \tag{2.21}$$

where the integration $\int \mathrm{d}v_{\rm int}^{(S)}$ is over the internal spatial co-ordinates of the α-particle containing nucleons (1234).

In calculating $\langle \mathrm{exc}\,|H_{\rm int}|\,\mathrm{exc}\rangle$ in (2.9), we use the approximation

$$\begin{aligned} \langle 0\,|\,\mathrm{operator}\cdot H_{\rm int}\,|\,0\rangle &= \langle 0\,|\,H_{\rm int}\cdot \mathrm{operator}\,|\,0\rangle \\ &\to \langle 0\,|\,\mathrm{operator}\,|\,0\rangle\cdot\langle 0\,|\,H_{\rm int}\,|\,0\rangle \end{aligned} \tag{2.22}$$

(this formula would be exact if $\Psi_0^{(\alpha)}$ were the exact ground state wave-function of an α-particle). $\langle \mathrm{exc}\,|H_{\rm int}|\,\mathrm{exc}\rangle$ is then expressible in terms of (2.18), (2.20), and (2.21), and the expression $\langle 0|V_{\alpha\alpha}H_{\rm int}V_{\alpha\alpha}|0\rangle$. If we write $H_{\rm int} = K_{\rm int}+V_{\rm int}$, where $K_{\rm int}$ and $V_{\rm int}$ are respectively the kinetic and potential internal energies, then $\langle 0|V_{\alpha\alpha}K_{\rm int}V_{\alpha\alpha}|0\rangle$ is just like (2.20) except that $K_{\rm int}$ appears between each pair of V's. The evaluation of $\langle 0|V_{\alpha\alpha}V_{\rm int}V_{\alpha\alpha}|0\rangle$ is straightforward but lengthy, and the formulae will not be given.

2.4. EVALUATION OF INTEGRALS

All spatial integrals, with the exception of those occurring in the kinetic energy, can be evaluated with the aid of the formula [8])

$$\begin{aligned} &\int\left(\prod_{i=1}^{n}\mathrm{d}\mathbf{x}_i\right)\exp\left(-\sum_{j,k=1}^{n}A_{jk}\mathbf{x}_j\cdot\mathbf{x}_k+\sum_{l=1}^{n}\boldsymbol{\beta}_l\cdot\mathbf{x}_l\right) \\ &= \pi^{\frac{3n}{2}}|A|^{-3/2}\exp\left[\tfrac{1}{4}\sum_{i,j=1}^{n}(A^{-1})_{ij}\boldsymbol{\beta}_i\cdot\boldsymbol{\beta}_j\right]; \end{aligned} \tag{2.23}$$

here the quantities A_{jk} are constants; $|A|$ is the determinant of the matrix A; A^{-1} is the matrix inverse of A, and the $\boldsymbol{\beta}_i$ are constant vectors. The integrations in (2.23) extend over all space for each of the $\mathbf{x}_i$.

The spatial integrals arising from the kinetic energy can all be expressed as derivatives of the result (2.23) with respect to the A_{jk} and the $\boldsymbol{\beta}_i$.

The work can be considerably simplified by applying linear orthogonal transformations to the vector variables of integration. In this way each of the 6×6 matrices occurring can be reduced to at worst a single 3×3 block on the diagonal, the rest of the matrix being diagonal.

2.5. ROSENFELD MIXTURE

An important feature of the potential (2.14a) is that $a_0 = 0$. As a consequence, we have $\langle 0|V_{\alpha\alpha}|0\rangle = 0$, (from (2.18)), and in $\langle 0|V_{\alpha\alpha}^2|0\rangle$ only the term $48(a_s^2+\ldots)$ remains ((2.20)). The polarisation mechanism now

leads only to a spin and charge dependent correlation of the motion of the nucleons in the different α-clusters.

We adjust the parameter A in (2.5) and (2.8) so as to make V_{POL} negative and numerically a maximum. As a first approximation, we replace the denominator in (2.8) by 1, when we obtain $A = -1/(\Delta E)_{\mathrm{R}}$. (We shall use the suffix R to denote that $(\Delta E)_{\mathrm{R}}$ refers to the Rosenfeld mixture.) To obtain a better approximation, we expand V_{POL} in powers of $V_{\alpha\alpha}/(\Delta E)_{\mathrm{R}}$, noting that $(\Delta E)_{\mathrm{R}}^{(1)}/(\Delta E)_{\mathrm{R}}^{(0)} = \mathrm{O}(V_{\alpha\alpha}/\Delta E_{\mathrm{R}})$. In this way we obtain

$$V_{\mathrm{POL}} = -\frac{\langle 0|V_{\alpha\alpha}^2|0\rangle}{(\Delta E)_{\mathrm{R}}^{(0)}}\left[1-\frac{\langle \mathrm{exc}|V_{\alpha\alpha}|\mathrm{exc}\rangle}{(\Delta E)_{\mathrm{R}}^{(0)}}+\mathrm{O}\left(\frac{V_{\alpha\alpha}^2}{(\Delta E)_{\mathrm{R}}^{(0)2}}\right)\right]. \tag{2.24}$$

We have

$$|\langle \mathrm{exc}|V_{\alpha\alpha}|\mathrm{exc}\rangle| = \left|\frac{\langle 0|V_{\alpha\alpha}^3|0\rangle}{\langle 0|V_{\alpha\alpha}^2|0\rangle}\right| = w|\langle 0|V_{\alpha\alpha}^2|0\rangle^{\frac{1}{2}}|. \tag{2.25}$$

We shall put $w = 1$ for the purpose of a rough estimate. The numerical results (§ 3) will show that the second term in the square bracket in (2.24) is small compared with the first.

2.6. SERBER POTENTIAL

This potential (2.14b) has $a_0 \neq 0$. Two polarisation processes now occur. The a_0 term, which is independent of $\boldsymbol{\sigma}$ and $\boldsymbol{\tau}$, leads to a mutual distortion of the α-clusters from a spherically symmetric to a sort of spheroidal shape, the axis of symmetry lying along the line joining the mass centres. The spheroids are prolate (oblate) if $a_0 < 0$ (> 0). In contrast to the a_0 term, the a_σ, a_τ, and $a_{\sigma\tau}$ terms lead to the same sort of spin and charge dependent correlation of the motion of nucleons in the two different α-clusters as for the Rosenfeld mixture. To take the difference between the two types of polarisation into account, we replace the trial wave function (2.5) by

$$\Phi = [1+A_1(V_{\alpha\alpha 1}-\langle 0|V_{\alpha\alpha 1}|0\rangle)+A_2 V_{\alpha\alpha 2}]\Psi_0^{(\alpha)}\Psi_0^{(\alpha)}, \tag{2.26}$$

where $V_{\alpha\alpha 1}$ and $V_{\alpha\alpha 2}$ respectively are the a_0 and the $(a_\sigma, a_\tau, a_{\sigma\tau})$ parts of the α-α interaction potential.

We then calculate the expectation value of $H_{\mathrm{int}}+V_{\alpha\alpha}$ with the wave-function (2.26). In a way analogous to the derivation of (2.7) and (2.8), one obtains for the polarisation energy

$$\begin{aligned} V_{\mathrm{POL}} = \{&[2A_1+A_1^2(\Delta E)_1](\langle 0|V_{\alpha\alpha 1}^2|0\rangle-\langle 0|V_{\alpha\alpha 1}|0\rangle^2) \\ &+[2A_2+(\Delta E)_2 A_2^2]\langle 0|V_{\alpha\alpha 2}^2|0\rangle+2A_1A_2\langle 0|V_{\alpha\alpha 2}^2(V_{\alpha\alpha 1}-\langle 0|V_{\alpha\alpha 1}|0\rangle)|0\rangle\} \\ &\cdot\{1+A_1^2(\langle 0|V_{\alpha\alpha 1}^2|0\rangle-\langle 0|V_{\alpha\alpha 1}|0\rangle^2)+A_2^2\langle 0|V_{\alpha\alpha 2}^2|0\rangle\}^{-1}. \end{aligned} \tag{2.27}$$

In deriving (2.27), we have used the results $\langle 0|V_{\alpha\alpha 2}|0\rangle = 0$, $\langle 0|V_{\alpha\alpha 1}V_{\alpha\alpha 2}|0\rangle = 0$, $\langle 0|V_{\alpha\alpha 1}^2 V_{\alpha\alpha 2}|0\rangle = 0$, and $\langle 0|V_{\alpha\alpha 1}H_{\mathrm{int}}V_{\alpha\alpha 2}|0\rangle = 0$ which follow from (2.19); we have used the notation

$$(\Delta E)_1 = (\Delta E)_1^{(0)} + (\Delta E)_1^{(1)}, \qquad (\Delta E)_2 = (\Delta E)_2^{(0)} + (\Delta E)_2^{(1)}, \quad (2.28a)$$

with

$$\begin{aligned}(\Delta E)_1^{(0)} &= \langle \text{exc } 1|H_{\text{int}}|\text{exc } 1\rangle - \langle 0|H_{\text{int}}|0\rangle,\\ (\Delta E)_1^{(1)} &= \langle \text{exc } 1|V_{\alpha\alpha 1}|\text{exc } 1\rangle - \langle 0|V_{\alpha\alpha 1}|0\rangle,\end{aligned} \quad (2.28b)$$

$$\begin{aligned}(\Delta E)_2^{(0)} &= \langle \text{exc } 2|H_{\text{int}}|\text{exc } 2\rangle - \langle 0|H_{\text{int}}|0\rangle,\\ (\Delta E)_2^{(1)} &= \langle \text{exc } 2|(V_{\alpha\alpha 1}+V_{\alpha\alpha 2})|\text{exc } 2\rangle - \langle 0|V_{\alpha\alpha 1}|0\rangle,\end{aligned} \quad (2.28c)$$

where

$$\langle \text{exc } i \mid \text{operator} \mid \text{exc } i\rangle \equiv \frac{\langle 0|(V_{\alpha\alpha i} - \langle 0|V_{\alpha\alpha i}|0\rangle)\ \text{operator}\ (V_{\alpha\alpha i} - \langle 0|V_{\alpha\alpha i}|0\rangle)|0\rangle}{\langle 0|(V_{\alpha\alpha i} - \langle 0|V_{\alpha\alpha i}|0\rangle)^2|0\rangle}. \quad (2.29)$$

The symbols $\langle \text{exc } 1| \ldots | \text{exc } 1\rangle$ and $\langle \text{exc } 2| \ldots | \text{exc } 2\rangle$ signify averages over the mixtures of excited states produced by the operation of $V_{\alpha\alpha 1}$ and $V_{\alpha\alpha 2}$ respectively on $\Psi_0^{(\alpha)}\,\Psi_0^{(\alpha)}$.

We adjust the constants A_1 and A_2 in (2.27) so as to make V_{POL} negative and numerically as large as possible. As a first approximation, we replace the denominator by 1, and neglect the term $2A_1A_2\ldots$ in the numerator. The minimum then occurs for $A_1 = -1/(\Delta E)_1$, $A_2 = -1/(\Delta E)_2$. Knowing the orders of magnitude of A_1 and A_2, we then obtain a better approximation by expanding V_{POL} in powers of $(V_{\alpha\alpha}/\Delta E)$. In the course of this expansion we also split up $(\Delta E)_1$ and $(\Delta E)_2$ into the two terms in (2.28a), where $(\Delta E)_{1,2}^{(1)}/(\Delta E)_{1,2}^{(0)} = \mathrm{O}(V_{\alpha\alpha}/\Delta E)$. We obtain

$$\begin{aligned}V_{\text{POL}} = &-\frac{(\langle 0|V_{\alpha\alpha 1}^2|0\rangle - \langle 0|V_{\alpha\alpha 1}|0\rangle^2)}{(\Delta E)_1^{(0)}}\left[1 - \frac{(\langle \text{exc } 1|V_{\alpha\alpha 1}|\text{ exc } 1\rangle - \langle 0|V_{\alpha\alpha 1}|0\rangle)}{(\Delta E)_1^{(0)}} + \mathrm{O}\left(\frac{V_{\alpha\alpha}}{\Delta E}\right)^2\right]\\ &-\frac{\langle 0|V_{\alpha\alpha 2}^2|0\rangle}{(\Delta E)_2^{(0)}}\left[1 - \frac{(\langle \text{exc } 2|(V_{\alpha\alpha 1}+V_{\alpha\alpha 2})|\text{ exc } 2\rangle - \langle 0|V_{\alpha\alpha 1}|0\rangle)}{(\Delta E)_2^{(0)}} + \mathrm{O}\left(\frac{V_{\alpha\alpha}}{\Delta E}\right)^2\right]\\ &+\frac{2\langle 0|V_{\alpha\alpha 2}^2(V_{\alpha\alpha 1} - \langle 0|V_{\alpha\alpha 1}|0\rangle)|0\rangle}{(\Delta E)_1^{(0)}(\Delta E)_2^{(0)}}\left[1 + \mathrm{O}\left(\frac{V_{\alpha\alpha}}{\Delta E}\right)\right].\end{aligned} \quad (2.30)$$

The correction terms written out in full in the square brackets, and the term involving both $(\Delta E)_1^{(0)}$, and $(\Delta E)_2^{(0)}$ are smaller by a factor $\mathrm{O}(V_{\alpha\alpha}/\Delta E)$ than the terms $(\langle 0|V_{\alpha\alpha 1}^2|0\rangle - \langle 0|V_{\alpha\alpha 1}|0\rangle^2)/(\Delta E)_1^{(0)}$ and $\langle 0|V_{\alpha\alpha 2}^2|0\rangle/(\Delta E)_2^{(0)}$. For the purpose of a rough estimate of the correction term in the first square bracket of (2.30), we take

$$\begin{aligned}\left|\frac{\langle \text{exc } 1|V_{\alpha\alpha 1}|\text{ exc } |1\rangle - \langle 0|V_{\alpha\alpha 1}|0\rangle}{(\Delta E)_1^{(0)}}\right| &= \left|\frac{\langle 0|(V_{\alpha\alpha 1} - \langle 0|V_{\alpha\alpha 1}|0\rangle)^3|0\rangle}{\langle 0|(V_{\alpha\alpha 1} - \langle 0|V_{\alpha\alpha 1}|0\rangle)^2|0\rangle(\Delta E)_1^{(0)}}\right|\\ &\approx \frac{|\langle 0|(V_{\alpha\alpha 1} - \langle 0|V_{\alpha\alpha 1}|0\rangle)^2|0\rangle^{\frac{1}{2}}|}{(\Delta E)_1^{(0)}},\end{aligned} \quad (2.31)$$

and for the correction term in the second square bracket

$$\left|\frac{\langle \text{exc } 2|(V_{\alpha\alpha 1}+V_{\alpha\alpha 2})|\text{exc } 2\rangle - \langle 0|V_{\alpha\alpha 1}|0\rangle}{(\Delta E)_2{}^{(0)}}\right|$$

$$= \left|\frac{\langle 0|[V^3_{\alpha\alpha 2}+V^2_{\alpha\alpha 2}(V_{\alpha\alpha 1}-\langle 0|V_{\alpha\alpha 1}|0\rangle)]|0\rangle}{\langle 0|V^2_{\alpha\alpha 2}|0\rangle (\Delta E)_2{}^{(0)}}\right| \tag{2.32}$$

$$\approx \left|\frac{\langle 0|V^2_{\alpha\alpha 2}|0\rangle^{\frac{1}{2}}}{(\Delta E)_2{}^{(0)}}\right| + \left|\frac{\langle 0|(V_{\alpha\alpha 1}-\langle 0|V_{\alpha\alpha 1}|0\rangle)^2|0\rangle^{\frac{1}{2}}}{(\Delta E)_2{}^{(0)}}\right|.$$

For a rough estimate of the term $2\ldots/(\Delta E)_1{}^{(0)}(\Delta E)_2{}^{(0)}$, we take

$$\left|\frac{2\langle 0|V^2_{\alpha\alpha 2}(V_{\alpha\alpha 1}-\langle 0|V_{\alpha\alpha 1}|0\rangle)}{(\Delta E)_1{}^{(0)}(\Delta E)_2{}^{(0)}}\Big|0\rangle\right| \approx \left|\frac{2\langle 0|V^2_{\alpha\alpha 2}|0\rangle\langle 0|(V_{\alpha\alpha 1}-\langle 0|V_{\alpha\alpha 1}|0\rangle)^2|0\rangle^{\frac{1}{2}}}{(\Delta E)_1{}^{(0)}(\Delta E)_2{}^{(0)}}\right|. \tag{2.33}$$

The numerical results in § 3 have been calculated by replacing the square brackets in (2.30) by 1, and by neglecting the term $2\ldots/(\Delta E)_1{}^{(0)}(\Delta E)_2{}^{(0)}$. We shall show in § 3 that this approximation is justified.

2.7. PERTURBATION THEORY

Instead of using the variational method discussed above, we could try to obtain the lowest eigenvalue of (2.4b) by a perturbation method *. Φ would be expanded in terms of the internal eigenfunctions of the systems of nucleons (1234) and (5678). The procedure would be analogous to the calculation of interatomic Van der Waals forces by perturbation theory (see, e.g., ref. [5])), except that in the atomic problem the nuclei are regarded as fixed, while in the nuclear problem it is the mass centres of the α-clusters which are fixed.

The expression for E_{int} given by perturbation theory is like (2.6), except that $E_0{}^{(1)}$ and V_{D} now have to be calculated with the exact ground state internal eigenfunctions of the two α-clusters, and V_{POL} is replaced by

$$V^{(p)}_{\text{POL}}(\mathbf{X}) = -\sum_{ij}{}' \frac{|\langle 0|V_{\alpha\alpha}|ij\rangle|^2}{E_i{}^{(1)}+E_j{}^{(1)}-2E_0{}^{(1)}}, \tag{2.34}$$

where $E_i{}^{(1)}$ is the internal energy of an α-cluster in its ith excited state, and where we have used the notation

$$\langle 0|\text{ operator }|ij\rangle$$

$$= \int \mathrm{d}v_{\text{int}}\, \Psi_0{}^{(\alpha)}(1234)\Psi_0{}^{(\alpha)}(5678)\text{ operator }\Psi_i{}^{(\alpha)}(1234)\Psi_j{}^{(\alpha)}(5678), \tag{2.35}$$

where $\Psi_i{}^{(\alpha)}(1234)$ is the internal wave function of the nucleons (1234) in the ith excited state. The prime on Σ in (2.34) indicates that the term with $i = j = 0$ is to be omitted.

† This perturbation procedure, starting as it does from equation (2.4b), is different from the one quoted in § 2.1 as establishing the validity of the ground state V_{POL} also in the region of low excitation energies. Both methods give the same results for the polarisation energy.

We again write $V_{\alpha\alpha} = V_{\alpha\alpha 1}+V_{\alpha\alpha 2}$, where $V_{\alpha\alpha 1}$ and $V_{\alpha\alpha 2}$ are defined as in (2.26). We now note that $\langle 0|V_{\alpha\alpha 1}|ij\rangle$ vanishes because of spin orthogonality, unless both the functions $\Psi_i^{(\alpha)}$ and $\Psi_j^{(\alpha)}$ contain a spin-charge Slater determinant D, and that $\langle 0|V_{\alpha\alpha 2}|0\rangle$ vanishes if both $\Psi_i^{(\alpha)}$ and $\Psi_j^{(\alpha)}$ contain a D (because of (2.19). Therefore there are no $\langle V_{\alpha\alpha 1}V_{\alpha\alpha 2}\rangle$ cross terms in (2.34), and we have

$$V_{\mathrm{POL}}^{(p)}(\mathbf{X}) = -\sum_{ij}{}' \frac{|\langle 0|V_{\alpha\alpha 1}|ij\rangle|^2+|\langle 0|V_{\alpha\alpha 2}|ij\rangle|^2}{E_i^{(1)}+E_j^{(1)}-2E_0^{(1)}} \qquad (2.36)$$
$$= V_{\mathrm{POL}1}^{(p)}+V_{\mathrm{POL}2}^{(p)}.$$

Upper limits for the absolute values of $V_{\mathrm{POL}1}^{(p)}$ and $V_{\mathrm{POL}2}^{(p)}$ are obtained if we replace the energy denominators by the smallest, which we denote by $(\Delta E)_1^{(p)}$, and $(\Delta E)_2^{(p)}$. Thus we have finally

$$|V_{\mathrm{POL}1}^{(p)}| \leqq \frac{1}{(\Delta E)_1{}^{(p)}} \sum_{ij}{}' |\langle 0|V_{\alpha\alpha 1}|ij\rangle|^2 = \frac{1}{(\Delta E)_1{}^{(p)}} (\langle 0|V_{\alpha\alpha 1}^2|0\rangle - \langle 0|V_{\alpha\alpha 1}|0\rangle^2), \qquad (2.37a)$$

$$|V_{\mathrm{POL}2}^{(p)}| \leqq \frac{1}{(\Delta E)_2{}^{(p)}} \sum_{ij}{}' |\langle 0|V_{\alpha\alpha 2}|ij\rangle|^2 = \frac{1}{(\Delta E)_2{}^{(p)}} \langle 0|V_{\alpha\alpha 2}^2|0\rangle, \qquad (2.37b)$$

where we have used closure, and the result $\langle 0|V_{\alpha\alpha 2}|0\rangle = 0$.

For the Rosenfeld mixture and for the $V_{\alpha\alpha 2}$ part of the Serber potential, the lowest excited state is one in which both α-clusters are excited, because the matrix elements of $V_{\alpha\alpha}$ (or $V_{\alpha\alpha 2}$) between the ground-ground state and another state in which only one α-cluster is excited vanishes according to (2.19). Since no excited bound state of the α-particle is known [9]), we must put

$$[(\Delta E)_2{}^{(p)},\ (\Delta E)_{\mathrm{R}}{}^{(p)}] = 2(E_{\mathrm{H}^3}-E_0^{(1)}) = 39.6\ \mathrm{MeV}, \qquad (2.38a)$$

where $E_0^{(1)}$ is the internal energy of the α-particle in the ground state (excluding rest masses), and E_{H^3} is that of the triton. The $V_{\alpha\alpha 1}$ part of the Serber potential is independent of the mechanical intrinsic spin and isobaric spin variables; it follows that only one α-cluster is excited in the lowest state of internal excitation produced by $V_{\alpha\alpha 1}$. We therefore have

$$(\Delta E)_1{}^{(p)} = 19.8\ \mathrm{MeV}. \qquad (2.38b)$$

Although we do not know the exact ground state wave function, we shall still use the limits (2.37a, b) with the approximate form (2.15), (2.16) of $\Psi_0^{(\alpha)}$ to supplement the variational calculations.

3. Results

3.1. α-PARTICLE RADIUS AND SEPARATION

The nuclear potential enters into the formulae (2.24) and (2.30) for V_{POL} in two ways: directly through $V_{\alpha\alpha}$, and indirectly through $\Psi_0^{(\alpha)}$. In the

approximate form (2.16) which we have used for $\Psi_0^{(\alpha)}$, the only free parameter is β, which determines the radius (see (2.17)). The most consistent procedure is to adjust this radius by minimising $E_0^{(1)}$, the energy of the α-particle (see (2.21)). With the Gaussian potential (2.11), the radii corresponding to the minimum are $\varrho_\alpha = 1.34\times10^{-13}$ cm for the first set of parameters and $\varrho_\alpha = 1.06\times10^{-13}$ cm for the second. These radii are somewhat smaller than is indicated by the scattering of 188 MeV electrons which gives $\varrho_\alpha = (1.4\pm0.15)\times10^{-13}$ cm for the distribution of the charge centres of the individual protons [10]). Actually, $E_0^{(1)}$ is not very sensitive to ϱ_α (see table 3.1), so that we can consider a wide enough range of radii to cover all possibilities without getting too bad a value for $E_0^{(1)}$. The calculations reported here were done before the latest radii from electron scattering became available, and therefore cover a somewhat wider range than is now necessary.

TABLE 3.1

Dependence of the theoretical binding energy of the α-particle on the radius (see (2.21))

$\varrho_\alpha(10^{-13})$ cm)		1.06	1.1	1.34	1.4	1.8
$E_0^{(1)}$ (MeV)	1st of set parameters (2.11)		19	24	24	18
	2nd set of parameters (2.11)	40	40		32	19

(The experimental binding energy of the α-particle is 28.2 MeV).

The distances of separation which are interesting range from about 5×10^{-13} cm down to $2\text{-}3\times10^{-13}$ cm. The upper limit is set by the known densities of nuclei and by the moments of inertia which α-nuclei must have to account for rotational levels [11]). The lower limit is set by the demand that the α-clusters should not overlap too much because the argument by which the formulae for V_{POL} were derived is valid only if E_{Int} is the dominant interaction in (2.2), i.e. if the nucleon exchange term is unimportant.

3.2. ROSENFELD MIXTURE

The results are shown in table 3.2. These results were calculated from formula (2.24), with the use of (2.9) and (2.20). The mean excitation energies $(\Delta E)_R^{(0)}$ for the Gaussian potential and some of the detailed figures are shown in table 3.3. (In all the tables, G1 stands for the first Gaussian potential, G2 for the second, and Y for the Yukawa shape.)

Since $(\Delta E)_R^{(0)}$ (see columns 6 and 7 of table 3.3) is almost independent of X in a range where the Gaussian potential goes through a wide range of slopes and curvatures, and since the two sets of parameters we have used give results for $(\Delta E)_R^{(0)}$ which are little different, it is clear that $(\Delta E)_R^{(0)}$

TABLE 3.2

Polarisation energy with the Rosenfeld mixture.

ϱ_α 10^{-13} cm	X 10^{-13} cm	G1 MeV	G2 MeV	Y MeV
1.1	2	−1.2	−2.9	−2.6
	3	−0.53	−0.91	−0.6
	4	−0.14	−0.12	−0.06
	5	−0.02	−0.01	−0.004
1.4	2	−2.7	−5.7	−4.9
	3	−1.2	−2.2	−1.6
	4	−0.44	−0.50	−0.30
	5	−0.09	−0.06	−0.04
1.8	2	−5.1	−9.5	−7.8
	3	−2.6	−4.4	−3.3
	4	−1.2	−1.5	−1.1
	5	−0.36	−0.36	−0.26

TABLE 3.3

Details for the Rosenfeld mixture

ϱ_α 10^{-13} cm	X 10^{-13} cm	$\langle 0\|V_{\alpha\alpha}^2\|0\rangle$ (MeV²)			$(\Delta E)_R^{(0)}$ (MeV)		$\frac{\langle 0\|V_{\alpha\alpha}^2\|0\rangle^{\frac{1}{2}}}{(\Delta E)_R^{(0)}}$	
		G1	G2	Y	G1	G2	G1	G2
1.1	2	206	597	444	170	205	0.08	0.12
	3	86.7	173	105	165	190	0.05	0.07
	4	21.8	21.2	9.94	153	180	0.03	0.03
	5	2.46	0.994	0.586	146	174	0.01	0.01
1.4	2	336	848	617	126	148	0.15	0.20
	3	152	308	201	122	141	0.10	0.12
	4	50.5	66.6	38.4	115	134	0.06	0.06
	5	9.53	7.34	4.32	110	130	0.03	0.02
1.8	2	455	984	694	89	104	0.24	0.30
	3	229	446	298	89	102	0.17	0.21
	4	97.4	151	95.7	85	98	0.12	0.13
	5	29.4	34.0	21.2	81	96	0.07	0.06
1	2	3	4	5	6	7	8	9

must be rather insensitive to the shape of the nuclear potential. We have therefore not calculated $(\Delta E)_R^{(0)}$ for the Yukawa potential, but have used instead the values for the first set of Gaussian parameters.

The calculations with the Yukawa potential were made by replacing $\exp(-r/1.37)/(r/1.37)$ by $1.19\exp(-0.571r^2)+0.0866\exp(-0.0978r)$. This approximation is illustrated in fig. 3.1.

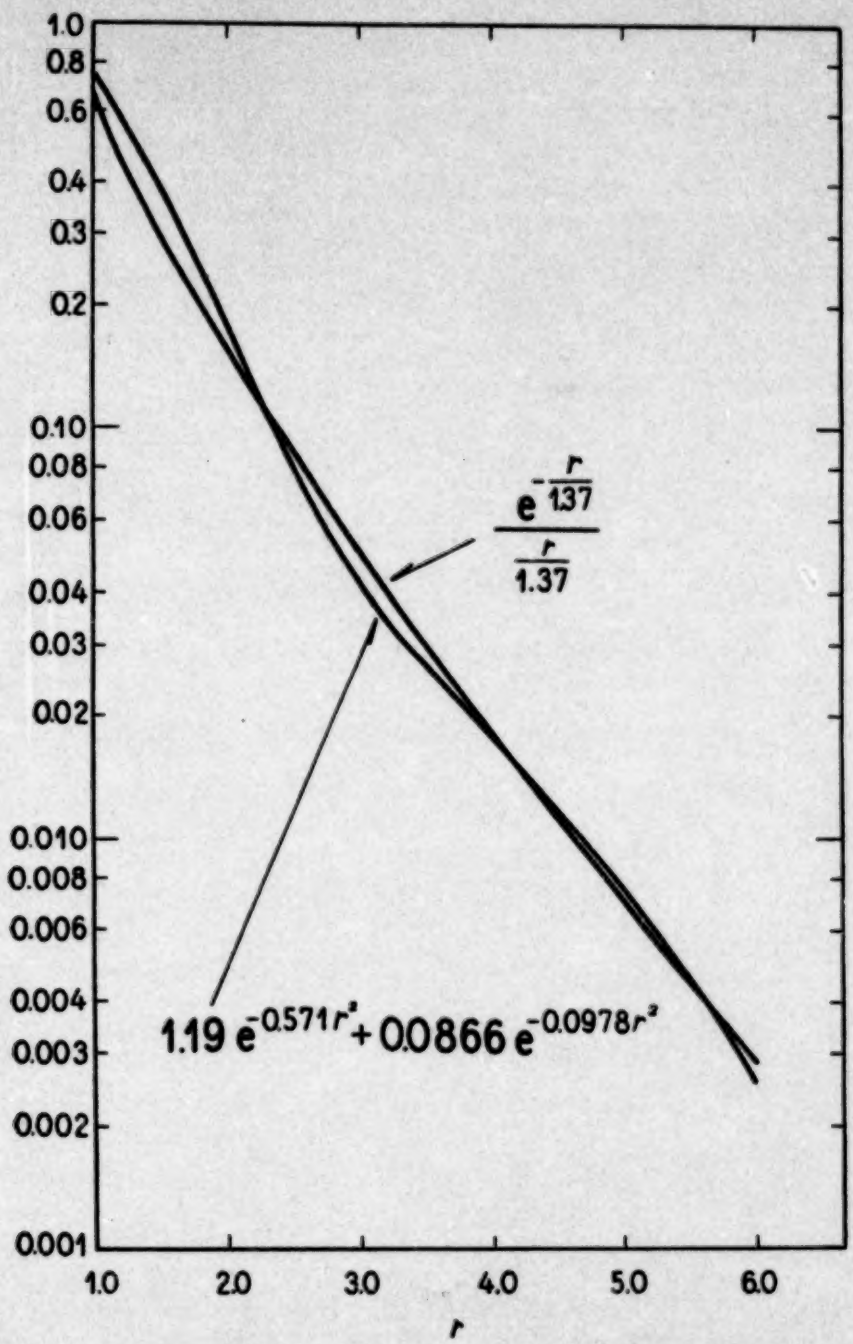

Fig. 3.1. Approximation for the Yukawa potential.

In calculating the results of table 3.2, we have made the following approximations:

(1) We have neglected the correction term $w|\langle 0|V_{\alpha\alpha}^2|0\rangle|^{\frac{1}{2}}$ in equations (2.24) and (2.25). The figures in columns 8 and 9 of table 3.3 show that this approximation is justified.

(2) In the whole discussion we have neglected the term $\Delta K(\mathbf{X})$ (equations (2.2 and (2.3)) which should strictly have been counted as part of the polarisation energy. Putting $A \approx -1/(\Delta E)_R^{(0)}$, we find from (2.3), (2.5), and (2.24) that

$$\Delta K(\mathbf{X}) \approx \frac{\hbar^2}{2\mu}\langle 0|\left[\nabla_{\mathbf{X}}\frac{(V_{\alpha\alpha}(\mathbf{X})-\langle 0|V_{\alpha\alpha}(\mathbf{X})|0\rangle)}{(\Delta E)_R^{(0)}}\right]^2|0\rangle$$
$$\approx \frac{\hbar^2}{2\mu}\cdot\frac{1}{\lambda^2}\cdot\frac{V_{\mathrm{POL}}}{(\Delta E)_R^{(0)}} \tag{3.1}$$

to the lowest order in $(V_{\alpha\alpha}/\Delta E)$; here we have put $\nabla_{\mathbf{X}} \to 1/\lambda$ (where $\lambda =$ range of the nuclear forces $\approx 10^{-13}$ cm); μ is the reduced mass of two α-particles. Since $(\Delta E)_R^{(0)} \approx 100$ MeV, we have $\Delta K \approx 0.1\, V_{\mathrm{POL}}$, so that ΔK is negligible in comparison with V_{POL}.

3.3. SERBER POTENTIAL

The results for the Serber potential are shown in table 3.4. These results were calculated from formula (2.30) with the use of (2.28a, b, c), (2.18), and (2.20); (in (2.20) the a_0 term is $\langle 0|V_{\alpha\alpha 1}^2|0\rangle$, and the rest is $\langle 0|V_{\alpha\alpha 2}^2|0\rangle$; also we have here $\langle 0|V_{\alpha\alpha}|0\rangle = \langle 0|V_{\alpha\alpha 1}|0\rangle$).

TABLE 3.4

Polarisation energy with the Serber potential

ϱ_α 10^{-13} cm	X 10^{-13} cm	G1 MeV	G2 MeV	Y MeV
1.1	3	−0.70	−0.97	−0.97
	4	−0.23	−0.11	−0.082
	5	−0.023	−0.004	−0.0074
1.4	3	−1.3	−2.02	−1.8
	4	−0.47	−0.42	−0.34
	5	−0.084	−0.04	−0.037
1.8	3	−2.9	−3.8	−2.6
	4	−1.1	−1.20	−0.87
	5	−0.31	−0.25	−0.19

The mean excitation energies $(\Delta E)_1^{(0)}$ and $(\Delta E)_2^{(0)}$ for the Gaussian potential, and some of the detailed figures are shown in table 3.5. We see that $(\Delta E)_2^{(0)}$ is almost independent of X and is almost the same for the two sets of Gaussian parameters. $(\Delta E)_1^{(0)}$, in contrast to $(\Delta E)_2^{(0)}$, shows a strong dependence on X when $X \leqq 3\times 10^{-13}$ cm, and flattens out for higher values of X. At small values of X (not given in table 3.5), our values of $(\Delta E)_1^{(0)}$ even become negative; however, from the definition (2.28b), it is clear that $(\Delta E)_1^{(0)}$ cannot be negative, and we are therefore forced to ascribe

TABLE 3.5

ϱ_α	X	$\langle 0\|V_{\alpha\alpha 1}\|0\rangle$ (MeV)			$\langle 0\|V_{\alpha\alpha 1}{}^2 1\|0\rangle - \langle 0\|V_{\alpha\alpha 1}\|0\rangle^2$ (MeV^2)			$\langle 0\|V_{\alpha\alpha 2}{}^2\|0\rangle$ (MeV^2)		
10^{-13}cm	10^{-13}cm	G1	G2	Y	G1	G2	Y	G1	G2	Y
1.1	3	−21.8	−14.6	−16.0	35.0	63.7	37.7	27.0	53.8	31.5
	4	− 5.71	− 2.34	− 5.53	8.70	6.81	3.06	6.80	6.59	2.98
	5	− 1.02	− 2.24	− 2.20	0.850	0.253	0.310	0.764	0.309	0.17
1.4	3	−22.1	−16.8	−17.4	54.2	98.4	60.6	47.1	95.8	60.4
	4	− 7.17	− 3.94	− 6.43	18.7	20.3	11.4	15.7	20.7	11.6
	5	− 1.69	− 0.61	− 2.47	3.14	1.86	1.26	2.96	2.28	1.30
1.8	3	−21.0	−17.4	−17.5	67.2	116.9	75.2	71.4	139	90.0
	4	− 8.67	− 5.96	− 7.64	31.4	41.6	25.6	30.4	47.1	28.8
	5	− 2.79	− 1.5	− 3.07	9.08	8.57	5.55	9.14	10.6	6.37
1	2	3	4	5	6	7	8	9	10	11

the anomalous results to the approximations we have made, i.e. to the use of an approximate ground state wavefunction for the α-particle, and to the replacement $H_{\text{int}}|0\rangle \to \langle 0|H_{\text{int}}|0\rangle|0\rangle$. Since the anomalous results occur only for $X < 3\times 10^{-13}$ cm, while the results for $X > 3\times 10^{-13}$ cm appear reasonable, we have used only the latter. For the results with the Yukawa potential, we have again used the Gaussian values (first set of parameters) of $(\Delta E)_2{}^{(0)}$; for $(\Delta E)_1{}^{(0)}$ we have taken 50 MeV.

The following approximations were made in calculating the results for the Serber potential:

(1) We have neglected the correction terms in the square brackets in equation (2.30). From the estimates (2.31), (2.32), and (2.33), and columns 16—21 of table 3.5 we see that this approximation is justified.

(2) We have neglected the term ΔK in (2.2) and (2.3). Putting $A_1 \approx -1/(\Delta E)_1{}^{(0)}$, $A_2 \approx -1/(\Delta E)_2{}^{(0)}$, and using (2.3) and (2.26), we obtain, to the lowest order in $(V_{\alpha\alpha}/\Delta E)$

$$\Delta K = \frac{\hbar^2}{2\mu}\langle 0|\left[\nabla_{\mathbf{X}}\left(\frac{V_{\alpha\alpha 1}(\mathbf{X})-\langle 0|V_{\alpha\alpha 1}(\mathbf{X})|0\rangle}{(\Delta E)_1{}^{(0)}}+\frac{V_{\alpha\alpha 2}(\mathbf{X})}{(\Delta E)_2{}^{(0)}}\right)\right]^2|0\rangle$$

$$=\frac{\hbar^2}{2\mu}\left\{\langle 0|\left[\nabla_{\mathbf{X}}\left(\frac{V_{\alpha\alpha 1}(\mathbf{X})-\langle 0|V_{\alpha\alpha 1}(\mathbf{X})|0\rangle}{(\Delta E)_1{}^{(0)}}\right)\right]^2|0\rangle+\langle 0|\left[\nabla_{\mathbf{X}}\frac{V_{\alpha\alpha 2}}{(\Delta E)_2{}^{(0)}}\right]^2|0\rangle\right\}$$

$$\approx\frac{\hbar^2}{2\mu}\cdot\frac{1}{\lambda^2}\cdot\left(\frac{V_{1\text{POL}}}{(\Delta E)_1{}^{(0)}}+\frac{V_{2\text{POL}}}{(\Delta E)_2{}^{(0)}}\right)\approx 10\left(\frac{V_{1\text{POL}}}{(\Delta E)_1{}^{(0)}}+\frac{V_{2\text{POL}}}{(\Delta E)_2{}^{(0)}}\right)\text{MeV};\quad (3.2)$$

here we have used the results $\langle 0|V_{\alpha\alpha 1}|0\rangle = 0$, $\langle 0|V_{\alpha\alpha 1}V_{\alpha\alpha 2}|0\rangle = 0$, and we have replaced $\nabla_{\mathbf{X}}$ by $1/\lambda$. Since $(\Delta E)_1{}^{(0)} > 30$ MeV, and $(\Delta E)_2{}^{(0)} \approx 100$ MeV, we see that ΔK is always small compared with V_{POL}.

Details for the Serber potential

$(\Delta E)_1^{(0)}$ (MeV)		$(\Delta E)_2^{(0)}$ (MeV)		Estimates of Correction Terms					
G1	G2	G1	G2	(2.31)		(2.32)		(2.33) MeV	
69	97	145	171	0.09	0.08	0.08	0.09	0.03	0.05
49	93	136	164	0.06	0.03	0.04	0.03	0.006	0.002
51	102	130	162	0.02	0.005	0.01	0.006	0.0002	0.00002
60	77	110	129	0.12	0.13	0.13	0.15	0.10	0.19
58	79	104	124	0.07	0.06	0.08	0.07	0.02	0.02
57	85	100	123	0.03	0.02	0.04	0.02	0.002	0.0007
33	50	81	96	0.25	0.22	0.21	0.23	0.44	0.63
47	60	78	93	0.12	0.11	0.14	0.14	0.10	0.11
48	64	75	92	0.06	0.05	0.08	0.07	0.02	0.01
12	13	14	15	16	17	18	19	20	21

3.4. PERTURBATION THEORY

According to § 2.7, an upper limit to $|V_{\mathrm{POL}}|$ is obtained from perturbation theory if one replaces (ΔE) by $(\Delta E)^{(p)}$, which was defined as the lowest excitation energy among the states excited by the interaction potential $V_{\alpha\alpha}$. Comparing the values of $(\Delta E)^{(p)}$ given in (2.38a, b) with the results shown in tables 3.3 and 3.5, we see that the upper limits are larger than the results from the variational calculation by a factor of between two and four.

4. Non-additive Polarisation Forces

The polarisation energy between α-clusters is non-additive for some exchange types of the nucleon-nucleon potential [4]). According to equation (7.6) of reference [4]), perturbation theory gives for the non-additive polarisation energy between 3 α-clusters

$$V_{\mathrm{POL\ na}} = -\sum_{i\neq 0} \frac{\langle 000|V_{\alpha 1\alpha 2}|i00\rangle\langle i00|V_{\alpha 1\alpha 3}|000\rangle}{E_{i00}-E} + \text{similar terms (21, 23) and (31, 32).} \tag{4.1}$$

In equation (4.1) the three α-clusters are denoted by 1, 2, and 3; $V_{\alpha 1\alpha 2}$ is the interaction potential between α-clusters 1 and 2. The exchange of nucleons between the α-clusters has been neglected. The symbol $|ijk>$ represents the state in which α-clusters 1, 2, and 3 respectively are in the ith, jth, and kth state of internal excitation; E_{ijk} stands for $(E_i^{(1)}+E_j^{(1)}+E_k^{(1)})$, where $E_i^{(1)}$ is the internal energy of a free α-particle in the ith excited state; (if the α-particle is disrupted, then $E_i^{(1)}$ contains everything but the kinetic energy of mass-centre motion). E is the total energy (ex-

cluding rest-masses of the nucleons) of the system of three α-particles. If the system is not too highly excited then we can put † $E \approx 3E_0^{(1)}$, so that

$$E_{i00} - E \approx E_i^{(1)} - E_0^{(1)}. \tag{4.2}$$

We note that in (4.1) we have, by integrating over the co-ordinates of α-cluster 3,

$$\langle 000|V_{\alpha 1\alpha 2}|i00\rangle = \langle 0_1\, 0_2|V_{\alpha 1\alpha 2}|i_1\, 0_2\rangle,$$

where we have put in the suffices to show that in $\langle 0_1\, 0_2|$ both cluster 1 and 2 are in the ground state, while in $|i_1\, 0_2\rangle$ cluster 1 is in the ith state of internal excitation, and cluster 2 is in the ground state. If $V_{\alpha 1\alpha 2}$ is a sum of central potentials then the only term which survives the integration $\langle 0_2| \ldots |0_2\rangle$ is the term in a_0; the other terms vanish because of (2.19). We therefore see from (2.14b) that the Serber potential gives a non-additive polarization energy, while the Rosenfeld mixture (2.14a) does not. In calculating V_{POL} for the Serber potential, we can therefore replace $V_{\alpha 1\alpha 2}$ by $V_{\alpha 1\alpha 2\,1}$, i.e. the part containing a_0.

We have estimated $V_{\text{POL na}}$ from (4.1) for the case where the mass centres of the three α-clusters are at the apices of a fixed equilateral triangle of length of side X. Denoting this restricted value of $V_{\text{POL na}}$ by $V^{\Delta}_{\text{POL na}}(X)$, we have from (4.1) and (4.2)

$$V^{\Delta}_{\text{POL na}}(X) \approx -3\sum_{i\neq 0} \frac{\langle 000|V_{\alpha 1\alpha 2\,1}|i00\rangle\langle i00|V_{\alpha 1\alpha 3\,1}|000\rangle}{E_i^{(1)} - E_0^{(1)}}. \tag{4.3}$$

We replace the denominators in (4.3) by a suitable mean value $(\Delta E)_{\text{na}}$ so that by the use of closure (4.3) becomes

$$V^{\Delta}_{\text{POL na}}(X) \approx -\frac{3}{(\Delta E)_{\text{na}}}\left[\langle 0_1\, 0_2|V_{\alpha 1\alpha 2\,1}|0_2\rangle\langle 0_3|V_{\alpha 1\alpha 3\,1}|0_1\, 0_3\rangle - |\langle 0_1\, 0_2|V_{\alpha 1\alpha 2\,1}|0_1\, 0_2\rangle|^2\right], \tag{4.4}$$

where we have again used the symmetry between the three α-clusters. We have calculated the value of the expression (4.4) for $X = 3$, 4, and 5×10^{-13} cm, taking

$$(\Delta E)_{\text{na}} = 50 \text{ MeV}, \tag{4.5}$$

since we have here an a_0 type polarization for which we found $(\Delta E)_1^{(0)} \approx$ 50 MeV for $X \geqq 3\times 10^{-13}$ (see table 3.5).

The integrals appearing in (4.4) have been evaluated for nuclear forces with the Gaussian radial dependence (first set of parameters). The integrals

† Not $2E \approx 3E_0^{(1)}$ as stated in ref. [4]).

were evaluated with the aid of formula (2.23). The results are shown in table 4.1.

TABLE 4.1

Non additive polarization energy for three α-clusters

ϱ_α	X	$V^d_{\text{POL na}}$ (G1)
10^{-13} cm	10^{-13} cm	MeV
1.1	2	+0.13
	3	+0.01
	4	−0.0006
1.4	2	+0.2
	3	+0.05
	4	+0.001
1.8	2	+0.02
	3	+0.09
	4	+0.01

5. Discussion

The α-particle model demands an attraction between α-particles with an expectation value of about 5 MeV per nearest neighbour pair at an average separation of from 3 to 4×10^{-13} cm [11]). In considering the role of the polarization forces in providing this attraction, there are two qualitatively different situations to be discussed: Either the nuclear potential does not have a direct component, when V_{POL} is the only source of attraction, or the nuclear potential does have a direct component, when there is a direct attraction in addition to the polarization attraction.

As an example of a potential without a direct component, we have considered the Rosenfeld mixture. The results given in table 3.2 show that the magnitude of the expectation value of the polarization attraction cannot be more than 1, or at most 2 MeV. It follows that with central forces between nucleons, the polarization forces between α-particles are too weak to account by themselves for the attraction required by the α-particle model. This conclusion is based on our variational calculation which underestimates the magnitude of V_{POL} [4]). An upper limit is set by the perturbation method described in § 3.4 by which for example the Gaussian potential (2.11) with the second set of parameters and with $\varrho_\alpha = 1.4\times10^{-13}$ cm gives $V_{\text{POL}} = -7.8$ MeV at a separation of 3×10^{-13} cm, and -1.7 MeV at 4×10^{-13} cm; these magnitudes come quite close to the requirement of the α-particle model. However, because of the stationary character of the

energy guaranteed by Rayleigh's principle, we believe that the variational results represent the true situation.

The second possibility we have to consider is that the nuclear potential might contain a direct tail, in which case the polarization energy would supplement the direct attraction between α-particles. As an example of a potential with a direct tail, we have considered the Serber potential. The results given in table 3.4 show that the magnitude of the expectation value of the polarization energy here is 1 to 2 MeV, as with the Rosenfeld mixture. It follows that with central forces, the polarization energy is of the order of the α-α binding energy per pair of nearest neighbours [11]), but cannot form more than a minor part of the total attraction between α-particles. The conclusion is again based on our variational calculation, and the upper limit set by the perturbation method is substantially bigger. A direct tail in the nuclear potential leads to a non-additive component in the polarization energy whose physical origin has been explained in the introduction. Our estimates of this energy for three α-particles show it to be negligible

The polarization process not only leads to an attraction between α-particles; as has been pointed out by Heisenberg [2]) it also tends to dissolve them by excitation. Let us consider two α-particles. By perturbation theory, one may estimate the probability of excitation of the internal motion of the α-particles to be

$$(1/\Delta E)^2(\langle 0|V_{\alpha\alpha}^2|0\rangle - \langle 0|V_{\alpha\alpha}|0\rangle^2)$$

for a given distance of separation of the mass centres; (the notation has been explained in the introduction). This probability may be written $V_{\mathrm{POL}}/\Delta E$; if we average over the mass centre separations, we find for the average probability of excitation $\langle V_{\mathrm{POL}}\rangle/\Delta E$, where $\langle V_{\mathrm{POL}}\rangle$ is the expectation value of V_{POL}, and where we have used the fact that according to tables 3.3 and 3.5 ΔE is almost independent of the distance of separation. If we put, in accordance with our results, $\langle V_{\mathrm{POL}}\rangle \approx 1.5$ MeV, $\Delta E \approx 100$ MeV, we get $\langle V_{\mathrm{POL}}\rangle/\Delta E \approx 1.5\ \%$. This very small probability of excitation holds for the polarization forces calculated from a central nuclear potential, and as we have seen, these are too weak to bind α-particles. If, perhaps through the action of tensor forces, the polarization forces were strong enough to bind α-particles together, we would have $\langle V_{\mathrm{POL}}\rangle \approx 5$ MeV; putting $\Delta E \approx 100$ MeV, as is appropriate for the correlation type of polarization (see table 3.5), we get $\langle V_{\mathrm{POL}}\rangle/\Delta E \approx 5\ \%$.

If there are more than two α-particles, then as long as one ignores nucleon exchange, one can treat the effect of the interaction potentials $V_{\alpha(\alpha)}$ separately.

We shall neglect the non-additive polarisation energy since this was found to be very small in § 4. Moreover, because of the short range of nuclear

forces, one need take into account only the interaction of neighbouring α's. Each such pair of neighbours will produce in one another an average probability of excitation $\langle V_{\mathrm{POL}}\rangle/\Delta E$, as for the single pair we have just considered. If an α-particle has N neighbours, then the probability of its being excited will be $N\langle V_{\mathrm{POL}}\rangle/\Delta E$. Since $N \leqq 12$, it follows that the polarization could never have any serious dissolving effect for the value $\langle V_{\mathrm{POL}}\rangle\Delta E \approx 1.5\ \%$ which we have calculated with central forces. On the other hand if the tensor force polarization were strong enough to provide the attraction required by the α-particle model, then solution through polarization would become serious in the heavier nuclei (say $A \geqq 40$) where there would be some completely surrounded α-particles; in the light α-nuclei where each α has only three or four neighbours, solution by polarization would still not be serious.

6. Conclusion

Central forces between nucleons lead to a negative polarization energy between α-particles. This polarization energy is of the order of magnitude of the α-α binding energy per pair of nearest neighbours, but is too small to account by itself for the attraction between α-particles required by the α-particle model. The extent of the solution of α-particles engendered by their mutual polarization is never serious for $A \leqq 40$ where it offers no difficulty to the α-particle model.

We are indebted to Professor L. Rosenfeld for his criticism and encouragement. We would also like to express our sincere appreciation of the help of the staff of the Manchester University Electronic Computor with much of the numerical work. One of us (A.S.R.) held a research grant from the British Rayon Research Institute while this work was done.

References

1) A. Herzenberg, Nuclear Physics **3** (1957) 1
2) W. Heisenberg, Zeits. f. Phys. **96** (1935) 473
3) H. Margenau, Phys. Rev. **59** (1941) 37
4) A. Herzenberg, Nuovo Cimento, **1** (1955) 1008
5) L. I. Schiff, (McGraw Hill, 1949) p. 177
6) L. Rosenfeld, Nuclear Forces (North-Holland Publishing Co., 1949)
7) J. M. Blatt and J. D. Jackson, Phys. Rev. **76** (1949) 18
8) A. L. Aitken, Determinants and Matrices (Oliver and Boyd Ltd., 1948) p. 138, ex. 25
9) R. M. Eisberg, Phys. Rev. **102** (1956) 1104
J. Benveniste and B. Cork, Phys. Rev. **89** (1953) 422
10) R. Hofstadter and R. W. McAllister, Phys. Rev. **102** (1956) 851
11) A. Herzenberg, Nuovo Cimento, **1** (1955) 986

Nuclear Physics **3** (1957) 336—339; *North-Holland Publishing Co., Amsterdam*

THE POLARIZATION OF 173 MeV PROTONS INELASTICALLY SCATTERED BY CARBON

H. TYRÉN, PETER HILLMAN † and A. JOHANSSON
The Gustaf Werner Institute for Nuclear Chemistry, University of Uppsala

Received 27 December 1956

This is a preliminary report of an experiment designed to measure the polarization of high energy protons inelastically scattered from nuclei. Recent experiments at 96 [1]) and 180 [2]) MeV have shown that there are peaks in the inelastic proton energy spectra for light elements, corresponding to various excited nuclear states. References [3]) and [4]) report experiments essentially on the *asymmetry* in the inelastic scattering of polarized protons corresponding to excitation of the 4.4 MeV level in carbon, using the standard double scattering technique, in which the first scatterer merely provides a beam of polarized protons at a fixed angle. In the present experiment, in which the *polarization* is measured, the second scatterer is merely a fixed analyzer, and only the *first* angle is varied.

The general experimental arrangement is as shown in ref. [2]) The heart of the experiment is the method of separating the first scattered protons in a 90° magnetic analyzer, which can be rotated about the scatterer. The resolution of the system corresponds to about two MeV full width at half height, so that clear separation of various inelastic peaks is obtained. The number of protons in the magnet image is usually less than about 100/sec, so that a thick analyzing scatterer and large geometries are necessary. These make it impossible to measure the analyzing power by the usual method of making the first and second scattering situations nearly identical. They also make it difficult to calculate the analyzing power from published results sufficiently accurately, as well as to obtain the necessary geometrical symmetry. Therefore the relation between the measured asymmetry and the polarization of the incident particles is determined empirically by using protons of known polarization. These are obtained by elastic scattering from carbon, for which accurate polarizations are known at 137 [5]), 155 [3]), and 220 [4]) MeV.

The analyzing scatterer is carbon, and the double scattered protons are counted simultaneously to the left and right in two symmetrically placed plastic scintillators in coincidence with a single narrow scintillator, imme-

† CERN (European Organisation for Nuclear Research, theoretical study division). On leave of absence from AERE, Harwell, England.

diately in front of the carbon, which defines the beam. An anticoincidence counter detecting unscattered protons reduces the high accidental coincidence rate due to the low ($\approx 1/400$) duty cycle of the 185 MeV regenerated

TABLE I

Polarization by Carbon in Percent

Angle	Elastic	4.4 MeV Level
9.7°		53±15
11.7		43±10
14.7		63± 8
19.7		89± 7
23.7	66±7	91± 8
26.7	−2±12	87±13
29.7	−28±15	53±12
32.2	−4±16	17±11
34.7	78±23	2±16

external proton beam of the synchrocyclotron. A mean of approximately 1/200 of the particles incident on the analyzing scatterer is counted in each counter. The analyzing power of the system is found to be about 45 %, dropping slightly with decreasing energy.

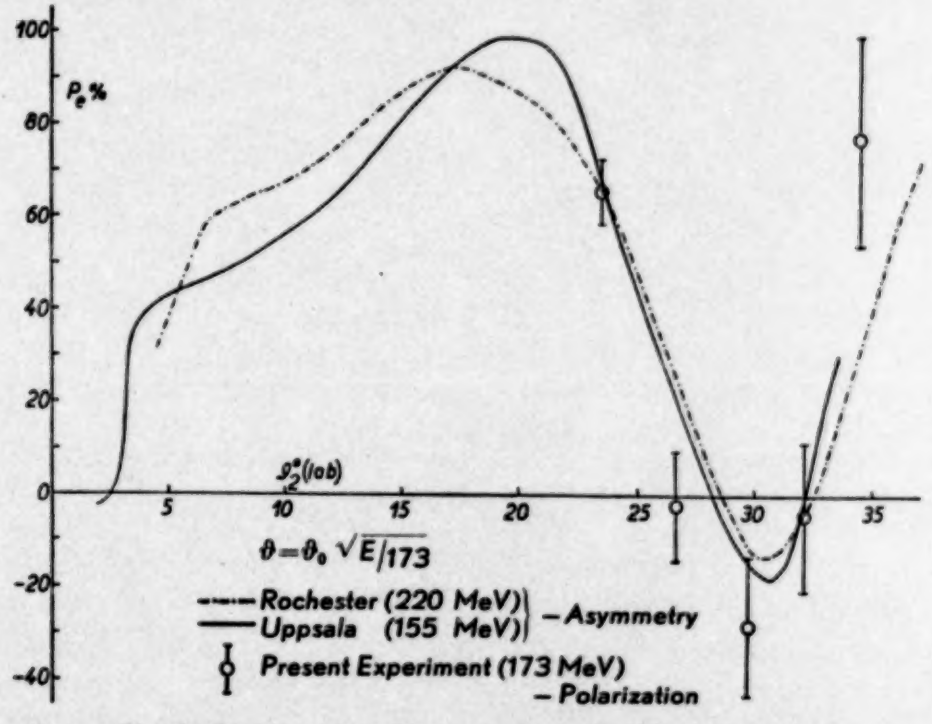

Fig. 1. Elastic asymmetry and polarization from carbon.

Aside from statistical errors and the small uncertainties in the carbon elastic polarizations used for the calibration, the only experimental errors are those arising from differences in the experimental conditions between

the "calibration" and "measurement" situations. Various checks have shown these to be small.

There may also be a contamination of the measured particles by stray particles or those from underlying or adjoining peaks. For the 4.4 MeV level of carbon on which we report here there are no nearby levels, and few stray particles, and only at angles less than about 10° is there an appreciable contamination from the very large elastic peak.

The calibration was carried out with the unpolarized direct beam and with protons elastically scattered at 6° to 19.7°. In table I we give our measured values of the polarizations of protons elastically scattered from carbon beyond 20°, and scattered from the 4.4 MeV level of carbon. The mean

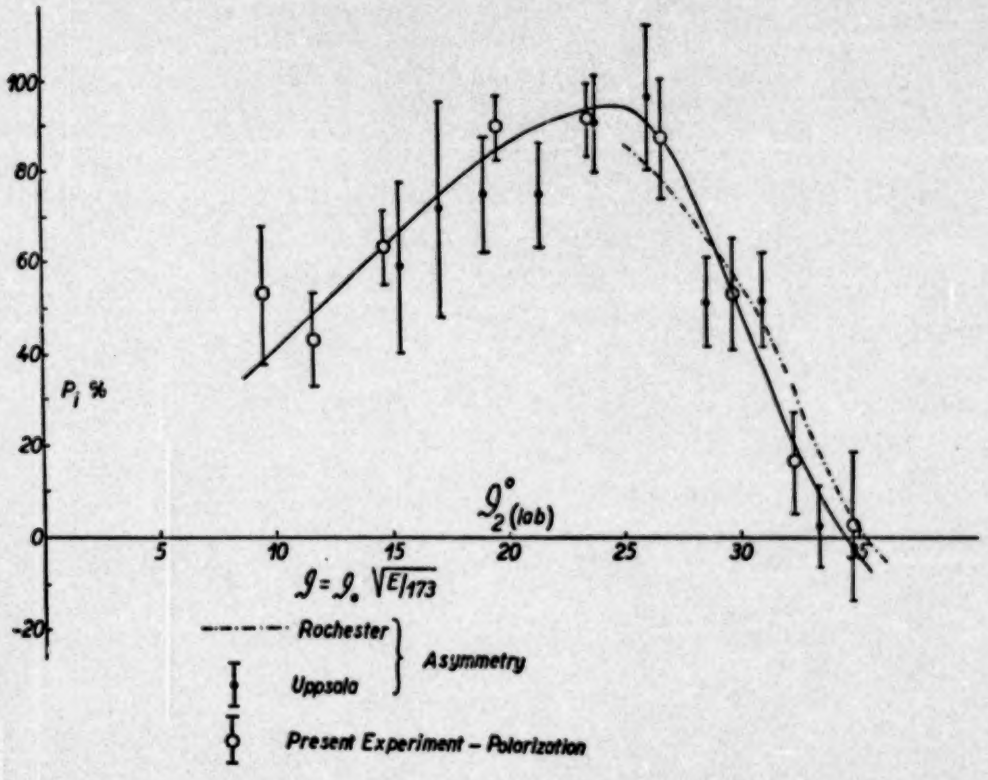

Fig. 2. Asymmetry and polarization from carbon 4.4 MeV level.

scattering energy was 173 MeV, and the angular resolution $\pm 0.8°$ total. Measurements are in progress on the 9.6, 15.0, 19.0 and 21.9 MeV levels and on extending the present results. The errors shown are standard deviations. They do not include the calibration error, which would contribute about an additional $\pm$ 5% to the quoted errors, but is not independent from point to point.

After adjusting the angle scale by the square root of the ratio of the energies, the present results for both the elastic and the 4.4 MeV polarizations agree very well with the asymmetries measured at 155 MeV and 220 MeV, as shown in figs. 1 and 2. As pointed out by Th. Maris [6]), there is no a priori

reason to expect this result, and it is apparently a significant physical fact

We are obliged to Prof. The Svedberg for his interest and support. We had frequent discussions with Dr. Th. A. J. Maris, whose enthusiasm is gratefully acknowledged. We thank Mr. Å. Svanheden, B. Hemryd and the cyclotron crew for technical cooperation, and Mr. B. Smith for vital electronic assistance. One of us (P. H.) is a CERN Fellow, and wishes to thank that organization. The work has been supported by the Swedish Atomic Energy Commission.

References

1) K. Strauch and F. Titus, Phys. Rev. **104** (1956) 191
2) H. Tyrén and Th. A. J. Maris, Nuclear Physics **2** (1956/57) 52
3) R. Alphonce, A Johansson, and G. Tibell, Nuclear Physics **3** (1957) 185
4) W. G. Chesnut, E. M. Hafner, and A. Roberts, Phys. Rev. **104** (1956) 449
5) J. M. Dickson and D. C. Salter, reported at the Amsterdam Conference (1956)
6) Th. A. J. Maris, Nuclear Physics **3** (1957) 213

Nuclear Physics **3** (1957) 340—343; *North-Holland Publishing Co., Amsterdam*

SUR LA DIFFUSION D'ÉLECTRONS DE HAUTE ÉNERGIE PAR LES NOYAUX

J. REIGNIER †

Department of Theoretical Physics, University of Manchester

Reçu le 21 décembre 1956

Abstract. The model dependence of the scattering of high energy electrons is discussed on the basis of equivalence laws. It is shown that even at very high energies the angular distribution is insensitive to the central part of the density distribution, but can provide information about the surface region.

1. Conditions d'Equivalence

Dans un article récent [1]), le Professeur L. Rosenfeld attire l'attention sur le traitement analytique de la diffusion d'électrons de haute énergie par les noyaux et signale que d'après les conditions d'équivalence établies [2]) il faut s'attendre à ce qu'à très haute énergie, la section efficace de diffusion devienne insensible à la distribution de la charge. Nous voudrions préciser cette question par une discussion basée sur les lois d'équivalence.

Par définition, deux répartitions sont „équivalentes du point de vue de l'onde partielle j et à l'énergie E" si le déphasage de cette onde partielle, de moment angulaire total j (en unité $\hbar$), est le même pour les deux répartitions à l'énergie considérée. Nous avons montré [2]) que la condition d'équivalence de deux répartitions du point de vue de l'onde partielle j et à l'énergie E était l'égalité de

$$\int_0^{r_1} V(r) r \, [J_j^2(Er) + J_{j+1}^2(Er)] \mathrm{d}r \tag{1}$$

pour les deux répartitions. $V(r)$ est le potentiel, r_1 est un point extérieur aux deux répartitions (les unités sont $\hbar = 1$, $c = 1$, $m = 1$). En intégrant deux fois par parties, en utilisant l'équation au potentiel et le fait que le potentiel est coulombien en r_1 pour les deux répartitions, on obtient comme condition d'équivalence, l'égalité de

$$\int_0^{\infty} \varrho(r) r^2 \mathscr{I}_j(Er) \mathrm{d}r; \tag{2}$$

$\varrho(r)$ est la densité d'électricité et $\mathscr{I}_j(x)$ est défini par

$$\mathscr{I}_j(x) \equiv \int_0^x \left\{ J_j^2(x') + J_{j+1}^2(x') - \frac{2j+1}{x'} J_j(x') J_{j+1}(x') \right\} \mathrm{d}x'. \tag{3}$$

La fonction $\mathscr{I}_j(x)$ est nulle à l'origine, positive et toujours croissante pour

† En congé de l'Université Libre de Bruxelles.

$x > 0$. Il est aisé de voir qu'à basse énergie, c'est-à-dire pour $ER \ll j$ où R est de l'ordre des dimensions nucléaires †, cette condition se réduit à la condition de Bodmer [3]), à savoir l'égalité de

$$\int_0^\infty \varrho(r) r^{2j+3} \mathrm{d}r \qquad (ER \ll j). \tag{4}$$

La condition (2) montre que la diffusion d'électrons est insensible aux valeurs centrales de $\varrho(r)$: du fait que $\mathcal{J}_j(x)$ est nulle à l'origine et ensuite toujours croissante, les valeurs superficielles de la densité sont beaucoup plus importantes que les valeurs centrales. Cependant, si l'énergie croît, $\mathcal{J}_j(Er)$ peut déjà prendre de très grandes valeurs pour r petit et il est intéressant de considérer ce que devient la condition (2) quand l'énergie augmente indéfiniment. Le passage à la limite montre que pour $ER >>> j$, la condition d'équivalence devient l'égalité de

$$\int_0^\infty \varrho(r) r^2 \log r \, \mathrm{d}r \qquad (ER >>> j). \tag{5}$$

2. Discussion

(1) On voit que la loi d'équivalence est la même pour toutes les ondes partielles $j <<< ER$. Toutes ces ondes partielles ne dépendent donc que d'un seul paramètre qui peut être par exemple le „rayon logarithmique équivalent" défini par

$$\log R_{\mathrm{eq}} = 1/3 + \langle \log r \rangle; \tag{6}$$

$\langle \log r \rangle$ est la valeur moyenne de $\log r$ prise sur le noyau avec la fonction de poids $\varrho(r)$ et R_{eq} est le rayon de la sphère homogène dont le $\langle \log r \rangle$ est le même que celui de la distribution considérée. On remarquera que pour une onde partielle donnée, la condition d'équivalence à très haute énergie, (5), est moins stricte qu'à basse énergie, (4).

En ce qui concerne la section efficace de diffusion, il faut tenir compte de ce que le nombre d'ondes partielles dont le déphasage est influencé par le volume fini du noyau croît à peu près linéairement avec l'énergie (par exemple, pour le plomb ce nombre est environ: 1 jusqu'à 20 MeV, 5 de 80 à 100 MeV, 10 de 180 à 200 MeV). A très haute énergie, les premières ondes partielles ($j \ll ER$) dépendent d'un seul et même paramètre; les autres ondes partielles dépendent chacune d'un paramètre différent, (2), lequel se réduit à (4) pour les dernières ($j > ER$). La section efficace de diffusion dépend donc du modèle par un certain nombre de paramètres. L'importance des dernières ondes partielles est d'ailleurs probablement négligeable devant celle des premières, ce qui réduit le nombre de ces paramètres.

La figure ci-jointe illustre ces conclusions. Nous avons considéré l'équi-

† Par exemple, en unités usuelles, R peut être pris égal à $1.2 \times 10^{-13} A^{1/3}$ cm.

valence d'une sphère chargée en surface de rayon r_s et d'une sphère homogène de rayon r_h. Pour chaque valeur de j et de Er_h, la condition (2) détermine le rapport r_s/r_h. Ce rapport est porté sur le graphique pour quelques valeurs † de j en fonction de Er_h et aussi en fonction de l'énergie pour un noyau Pb de rayon $1.18\times10^{-13}A^{\frac{1}{3}}$ cm. On remarque qu'à 180 MeV, la valeur limite $r_s/r_h = \exp(-1/3)$ est bien près d'être atteinte pour les ondes $j = \frac{1}{2}$

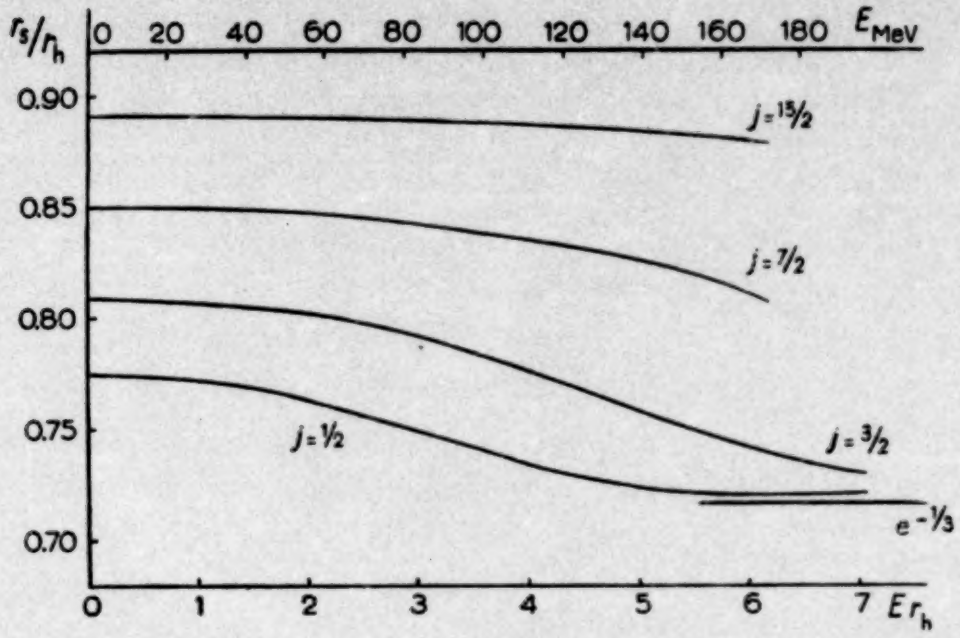

et $j = 3/2$. D'un autre côté, à la même énergie l'onde $j = 15/2$ obéit pratiquement encore à la condition de Bodmer.

A très haute énergie, le rayon logarithmique équivalent est probablement un paramètre fondamental de la diffusion d'électrons par les noyaux.

(2) La loi d'équivalence (5) montre d'autre part que même à très haute énergie et pour les petites valeurs de j, le déphasage des ondes partielles est pratiquement insensible aux valeurs centrales de la densité: nous pouvons changer assez fortement les valeurs centrales de $\varrho(r)$ sans changer beaucoup le rayon logarithmique équivalent. La diffusion d'électrons (même de très haute énergie) par les noyaux ne peut donc pas préciser le centre de la distribution d'électricité. Par contre, elle peut donner une image en principe de plus en plus detaillée de la densité aux valeurs pas trop petites de r et en particulier à la surface du noyau.

Il faut toutefois remarquer que le début du domaine des très hautes énergies ($\approx$ 200 MeV) est également le seuil où les effets dûs à la granulation de la charge électrique du noyau peuvent devenir importants.

† Les courbes $j = \frac{1}{2}$ et $j = 3/2$ ont été calculées au Laboratoire de Calcul Numérique de l'Université Libre de Bruxelles.

Je remercie vivement Monsieur le Professeur L. Rosenfeld pour d'intéressantes discussions.

Bibliographie

1) L. Rosenfeld, Nuclear Physics **2** (1956/57) 450 †
2) J. Reignier, Bull. Acad. Roy. Belg., Cl. Sc. **41** (1955) 151; **42** (1956) 173
3) A. R. Bodmer, Proc. Phys. Soc. A **66** (1953) 1041

† [The papers mentioned in this note aim at a treatment of the problem of the "equivalence" of charge distributions for scattering as comprehensive and rigorous as possible. The first discussion of this problem is due to H. Feshbach, Phys. Rev. **84** (1951) 1206 (L.R.)]

Nuclear Physics **3** (1957) 348; *North-Holland Publishing Co., Amsterdam*

BOOK REVIEW

E. BRODA und T. SCHONFELD, *Die technischen Anwendungen der Radioaktivität* (Verlag Technik, Berlin — Porta Verlag, München, 1956. × + 313 p. 19 DM).

The first quarter of this book is devoted to a simple and straightforward account of the fundamentals of natural and induced radioactivity, including methods of detection and measurement. This section is moderately well illustrated and is of a standard appropriate to first year University studies.

The remaining portion of the book attempts to cover the whole range of technical and scientific applications of radioactivity, including biological as well as physical and chemical aspects. The treatment of particular topics is brief and varies from section to section. The section on the use of radioactive material in chemical analysis reads like an uncritical compilation of abstracts, whereas that on the measurement of thickness by radiation methods shows an attempt to evaluate the field of application of the various possible methods. The small size and wide scope of the book means that the general level of treatment must be uncritical and the chief potential value of the work is as a bibliography of original papers. Here, unfortunately, the method of listing and renumbering references afresh on every page reduces the bibliographical elegance of the work.

H. J. Axon

ERRATA

Properties of Low Lying Levels in Mg^{25}, by H. E. Gove, G. A. Bartholomew, E. B. Paul and A. E. Litherland (Nuclear Physics **2** (1956/57) 132—146).

In line 4 of the abstract instead of 51 : 49 read 49 : 51. In figure 9 the two numbers 51 and 49 for the branching of the 0.98 MeV level in Mg^{25} should be reversed.

The papers by Th. A. J. Maris and H. Tyrén (Nuclear Physics **3** (1957) 35) and by H. Tyrén and Th. A. J. Maris (Nuclear Physics **3** (1957) 52) have been printed in the wrong order. These papers (in contradistinction to their authors)would be perfectly commutable if they did not refer to each other by the words 'preceding' and 'following', which are not invariant with respect to inversion.

D. C. PEASLEE, Nuclear surfaces and zero-energy scattering 255

A. N. MITRA, The fluctuation problem in μ-meson bursts 262

N. L. SVANTESSON, A scintillation spectrometer study of the photodisintegration of O^{16} 273

G. N. FOWLER and A. W. WOLFENDALE, On the interactions of fast μ-mesons 299

J. B. BELLICARD, A. MOUSSA et S. K. HAYNES, Etude des électrons Auger-K émis par le zinc 65 307

A. HERZENBERG and A. S. ROBERTS, Studies in the α-particle model of nuclei IV. The polarisation forces between α-clusters in nuclei. 314

H. TYRÉN, PETER HILLMAN and A. JOHANSSON, The polarization of 173 MeV protons inelastically scattered by carbon 330

J. REIGNIER, Sur la diffusion d'électrons de haute énergie par les noyaux . 340

Book Review 344

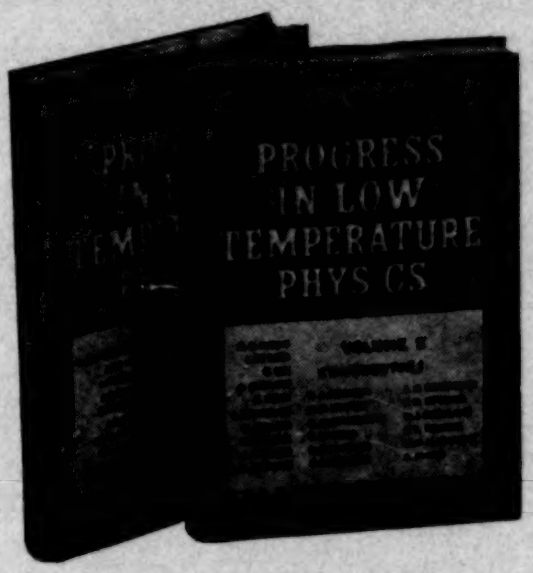

Just out

THE SECOND VOLUME

of

PROGRESS IN LOW TEMPERATURE PHYSICS

Edited by C. J. GORTER

Professor of Physics, Leiden

Contributors:

K. R. ATKINS
J. DE BOER
D. BIJL
A. H. DAANE
C. DOMB
J. S. DUGDALE
M. DURIEUX
H. VAN DIJK
C. J. GORTER
L. D. JENNINGS
V. A. JOHNSON
H. C. KRAMERS
K. LARK-HOROVITZ
S. LEGVOLD
B. T. MATTHIAS
D. SHOENBERG
E. H. SONDHEIMER
F. H. SPEDDING
M. J. STEENLAND
H. A. TOLHOEK
D. H. N. WANSINK
P. WINKEL

6x9'' . x + 480 PAGES . 180 ILLUS. GUILDERS 42.— (84 s)

NORTH-HOLLAND PUBLISHING COMPANY — AMSTERDAM

Send your order to your bookseller or directly to the publisher

Editorial Board

K. B. Adams
E. Amaldi
H. L. Anderson
K. T. Bainbridge
C. J. Bakker
P. R. Bell
R. E. Bell
S. de Benedetti
A. Berthelot
H. Brinkman
G. von Dardel
M. Deutsch
W. Gentner
P. C. Gugelot
H. Halban
O. Haxel
M. de Hemptinne
P. Huber
D. J. Hughes
S. Kikuchi
J. Koch
S. Livingston
E. M. McMillan
P. B. Moon
M. L. Oliphant
W. Paul
A. S. Rao
G. Salvini
P. Savić
P. Scherrer
C. Schmelzer
A. de Shalit
H. W. B. Skinner
R. Tangen
D. Taylor
S. du Toit
O. Wernholm
R. R. Wilson
S. D. Winter

NUCLEAR INSTRUMENTS

A journal on accelerators, instrumentation and techniques in nuclear physics

EDITOR: K. SIEGBAHN
UPPSALA

Papers to be published shortly

B. ASTRÖM, Scintillation spectrometer with constant relative channel width

C. J. BATTY, The loading of nuclear emulsions with water

L. FAVRE, Démultiplicateurs électroniques d'impulsions (I+II)

D. C. BROWN, A transistorized radiation monitor

G. BRONCHA, H. BRUCK, J. HAMELIN, G. NEYRET and T. BOLZINGER, Le test des blocks de l'électro-aimant du synchrotron de Saclay

K. O. NIELSEN and O. SKILBREID, Continuous scanning in two directions of the ion beam in an electromagnetic isotope separator

E. R. RAE and F. W. K. FIRK, An application of magnetic tape recording to neutron time of flight spectroscopy

Nuclear Instruments is published in bi-monthly issues.

Subscription price 130 *sh*; $ 17.00, *postfree.*

NORTH-HOLLAND PUBLISHING COMPANY AMSTERDAM